Theoretical and Experimental Investigations of an Adsorption Heat Pump with Heat Transfer between two Adsorbers

Von der Fakultät Energietechnik der Universität Stuttgart zur Erlangung der Würde eines Doktors der Ingenieurwissenschaften (Dr.–Ing.) genehmigte Abhandlung

Vorgelegt von

Dirk Schawe

aus Bad Cannstatt

Hauptberichter:	Prof. Dr. M. Groll
Mitberichter:	Prof. Dr. F. Meunier
	Prof. Dr. E. Hahne

Tag der Einreichung:	30.03.1999
Tag der mündlichen Prüfung:	21.12.2000

Institut für Kernenergetik und Energiesysteme der Universität Stuttgart

2001

Preface

I am grateful to the *Stiftung Energieforschung Baden–Württemberg* sponsoring this project enabling me to achieve in this context the following dissertation.

Especially I wish to express my sincere thanks to my supervisor Françis Meunier (Professor at *Conservatoire National des Arts et Métiers, Institut Français du Froid Industriel, CNAM–I.F.F.I.*, France) for his creative influence, his warm friendship and for his direct and indirect support to my thesis, teaching me all the secrets of adsorption.

As well I am very much obliged to Michel Pons (*Laboratoire d'Informatique pour la Mécanique et les Sciences de l'Ingénieur, CNRS–LIMSI*, France) for many discussions and helpful suggestions and annotations, especially for his proposal of the double–effect adsorption heat pump cycle. Jean–Jacques Guilleminot, another researcher at *CNRS–LIMSI*, I thank for hacking a computer program simulating an unsteady adsorption heat pump process, and for leaving me this program.

Furthermore I take the opportunity to thank for all help I received from the management of the *Fraunhofer Institute for Solar Energy Systems* in Freiburg (Germany), allowing me to use their facilities for laboratory experiments.

I would also like to express my gratitude to Manfred Groll (Professor at the *Institute for Nuclear Technology and Energy Systems*, University of Stuttgart, Germany) and to Erich Hahne (Professor at the *Institute of Thermodynamics and Thermal Engineering*, University of Stuttgart, Germany) for their appreciated contributions.

Freiburg, November 1998 Dirk Schawe

Abstract

Two thermally powered and quasi–continuously working heat pumps with two adsorbers effected by the principles of adsorption are investigated. In contrast to adsorption heat pumps with a single adsorber these systems deal with a multiple heat and mass transformation between two different adsorptive materials to obtain higher performances. The adsorptive characteristics of both adsorbents should be designed in a way that the heat released from both the desorption–cycle as well as the adsorption–cycle of an adsorbent of strong affinity will desorb the adsorbent of weak affinity. This process is called a two–stage triple–effect cycle which will be investigated in this report. The second investigated cycle uses only the adsorption heat released from the adsorbent of strong affinity to desorb the adsorbent of weak affinity. This is called a single–stage double–effect cycle. Calculations based on a simplified steady–state adsorption heat pump process result in COPs for both cycles between 0.5 and 1.0 with a zeolite/silica gel/water triple. More accurate dynamic numerical simulations of the promising single–stage double–effect cycle taking into account the consolidated adsorbent developed by the french laboratory CNRS–LIMSI (Meunier et al.) reduced the COP to 0.3 – 0.6. The value of the COP is highly dependent on the heat transfer characteristics of the adsorbent/heat exchanger connection, on their thermal conductivities, and in case of a consolidated adsorbent of its permeability. The COPs reached with the experimental setup are between 0.3 und 0.4, although the overall heat transfer coefficient of the employed finned tube heat exchanger (26–46 $W/m^2 K$) is acceptable. The main problems are the measured low amounts of condensation heat.

Contents

List of Figures

List of Tables

Nomenclature

❑ Basic Units

A	Ampere (electric current I)
Å	Angstrom (10^{-10} m; wavelength λ)
cm	Centimeter (10^{-2} m; length L)
°C	Degree centigrade (temperature T)
J	Joule (Nm; energy E)
kg	Kilogram (mass m)
kJ	Kilojoule (10^3 J; energy E)
kW	Kilowatt (10^3 W; power $\dot{E}$)
K	Kelvin (absolute temperature T)
m	Meter (length L)
mm	Millimeter (10^{-3} m; length L)
N	Newton ($^{\mathrm{kg\,m}}/_{\mathrm{s}^2}$; force F)
Pa	Pascal ($^{\mathrm{N}}/_{\mathrm{m}^2}$; pressure P; stress τ)
s	Second (time t)
Torr	Torr (133.32 Pa; pressure P)
VDC	Volt (direct–current voltage V)
W	Watt ($^{\mathrm{J}}/_{\mathrm{s}}$; power $\dot{E}$)
Ω	Ohm ($^{\mathrm{V}}/_{\mathrm{A}}$; electric resistance R)

❑ Symbols

A	Cross–sectional area of a heat exchanger tube [m^2]
c	Specific heat capacity [$^{\mathrm{J}}/_{\mathrm{kg\,K}}$]
c_c	Gaseous working fluid concentration in the adsorbent [$^{\mathrm{kg}}/_{\mathrm{m}^3}$] *(Eqs. 9.28, 9.29, and 9.31)*
d	Interior tube diameter [m]
d_0	Interior diameter of the consolidated adsorbent [mm] *(chapter 9)*
d_1	External diameter of the consolidated adsorbent [mm] *(chapter 9)*
D	Diffusion coefficient [$^{\mathrm{m}^2}/_{\mathrm{s}}$]
e	Mass specific energy [$^{\mathrm{J}}/_{\mathrm{kg}}$]
E	Energy [J]
$\dot{E}$	Heat flux [$^{\mathrm{J}}/_{\mathrm{s}}$]
f	Friction factor [–] *(Eqs. 7.27 and 7.28)*
ΔF	Specific free energy of adsorption [$^{\mathrm{J}}/_{\mathrm{kg}}$]
h	Heat transfer coefficient [$^{\mathrm{W}}/_{\mathrm{m}^2\,\mathrm{K}}$]
H	Heat loss [$^{\mathrm{W}}/_{\mathrm{K}}$] *(chapter 9)*
$-\Delta H$	Latent heat of adsorption [$^{\mathrm{J}}/_{\mathrm{kg}}$]

I	Electric current [A]
$\mathbf{J}$	Mass flux [$^{kg}/_{m^2\,s}$]
k	Thermal conductivity [$^{W}/_{m\,K}$]
K	Permeability [m^2]
K	K–factor [$^{impulses}/_{litre}$] *(page 58)*
l	Length of a heat exchanger tube [m]
L	Latent heat of vaporization [$^{J}/_{kg}$]
m	Adsorbent mass [kg]
$\dot{m}$	Mass flow rate [$^{kg}/_{s}$]
M	Molecular weight [$^{kg}/_{mol}$]
Nu	Nusselt number [–]
p	Pressure [$^{N}/_{m^2}$]
P	Power [$^{J}/_{s}$]
Pr	Prandtl number [–]
q	Adsorbent concentration [$^{kg}/_{kg}$]
q_0	Maximum adsorbent concentration [$^{kg}/_{kg}$]
Δq	Difference between poor and rich sorbate concentration [$^{kg}/_{kg}$]
Δr	Wall thickness [m] *(chapter 9)*
R_e	Electric resistance [Ω] *(Eq. 6.1)*
R_i	Thermal resistance [$^{K}/_{W}$]
$\Re$	Universal gas constant [8.314 $^{J}/_{mol\,K}$]
R	Specific gas constant [$^{J}/_{kg\,K}$]
Re	Reynolds number [–]
t	Time [s]
Δt	Time interval [s]
T	Temperature [K]
U	Overall heat transfer coefficient [$^{W}/_{m^2\,K}$]
v	Velocity [$^{m}/_{s}$]
$\mathbf{v}$	Velocity vector [$^{m}/_{s}$] *(Eq. 9.30)*
V	Volume [m^3]
$\dot{V}$	Volume flow rate [$^{m^3}/_{s}$]
$\dot{V}_b$	Programmed volume flow rate [$^{m^3}/_{s}$] *(Eq. 6.4)*
W	Adsorption volume [$^{m^3}/_{kg}$]

❑ Greek Symbols

α	Thermal diffusivity [$^{m^2}/_{s}$]
β	Expansion coefficient [$^{1}/_{K}$] *(Eq. B.19)*
ϵ	Heat exchanger effectiveness [–]
ε	Porosity of consolidated adsorbant [–] *(Eq. 9.28)*
μ	Dynamic viscosity [$^{kg}/_{m\,s}$]
μ_D	Dipole moment [Debye] *(appendix C)*
ν	Kinematic viscosity [$^{m^2}/_{s}$]
ϕ	Binding energy [$^{J}/_{kg}$]
ϕ_d	Differential binding energy [$^{J}/_{kg}$] *(Eq. B.17)*
ϕ_i	Integral binding energy [$^{J}/_{kg}$] *(Eq. B.20)*
ρ	Density [$^{kg}/_{m^3}$]
υ	Specific volume [$^{m^3}/_{kg}$]

❑ Subscripts

a	Adsorption
amb	Ambient
ar	Adsorber
$arhx$	Heat exchanger inserted in the adsorber tank
at	Adsorbent
aw	Adsorbed working fluid (adsorbate)
b	Boiling point *(appendix C)*
c	Condensation
$calc$	Calculated
chx	Condenser heat exchanger
$crit$	Critical values *(appendix C)*
d	Desorption
d/a	Desorption/adsorption
$diff$	Difference
dv	Dead volume
e	Evaporation
ehx	Evaporator heat exchanger
eng	Expanded natural graphite
exp	Experimental
fin	Fin of the heat exchanger
fp	Freezing point *(appendix C)*
h	High (concentration)
htf	Heat transfer fluid
hx	Adsorber heat exchanger without adsorbent
$hxat$	Adsorber heat exchanger with adsorbent
i	Interior
in	Inlet
is	Insulation
l	Low (concentration)
$loss$	Loss coefficient
m	Mean value
max	Maximum value
$mean$	Mean, average value
$meas$	Measured value
oil	Thermal oil
out	Outlet
s	Saturated
sc	Sorption chamber (adsorber without heat exchanger and adsorbent)
sim	Simulated
tp	Triple point *(appendix C)*
w	Working fluid
$wall$	Wall of a tank
z	Driving heat
0	Basic value
1	Low temperature level
2	Temperature after isosteric heating
3, 5	High temperature level
4	Temperature after isosteric cooling

❑ Superscripts

’	Belonging to LT–cycle or weak affinity adsorbent, respectively
ar	Adsorber
c	Condensation
calc	Calculated
eff	Effective
exp	Experimental
$\bar{h}$	Convective heat transfer
hxat	Heat exchanger with adsorbent
k	Thermal conduction
loss	Heat loss
rad	Radiation heat transfer
sens	Sensible heat

Chapter 1

German Summary — Deutsche Zusammenfassung

1.1 Einleitung

Mit *Adsorption* wird ein Vorgang bezeichnet, bei welchem ein Stoff – das *Adsorptiv* – an einer Substanz meist anderen Aggregatzustands – dem *Adsorbens* – allein durch Oberflächenkräfte, nicht durch chemische Bindungen anhaftet. Damit ist die Adsorption nichts anderes als eine Bindung, also eine Verdichtung von Molekülen aus einer fluiden Phase an einer Phasengrenze bzw. Festkörperoberfläche. Eine Bindung steht immer in Verbindung mit einem Energieumsatz; die Adsorption ist eine exotherme Reaktion. Der umgekehrte Prozess ist die *Desorption*, bei der das Adsorptiv von seinem Adsorbens unter Einsatz von Energie getrennt wird und einen Phasenwechsel erfährt.

Großtechnisch wird die Adsorption zur Trocknung, Abgasreinigung, Sorptionskatalyse und zum Ionenaustausch eingesetzt. Da die Adsorption ein thermisches Verfahren ist, lassen sich mit ihr Kreisprozesse auf unterschiedlichen Temperatur– und Druckniveaus realisieren, wie z.B. bei einem offenen oder geschlossenen Wärmepumpenprozess.

Der Begriff der *Wärmepumpe* oder auch der *Kältemaschine* steht für eine Maschine, die unter Einsatz von Energie ein warmes System aufwärmt, dabei ein kaltes System gleichzeitig abkühlt. Die zugeführte Energie kann in Form mechanischer Arbeit erbracht werden, wie es bei einer elektrischen Verdichterwärmepumpe der Fall ist, oder in Form von thermischer Arbeit bzw. thermischer Verdichtung. Letzteres wird bei den Sorptionswärmepumpen eingesetzt und hat den Vorteil der direkten Nutzung fossiler Brennstoffe ohne den Konversionsschritt der Stromerzeugung. Solche Sorptionswärmepumpen, ausschließlich basierend auf dem physikalischen Prozess der Adsorption, sollen in dieser Dissertation behandelt werden.

Die einfachste Adsorptionswärmepumpe besteht aus einem Adsorber mit integriertem Sorptionswärmetauscher *(Wärmetauscher/Adsorbens–Matrix)*, einem Verdampfer und einem Kondensator. Der thermodynamische Kreisprozess ist in Abb. 1.1 dargestellt. Sie arbeitet periodisch. Dies kann jedoch durch die Anordnung mehrerer phasenverschoben arbeitender Adsorber ausgeglichen werden. Ein wesentlicher Nachteil ist, daß die Nutzwärmeabgabe über einen großen Temperaturbereich von T_3 bis T_c erfolgt.

Dieser Nachteil kann durch Wärmetransformation zwischen einer endlichen Anzahl von Adsorbern kompensiert werden. Hierbei wird versucht mit einem Hochtemperaturprozess einen Niedertemperaturprozess anzutreiben. Dabei kann sowohl die Adsorptionswärme und die Kondensationswärme des Hochtemperaturprozesses (→ **Tripel–Effekt–Kreisprozess**), als auch nur die Adsorptionswärme (→ **Doppelt–Effekt–Kreisprozess**) zur Regenerierung des Niedertemperatur-

prozesses eingesetzt werden. Eine ausführliche Erläuterung zur Bezeichnungsweise der beiden Zyklen wird in dem Unterkapitel 3.2 aufgezeigt.

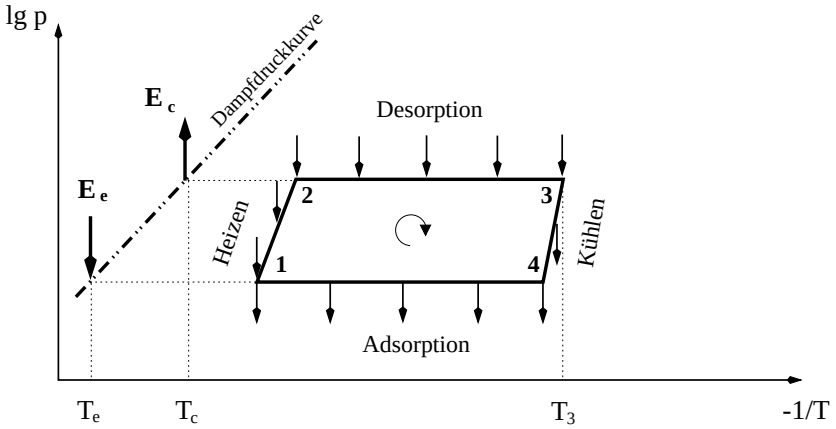

Abbildung 1.1: Adsorptionswärmepumpe mit einem Adsorber.

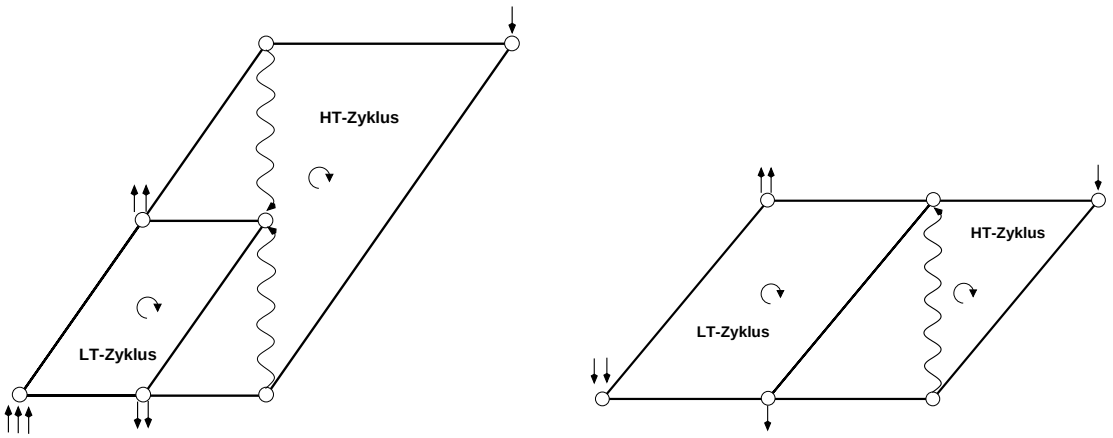

(a) (b)

Abbildung 1.2: (a) Tripel–Effekt–Kreisprozess und (b) Doppelt–Effekt–Kreisprozess.

Im ersten Abschnitt dieser Dissertation (Kapitel 4) werden die zuvor kurz vorgestellten zwei Adsorptionswärmepumpen (**AHP**) mit erhöhter Leistungszahl näher erläutert, deren Effizienz abgeschätzt und untereinander verglichen. Diese theoretischen Betrachtungen wurden mittels experimentellen Untersuchungen verifiziert. Aufgrund der beschränkten finanziellen Mittel konnte jedoch nur ein Labormeßstand einer Adsorptionswärmepumpe mit einem Adsorber realisiert werden. Zum Ende des zweiten Abschnitts (Abschnitt 7.6.2) wurde versucht, mit den gewonnenen Meßergebnissen Rückschlüsse auf die Leistungszahlen der beiden vorgestellten Mehrfach–Effekt–Kreisprozesse zu ziehen. In einem abschließenden dritten Teil (Kapitel 9) wird noch der vielversprechende Doppelt–Effekt–Kreisprozess mit Hilfe eines physikalischen instationären Modells numerisch simuliert.

In dieser deutschen Zusammenfassung werden die Kreisprozesse und der Labormeßstand dargestellt und die theoretischen und praktischen Ergebnisse zusammengefaßt.

1.2 Theoretische Untersuchungen zweier Mehrfach–Effekt–Kreisprozesse

1.2.1 Der Tripel–Effekt–Kreisprozess

Die Adsorptionswärmepumpe besteht aus zwei getrennten Adsorbern (**AdR**), die über Wärmeträgerrohre miteinander verbunden sind. Einer von beiden Adsorbern ist für hohe Temperaturen ausgelegt *(→ HT–AdR)* und der andere für niedrige Temperaturen *(→ LT–AdR)*. Beide Adsorber werden durch einen vorgeschalteten Verdampfer mit gasförmigem Arbeitsstoff versorgt. Auf der dem Verdampfer gegenüberliegenden Seite der Adsorber ist für jeden Adsorber ein Kondensator (**Cond**) angeordnet. Beide Adsorber sind mit dem jeweiligen Sorptionsmittel befüllt. Das Sorptionsmittel, mit dem der HT–AdR befüllt wird *(HT–Adsorbens)*, zeichnet sich dadurch aus, daß der Arbeitsstoff mit vergleichsweise großen Bindungskräften gebunden wird. Daraus resultiert, daß hohe Temperaturen zur Austreibung *(Desorption, Regenerierung)* des Arbeitsstoffs notwendig sind ($\approx 300°C$). Das zweite Sorptionsmittel *(LT–Adsorbens)* wird in seinen Bindungseigenschaften so gewählt, daß die bei der Adsorption und Desorption des HT–Adsorbens freiwerdende Wärme auf einem genügend hohen Temperaturniveau und in ausreichender Menge vorliegt, um das LT–Adsorbens vollständig zu regenerieren. Das LT–Adsorbens muß demnach deutlich niedrigere Bindungskräfte besitzen als das HT–Adsorbens, um bereits bei Regenerationstemperaturen im Bereich von 90° bis $140°C$ einen niedrigen Beladungszustand zu erreichen. Die hier vorgestellte Tripel–Effekt–Adsorptionswärmepumpe durchläuft für jeden Adsorber in einem eigenen Kreisprozess die Zustandsänderungen 1–2–5–3–4–1 *(→ HT–Kreisprozess)* und 1'–2'–3'–4'–1' *(→ LT–Kreisprozess)*. Mit Beginn der Zustandsänderung 2–5 des HT–Kreisprozesses wird der HT–Kondensator mit dem LT–Adsorber thermisch über einen flüssigen Wärmeträger verbunden. Der LT–Adsorber befindet sich jedoch auf der Temperatur $T_{1'}$ bzw. $T_{c'}$. Da die Kondensationswärme des HT–Kreisprozesses den LT–Kreisprozess aufheizen soll, muß der Dampfdruck im HT–Kondensator während der Kondensation bzw. während der Desorption des HT–Adsorbens steigen. Dies zu realisieren ist eine Schwierigkeit des Tripel–Effekt–Kreisprozesses.

Unter Berücksichtigung der Zusammenschaltung der beiden Kreisprozesse läßt sich die Arbeitsweise dieser Adsorptionswärmepumpe in vier Sequenzen einteilen.

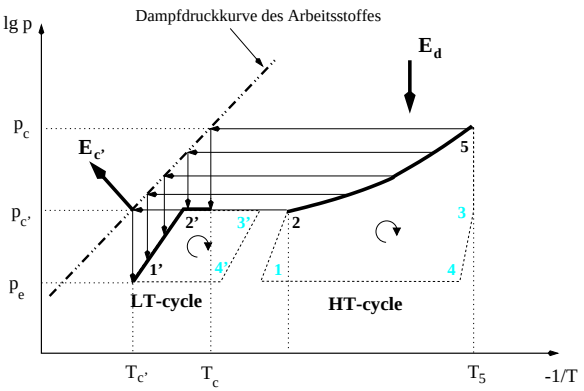

1. Sequenz: Desorption im HT–AdR *(2 → 5)*

Das Adsorbens hoher Bindungsenergie im HT–AdR wird auf eine maximale Temperatur T_5 und auf einen Druck p_c aufgeheizt und dabei desorbiert *(hohes Temperaturniveau, 2→5)*. Unter Zufuhr der Desorptionswärme E_d desorbiert der Arbeitsstoff und kondensiert mit steigendem Druck von $p_{c'}$ nach p_c im HT–Cond. Die Kondensationswärme wird an LT–AdR übertragen. Das Adsorbens niedriger Bindungsenergie im LT–AdR wird dabei isoster aufgeheizt *(1'→2')*. Sofern die Temperatur T_c höher ist als $T_{2'}$, beginnt bereits die isobare Desorption des LT–Adsorbens *(2'→3')*. Der desorbierte Arbeitsstoff kondensiert bei einem Druck $p_{c'}$ im LT–Cond. Die freiwerdende Kondensationswärme $E_{c'}$ *(mittleres Temperaturniveau)* kann als Nutzenergie abgeführt werden. Der Verdampfer ist inaktiv.

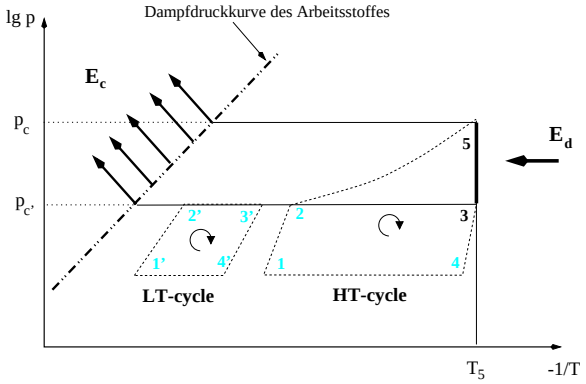

2. Sequenz: Isotherme Desorption im HT–AdR *(5 → 3)*

Nach Erreichen der Desorptionsendtemperatur T_5 wird das HT–Adsorbens isotherm desorbiert. Dabei sinkt der Druck von p_c auf $p_{c'}$. Dazu wird der HT–Cond direkt mit der Wärmesenke verbunden. Während dieser Sequenz sind Verdampfer, LT–Cond und LT–AdR außer Betrieb.

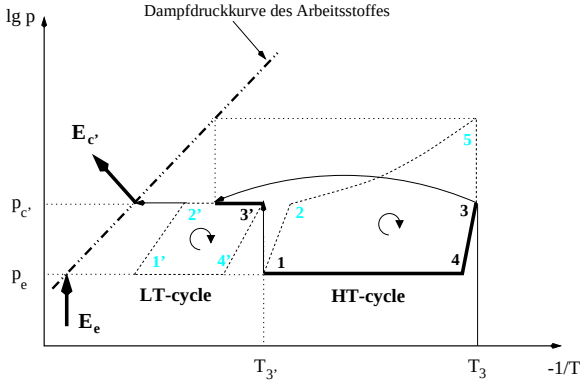

3. Sequenz: Adsorption im HT–AdR *(3 → 1)*

HT–AdR wird mit LT–AdR mittels eines Wärmeträgers thermisch verbunden. Dabei wird HT–AdR zunächst gekühlt, bis sich im Adsorber ein Druck p_e einstellt *(3→4)*. Danach erfolgt die isobare Adsorption des HT–Adsorbens *(4→1)*, wobei die freiwerdende Adsorptionswärme ebenfalls ans LT–Adsorbens zur seiner Desorption übertragen wird *(2'→3')*. Die freiwerdende Kondensationswärme $E_{c'}$ steht als Nutzwärme an der Wärmesenke zur Verfügung. HT–Cond ist inaktiv.

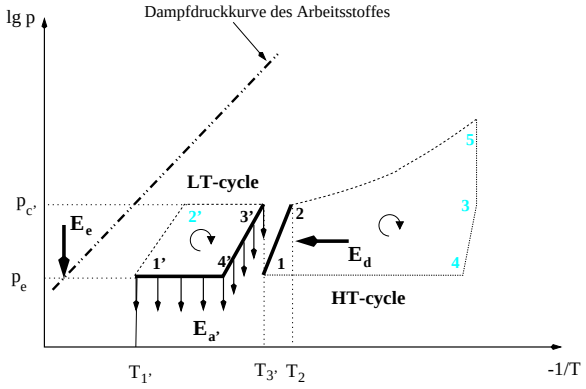

4. Sequenz: Adsorption im LT–AdR *(3' → 1')* und isosteres Aufheizen des HT–AdR *(1 → 2)*

Der LT–AdR wird mit der Wärmesenke verbunden; dabei sinkt der Druck auf p_e *(3'→4')*. Anschließend erfolgt die Adsorption von gasförmigem Arbeitsstoff *(niedriges Temperaturniveau)* am LT–Adsorbens *(4'→1')*. Die Adsorptionswärme $E_{a'}$ kann als Nutzenergie abgeführt werden. Gleichzeitig steigt der Druck im HT–AdR isoster von p_e auf $p_{c'}$ *(1→2)*. HT–Cond und LT–Cond sind außer Betrieb.

Die Leistungszahl des Tripel–Effekt–Kreisprozesses wurde mittels numerischer Computersimulationen abgeschätzt. Das Simulationsprogramm basiert auf einem statischen Sorptionsprozess, der die sensiblen Wärmen des Arbeitsstoffs und des Adsorbens und die Adsorptionsenthalpie, bestehend aus der Bindungswärme und der Verdampfungsenthalpie des Arbeitstoffs, berücksichtigt. Zusätzlich wird noch die sensible Wärme eines Wärmetauschers eingerechnet, der ein angenommenes Massenverhältnis bezogen auf das Adsorbens von 2:1 besitzt. Die Leistungszahl COP *(coefficient of performance)* des Tripel–Effekt–Kreisprozesses kann mit Hilfe der COPs der beiden Einzelprozesse HT–Kreisprozess und LT–Kreisprozess ausgedrückt werden:

$$\mathrm{COP} = \underbrace{\frac{|e_e|}{e_z}}_{\mathrm{COP}_{HT}} + \underbrace{\frac{|e_{e'}|}{e_{d'}}}_{\mathrm{COP}_{LT}} \left(1 + \underbrace{\frac{|e_e|}{e_z}}_{\mathrm{COP}_{HT}}\right) = \mathrm{COP}_{HT} + \mathrm{COP}_{LT}\,(1 + \mathrm{COP}_{HT}) \tag{1.1}$$

Die numerischen Simulationen wurden an vier verschiedenen Sorptionsmittelpaarungen vorgenommen; drei Silikagel/Zeolith 13X– und eine Zeolith 13X/Zeolith 13X–Paarung. Der Arbeitsstoff ist jeweils Wasser. Untersucht wurde der Einfluß der drei Temperaturniveaus auf den COP:

1. Temperatur der Wärmequelle T_e,
2. Temperatur der Wärmesenke $T_{c'}$ und
3. Desorptionsendtemperatur des HT–Kreisprozesses T_5

Dabei zeigte vor allem die Wahl der Kondensationstemperatur des LT–Kreisprozesses *(= Temperatur der Wärmesenke)* einen bedeutsamen Einfluß auf die Leistungszahl (siehe Abb. 1.3). Die Veränderung der beiden anderen Temperaturniveaus ließ den COP weniger signifikant schwanken.

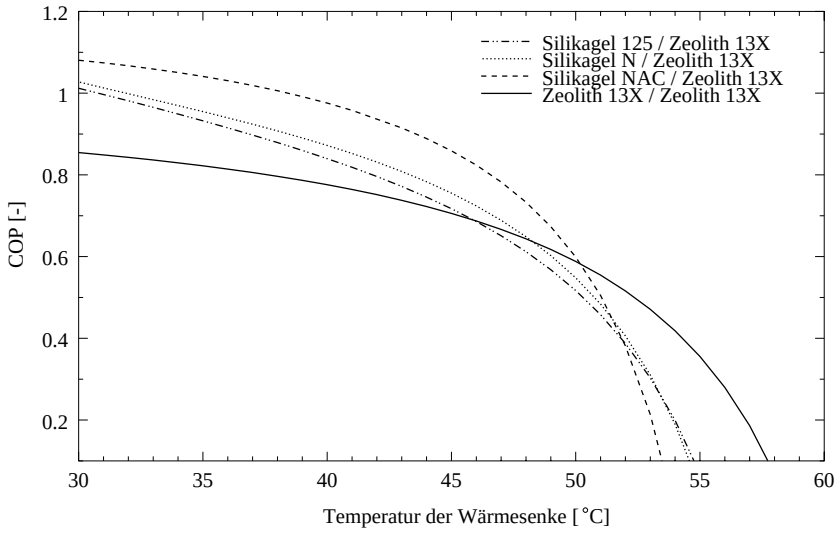

Abbildung 1.3: COP als Funktion der Kondensationstemperatur ($T_e = 7°\mathrm{C}$, $T_3 = 280°\mathrm{C}$, $p_c = 500$ mbar, $T_1 = T_{3'} = 106°\mathrm{C}$).

Vergleicht man in Abb. 1.3 die einzelnen Materialkombinationen untereinander, so zeigen die Silikagel/Zeolith–Kombinationen bis zu einer Kondensationstemperatur von 46°C bessere Leistungszahlen als die reine Zeolithkombination. Überraschend ist jedoch, daß die Zeolithkombination bei höheren Temperaturen den Silikagel/Zeolith–Kombinationen überlegen ist, ihr Kurvenverlauf insgesamt weniger schwach abfällt. Dies wird dadurch begründet, daß mit zunehmender Kondensationstemperatur die Beladungsbreite bei den Silikagel/Zeolith–Kombinationen sich stärker verringert als bei der Zeolithkombination.

1.2.2 Der Doppelt–Effekt–Kreisprozess

Im Unterschied zur Tripel–Effekt–AHP arbeitet die Doppelt–Effekt–AHP auf nur zwei Druckniveaus. Dadurch kann nur die Adsorptionswärme des HT–Kreisprozesses genutzt werden, um den LT–Kreisprozess zu regenerieren. Die Kondensationswärme des HT–Kreisprozesses wird direkt an

die Wärmesenke abgeführt. Durch diesen Schritt kann die Anzahl der Sequenzen auf zwei reduziert werden, wobei der HT–Kreisprozess die Zustandsänderungen 1–2–3–4–1 und der LT–Kreisprozess 1'–2'–3'–4'–1' durchläuft. Zudem erlaubt der wechselseitige Betrieb von Verdampfung und Kondensation die Einsparung eines Kondensators gegenüber der Tripel–Effekt–AHP.

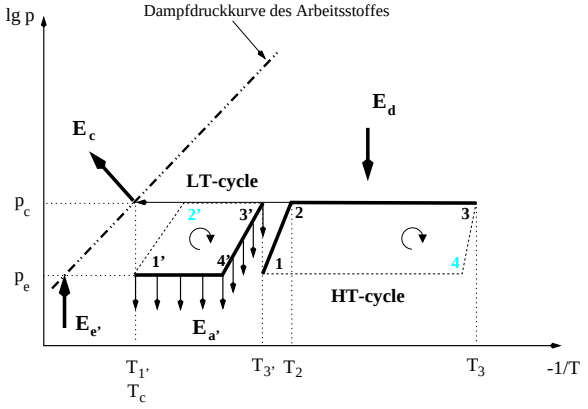

1. Sequenz: Desorption im HT–AdR *(1 → 3)* und Adsorption im LT–AdR *(3' → 1')*

Das Adsorbens hoher Bindungsenergie im HT–AdR wird auf eine maximale Temperatur T_3 aufgeheizt und dabei desorbiert *(hohes Temperaturniveau, 2⟶3)*. Der desorbierte Arbeitsstoff kondensiert bei einem Druck p_c im HT–Cond. Die Kondensationswärme steht als Nutzwärme an der Wärmesenke zur Verfügung. Gleichzeitig ist der LT–AdR mit der Wärmesenke verbunden, um diesen zu kühlen *(3'⟶4')*. Nach Erreichen des Verdampfungsdruckes p_e erfolgt die Adsorption im LT–AdR *(4'⟶1')*. Die Adsorptionswärme steht ebenfalls an der Wärmesenke *(mittleres Temperaturniveau)* zur weiteren Nutzung bereit.

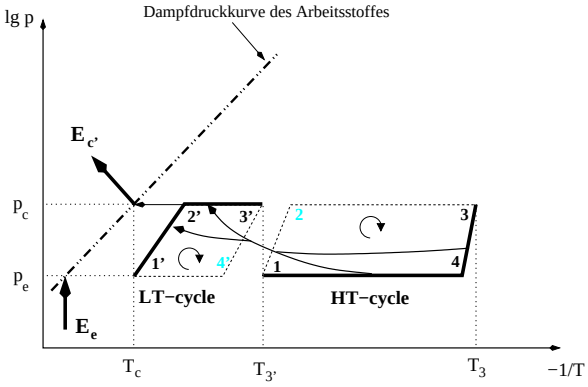

2. Sequenz: Adsorption im HT–AdR *(3 → 1)*

HT–AdR wird mit LT–AdR thermisch verbunden. Dabei wird HT–AdR heruntergekühlt bis der Verdampfungsdruck p_e erreicht wird *(3⟶4)*. Es folgt die Adsorption von gasförmigem Arbeitsstoff *(niedriges Temperaturniveau)* am HT–Adsorbens *(4⟶1)*. Die freiwerdende Adsorptionswärme wird benutzt, um das LT–Adsorbens aufzuheizen *(1'⟶2')* und zu desorbieren *(2'⟶3')*. Dabei kondensiert der Arbeitsstoff bei einem Druck p_c im LT–Cond, und die Kondensationswärme $E_{c'}$ wird an die Wärmesenke abgeführt. HT–Cond ist inaktiv.

Die Leistungszahl des Doppelt–Effekt–Kreisprozesses wurde mittels numerischer Computersimulationen abgeschätzt, die auf den gleichen Annahmen beruhen wie beim zuvor beschriebenen Tripel–Effekt–Kreisprozess. Der COP läßt sich ebenfalls als Summe der COPs der einzelnen Kreisprozesse schreiben:

$$\mathrm{COP} = \underbrace{\frac{|e_{e'}|}{e_{d'}}}_{COP_{LT}} + \underbrace{\frac{|e_e|}{e_z}}_{COP_{HT}} = \mathrm{COP}_{LT} + \mathrm{COP}_{HT} \tag{1.2}$$

Auch hier wurde der COP in Abhängigkeit von den drei Temperaturniveaus für vier unterschiedliche Materialkombinationen berechnet. Die Ergebnisse sind denen des Tripel–Effekt–Kreisprozesses ähnlich. Nur der COP ist insgesamt um maximal 0.1 geringer. Die Leistungszahl wird ebenfalls am

stärksten von der Kondensationstemperatur beeinflußt. Ein sehr wesentlicher Unterschied zwischen den beiden vorgestellten Kreisprozessen zeigt sich in der Entwicklung des COP's in Abhängigkeit der Desorptionsendtemperatur. Während beim Tripel–Effekt–Kreisprozess der COP mit steigender Desorptionsendtemperatur fast linear zunimmt, gibt es beim Doppelt–Effekt–Kreisprozess ein Maximum bzw. eine Temperatur, ab der sich der COP nahezu nicht mehr verändert, wie es in Abb. 1.4 markiert ist. Der Doppelt–Effekt–Kreisprozess erreicht sein Maximum bei ca. 220°C. Um beim Tripel–Effekt–Kreisprozess den gleichen COP–Bereich zu erreichen, sind je nach Materialkombination Temperaturen von 250° bis 262°C notwendig. Die geringere Maximaltemperatur des Doppelt–Effekt–Kreisprozesses hat in der praktischen Auslegung einer solchen Maschine den nicht zu unterschätzenden Vorteil der wesentlich geringeren Komponentenkosten.

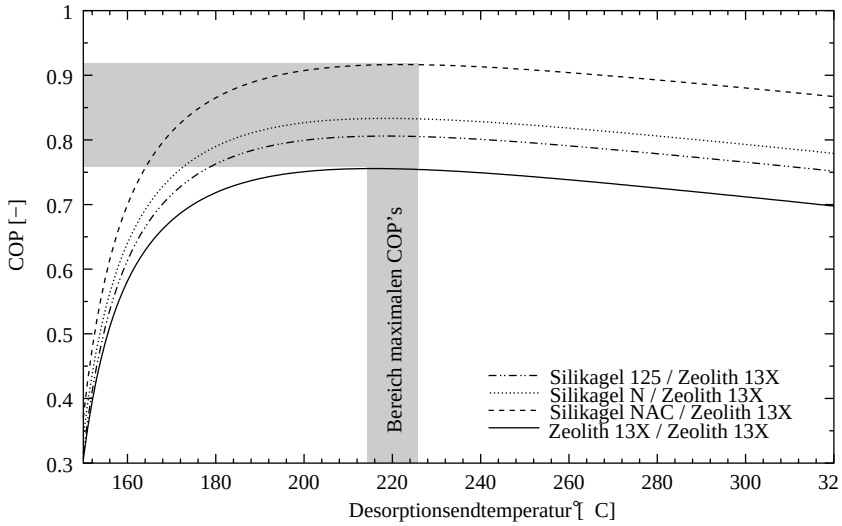

Abbildung 1.4: COP als Funktion der Regenerationstemperatur ($T_e = 7°C$, $T_{1'} = 40°C$, $T_1 = T_{3'} = 106°C$).

1.3 Laboraufbau einer Adsorptionswärmepumpe mit einem Adsorber

1.3.1 Der Laboraufbau

Der Testaufbau besteht im wesentlichen aus

- einem Verdampfer und einem baugleichen Kondensator, beide ausgeführt als zylinderförmige Edelstahlbehälter mit eingelegtem innen und außen beripptem Kupferrohr (überfluteter Verdampfer),
- einem Adsorber, d.h. einem Vakuumbehälter aus Edelstahl AISI 304L,
- einem Lamellenwärmetauscher, zwischen dessen Lamellen sich das eingeschüttete Adsorbens befindet (siehe Abb. 1.6),
- drei Thermostaten, welche die Energieversorgung übernehmen und im Falle von Verdampfer/Kondensator mit Wasser, im Falle des Sorptionswärmetauschers mit Thermoöl betrieben werden,
- einer Vakuumpumpe *(notwendig bei der Verwendung von Wasser als Arbeitsstoff)*,

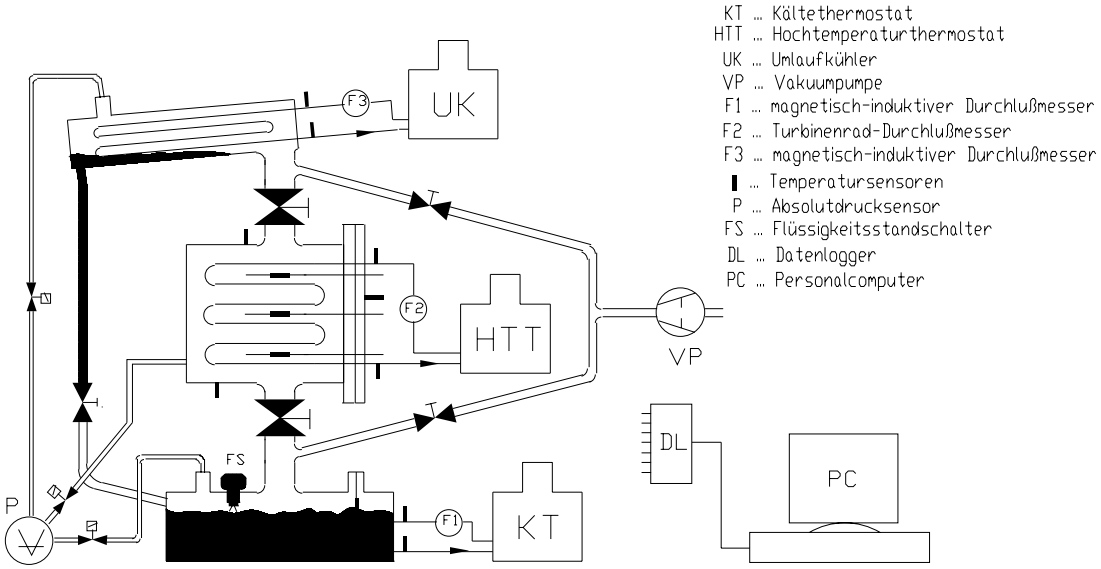

Abbildung 1.5: Labormeßstand einer Adsorptionswärmepumpe mit einem Adsorber.

- der Sensorik (Durchflußmesser, Drucksensor und mehrere Temperatursensoren) und
- der Meßwerterfassung, die von einem Datenlogger (Multiplexer und Signalwandler) kontrolliert wird und die Daten seriell an einen Personal Computer zur Speicherung und Bearbeitung weiterleitet.

Das Herzstück des Sorptionsmeßstandes ist der Lamellenwärmetauscher, der die wärmeleitende Verbindung zwischen dem im Grunde gut isolierenden Adsorptionsmittel und dem Wärmeträger herstellt. Der Lamellenwärmetauscher ist vollständig aus Kupfer hergestellt und besteht aus 44 Lamellen (Stärke: 0.15 mm), die senkrecht zu ihrer Oberfläche von 36 miteinander verbundenen 1/8–Zoll Rohren durchbrochen sind. Zwischen die Lamellen wird das Sorptionsmittel gefüllt, das von einem umspannten feinmaschigen Edelstahlnetz am Herausrieseln gehindert wird. Der Lamellenabstand wurde so gewählt, daß jedes Adsorbenskorn mindestens einen Berührungspunkt mit einer metallischen Oberfläche hat. Unter der Annahme einer vollständig turbulent ausgebildeten Rohrströmung liegt der Wärmedurchgangskoeffizient des zeolithgefüllten Lamellenwärmetauschers temperaturabhängig zwischen 26 und 46 $^{\mathrm{W}}/_{\mathrm{m}^2\,\mathrm{K}}$. Douss et al. [16] hat mit einem ähnlichen Wärmetauscher 18 $^{\mathrm{W}}/_{\mathrm{m}^2\,\mathrm{K}}$ ermittelt.

Abbildung 1.6: Lamellenwärmetauscher.

1.3.2 Experimentelle Untersuchungen

Die experimentellen Untersuchungen wurden an drei Stoffsystemen durchgeführt:

1. Silikagel Grace 125/Wasser

2. Silikagel Grace 125/Methanol

3. Zeolith 13X/Wasser

Zu den Silikagel Grace 125/Methanol–Messungen sind in dieser Dissertation keine Ergebnisse veröffentlicht, da sich die Eigenschaften des Silikagels nach einigen Meßzyklen dahingehend veränderten, daß die Adsorptionsfähigkeit verloren ging und das Silikagel sich von glasig weiß nach dunkelbraun verfärbte. Auch der Austausch des Methanols durch Wasser zeigte keine erneutes Adsorptionsvermögen des Silikagels. Die Verfärbung des Silikagels deutet auf Kohlenstoff hin. Eine Ursache für die Anlagerung von Kohlenstoff könnte in den Verdampfer eingedrungenes verdampftes Vakuumpumpenöl sein.

Zu den verbleibenden beiden Stoffsystemen sind eine große Anzahl von Messungen unter verschiedenen Bedingungen gemacht worden. Jedoch werden in dieser Dissertation nur Meßergebnisse präsentiert, die Rückschlüsse auf die vorgestellten Mehrfach–Effekt–Kreisprozesse zulassen und mit denen die Verluste des Adsorbers bestimmt werden können.

Zur Durchführung von Messungen wird der Wärmetauscher, wie er in Abb. 1.6 abgebildet ist, komplett mit dem vorgesehenen Adsorbens befüllt, in den Adsorber eingeführt und vakuumdicht verschlossen. Der Verdampfer wird mit entgastem Arbeitsstoff befüllt. Da Wasser als Kältemittel eingesetzt wird, muß die gesamte Anlage evakuiert und auf Lecks kontrolliert werden. Die drei Thermostaten sind auf ihre gewünschte Temperatur zu stabilisieren. Ein kompletter Kreisprozess läuft dann wie folgt ab:

Desorption

1. Alle drei Ventile sind geschlossen.

2. Der Adsorber wird aufgeheizt und Ventil 2 geöffnet sobald der Dampfdruck im Adsorber den Kondensationsdampfdruck übersteigt.

3. Nach Erreichen der Desorptionsendtemperatur wird Ventil 2 geschlossen und Ventil 3 zur Rückführung des Kondensats in den Verdampfer kurzzeitig geöffnet und dann wieder geschlossen, ohne einen Druckausgleich zwischen den beiden Behältern herbeizuführen.

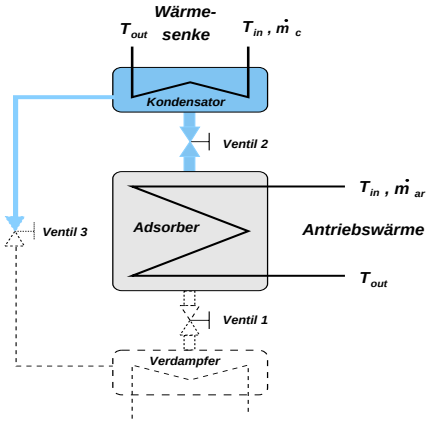

Adsorption

1. Der Adsorber wird mit der Wärmesenke verbunden und dabei gekühlt.

2. Sobald der Dampfdruck im Adsorber unter den Verdampfungsdruck des Arbeitstoffs sinkt, wird Ventil 1 geöffnet. Die Adsorption wurde eingeleitet.

3. Nach Erreichen der eingestellten Temperatur der Wärmesenke wird Ventil 1 geschlossen und der Kreisprozess ist beendet.

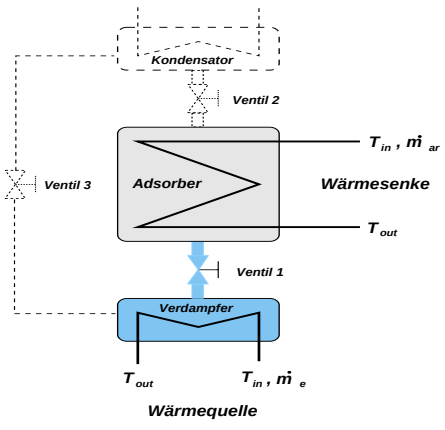

Jede abgeschlossene Messung umfaßt vier aufeinanderfolgende Desorptions/Adsorptions–Sequenzen, wobei die letzten drei von der Datenerfassung aufgezeichnet werden. Eine solche

Sequenz zeigt Abb. 1.7. Ihr fehlt der Wärmefluß des Verdampfers, der leider aufgrund der zu großen Trägheit des Verdampfers nicht erfaßt werden konnte.

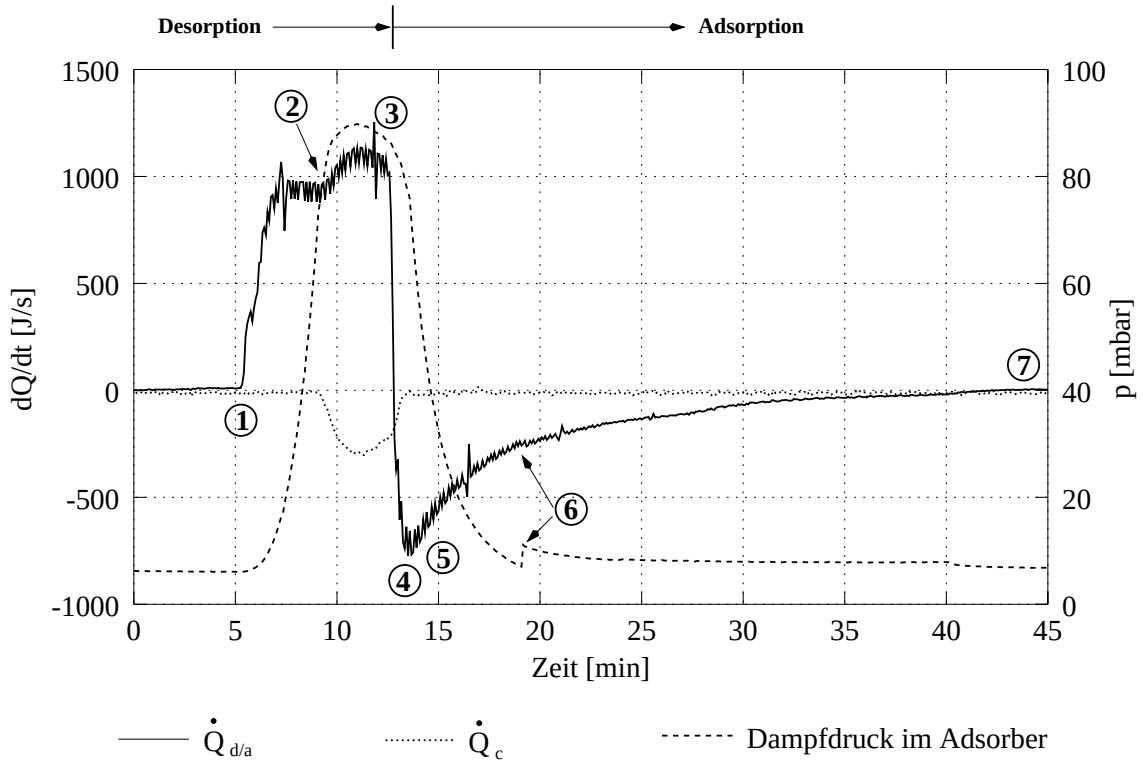

Abbildung 1.7: Wärmeflüsse von Adsorber und Kondensator und der Druckverlauf im Adsorber für eine Desorptions/Adsorptions–Sequenz.

Die Ermittlung der Wärmeflüsse erfolgt mittels der Gleichung

$$\dot{E} = \rho(T_{mean})\,\dot{V}\,c_{htf}(T_{mean})\,\Delta T. \tag{1.3}$$

worin ρ die Dichte, $\dot{V}$ der Volumenstrom und c_{htf} die Wärmekapazität des Wärmeträgers sind. ΔT ist hierbei die Differenz zwischen der Vorlauftemperatur zur Zeit t und einer errechneten Rücklauftemperatur, die ein Fluidteilchen zur Zeit $t+\Delta t$ haben würde, das zur Zeit t den Vorlauf passiert hat.

Die Dissertation präsentiert insgesamt fünf ausgesuchte Messungen, vier davon mit Silikagel Grace 125/Wasser und eine mit Zeolith 13X/Wasser. Drei Silikagel–Messungen unterscheiden sich nur durch ihre Kondenstionstemperatur und weisen ungefähr die gleiche Verdampfungstemperatur wie die Zeolith–Messung auf. Die verbleibende Silikagel–Messung wurde mit erhöhter Verdampfertemperatur durchgeführt. Neben den reinen Meßergebnissen finden sich in Tabelle 7.1 noch Angaben

zu Wärmeverlusten und zu berechneten Leistungszahlen.

Allen Meßergebnissen war gemein, daß die ermittelten Kondensationswärmen deutlich unter den berechneten lagen. Eine Ursache liegt sicherlich darin begründet, daß Kondensation nicht nur an dem Wärmetauscher erfolgt, sondern daß man auch mit parasitärer Kondensation rechnen muß, die an den Wänden der Anschlußteile zwischen Adsorber und Kondensator auftritt. Außerdem ist der Kondensator für die anfallenden Kondensationsmengen überdimensioniert, d.h. man muß mit beachtlichen Verlusten rechnen, deren quantitative Erfassung sehr schwierig ist.

Berechnet man aus den Meßergebnissen die verlustberichtigten und massenspezifischen Wärmen wie Adsorptions–, Desorptions– und Kondensationsenergie, so lassen sich die Leistungszahlen des Doppelt–Effekt– und Tripel–Effekt–Kreisprozesses berechnen. Die Ergebnisse sind in Tabelle 7.2 dargestellt und zeigen verglichen mit den vom Computer simulierten Werten einen deutlich geringerer Leistungszahl. Die Differenz verringert sich jedoch mit steigender Kondensationstemperatur. Auch hier liegt die Ursache hauptsächlich wieder in den zu gering gemessenen Kondensationswärmen.

1.4 Schlußwort

Leistungszahlverbesserungen lassen sich bei Adsorptionswärmepumpen im wesentlichen durch Wärme– und Massentransformationen erreichen. Sie sind jedoch meist verbunden mit einer aufwendigeren Konstruktion. Dies gilt vor allem für die in der vorliegenden Dissertation vorgestellte Tripel–Effekt–AHP. Anders verhält es sich bei der ebenfalls präsentierten Doppelt–Effekt–AHP. Sie besitzt im Vergleich zur einstufigen AHP mit nur einem Adsorber nur wenig mehr Bauteile, die zudem noch für geringere Maximaltemperaturen ausgelegt sein dürfen. Zudem arbeitet sie nur mit zwei Sequenzen, die im Gegensatz zur einstufigen AHP kontinuierlich Wärme an der Wärmesenke abgeben und gleichzeitig den Verdampfer kontinuierlich kühlen.

Daneben gibt es noch die Leistungszahlverbesserungen durch geeignete Konstruktionen und aufeinander abgestimmte Komponentenauslegung. Hierbei sind folgende Einflußgrößen von Bedeutung:

- Optimierung des Wärmeübergangs zwischen dem Adsorbens und dem Wärmetauscher bzw. dem Wärmeträger.
- Entwicklung von Adsorbentien, die in ihrem Betriebstemperaturbereich den größten Beladungshub aufweisen sollten.
- Komponenten einfacher Bauweise sind zu verwenden, die stabil und leicht sind und keine beweglichen Teile aufweisen.

Chapter 2

Introduction

The physical process of adsorption is widely used for drying, purification and separation processes, ion exchange and catalysis. All these techniques use only the adsorption of gaseous or liquid molecules on highly porous materials. But adsorption is accompanied by evolution of heat. This heat is normally treated as waste heat, but if the adsorption process is adapted to an open or closed heat pump cycle, then this released heat might be useful for heating or air conditioning buildings or refrigeration for example.

The *heat pump* is a system that receives heat from a colder body and delivers heat to a hotter body, not in violation of the second law, but by virtue of a work or heat input. If a heat pump operates with thermal compression we talk about an *adsorption heat pump* (short: **AHP**). Such adsorption heat pumps differ fundamentally from vapor–compression heat pumps, because the adsorption system converts heat of a given temperature to heat of another temperature without any intermediate use of mechanical work, provided by an electric compressor or gas engine.
Comparing an AHP with a vapor–compression heat pump the following pros and cons can be raised:

Adsorption heat pump

+	direct use of fossil energy
+	operation with energy sources like waste heat or solar energy is possible which causes no greenhouse–effect
+	environmentally friendly fluids like water, alcohols, ammonia or hydrogen are utilized
+	sufficiently high performances can be reached with multi–effect systems
−	additional infrastructure like gas pipeline or oil tank is necessary
−	cost–intensive components are necessary (depending on the maximum desorption temperature)
−	design volume larger

Vapor–compression heat pump

+	no further infrastructure than electricity is necessary
+	compact designs
−	fossil energy is converted from heat to electricity and then back to heat

From the list above we can see that AHPs have the most significant advantage compared to their vapor-compression counterparts concerning the impact on the environment, viz. zero ODP – *Ozone Depletion Potential* and zero GWP – *Global Warming Potential*, and they can utilize alternative energy sources like waste heat or solar heat.

A comprehensive state of the art review on the feasibilities of solid sorption systems — adsorption and chemical reaction of salts and hydrates — is presented by Meunier [62].

In the first part of this dissertation two different AHPs with increased efficiency, a two–stage triple– and a single–stage double–effect AHP, are investigated comparing their performances and their design possibilities with respect to simplification. We will discover that the double–effect AHP cycle will become a promising solution. Therefore the third part is dedicated to its dynamic operation investigated through computer simulation. The second part describes the single–adsorber experimental setup which was the only possible way to become acquainted with the real adsorption process, because of financial restriction. A further goal of the experimental setup is to draw the conclusion from the experimental single–adsorber results back to the theoretical multi–effect cycle results of the first part of this report. The dissertation is closed with an extensive appendix giving the reader mathematical concepts and a variety of physical properties of the used adsorbents and working fluids.

Chapter 3

A Brief Introduction to Adsorption Principles

The fundamentals of adsorption processes in general, i.e. for the customary applications as gas separation, purification, etc., are described by Ruthven [80], Yang [93] and in German by Kast [43], and in two ancient publications by Blüh and Stark [8] and Hückel [39]. Suzuki [87] is the only author who dedicated one chapter to the adsorption for energy conversion.

A recommended book with a complete collection of heat conversion systems based on Rankine cycles with their design rules was edited by Alefeld and Radermacher [3].

3.1 Phenomenon Adsorption

At the surface of solids unsaturated and relatively weak intermolecular forces of the van der Waals type and electrostatic forces are acting. Hence, when a solid is exposed to a gas, the gas molecules will form bonds with it and become attached, but not chemically bonded. This phenomenon is called **physical adsorption**. In cases the gas molecules form a chemical bond with the surface of the solid, we talk of **chemisorption**. The inverse process, the release of gas molecules from the solid surface is termed **desorption**.

The process of physical adsorption from a gaseous or liquid phase is invariably exothermic. The heat of adsorption which is released, when a sorbate attaches to a solid surface, consists of the binding energy, and in case of adsorption from a gaseous phase, of the latent heat of vaporization. Responsible for the binding energy are two groups of forces, the always acting van der Waals forces and the electrostatic interactions as polarization, dipole, and quadrupole interactions. The latter forces are mainly acting on adsorbents with ionic structure such as zeolites.

The van der Waals forces are divided into dispersion forces, whose attractive potential is mainly proportional to the inverse sixth–order distance r between the centers of two interacting molecules. On the other hand the finite size of the molecules causes a repulsive potential which is proportional to the inverse twelfth–order distance r. These repulsive forces distinguish physical adsorption from chemisorption, where changes in the electron shells of the atoms, especially of the valence electrons occur.

The electrostatic potentials in the area of the surface of ionic structured solids are caused by polarization, field–dipole and gradient–quadrupole interactions. If dipolar sorbate molecules like water or ammonia are attached by such an ionic structured solid, unusual high heat of adsorption is contributed.

3.1.1 Adsorption Equilibrium

An adsorbent inserted in a gaseous atmosphere of a certain composition will reach after a sufficiently long period equilibrium with the surrounding fluid, i.e. the amount of adsorbed and desorbed fluid molecules is equal. The amount of components adsorbed per mass of adsorbent q depends on the pressure p of the fluid phase and the temperature T of the adsorbent. So we can state for equilibrium the function $f(p, T, q)$ must be zero. Normally the amount adsorbed q is given as function of the pressure p at constant temperature T

$$q = f(p)|_T \tag{3.1}$$

This relation is called the *adsorption isotherm* at T.

There coexist many mathematical descriptions of the adsorption isotherm. Some of these models are derived from physics, while others are of empirical nature based on experimental data with an finite amount of empirical parameters. We distinguish three different approaches:

❶ Langmuir approach [47]

❷ Gibbs approach

❸ Potential theory, first introduced by Polanyi [2]

3.1.2 Langmuir Isotherm

The simplest isotherm is the Langmuir isotherm, a monolayer adsorption on homogeneous surfaces, assuming that

- each surface site of the adsorbent can accommodate only one molecule or atom,
- no interactions between the adsorbing molecules take place,
- each adsorbed molecule or atom is located at a specific place on the adsorbent surface, and
- all surface sites are energetically equal (homogeneous).

The Langmuir model has been modified by reducing its original list of assumptions. An important modification is to allow interactions between the adsorbed molecules which becomes pronounced for concentrations near saturation. Such a model taking into account weak interactions between neighboring molecules has been presented by Lacher [46] and Fowler and Guggenheim [24]. Another modification is to regard nonuniform surfaces, which is treated in the *Freundlich isotherm*. And the multilayer adsorption is studied intensively by Brunauer, Emmett and Teller [10], known as *BET model*.

3.1.3 Gibbs Isotherm

From the thermodynamic equilibrium conditions follows the analogy between the vapor–liquid–equilibrium and the adsorbate–gas–equilibrium, i.e. formally the pressure and volume will be replaced by the spreading pressure and the surface area. The chemical potential of the adsorbate which is treated as a two–dimensional entity, is then equal to that of the gas phase at equilibrium.

3.1.4 Potential Theory

The adsorption system is viewed as a gradual concentration of gas molecules toward the solid surface due to a potential field. The correlation between the sorptive potential, i.e. the work needed to compress the sorbate from pressure p to saturation pressure p_s, and the volume above the surface, i.e. the amount adsorbed on the surface regarded as liquid, is defined by the Dubinin–Polanyi *characteristic curve* (Dubinin and Astakhov [22]). This characteristic curve is assumed to be independent of temperature.

A more detailed approach to the Dubinin theory is introduced in appendix B.1 which treats the analysis of the thermogravimetrical measurements.

3.2 Cascade Adsorption Heat Pump Configurations

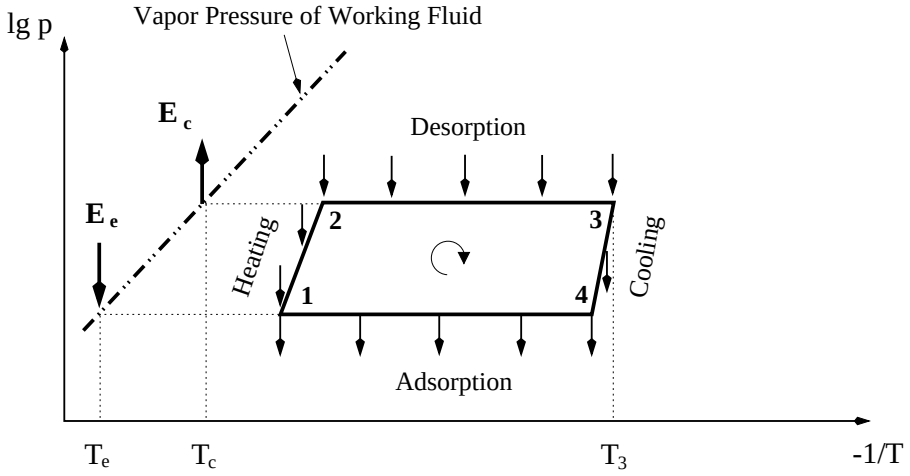

Figure 3.1: Intermittent cycle.

The simplest adsorption heat pump consists of a single adsorber filled with an adsorbent–heat exchanger compound connected through valves to an evaporator and a condenser. Low–temperature heat (T_e) released to the evaporator and high–temperature heat (T_3) to the adsorber result in an intermediate-temperature heat (T_c) output at the heat sink. One cycle is divided into four phases as pictured in Fig. 3.1: Heating ($1 \rightarrow 2$), Desorption ($2 \rightarrow 3$), Cooling ($3 \rightarrow 4$) and Adsorption ($4 \rightarrow 1$). During the desorption–, cooling– and adsorption–phase heat is released to the heat sink. And during the adsorption–phase heat is withdrawn from the evaporator. The heating–phase is not accompanied by a heat output. In both cases, the single–adsorber heat pump is used as heating device or refrigerator, the heating or cooling rates, respectively, are intermittent. Moreover, the heat sink is provided by large temperature swings from T_3 down to T_c.

The disadvantages of intermittent process and large temperature swings can be avoided by cascading regenerative cycles transferring heat from high–temperature adsorbers to low–temperature. In the literature many cascading cycles have been proposed. They might be divided into two groups with regard to the type of heat transfer occurring between two or more adsorbers. The first group deals with the process of *heat recovery* by circulating a heat transfer fluid between two adsorbers until their temperatures become equal (equivalent to the temperature distribution in a parallel flow heat exchanger). For example Douss et al. [19] operate with two different adsorptive materials, active carbon and zeolite, but with two working fluids, methanol and water, respectively. The working pairs are arranged in three adsorbers *(one for active carbon and two for zeolite)* and

two evaporators. The enforced heat recoveries are mainly heat transfers from the high temperature adsorber cooling it down to preheat the low temperature adsorber. The same principle of heat recovery is effected in the adsorptive air conditioning unit *(both adsorbers of equal size are filled with the same adsorptive material)* used by Poyelle et al. [72]. Supplementary they adapted a mass transfer sequence to the cycle in order to enlarge the mass of working fluid pumped in the cycle.

The second group works with the principle of *thermal regeneration*. First systems are pursued by Shelton et al. [84] and experimentally realized by Pons et al. [67], [68], [70] and [71]. These systems require innovative techniques to maintain temperature profiles in each adsorber during operation.

Additionally both types of heat transfer processes, the heat recovery and the thermal regeneration can be adapted by mass transfers between the adsorbers in order to enlarge the working fluid pumped around.

In the frame of this work we go back to the heat recovery cycles by proposing two cascading cycles which differ mainly with respect to the kind and number of heat recoveries. Both systems consist of two adsorbers filled with two adsorbents of different adsorptive characteristics. One adsorber contains an adsorptive material of weak affinity operating at a low temperature level *(LT–cycle)* and the other, material of strong affinity operating at a high temperature level *(HT–cycle)*. The number of condensers and evaporators depends on the type of configuration presented afterwards, and if one or two different working fluids are used. In the following some definitions are given which are used to classify the suggested cycles presented in the subsequent paragraphs:

- **Exchange Unit** ( ≙ ): This is the number of heat exchanges in which a phase change of working fluid occurs (Alefeld and Radermacher [3]).
- **Number of Stages:**
  - **1st Definition:** The number of basic cycles necessary to compose the system gives the number of stages (Alefeld and Radermacher [3]).
  - **2nd Definition:** Another commonly used definition for the stages of a heat pump system is to regard the pressure levels between which the system is operating.
- **Effectiveness:** The effectiveness of the system is the ratio of heat output at the evaporator (refrigeration) to heat input (driving heat) (Alefeld and Radermacher [3]).

In order to classify both suggested cycles (see Figs. 3.3(a) and 3.2(a)) we keep to the design rules for the configuration of heat conversion systems introduced by Alefeld and Radermacher [3]. For the number of stages we will use the commonly used definition (→ 2nd Definition) instead of the definition given by Alefeld and Radermacher [3]. Therefore we call a system which is operating between two pressure levels a single–stage system, as presented in Fig. 3.3(a), and a system operating between three pressure levels a two–stage system, as given in Fig. 3.2(a). In case of the first definition the two following presented cycles would both be of type two–stage.

The first configuration as illustrated in Fig. 3.2 uses two condensers, because they need to work simultaneously and one evaporator because only one working fluid is regarded. It operates on the principle that the condenser heat and the adsorption heat of the HT–cycle drive the LT–cycle. Two condensers are necessary because they work simultaneously. Therefore, one unit of heat input produces three units of refrigeration. Or expressed as heating efficiency, one unit of latent driving heat causes one unit of latent condenser heat and one unit of latent adsorption heat that are transferred to the LT–adsorber, and further two units of latent heat released by the LT–adsorbent.

In the sum, four units of latent heat are released at the heat sink. Applying the commonly used rules this configuration based on three pressure levels is two–staged and has seven exchange units with a triple cooling capacity (Fig. 3.2(b)). All these considerations together yield to a **Two–stage Triple–effect Adsorption Heat Pump.**

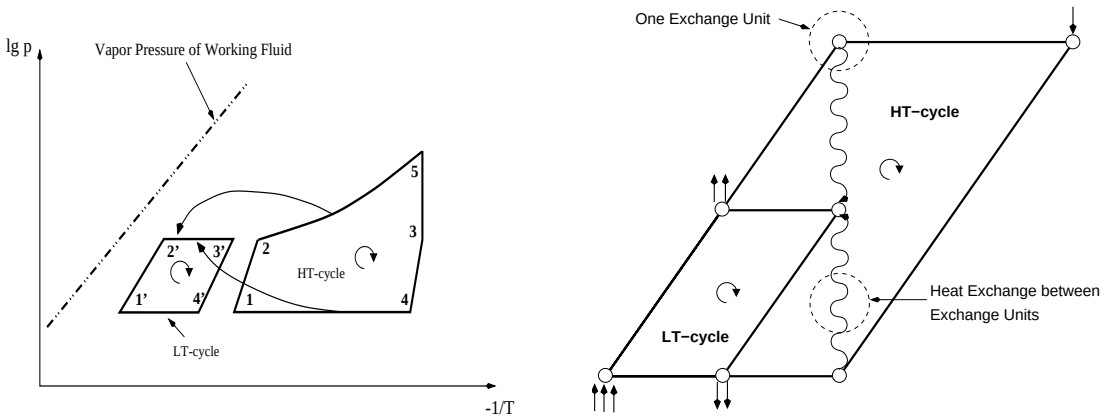

(a) (b)

Figure 3.2: (a) Triple–effect adsorption heat pump with two heat recoveries and (b) as topological graph.

Fig. 3.3 presents a cascade adsorption heat pump similar to the first configuration but with one heat recovery less. Only the HT–adsorber heat is used to drive the LT–adsorber. Since the condensation in the HT– and LT–cycle is out of phase, only one condenser is necessary, and because only one working fluid is taken into account, one evaporator will suffice. Therefore six exchange units achieve a cooling capacity of two, i.e. one unit of heat input produces two units of refrigeration. So the system will be defined as **Single–stage Double–effect Adsorption Heat Pump.**

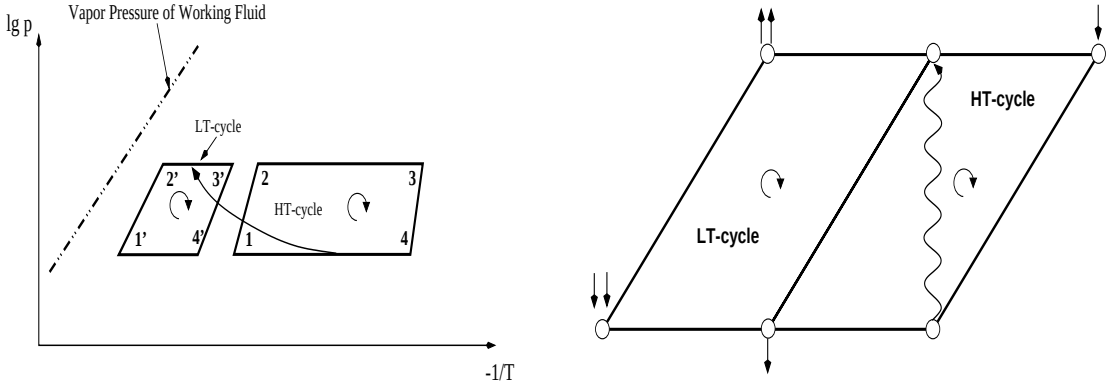

(a) (b)

Figure 3.3: (a) Double–effect adsorption heat pump with one heat recovery and (b) as topological graph.

An easy to realize modification of both cycles is to adapt mass transfer sequences to both configurations in order to enlarge the mass of working fluid pumped in the cycle and thereby the efficiency. For the triple–effect cycle one mass transfer can be introduced (Fig. 3.4), whereas the double–effect configuration allows two mass transfers (Fig. 3.5). As we will see later, the mass transfer while heating the LT–adsorber might be important because it enlarges the working fluid concentration to an area in the isosteric field, where the concentration change is high, i.e. where the isosteres are placed close together.

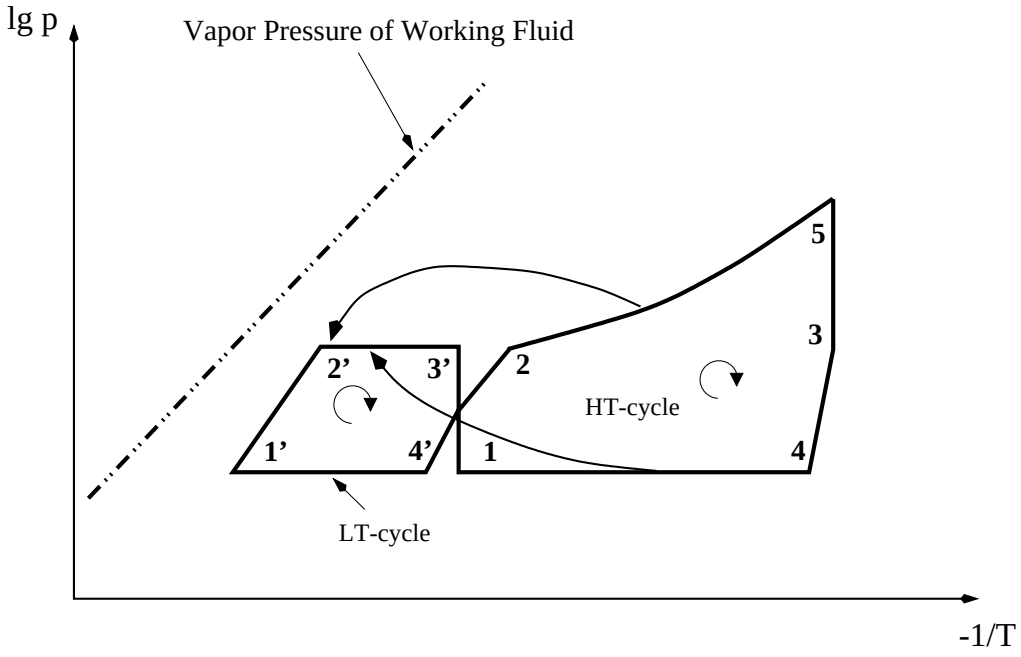

Figure 3.4: Triple–effect adsorption heat pump including one mass transfer.

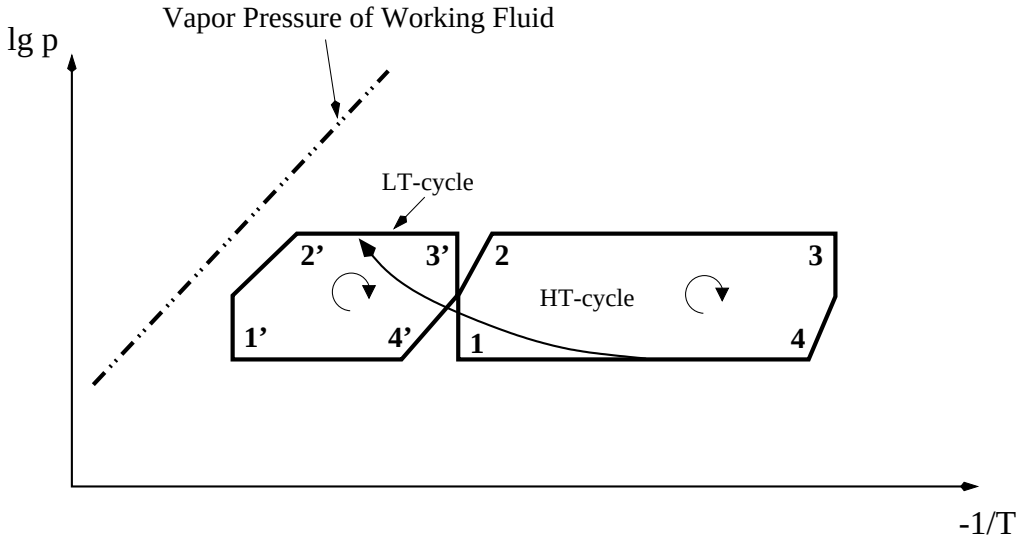

Figure 3.5: Double–effect adsorption heat pump including two mass recoveries.

Part I

Theoretical Investigations of Two Multi–Effect Adsorption Heat Pumps

Chapter 4

Triple–Effect and Double–Effect AHP–Cycles

4.1 Two–Stage Triple–Effect AHP–Cycle

4.1.1 Cycle and its Operation

The adsorption heat pump consists of two separate adsorbers (**AdR**) which are connected by a coolant loop. One adsorber is designed and used in a high–temperature mode *(→ HT–AdR)* and the other in a low–temperature mode *(→ LT–AdR)*. An evaporator supplies both adsorbers with gaseous working fluid. On the opposite side each adsorber is connected to a condenser (**Cond**). In case of using water or an alcohol as working fluid the whole system must be designed vacuum–tight. The adsorptive material filled in the HT–AdR *(HT–adsorbent)* is characterized by strong affinity to the working fluid resulting in high desorption temperatures ($\approx 300°$C). The adsorbent of the LT–AdR *(LT–adsorbent)* is a material of weak affinity with small sorbate concentrations at temperatures between 90° and 140°C. These two adsorptive materials with different affinities enable the regeneration of the weak affinity adsorbent through the heat released from one desorption/adsorption–sequence of the strong affinity adsorbent. The thermodynamic cascading cycle is shown in Fig. 4.1, a Clapeyron–diagram. The two adsorbents proceed through the steady state processes 1–2–5–3–4–1 (HT–cycle) for the HT–adsorbent and 1'–2'–3'–4'–1' (LT–cycle) for the LT–adsorbent. At state 2 of the HT–cycle the HT–condenser coolant circuit will be connected to the heat exchanger of the LT–adsorber which is at temperature $T_{1'}$ and $T_{c'}$, respectively (see 1^{st} Sequence in Fig. 4.2). Thus the condensation in the HT–condenser starts at pressure $p_{c'}$ increasing to p_c until desorption of the HT–adsorbent reaches its maximum temperature T_5 ($= T_3$). For this reason the change from state 2 to 5 of the HT–cycle cannot be isobaric desorption.

Connecting both thermodynamic cycles, the operation mode of this cascading adsorption heat pump can be divided into four sequences. At the beginning of the first sequence we will assume that both adsorbents are in an adsorbed state of equilibrium and the HT–adsorber was already heated isosterically (Fig. 4.1: $1 \rightarrow 2$).

1^{st} Sequence: Desorption in HT–AdR *($2 \rightarrow 5$)*

The adsorbent of strong affinity filled in HT–AdR will be desorbed by heating the adsorber to a maximum temperature T_5 and pressure p_c *(high–temperature level, 2→5)*. The desorbed gaseous working fluid condenses in HT–Cond with increasing pressure from $p_{c'}$ up to p_c. The condensation heat will be transferred by a coolant (e.g. thermal oil) to LT–AdR. The adsorbent in LT–AdR is heated up isosterically *(1'→2')* and when the temperature T_c is higher than $T_{2'}$ isobaric desorption starts, too *(2'→3')*. The desorbed working fluid from the LT–adsorbent condenses in the LT–Cond at pressure $p_{c'}$. The condensation heat $E_{c'}$ *(intermediate–temperature level)* is now available for

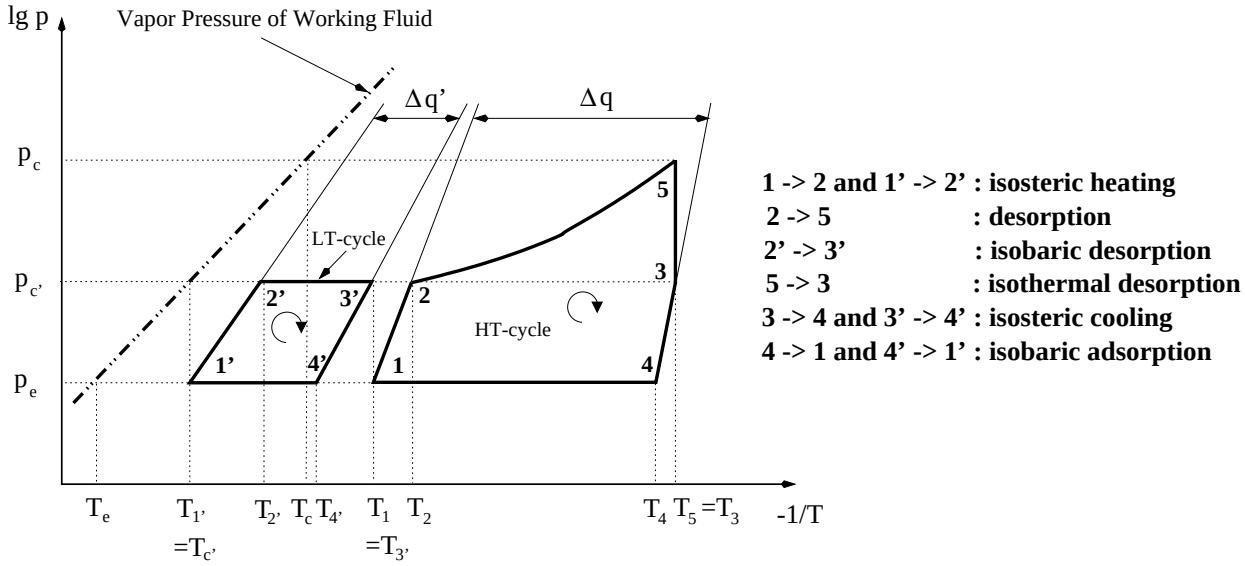

Figure 4.1: Thermodynamic cycles of the triple–effect AHP plotted in a Clapeyron–diagram. 1–2–5–3–4–1 for HT–adsorbent *(HT–cycle)* and 1'–2'–3'–4'–1' for LT–adsorbent *(LT–cycle)*.

further use at the heat sink. The evaporator is inactive.

2nd Sequence: Isothermal Desorption in HT–AdR *(5 → 3)*

After reaching the maximum desorption temperature T_5, the HT–adsorbent will be desorbed isothermally, while the HT–Cond is connected to the heat sink for heat output $E_c^{5\rightarrow 3}$. This will cause the decrease of the pressure in the HT–Cond from p_c back to $p_{c'}$. For this sequence, the evaporator, LT–Cond and LT–AdR are inactive.

3rd Sequence: Adsorption in HT–AdR *(3 → 1)*

In order to cool the HT–AdR down till the evaporation pressure p_e is reached, it will be thermally connected to the LT–AdR *(3→4)*. Afterwards evaporated working fluid *(low–temperature level, heat extraction)* will be adsorbed isobarically by the HT–adsorbent *(4→1)*. The released heat of adsorption is transferred through a coolant loop to the LT–AdR. Thereby the desorption of LT–adsorbent continues and finishes at $T_{3'}$ *(2'→3')*. The desorbed gaseous working fluid is liquefied in the LT–Cond at $p_{c'}$ by releasing heat $E_{c'}$ which will be available at the heat sink. The HT–Cond is inactive.

4th Sequence: Adsorption in LT–AdR *(3' → 1')* and Heating of HT–AdR *(1 → 2)*

The LT–AdR is cooled down till evaporation pressure p_e is reached, by connecting it to the heat sink *(3'→4')*. Afterwards gaseous working fluid evaporated at p_e by environmental heat transfer to the evaporator will be adsorbed by the LT–adsorbent *(4'→1')*. The released heat of adsorption $E_{a'}$ flows to the heat sink. Simultaneously HT–AdR is heated isosterically by an external heater from pressure p_e up to $p_{c'}$ *(1→2)*. During this cycle the HT–Cond and the LT–Cond are out of service.

The connections of both cycles during the four sequences are summarized in the following table:

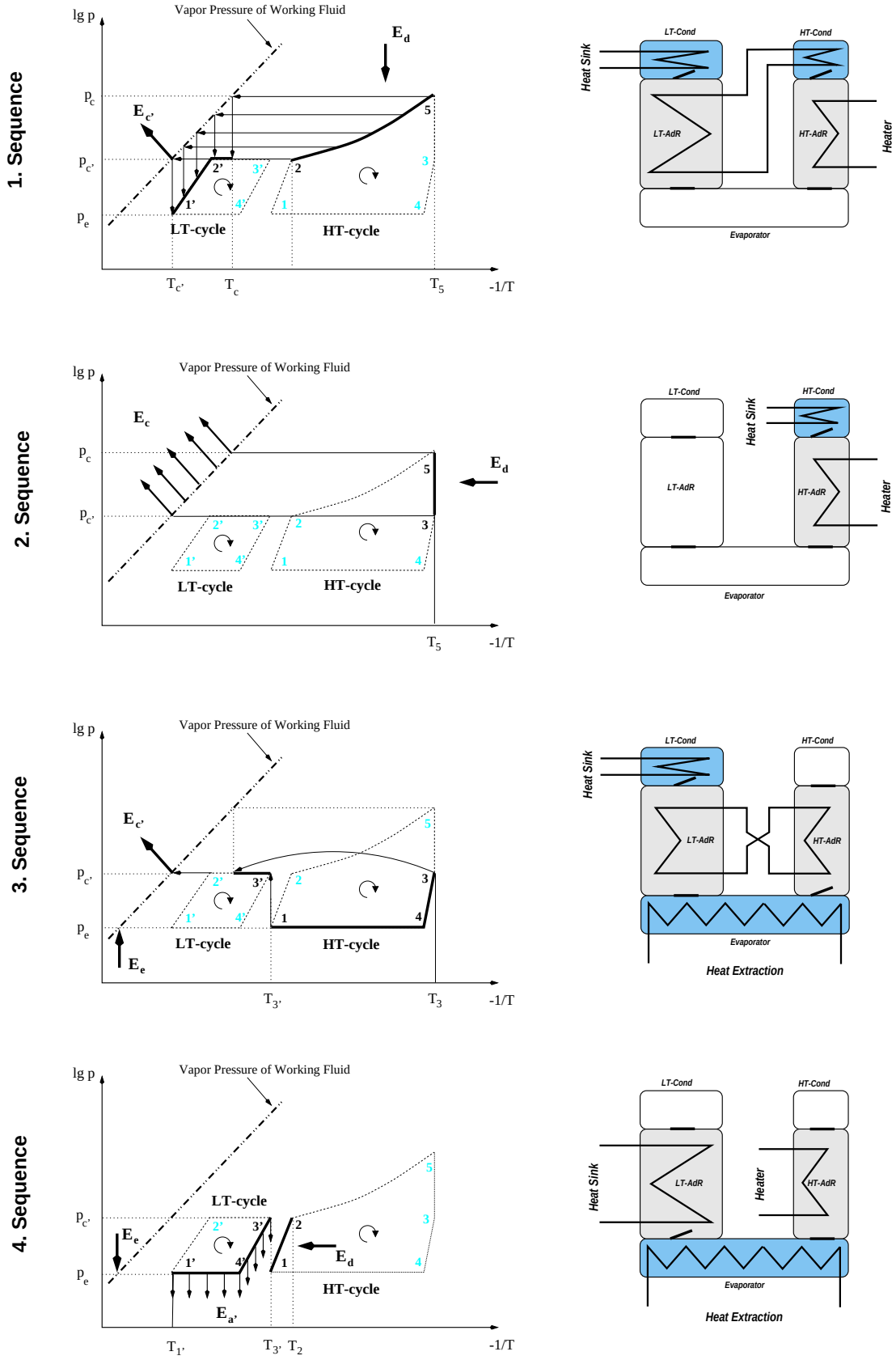

Figure 4.2: The four sequences of the two–stage triple–effect adsorption heat pump.

Sequence	Phase	**Thermal Connection**	**Flow of Working Fluid**
1	desorbing	heater → HT–AdR	HT–AdR → HT–Cond
	heat recovery	HT–Cond → LT–AdR	LT–AdR → LT–Cond
2	desorbing	heater → HT–AdR	HT–AdR → HT–Cond
3	adsorbing		evaporator → HT–AdR
	heat recovery	HT–AdR → LT–AdR	
4	adsorbing		evaporator → LT–AdR
	heating	boiler → HT–AdR	

As summary we could emphasize that the presented triple–effect AHP is essentially characterized by the special connection of two adsorbers associated with the use of two matched adsorptive materials. Both, the heat released while condensing the gaseous working fluid desorbed from the HT–adsorbent, as well the adsorption enthalpy from the HT–adsorbent have a sufficiently high–temperature level to achieve the regeneration of the LT–adsorbent.

4.1.2 Triple–Effect Cycle Performance

Computer simulations are performed. They consider a steady–state adsorption heat pump process *(assuming uniform temperatures, pressures and concentrations)* taking into account the sensible heat of the liquid and adsorbed working fluid and of the adsorbents, the latent heat of adsorption ΔH and furthermore the sensible heat of a copper heat exchanger assuming a mass fraction of two units exchanger mass per unit mass adsorbent. But no heat transfer coefficients are included. The thermodynamic cycles are assumed as ideal *(isobaric, isosteric and adiabatic processes)*.

The mathematical equations in a more comprehensive form are given in the appendix A.1. The mass fraction of both adsorbents $^{\mathrm{m'}}/_{\mathrm{m}}$ is expressed through the energy conservation of both interacting cycles that the adsorption plus the condensation heat of the HT–cycle must be equal to the necessary desorption heat of the LT–cycle.

$$m\,|e_a + e_c| = m'\,e_{d'} \quad \Rightarrow \quad \frac{m'}{m} = \frac{|e_a + e_c|}{e_{d'}} \tag{4.1}$$

With the mass fraction the COP of the whole triple–effect cycle is

$$\mathrm{COP} = \frac{|e_e + \dfrac{m'}{m}\,e_{e'}|}{e_z} \tag{4.2}$$

We are able to express the COP independently from the mass fraction, only in terms of the COP of the LT–cycle and of the HT–cycle. After replacing the mass fraction in Eq. 4.2 by Eq. 4.1 and some further transformations (see appendix A.1 assuming that $e_a \approx e_z$ and $e_c \approx e_e$ we receive for the COP the expression

$$\begin{aligned} \mathrm{COP} &= \underbrace{\frac{|e_e|}{e_z}}_{\mathrm{COP}_{HT}} + \underbrace{\frac{|e_{e'}|}{e_{d'}}}_{\mathrm{COP}_{LT}} \left(1 + \underbrace{\frac{|e_e|}{e_z}}_{\mathrm{COP}_{HT}}\right) \\ &= \mathrm{COP}_{HT} + \mathrm{COP}_{LT}\,(1 + \mathrm{COP}_{HT}) \end{aligned} \tag{4.3}$$

Both cycles as pictured in Fig. 4.1 and the fraction of the adsorbent masses are completely determined by the six initial values

❶ maximum condensation temperature $T_c \succ p_c$ (*intermediate*–temperature of HT–cycle)

❷ maximum desorption (regeneration) temperature $T_{3'}$ (*high*–temperature of LT–cycle)

❸ temperature T_1 (HT–cycle)

❹ temperature of the heat extraction $T_e \succ p_e$ (*low*–temperature of HT– and LT–cycle)

❺ temperature of the heat sink $T_{c'} \succ p_{c'}$ (*intermediate*–temperature of LT–cycle)

❻ maximum desorption temperature $T_5 = T_3$ (*high*–temperature of HT–cycle)

and one constraint equation

$$e_c(T_c) = \frac{m'}{m} e_{d'}(T_c) \tag{4.4}$$

expressing the energy equilibrium at temperature T_c for the condensation heat of the HT–cycle and the heat released from desorption of LT–adsorbent until T_c was reached, multiplied by the mass fraction. The isosteric fields necessary for the calculations have been obtained experimentally by a thermogravimetrical measuring device and analyzed by the *Theory of Dubinin* (see appendix B.1).

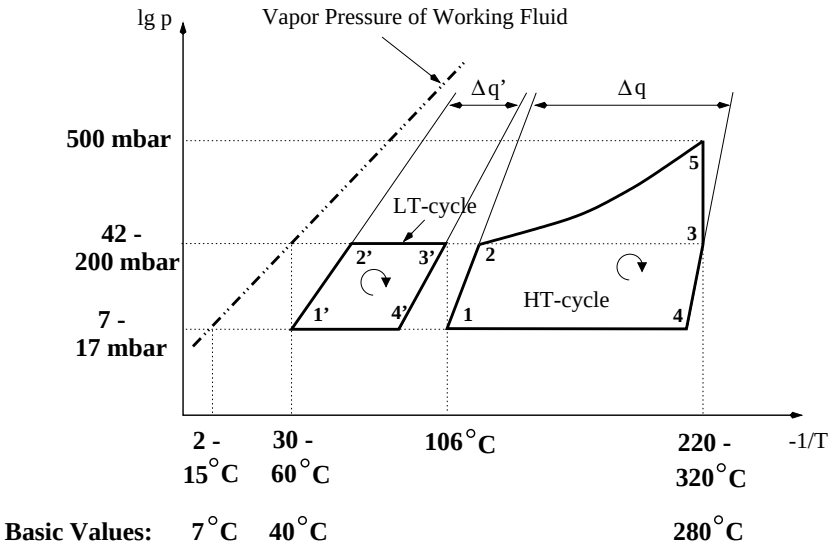

Figure 4.3: Initial values of the computer simulations.

The numerical simulations are performed with the four material combinations Silica Gel 125/Zeolite 13X, Silica Gel N/Zeolite 13X, Silica Gel NAC/Zeolite 13X and Zeolite 13X/Zeolite 13X, and water as working fluid. The calculations shall provide the influence of the three temperatures

① heat extraction (evaporation) temperature T_e (→ Fig. 4.4),

② heat sink temperature $T_{c'}$ (→ Fig. 4.5) and

③ maximum desorption (regeneration) temperature T_5 (→ Fig. 4.6)

on the COP of the triple–effect cycle. The numerical values of these three temperature levels and their remaining three initial conditions p_c, T_1 and $T_{3'}$ are specified in Fig. 4.3. The specific heat capacities of the materials are assumed as temperature independent:

$$\text{specific heat of silica gel} = 1.0\ {}^{\text{kJ}}/_{\text{kg K}}$$
$$\text{specific heat of zeolite} = 0.92\ {}^{\text{kJ}}/_{\text{kg K}}$$
$$\text{specific heat of the adsorbate} = 2.5\ {}^{\text{kJ}}/_{\text{kg K}}$$
$$\text{specific heat of copper heat exchanger} = 0.383\ {}^{\text{kJ}}/_{\text{kg K}}$$

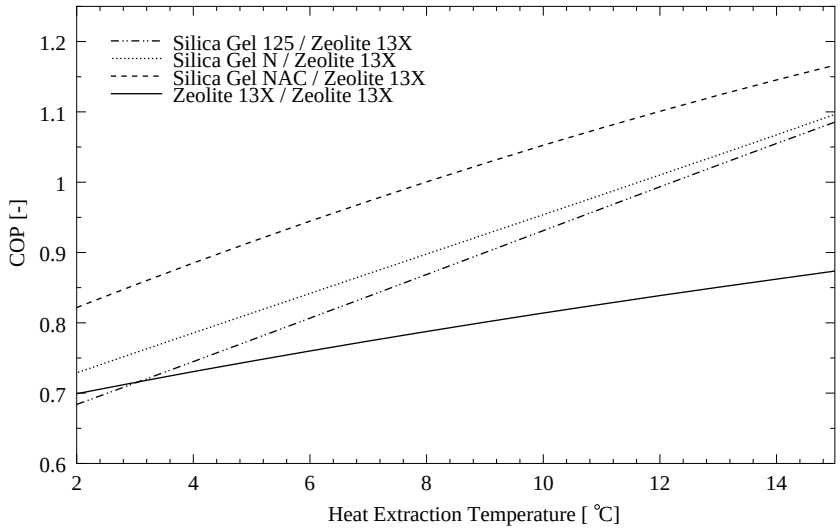

Figure 4.4: COP as function of the heat extraction (evaporation) temperature ($T_{1'} = 40°\text{C}$, $T_3 = 280°\text{C}$, $p_c = 500$ mbar, $T_1 = T_{3'} = 106°\text{C}$).

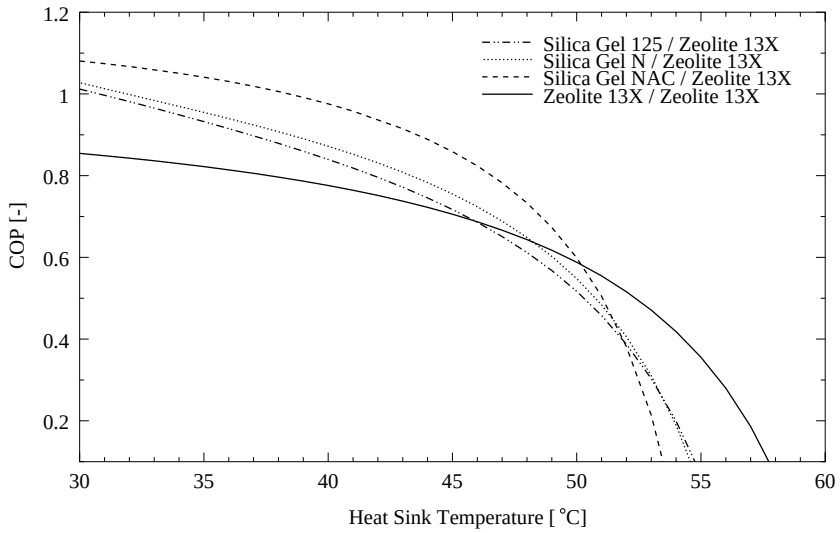

Figure 4.5: COP as function of the heat sink temperature ($T_e = 7°\text{C}$, $T_3 = 280°\text{C}$, $p_c = 500$ mbar, $T_1 = T_{3'} = 106°\text{C}$).

Comparing Figs. 4.4, 4.5 and 4.6 we can state that the strongest influence on the COP is caused by the heat sink temperature $T_{c'}$ (for three heat sink temperatures 30°, 40° and 50°C the COPs are tabulated in Table 4.1), and the weakest by the regeneration temperature of the HT–adsorbent T_5.

Following the curve shapes in Fig. 4.5 from low heat sink temperatures to higher values, we observe that till 46°C the COPs of the silica gel/Zeolite 13X–combinations are better than the

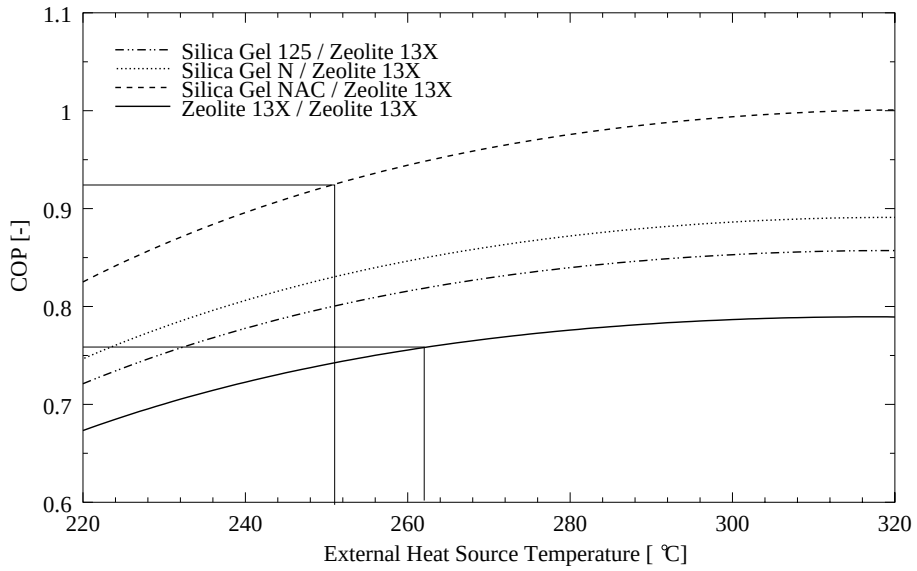

Figure 4.6: COP as function of the maximum desorption temperature ($T_e = 7°C$, $T_{1'} = 40°C$, $p_c = 500$ mbar, $T_1 = T_{3'} = 106°C$).

$T_e = 7°C$ ($p_e = 10$ mbar) / $T_3 = 280°C$ / $T_1 = T_{3'} = 106°C$ / $p_c = 500$ mbar									
	$T_{1'} = 30°C$ $p_{c'} = 43$ mbar $\Delta q = 115\,g/kg$			$T_{1'} = 40°C$ $p_{c'} = 74$ mbar $\Delta q = 111\,g/kg$			$T_{1'} = 50°C$ $p_{c'} = 124$ mbar $\Delta q = 107\,g/kg$		
LT–/HT–adsorbent	$\mathbf{\Delta q'}$	**COP**	$\mathbf{m'/m}$	$\mathbf{\Delta q'}$	**COP**	$\mathbf{m'/m}$	$\mathbf{\Delta q'}$	**COP**	$\mathbf{m'/m}$
Silica NAC/Zeo 13X	138	1.08	1.7	66	0.98	2.9	11	0.60	6.5
Silica 125/Zeo 13X	95	1.01	2.2	38	0.84	3.9	7	0.52	7.2
Silica N/Zeo 13X	106	1.03	2.0	45	0.87	3.6	8	0.55	6.7
Silica AF 25/Zeo 13X	95	1.01	2.2	39	0.84	3.8	7	0.52	7.1
Zeo 13X/Zeo 13X	69	0.85	2.3	39	0.78	3.2	13	0.59	5.2
Zeo Y/Zeo 13X	68	0.87	2.3	39	0.78	3.2	12	0.58	5.2
Zeo A/Zeo 13X	38	0.70	2.7	21	0.62	3.6	8	0.49	5.2

Table 4.1: Attainable COPs and their mass fractions of different adsorptive material combinations for three heat sink temperatures.

Zeolite 13X/Zeolite 13X–combination, but for higher temperatures the COP of the pure Zeolite 13X AHP will become better. The fact that the investigated silica gels have scarcely an advantage compared to zeolite is caused by the slight concentration changes $\Delta q'$ in the area where the LT–cycle is placed in the isosteric field; in this area the isosteres are widely spaced (see Fig. 4.7).

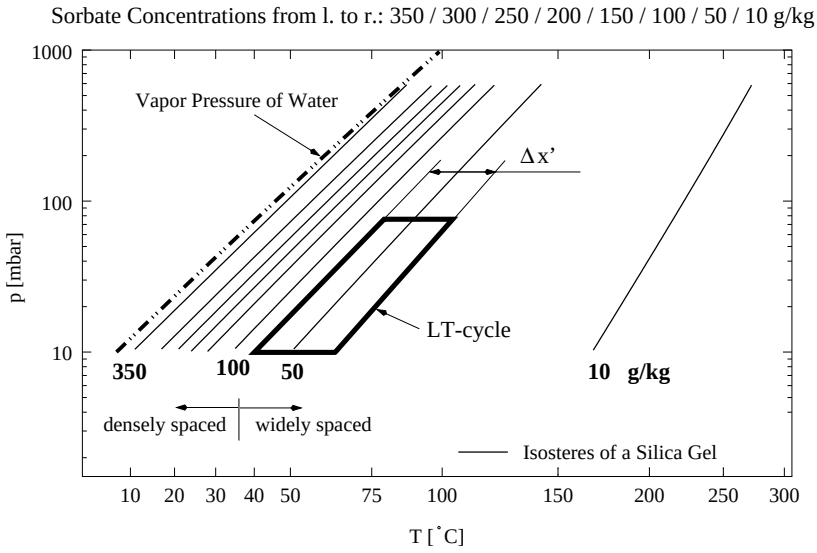

Figure 4.7: The LT–cycle plotted in an isosteric field of a silica gel which stands in for all other regarded silica gels.

Hence, zeolites in both adsorbers could be an acceptable choice for high heat sink temperatures. Some other zeolite–combinations should be investigated with the aim to improve the COP and getting closer to the silica gel/zeolite–curves for lower temperatures. In appendix B.2 two further zeolites are mentioned, a Zeolite A with 5Å pore diameter and a Na–Zeolite Y with the same pore diameter of 9Å as Zeolite 13X. The results are shown in Fig. 4.8 and listed in Table 4.1. With the regarded zeolite–combinations no pronounced improvement of the COP compared to Zeolite 13X/Zeolite 13X has been established. However in Fig. 4.8 the same effect as in Fig. 4.5 occurs: the lower the COP at 30°C, the flater the curve shape, i.e. the curves intersect at higher heat sink temperatures and the relatively lower COP at low sink temperature will become relatively higher at high heat sink temperature.

Till now we have only regarded the influence of the three temperature levels on the COP, but there are three other parameters p_c, T_1 and $T_{3'}$ which can be varied. Setting T_1 equal $T_{3'}$ will give the best COP, verified by numereous computer simulations. This reduces the changeable parameters to two which, however, cannot be varied independently from each other. Primarily it is the pressure p_c which shall be adapted to all other parameters because of the constraint Eq. 4.4. But it should be pointed out that increasing p_c from a lower limit due to fulfill Eq. 4.4 will not have any significant change on the COP nor on the mass fraction. A change of the temperature T_1 ($= T_{3'}$), 106°C ± 10 Kelvin, has a recognizable effect on the COP of the Silica Gel 125/Zeolite 13X–combination (see Fig. 4.11), and the Zeolite 13X/Zeolite 13X–combination (see Fig. 4.12), and even more on the mass fraction.

The effect of T_1 on the mass fraction is shown in two histograms of Fig. 4.9; the lower T_1, the higher the slope of the mass fraction rises with increasing heat sink temperature. For Zeolite 13X/Zeolite 13X this effect is a little bit weaker.

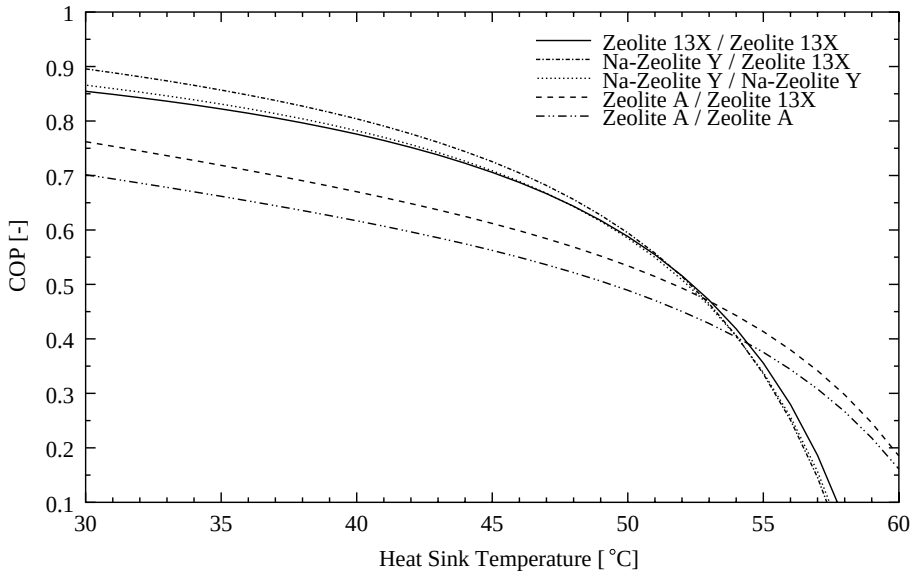

Figure 4.8: COP as function of the heat sink temperature for some zeolite–combinations ($T_e = 7°C$, $T_3 = 280°C$, $p_c = 500$ mbar, $T_1 = T_{3'} = 106°C$).

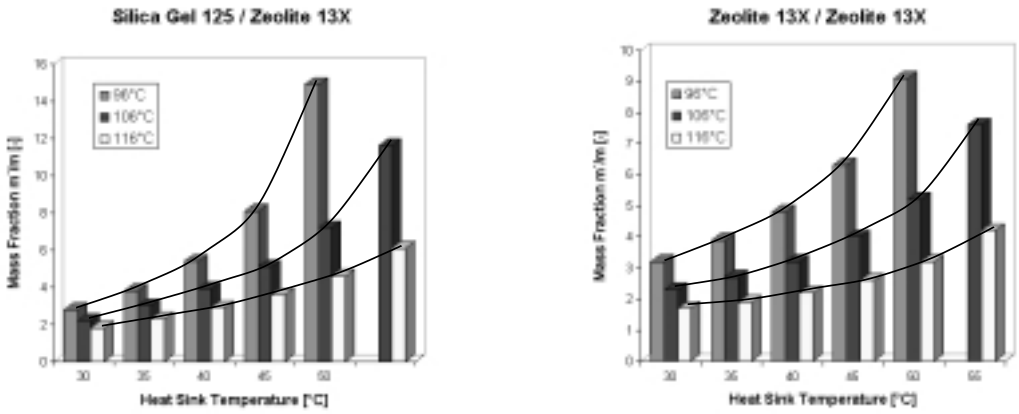

(a) (b)

Figure 4.9: (a) Mass fraction $^{m'}/_{m}$ for the material combinations Silica Gel 125/Zeolite 13X and (b) Zeolite 13X/Zeolite 13X as function of the heat sink temperature $T_{1'}$ for different T_1.

The curve shapes for Silica Gel 125/Zeolite 13X in Fig. 4.11 are almost identical with those for Zeolite 13X/Zeolite 13X in Fig. 4.12. For low heat sink temperatures, the 96°C–curve is highest, but with increasing heat sink temperature this curve drops below the other two. The reason is, that for a medium heat sink temperature the concentration change $\Delta q'$, and therefore the mass of working fluid pumped in the LT–cycle is lower than $\Delta q'$ for a higher T_1. This is illustrated in Fig. 4.10. Increasing T_1 means for a given heat sink temperature that the *rich* isostere stays in its position while the *poor* isostere moves to the right.

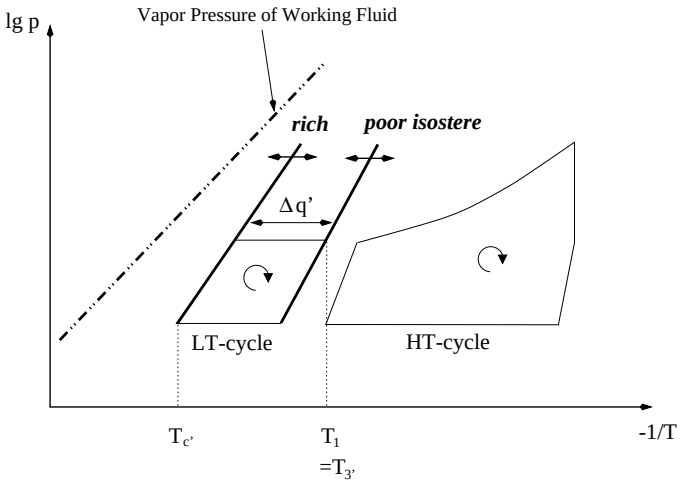

Figure 4.10: Illustrating of influence of T_1 on COP.

$$\Rightarrow \quad \Delta q'|_{116^\circ\,\mathrm{C}} > \Delta q'|_{106^\circ\,\mathrm{C}} > \Delta q'|_{96^\circ\,\mathrm{C}}$$

Further we can notice in Fig. 4.11 and 4.12 that with higher T_1 (106° and 116°C) the COP could not be improved for low heat sink temperatures.

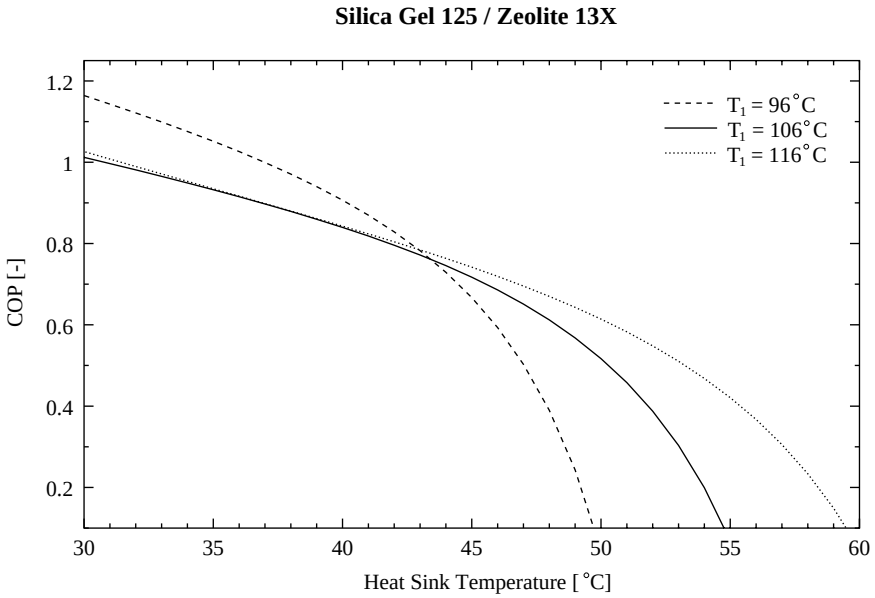

Figure 4.11: COP as function of the heat sink temperature for the Silica Gel 125/Zeolite 13X–combination at three different temperatures $T_1 = T_{3'}$ ($T_e = 7$°C, $T_3 = 280$°C, $p_c = 500$ mbar).

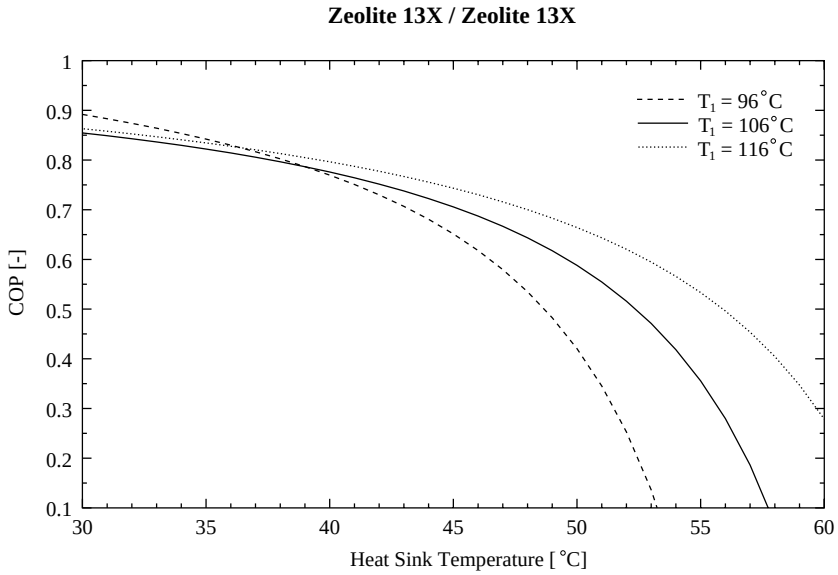

Figure 4.12: COP as function of the heat sink temperature for the Zeolite 13X/Zeolite 13X–combination at three different temperatures T_1 ($= T_{3'}$) ($T_e = 7°C$, $T_3 = 280°C$, $p_c = 500$ mbar).

4.2 Single–Stage Double–Effect AHP–Cycle

4.2.1 Cycle and its Operation

The main difference to the triple–effect AHP is, that this heat pump operates on only two instead of three pressure levels. This causes that only the adsorber heat of the HT–cycle is used as driving heat for the LT–cycle. Consequently the HT–adsorbent will proceed through the steady state processes 1–2–3–4–1, as illustrated in Fig. 4.13.

In this case one whole operation cycle runs through two sequences. At the beginning of the first sequence we assume as well that both adsorbents are in an adsorbed state of equilibrium.

1st Sequence: Desorption in HT–AdR *(1 → 3)* and Adsorption in LT–AdR *(3' → 1')*

The adsorbent of strong affinity filled in the HT–AdR will be heated and afterwards desorbed by heating the adsorber to a maximum temperature T_3 *(high–temperature level, 2→3)*. The desorbed gaseous working fluid is condensed. The condensation heat will be transferred by a coolant (e.g. thermal oil) to the heat sink. At the same time, the LT–adsorber is cooled down till evaporation pressure p_e is reached, by connecting it to the heat sink *(3'→4')*. Afterwards gaseous working fluid evaporated at p_e by environmental heat transfer to the evaporator will be adsorbed by the LT–adsorbent *(4'→1')*. The released heat of adsorption flows to the heat sink.

2nd Sequence: Adsorption in HT–AdR *(3 → 1)*

In order to cool the HT–AdR down till the evaporation pressure p_e is reached, it will be thermally connected to the LT–AdR *(3→4)*. Then evaporated working fluid *(low–temperature level, heat extraction)* will be adsorbed isobarically by HT–adsorbent *(4→1)*. The released heat of adsorption is transferred through a coolant loop to the LT–AdR for heating *(2'→3')* and desorbing LT–adsorbent completely till $T_{3'}$ is reached *(2'→3')*. The desorbed gaseous working fluid is liquefied in the condenser, releasing heat $E_{c'}$ which will be available at the heat sink.

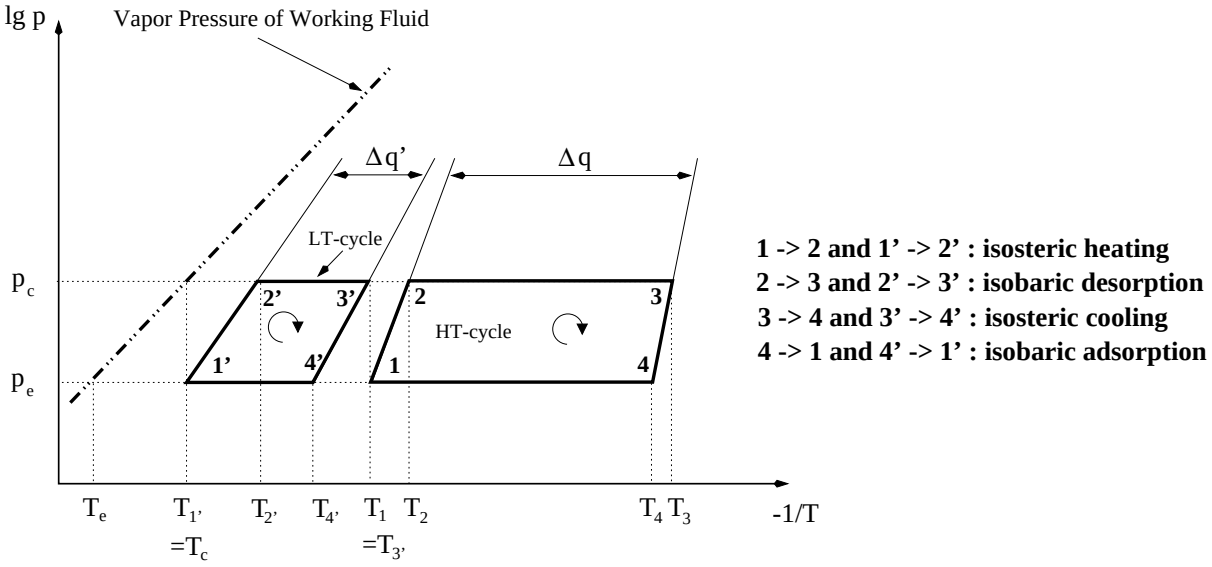

Figure 4.13: Thermodynamic cycles of the double–effect AHP plotted in a Clapeyron–diagram. 1–2–3–4–1 for HT–adsorbent *(HT–cycle)* and 1'–2'–3'–4'–1' for LT–adsorbent *(LT–cycle)*.

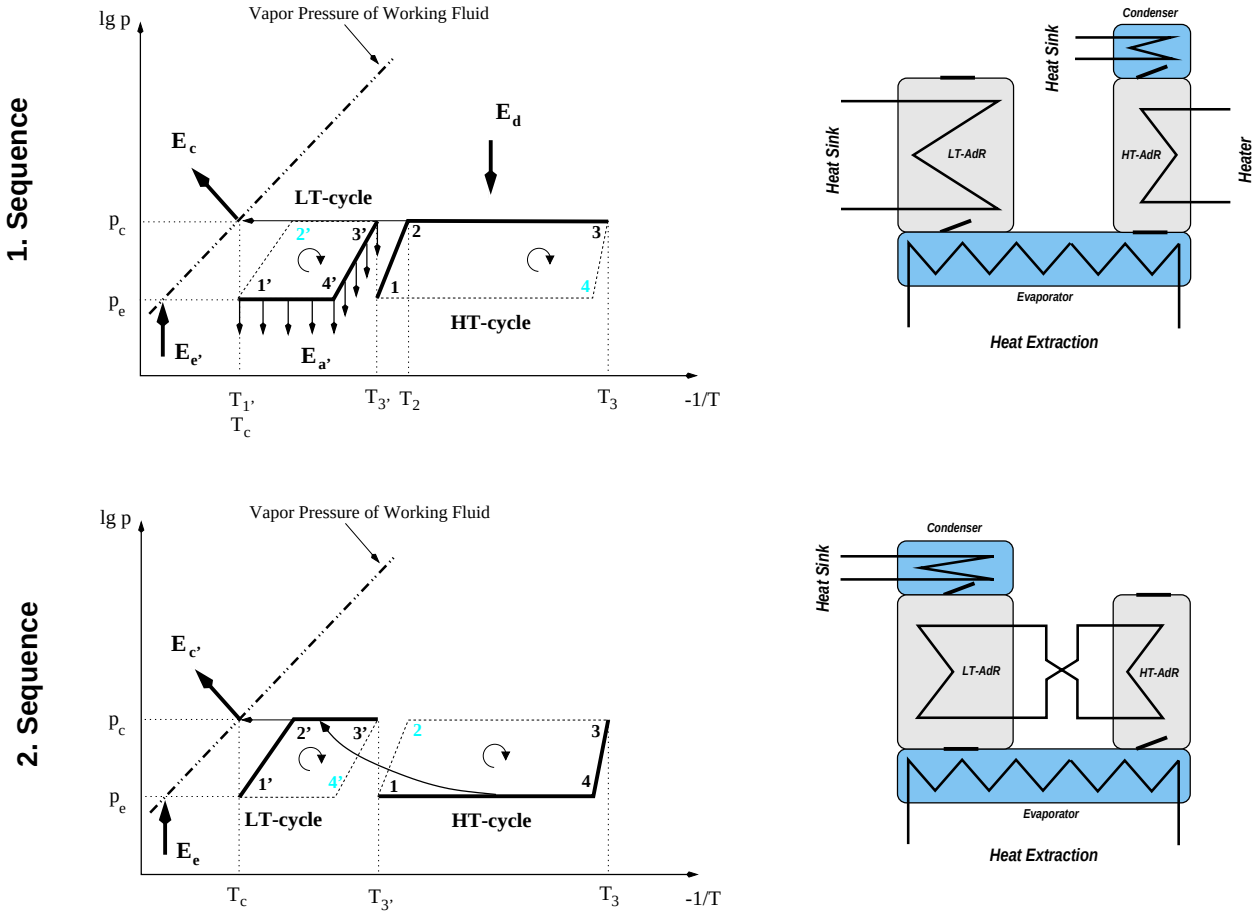

Figure 4.14: The two sequences of the single–stage double–effect adsorption heat pump.

The connections of both cycles during the two sequences are summarized in the following table:

Sequence	Phase	**Thermal Connection**	**Flow of Working Fluid**
1	desorbing	heater → HT–AdR	HT–AdR → condenser
	adsorbing		evaporator → LT–AdR
2	adsorbing		evaporator → HT–AdR
	desorbing	HT–AdR → LT–AdR	LT–AdR → condenser

As summary we could emphasize that the presented double–effect cycle is essentially characterized by one heat recovery which enables the condensation heat released from the HT–adsorbent to regenerate the LT–adsorbent.

4.2.2 Double–Effect Cycle Performance

In order to get a knowledge about the COP of this double–effect AHP the same approximated numerical computer simulations have been employed as already described in § 4.1.2. The complete equations are given in appendix A.2.

The mass fraction of both adsorbents $^{m'}/_{m}$ simplifies to the expression

$$m\,|e_a| = m'\,e_{d'} \quad \Rightarrow \quad \frac{m'}{m} = \frac{|e_a|}{e_{d'}} \tag{4.5}$$

meaning that adsorption heat released by the HT–adsorbent must be equal to the heat necessary for desorbing the LT–adsorbent.

In case of the double–effect cycle, the COP can be subdivided into a COP of the LT–cycle (COP_{LT}) and one of the HT–cycle (COP_{HT}), each independent from the mass fraction.

$$\mathrm{COP} = \frac{|e_e + \dfrac{m'}{m}\,e_{e'}|}{e_z} \tag{4.6}$$

With Eq. 4.5 we receive

$$\mathrm{COP} = \frac{|e_e + \dfrac{e_a}{e_{d'}}\,e_{e'}|}{e_z} \tag{4.7}$$

and assuming that $e_a \approx e_z$ the COP will become

$$\mathrm{COP} = \underbrace{\frac{|e_{e'}|}{e_{d'}}}_{COP_{LT}} + \underbrace{\frac{|e_e|}{e_z}}_{COP_{HT}} \tag{4.8}$$

In contrast to the triple–effect AHP, the double–effect AHP and its mass fraction is determined through five degrees of freedom because the sixth, the maximum pressure level of the HT–cycle is omitted. The heat pump is just operating at two pressure levels. The following five initial conditions remain:

❶ maximum desorption temperature $T_{3'}$ (*high*–temperature of LT–cycle)

❷ temperature T_1 (HT–cycle)

❸ temperature of the heat extraction $T_e \succ p_e$ (*low*–temperature of HT– and LT–cycle)

❹ temperature of the heat sink $T_c \succ p_c$ (*intermediate*–temperature of LT– and HT–cycle)

❺ maximum desorption temperature T_3 (*high*–temperature of HT–cycle)

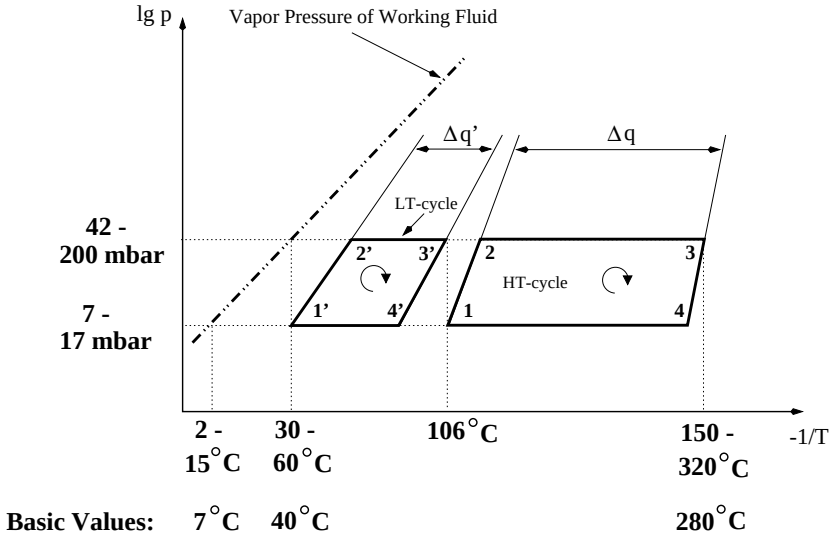

Figure 4.15: Initial values of the computer simulations.

The computer simulations are carried out for the same four material combinations as used in section 4.1.2 to simulate the triple–effect cycle (see section 4.1.2). The COPs are as well determined in dependence of the evaporation temperature T_e (→ Fig. 4.16), the heat sink temperature T_c (→ Fig. 4.17) and the maximum desorption temperature of the HT–cycle T_3 (→ Fig. 4.18). All the initial conditions are taken from section 4.1.2.

The double–effect cycle is as well strongly influenced by the heat sink temperature and less by the maximum desorption temperature. The only difference to the triple–effect cycle are the COPs which are lower by maximum 0.1 (compare Table 4.1 with Table 4.2).

The (COP vs. T_3)–curves have a rather flat maximum around 210°C to 230°C. For further increasing T_3, the COP will very slightly decrease. The reason for this behaviour is that the sensible heat becomes a little bit more significant than the latent heat of vaporization. This maximum COP is located for all investigated material combinations in the range of about 220°C ± 5 K. To receive the same COPs with the triple–effect cycle, a much higher temperature of about 250°C till 262°C is necessary (compare the emphasized regions in Fig. 4.18 with Fig. 4.6). That the desorption temperature can be reduced to values of about 200°C is a real advantage of the double–effect cycle when converting the theoretical cycle in a practical design, discussed more closely in chapter 5.

The double–effect cycle has two more variables left, T_1 and $T_{3'}$. Both are set equal for optimizing the COP as it was done for the triple–effect cycle. The results as shown in Fig. 4.19, 4.20 and 4.21 are similar to those of the triple–effect cycle and are subject to the same explanations. The only essential difference are the lower COPs and mass fractions as a function of the heat sink temperature.

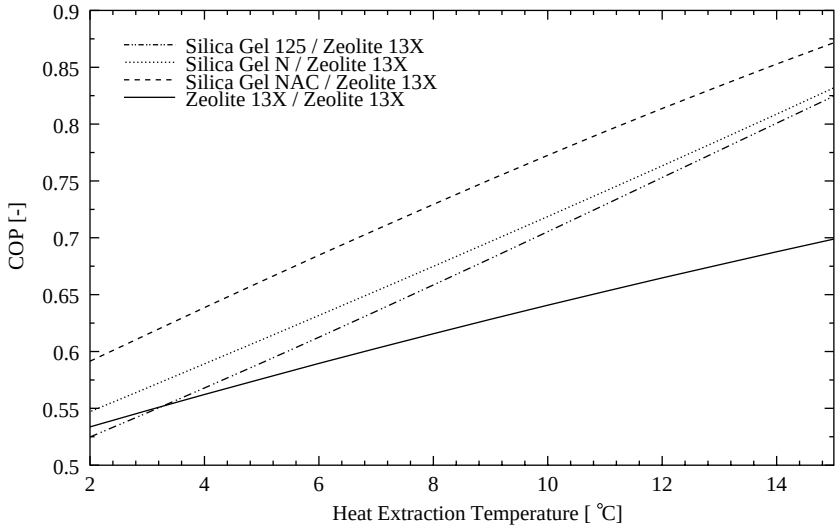

Figure 4.16: COP as function of the heat extraction temperature ($T_{1'} = 40°\mathrm{C}$, $T_3 = 280°\mathrm{C}$, $T_1 = T_{3'} = 106°\mathrm{C}$).

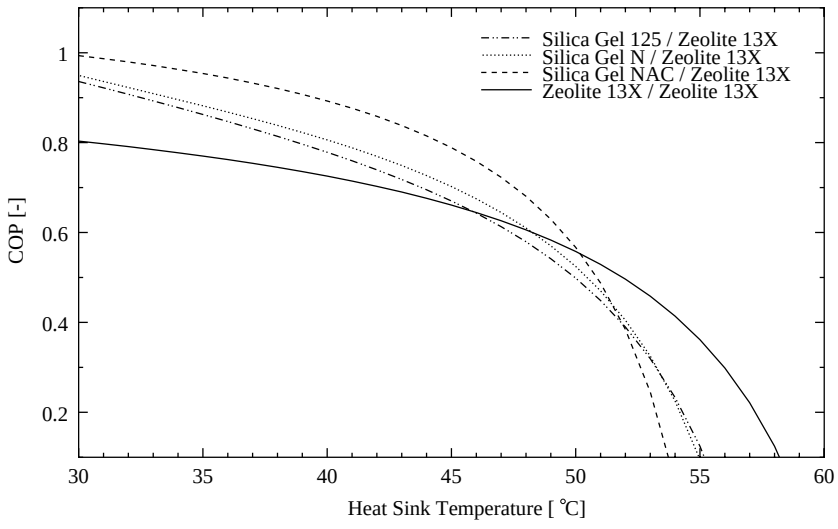

Figure 4.17: COP as function of the heat sink temperature ($T_e = 7°\mathrm{C}$, $T_3 = 280°\mathrm{C}$, $T_1 = T_{3'} = 106°\mathrm{C}$).

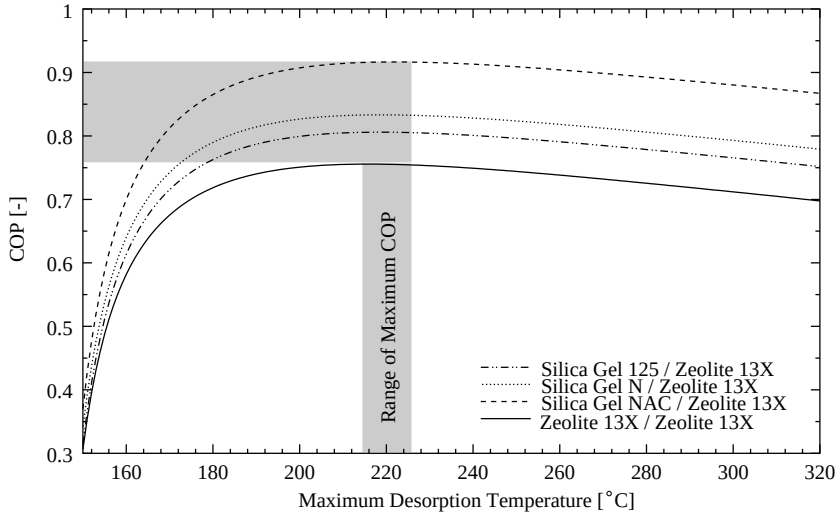

Figure 4.18: COP as function of the maximum desorption temperature ($T_e = 7°\text{C}$, $T_{1'} = 40°\text{C}$, $T_1 = T_{3'} = 106°\text{C}$).

$T_e = 7°\text{C}$ ($p_e = 10$ mbar) / $T_3 = 280°\text{C}$ / $T_1 = T_{3'} = 106°\text{C}$									
	$T_{1'} = 30°\text{C}$ $p_{c'} = 43$ mbar $\Delta q = 115\,{}^{\text{g}}/_{\text{kg}}$			$T_{1'} = 40°\text{C}$ $p_{c'} = 74$ mbar $\Delta q = 111\,{}^{\text{g}}/_{\text{kg}}$			$T_{1'} = 50°\text{C}$ $p_{c'} = 124$ mbar $\Delta q = 107\,{}^{\text{g}}/_{\text{kg}}$		
LT–/HT–adsorbent	$\mathbf{\Delta q'}$	**COP**	$\mathbf{{}^{m'}/_{m}}$	$\mathbf{\Delta q'}$	**COP**	$\mathbf{{}^{m'}/_{m}}$	$\mathbf{\Delta q'}$	**COP**	$\mathbf{{}^{m'}/_{m}}$
Silica NAC/Zeo 13X	138	0.99	1.4	66	0.89	2.3	11	0.57	5.3
Silica 125/Zeo 13X	95	0.93	1.8	38	0.78	3.1	7	0.50	5.8
Silica N/Zeo 13X	106	0.95	1.7	45	0.81	2.9	8	0.53	5.5
Silica AF 25/Zeo 13X	95	1.01	1.9	39	0.83	3.2	7	0.52	5.9
Zeo 13X/Zeo 13X	69	0.80	1.9	39	0.73	2.7	13	0.56	4.3
Zeo Y/Zeo 13X	68	0.81	2.0	39	0.73	2.7	12	0.55	4.4
Zeo A/Zeo 13X	38	0.67	2.63	21	0.59	3.1	8	0.47	4.3

Table 4.2: Attainable COPs and their mass fractions of different adsorptive material combinations for three heat sink temperatures.

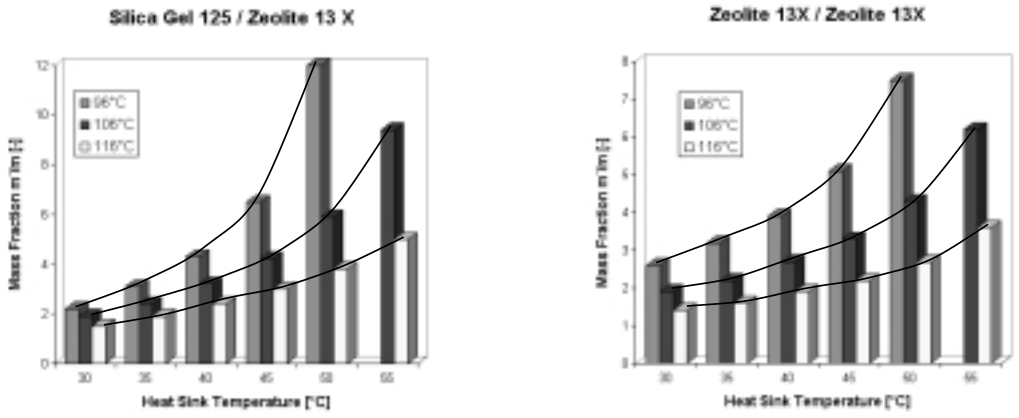

(a) (b)

Figure 4.19: (a) Mass fraction $^{m'}/_{m}$ for the material combinations Silica Gel 125/Zeolite 13X and (b) for Zeolite 13X/Zeolite 13X as function of the heat sink temperature $T_{1'}$ for different T_1.

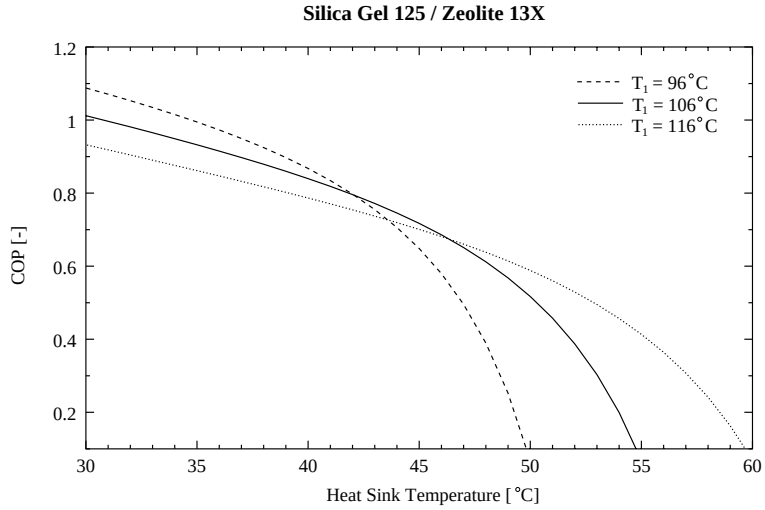

Figure 4.20: COP as function of the heat sink temperature for the Silica Gel 125/Zeolite 13X–combination at three different temperatures $T_1 = T_{3'}$ ($T_e = 7°C$, $T_3 = 280°C$).

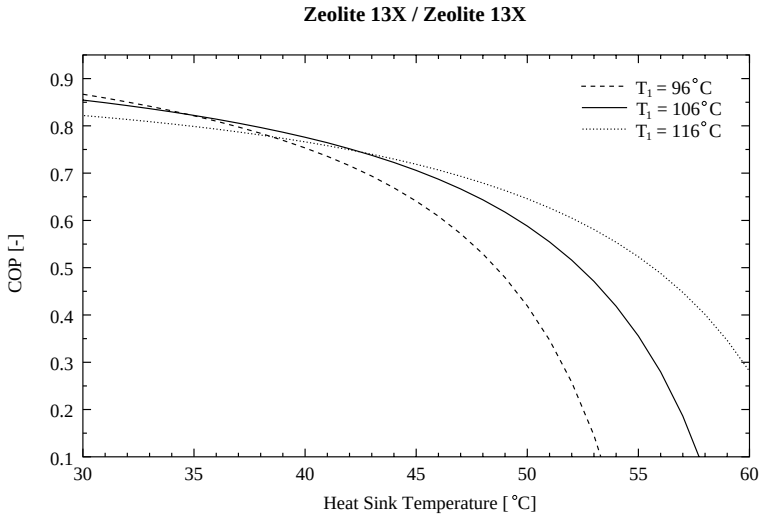

Figure 4.21: COP as function of the heat sink temperature for the Zeolite 13X/Zeolite 13X–combination at three different temperatures T_1 ($T_e = 7°\mathrm{C}$, $T_3 = 280°\mathrm{C}$).

Chapter 5

Both Cycles as Technical Designs

For the technical design of two–stage triple–effect and single–stage double–effect heat pumps, four requirements have to be considered:

1. **Costs:** The number of cost–intensive components must be minimized or by reducing the maximum desorption temperature. The latter is achieved on expense of the efficiency, more for the triple–effect than for the double–effect cycle, as the computer simulations have shown (compare Fig. 4.6 with Fig. 4.18).

2. **Simplification:** No complicated, but maintenance–free components with as far moving parts as possible should be installed. The automatic control engineering must be restricted to a minimum.

3. **Ecological Compatibility:** Normally all components and chemicals (adsorbents, working fluids, low temperature coolants) necessary for operating an AHP are ecologically harmless. The only exception might be the high temperature coolant (thermal oil), used to transfer heat from one adsorber to the other. For temperatures above 260°C as necessary for the triple–effect cycle only toxic, synthetic and organic thermal oils are available. The lower maximum regeneration temperature needed to operate a double–effect cycle efficiently might avoid such ecologically problematic thermal oils.

4. **Efficiency:** The efficiency has to surpass conventional systems, but in agreement with requirements 1, 2 and 3.

Due to these three requirements the designs are aligned on the following directives:

- Each adsorber has only one heat exchanger, although two heat exchangers would avoid valves. But there are two important arguments against installing two heat exchangers: first, the sensible heat of the heat exchanger and the circulating coolant will be at least doubled, and second, the development of an efficient heat exchanger–adsorbent compound will be complicated.

- The high temperature (> 200°C) coolant circuit should be operated by only one circulation pump.

- Additional valves should be used instead of circulation pumps if possible.

- 3–way valves might be replaced by a larger number of 2–way valves.

- The vacuum valves between adsorber and condenser or evaporator, respectively, might be replaced by check–valves which operate on pressure difference.

5.1 Design Suggestions for a Two–Stage Triple– and a Single–Stage Double–Effect AHP

For each configuration one design example is proposed in Fig. 5.3 and 5.4, respectively. Both designs are mainly based on the use of only one heat exchanger in each adsorber, and minimizing the number of pumps and valves (due to cost–reduction rather 2–way valves are installed than 3–way valves). Using two heat exchangers, especially in the LT–adsorber, has no advantage because it won't reduce the number of valves. Only if an additional pump is added, the valves can be reduced, but this won't make the system cheaper, simpler and more reliable.

An essential problem of the triple–effect cycle mentioned already in § 4.1.1, is to rise the pressure in the HT–condenser while the HT–adsorbent is desorbed. It is necessary that the outlet temperature of the LT–adsorber T_{ar}^{out} at time $t+\Delta t$ is higher than the inlet temperature of the HT–condenser T_c^{in} at time t (Fig. 5.1). Otherwise the pressure decreases which happens when the heat losses of the LT–adsorber become too large. Since no heat losses are considered in the numerical simulations, the pressure increases anyway. The problem of increasing the pressure in the HT–condenser as soon as heat losses of the adsorber are taken into account, and due to the requirement of simplifying the triple–effect cycle seems to be less attractive (a comprehensive comparison of both cascading configurations is given in Table 5.2). As well the simulation results do not differ much from those of the double–effect cycle. If two mass transfers are adapted to the double–effect, especially the mass transfer which will widen the LT–cycle to the left (see Fig. 5.2), i.e. to the area of the isosteric field where large concentration changes are achieved especially for silica gels, and it can be assumed that at least equal COPs can be obtained. Finally we can state, that from the four point of views, costs, simplification, ecological compatibility and efficiency (summarized in Table 5.1), the single–stage double–effect adsorption heat pump will definitely outdo the two–stage triple–effect AHP.

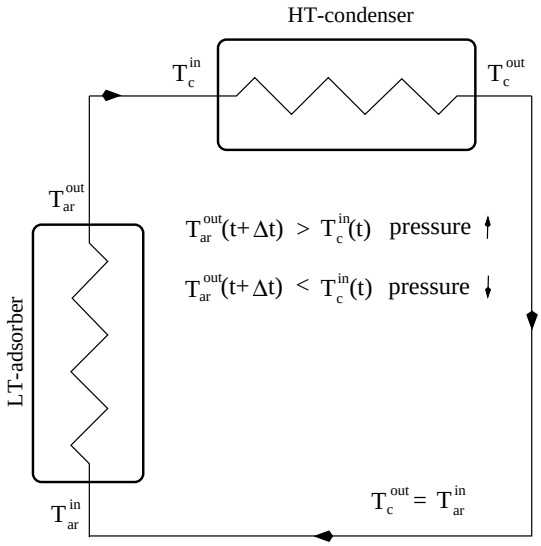

Figure 5.1: Rising pressure problem of the triple–effect cycle.

	3–effect	2–effect
cost	–	+
simplification	–	+
ecological compatibility	o	o
efficiency	o	o

Table 5.1: Comparison triple–effect and double–effect cycle: + ... advantage, – ... disadvantage, o ... same

	triple–effect	double-effect	single–effect
# of sequences	4	2	2
minimal desorption temperature T_3	≈260°C	≈200°C	140°–260°C
# of adsorbers	2	2	1
# of condensers	2	1	1
# of evaporators	1	1	1
# of circulation pumps:			
➢ designed for high temperature	1	1	1
➢ designed for low temperature	3	2	2
pumps working intermittently	2	0	3
pumps working continuously	2	3	0
# of 2–way fluid valves:			
➢ designed for high temperature	3	2	0
➢ designed for low temperature	4	2	0
# of vacuum valves	4	4	2
# of expansion valves	2	1	1
# of possible mass transfers	1	2	0

Table 5.2: Comparison of triple–, double– and single–effect cycle.

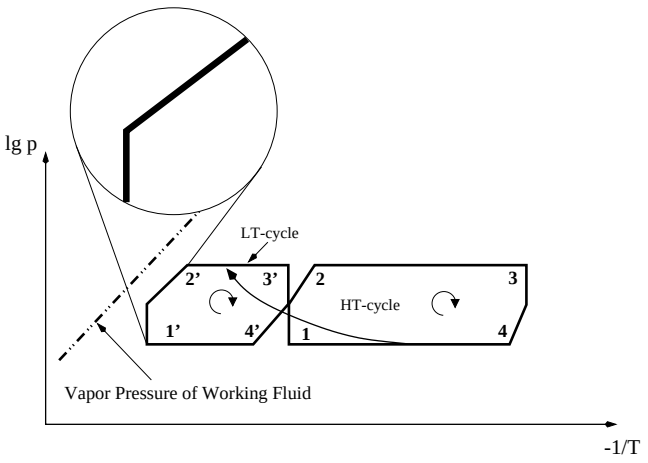

Figure 5.2: The two mass transfer sequences of the double–effect cycle enlarging the mass of working fluid pumped in both cycles.

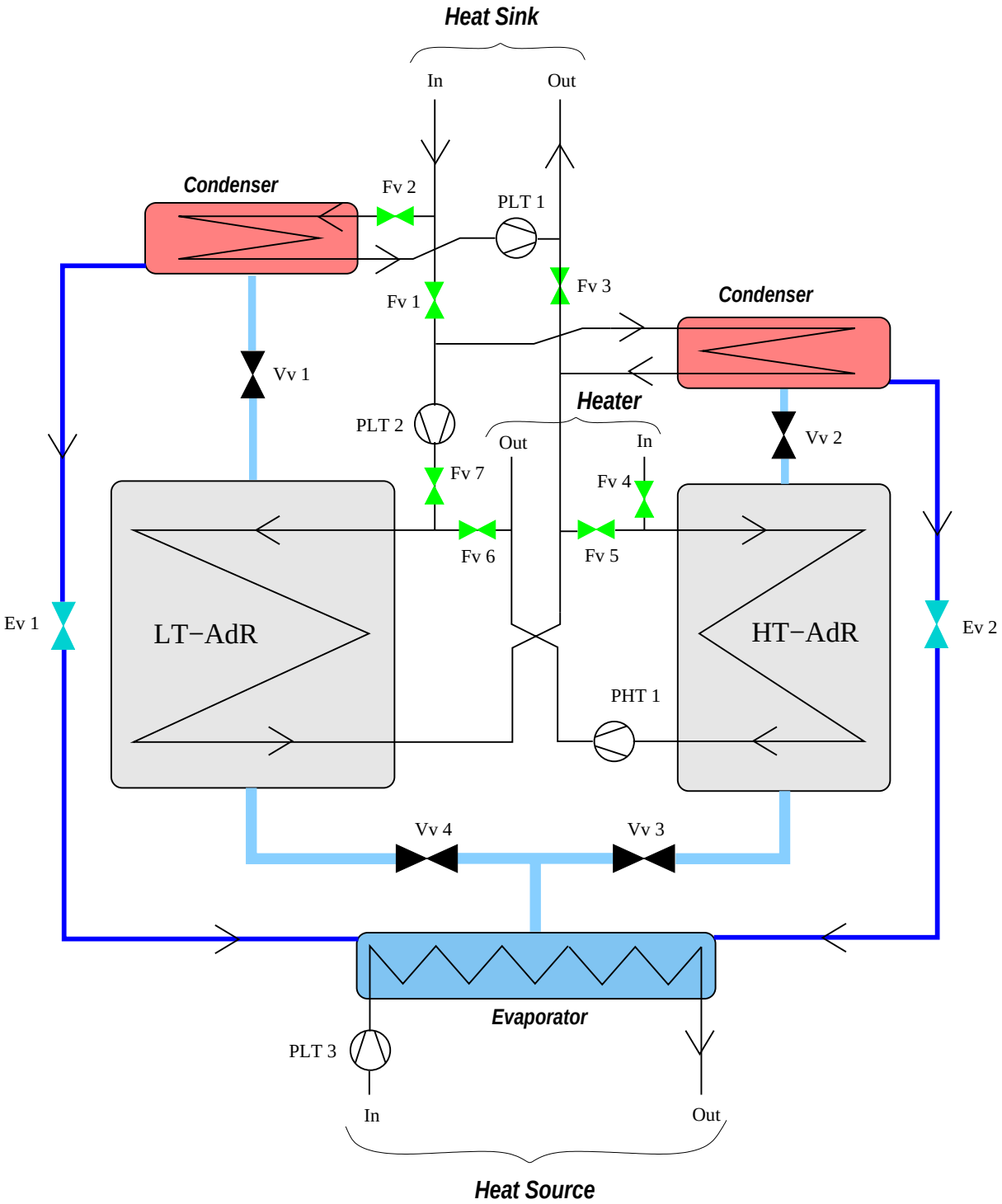

In ... Inlet−Flow
Out ... Outlet−Flow
PLT ... Circulation Pump (low temperature version)
PHT ... Circulation Pump (high temperature version)

Ev ... Expansion Valve
Fv ... Fluid Valve
Vv ... Vacuum Valve

Figure 5.3: Design of a two–stage triple–effect AHP with a minimal amount of components (5 main components) if just one heat exchanger per adsorber is used.

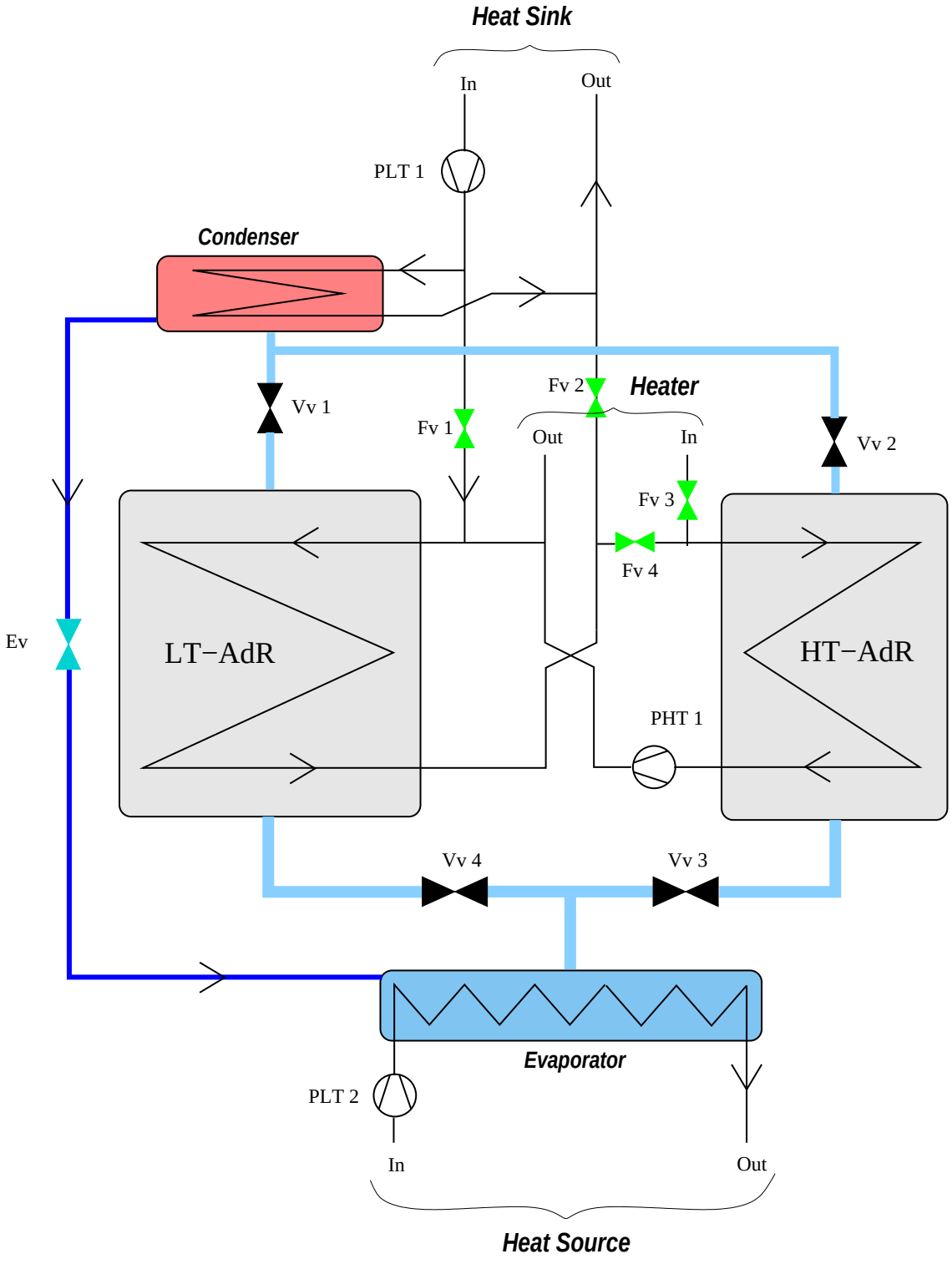

In ... Inlet−Flow
Out ... Outlet−Flow
PLT ... Circulation Pump (low temperature version)
PHT ... Circulation Pump (high temperature version)

Ev ... Expansion Valve
Fv ... Fluid Valve
Vv ... Vacuum Valve

Figure 5.4: Design of a single–stage double–effect AHP with a minimal amount of components (4 main components) if just one heat exchanger per adsorber is used.

Part II

The Experimental Single–Adsorber System

Chapter 6

The Experimental Single–Adsorber System

6.1 Design of an Experimental Setup with One Adsorber

In order to collect first experiences with closed solid sorption processes and to measure a heat exchanger design, presented thereafter, a laboratory breadboard assembly as shown in Figs. 6.1 and 6.2 was built up.

The experimental setup for closed solid sorption measurements consists of the following components:

- adsorber tank
- finned tube heat exchanger with adsorptive material filled between the fins
- evaporator
- condenser
- three baths (closed circulator heated bath, refrigerated bath, controlled–temperature re-circulator), responsible for heating, cooling and circulating the coolants
- vacuum pump
- manually switchable valves, solenoid valves and one diaphragm valve
- sensors: flow–meters, pressure transducer and platinum thermometers of type Pt 100
- measuring: data–logger (multiplexer with digital/analog–converter) transferring data to a personal computer
- adsorptive materials: silica gel and zeolite
- working fluid: water
- coolants: water and thermal oil

The individual components will be described in detail in the following sections.

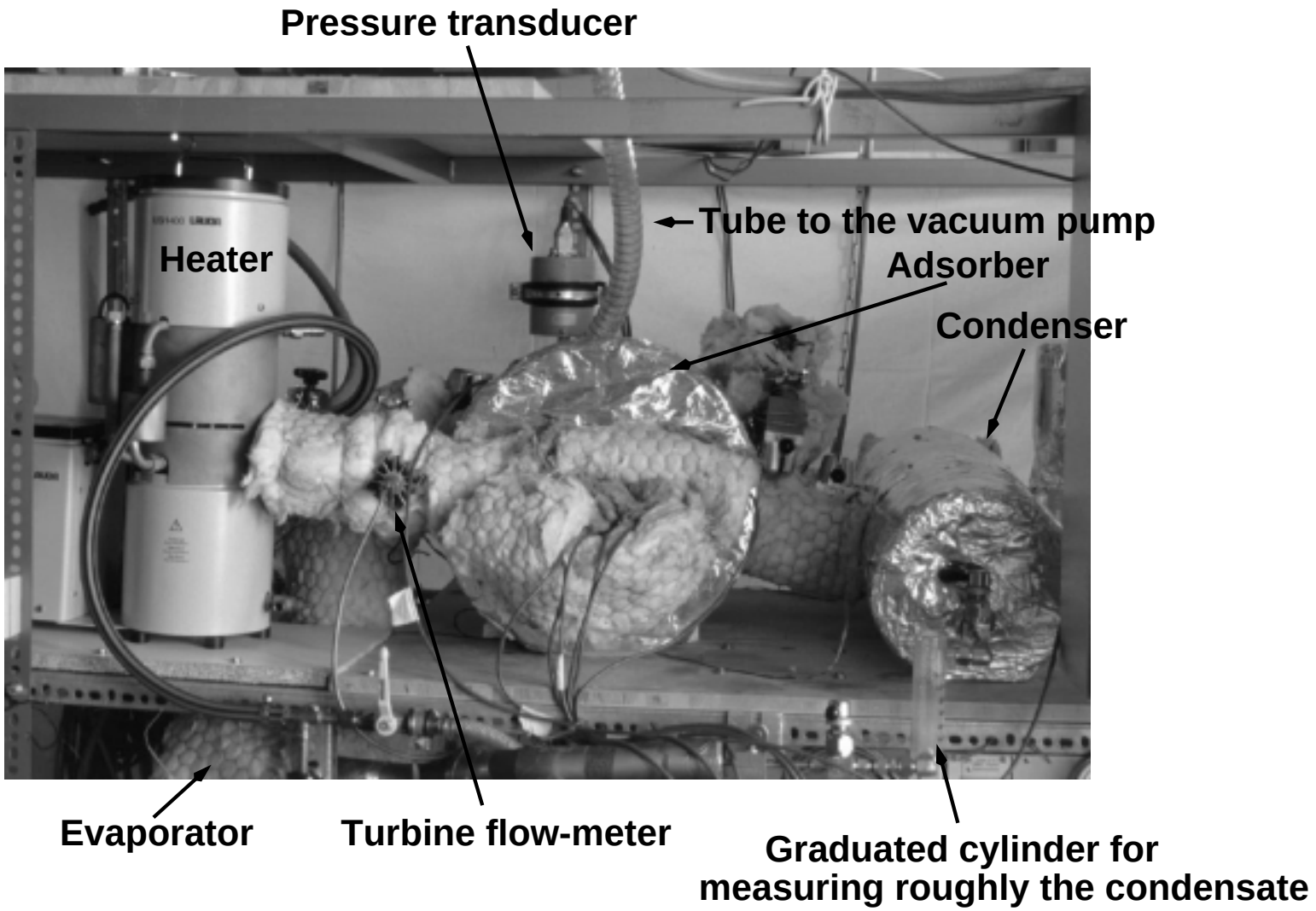

Figure 6.1: Photography of the insulated experimental solid sorption facility.

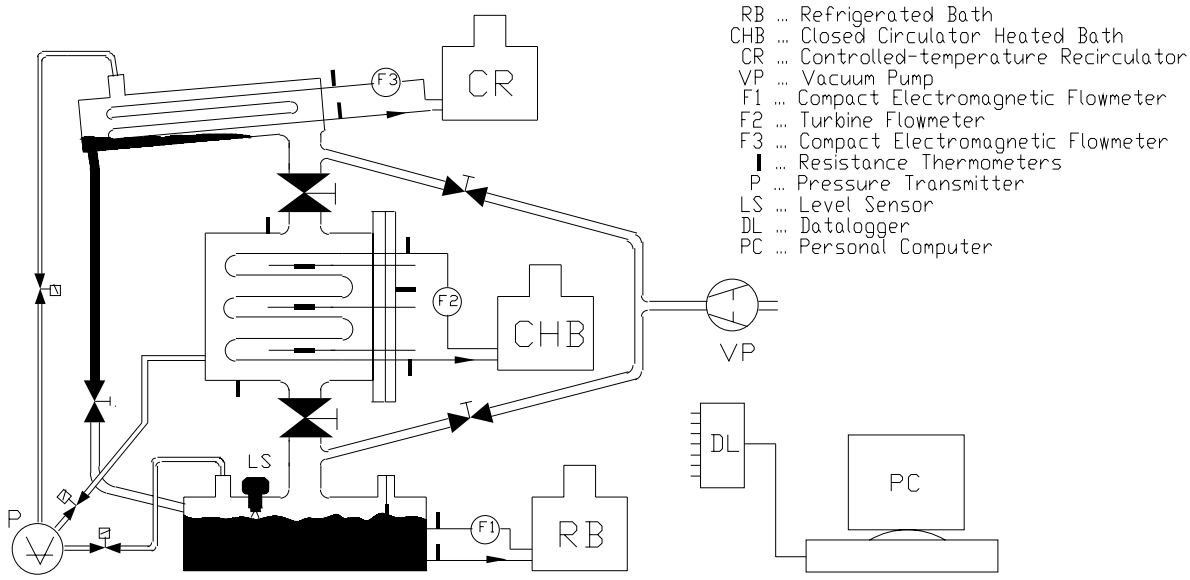

Figure 6.2: Schematic illustration of the experimental solid sorption facility (solid sorption heat pump with one adsorber).

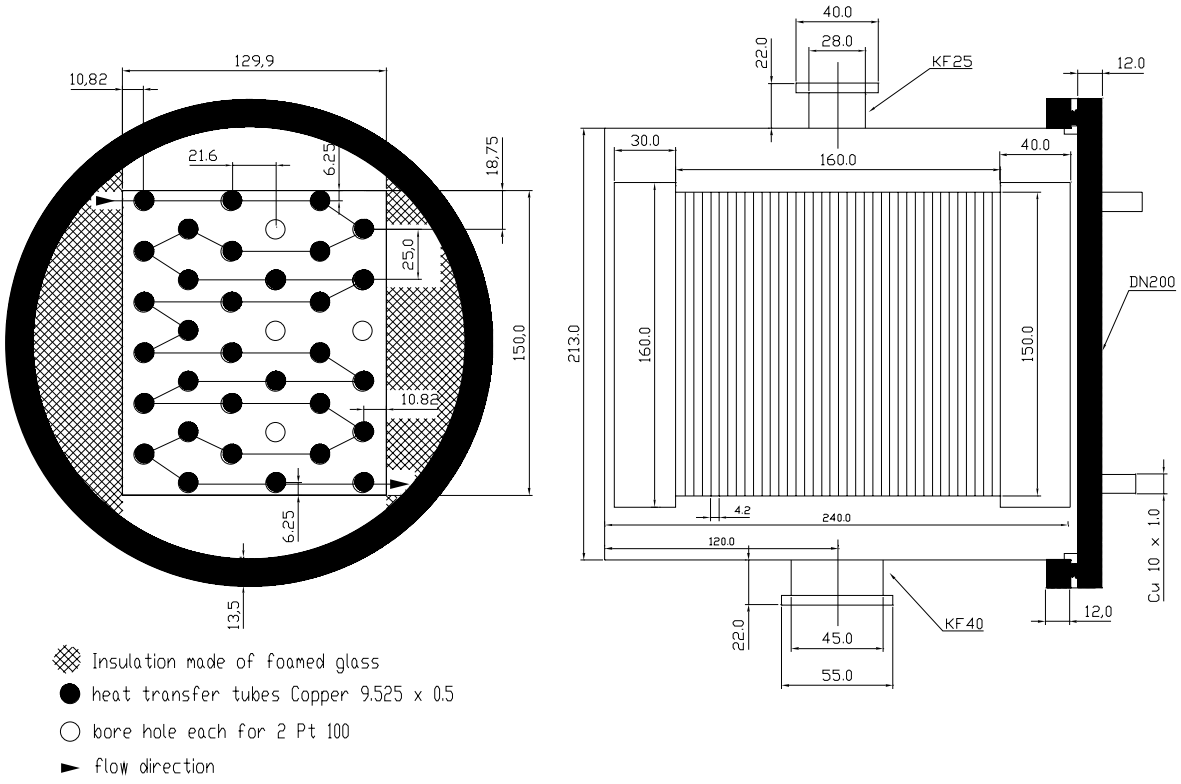

Figure 6.3: The finned tube heat exchanger placed in the adsorber tank.

6.1.1 The Adsorber with included Heat Exchanger

The cylindric adsorber is carried out as a vacuum–tight tank made of 3 mm stainless steel AISI 304L with a clamping flange fitting (Pneurop–ISO) DN 200 and two opposing small flange connections DN 25 and DN 40 (see Fig. 6.3). All flange connections are sealed over a center ring with a coated elastomer seal *(Viton)*. The DN 200 flange fitting is fixed vacuum–tight with clamps to the adsorber tank. The small flange fittings DN 25 and DN 40 are connected vacuum–tight to their counterparts with clamping rings.

The DN 200 flange fitting is furnished with six exactly positioned bore holes of equal diameter at which vacuum–tight A–lok to pipe butt–weld connections are welded. Two bore holes contain the inlet and outlet tube of the inserted finned tube heat exchanger. The remaining four flange holes are sized by one–sided closed copper tubes CU 10×1 mm. These copper tubes traverse the whole depth of the finned tube heat exchanger and are with its fins in close contact. They serve as retainer for four calibrated platinum thermometers of type Pt 100 which measure the temperature inside the heat exchanger.

The core component of the single–adsorber experimental adsorption heat pump, and mainly responsible for the quality and quantity of heat transfer is the heat exchanger and its connection to the adsorptive material. Not only the heat transfer from the heat exchanger surface to the adsorptive material is important for the efficiency of the heat pump, but also the mass fraction between the mass of the metal used for the heat exchanger and the mass of the adsorptive material in contact with the heat exchanger. The ratio should be as low as possible in order to reduce the heat capacity of the heat exchanger.

The measurements presented in the next chapter (§ 7) are performed with a finned tube heat exchanger (short: *FTHX*), which is a little more than twice as heavy as the adsorbent filled loosely in the space between the fins. A thin closed–meshed stainless steel net is bound around the exchanger to prevent the adsorptive material trickling out. The *FTHX* and its surrounding adsorber tank is pictured in Figure 6.4.

The finned tube heat exchanger consists of 32 copper tubes Cu 9.52×0.5 mm *(originally there are 36 bore holes in the fins, but four are retained for copper tubes closed on one side which contain the PT100 thermometers to measure the temperature inside the FTHX)* arranged in a pattern that fits to the punched holes in the fins (see Fig. 6.3). On this tube arrangement a package of 44 copper fins is slipped–on with a distance of 3.5 mm between them. After positioning the fins, the tubes are mechanically or hydraulically expanded in order to obtain a tight fit between fin and outer–tube surface. The tube connections are indicated in Fig. 6.3. The two square end–plates, one at each side of the fin–package, hide the connecting copper fittings. The gaps between these fittings are filled with a ceramic thermal insulation.

The adsorptive materials of type silica gel and zeolite have poor thermal conductive properties. The thermal conduction k for silica gel varies between 0.1 and 0.2 $^{W}/_{m\,K}$ (Bjurström et al. [7], Kast [43]) for a dry bed, and for moist zeolite it is about 0.18 up to 0.23 $^{W}/_{m\,K}$ (Sahnoune et al. [82]). Assuming average pellet diameters of 1.5–3.5 mm, the distance between the fins was set to 3.5 mm, i.e. each sorptive pellet has at least one contact point with a metallic surface.

The following table gives an overview about the technical properties of the whole adsorber:

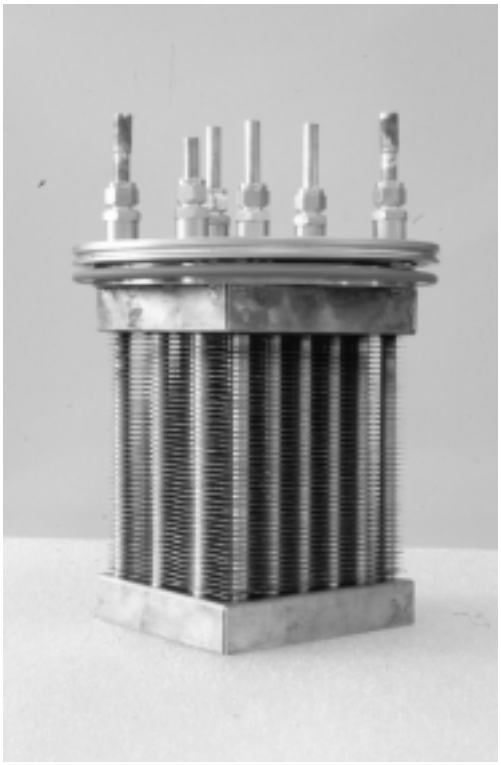

(a)

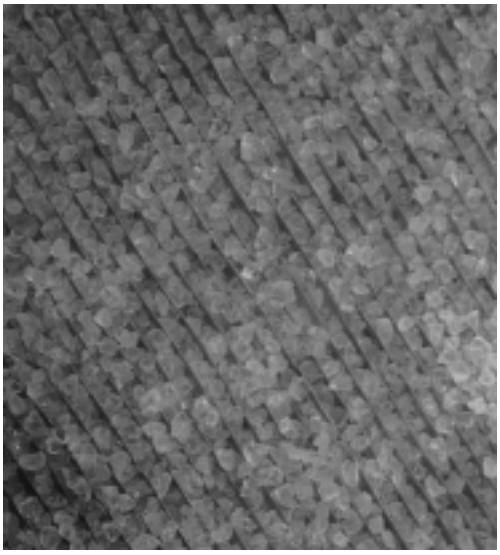

(b)

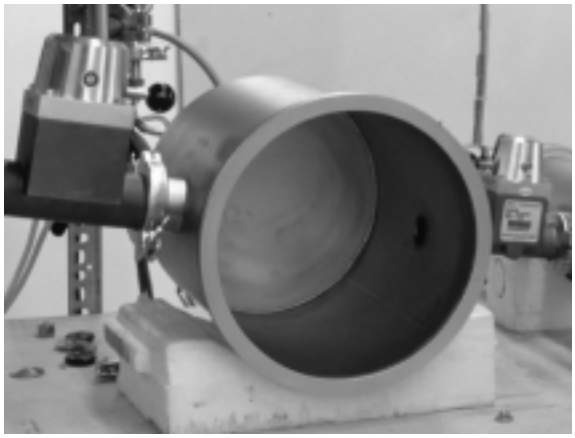

(c)

Figure 6.4: (a) Finned tube heat exchanger with fixed DN 200 flange fitting, center ring and elastomer seal, without filled in adsorptive. (b) Close–up photography of the adsorptive material – in this case Silica Gel Grace 125 – filled between the fins. (c) Adsorber tank, on the left the valved connection to the evaporator and on the right to the condenser.

Adsorber Tank	
dimensions	: see Fig. 6.3
material	: stainless steel AISI 304L
material of the sealing	: Viton
total mass	: 11676 g
wall thickness	: 3 mm
ISO–flange	: DN 200
connections	: DN 25 and DN 40

Finned Tube Heat Exchanger	
dimensions	: see Fig. 6.3
material	: copper
mass	: 3200 g
number of fins	: 44 + 2 end–plates
fin thickness	: 0.15 mm
distance between fins	: 3.5 mm
fin spacing	: 3.64 $^{\text{fins}}/_{\text{cm}}$
thickness of the end–plates	: 1.6 mm
number of heat exchanger tubes	: 32 bare copper tubes
dimensions of the tubes	: 9.525×0.5 mm
overall length of the tubes	: 7.3 m
exchange area on shell-side (fin area)	: 1.67 m^2
exchange area on coolant–side	: 0.2 m^2
net volume (volume between the fins)	: 3198.3 cm^3
mass of filled adsorptive material ($\varrho = 800\ \frac{g}{dm^3}$)	: $\approx$ 1500 g

6.1.2 Evaporator and Condenser

Evaporator and condenser are of identical construction. These Tube–and–shell heat exchangers are taken from a different application, i.e. they are not designed especially for the single–adsorber experimental adsorption heat pump. During the measurements it became obvious that the evaporator as well the condenser are not very well adapted to the experimental setup. But the financial resources of the project didn't allow to build new ones. Both are too large, especially if the evaporator is filled up with the working fluid no change of the coolant outlet temperature is observed during the adsorption process.

The component is a cyclindrical vacuum–tight tank made of stainless steel AISI 304L with two open ends (see Fig. 6.5(a)) which are sealed through an elastomer O–ring *(Viton)* stretched on a centering ring by a clamping flange fitting (Pneurop–ISO) DN 110. The heat transmission is performed by a coolant flowing through a bundle of copper U–tubes which have helically rolled fins on their inside and are corrugated on their outside (see Fig. 6.5(b)). Inlet and outlet are guided through bore holes in one flange fitting. The second opposing clamping flange fitting has a connection 8 mm in diameter. Through these two connections the condensate flows back from the

condenser to the evapotaor. In the middle of each container a flange with pipe is welded, DN 25 for the condenser and DN 40 for the evaporator, to connect them to the adsorber. The backflow of the condensate will be controlled by a manual diaphragm valve and not as usually implemented in vapor–compression heat pumps by an automatic expansion valve.

(a) (b)

Figure 6.5: The vacuum–tight tank (a) and the heat exchanger U–tube–bundle (b) of the evaporator and condenser, respectively.

Figure 6.5 shows the tank and the U–tube bundle heat exchanger serving as condenser and evaporator. The technical data are given in the following table:

Vacuum–tight Tank	
material	: stainless steel AISI 304L
material O–ring	: elastomer seal *(Viton)*
mass	: 8400 g
inside diameter	: 102 mm
overall length	: 540 mm
net volume	: 3900 cm^3
flange connections	: DN 40 bzw. DN 25

Heat Exchanger Tubes	
material	: copper
mass	: 1350 g
dimensions of the tubes	: 12.2×0.8 mm
overall length of the U–tube–bundle	: 2.3 m
external surface	: 0.3 m^2
internal surface	: 0.09 m^2

6.1.3 Coolants

The heat exchangers are provided with two different coolants (physical properties are given in appendix D):

- **Thermal oil:** Thermal oil is used as coolant for heating and cooling the sorption heat exchanger *(FTHX)*. This thermal oil is a synthetic, organic heat transfer medium which evaporates at normal pressure at temperatures over 360°C. This allows driving desorption temperatures over 300°C for zeolites.
- **Water:** The condenser and evaporator are cooled with distilled water by a temperature–controlled recirculator and refrigerated bath, respectively.

6.1.4 Adsorptive Materials and Working Fluids

A detailed description of the adsorptive materials is given in appendix B.2 and of the used working fluid water and some other ecologically acceptable ones in appendix C.

- **Adsorptive materials:** For the measurements the two commercially available adsorptive materials Silica Gel Grace 125 and Zeolite 13X are chosen.
- **Working fluid:** As working fluid distilled and demineralized water is used.

6.1.5 Installed Measuring Instruments

- **Temperature Sensors:** All temperature sensors are platinum resistance thermometers of type Pt100. The Class A platinum sensor is imbedded in a stainless steel protection tube of 3 mm in diameter with a silicone isolated $4 \times 0.25\ mm^2$ connecting wire carried out in 4–wire circuit. The temperature range is from $-50°$ up to $+400$°C. The sensors are provided with a current of 1 mA (also measured by the data–logger through a high–precision resistance) through a constant–current supply.
  Platinum has established itself as resistance material of choice. Its advantages include high chemical resistance, relatively easy workability, availability in highly pure form, and good reproducibility of its electrical properties. The properties, i.e. the electrical resistance and the permitted tolerances at different temperatures and some additional regulations are defined in the Standard IEC 751 in order to ensure universal interchangeability.
  The interrelationship between the electrical resistance R_e and the temperature T is covered by the n–order polynomial

$$R_e(T) = R_0\,(1 + A * T + B * T^2 + C * T^3 + \dots) \tag{6.1}$$

The term R_0 is referred to as the nominal value and represents the resistance at 0°C. According to IEC 751 the nominal value is 100.000 Ω. We therefore speak of a **PT100** temperature sensor. The coefficients *A, B, C, ...* describe the temperature–dependence of the resistance and result from calibration. *R(T)* is the resistance at temperature T calculated by Ohm's law from the measured voltage and current. For the measurement accuracy it will be adequate to reduce the n–order polynomial to a two–order one. According to IEC 751, for temperatures above 0°C it is possible to derive an explicit expression for the temperature:

$$T = \frac{-R_0\,A + \sqrt{((R_0\,A)^2 - 4\,R_0\,B\,(R_0 - R))}}{2\,R_0\,B} \tag{6.2}$$

According to IEC 751 the tolerance for Class A sensors is

$$\Delta T = \pm(0.15 + 0.002 \cdot |T|) \tag{6.3}$$

with $|T|$ temperature in °C.

☞ **Pressure Transducer:** The pressure is measured by an absolute pressure transducer of type MKS Baratron. The effects of ambient temperature fluctuations are greatly reduced by heating the sensor up to 150°C. The transducer is designed for a range from 1 Torr up to 1000 Torr and its electronic output is 4 to 20 mA or 0 to 10 VDC, and is linear with pressure over the full scale range, i.e. 1 mVDC corresponds to 1 Torr.

☞ **Compact Electromagnetic Flow–meter:** The two flow–meters installed in the coolant circuits of the evaporator and condenser work according to the electromagnetic principle. Both compact electromagnetic flow–meters have a nominal diameter of 10 mm of the Teflon–liner, reinforced with a stainless steel mesh. Because of the Teflon–liner the maximum temperature should not exceed 120°C and the electrical conductivity should not drop below 5 $\mu S/cm$ due to the measurement principle. The signal converter with a display for configuration, testing and control provides a 4–20 mA or 0–20 mA galvanic isolated current output. The volume–flow rate $\dot{V}$ will be determined from the measured current I_{meas}, the range of the chosen current output I_{diff} (16 mA or 20 mA) and the defined and programmed volume–flow rate range $\dot{V}_b$:

$$\dot{V} = \frac{I_{meas}}{I_{diff}}\,\dot{V}_b. \tag{6.4}$$

The optimum flow velocity should be 2–3 m/s and the recommended installation should be vertical with outlet up or horizontal but not at the highest point of a pipe. The straight minimum inlet flow length is set to 5× and the minimum outlet flow length to 2× the nominal diameter ensuring that the measuring tube is completely filled at all times. Strong electromagnetic fields in the vicinity of the flow–meter have to be avoided.

☞ **Turbine Flow–meter:** It is a mediate volume transmitter similar to a *Woltmann's Sail Wheel*. The volume passing through the tubes is measured by the mean velocity of the fluid. A light–weight turbine–wheel is carried concentrically in the tube body. Flow rectifiers ensure a laminar flow in the axial direction of the wheel. The fluid causes the wheel to rotate. The RPM of the turbine–wheel are directly proportional to the mean

flow velocity within the tube diameter and correspond to the volume flow over a wide range. An inductive pickup or a carrier–frequency pickup is screwed into the turbine flow–meter. The pickup will detect the RPM of the turbine–wheel through the non–magnetic turbine–body without magnetic drag and without coming into contact with the measuring medium.
The accuracy of the turbine flow–meter is defined by the factors linearity, corresponding to the instantaneous flow rate, and repeatability. Linearity usually amounts to ± 0.15 up to $\pm 1\%$ of the instantaneous flow rate within the linear measuring range of the turbine flow–meter. Repeatability gives the percentage difference between two measuring results at identical flow rates. It usually amounts to 0.05 up to 0.2%.
The turbine flow–meter is installed in the coolant circuit of the sorption heat exchanger. It is equipped with an inductive pickup for temperatures up to 350°C measuring the frequency of the turbine–wheel, which is converted into a current signal (0–20 mA) by a frequency–analog converter. The volume–flow rate is determined by the equation

$$\dot{V} = \frac{I_{meas}}{20\,mA}\,60\,\frac{f_{max}}{K}$$

$\dot{V}$ ... volume–flow rate [$^{l}/_{\mathrm{min}}$]
I_{meas} ... measured current [mA]
f_{max} ... maximum frequency [Hz]
K ... K–factor [$^{\mathrm{impulses}}/_{\mathrm{litre}}$]

The maximum flow rate of the turbine flow–meter can be limited. f_{max} is the appropriate frequency. The K–factor is obtained by calibration and defines the exact volume flow rate for the turbine flow–meter. Between the calibrated values the K–factor can be interpolated.
For installing the turbine flow–meter one should choose a straight part of the pipe, preferrably vertical with outlet up, and a length of straight pipe upstream of 10× turbine's nominal diameter and a length of straight pipe downstream of 5× turbine's nominal diameter.

6.1.6 Measuring Points

☞ **Temperatures:**

- 4 measuring points in the finned tube heat exchanger (the temperature of the filled–in adsorptive material cannot be measured separately)
- 2 measuring points at opposite outside surfaces of the adsorber
- 1 measuring point at the flange fitting of the adsorber tank
- ambient temperature
- inlet and outlet temperatures of the three coolants
- temperature of the liquid working fluid in the evaporator

☞ **Pressure:** With the pressure transducer the pressures in the evaporator, in the adsorber and in the condenser can be recorded one after another. For that the sensor has three outlets which are connected with solenoid valves to the components. The solenoid valves are controlled by the data transducer which gets the control–sequences from a computer program.

☞ **Flow rate:** In each of the three coolant circuits a flow–meter is installed (two compact electromagnetic and one turbine flow–meter).

6.1.7 The Transducer – Data–logger

The measuring signals of all built–in sensors are scanned through multiple data channels by a data–logger and then transmitted via an RS485 interface to a personal computer. The data–logger has galvanically isolated self–calibrating channels with high measuring accuracy and a 21 bit resolution which can be configured individually as Volt/mVolt–, 20 mA–, Pt100– and Thermocouple–channels (analog inputs, analog outputs, status inputs and switching outputs). Data storage and analyses and the control of the 0...10 V 16 bit switching outputs are taken over by a self–written computer program.

6.1.8 Further Components

- **Vacuum valves:** In the connections between the adsorber and the evaporator and condenser, respectively, and the two fittings to the vacuum pump manually operated valves are installed (leak tightness better than 10^{-9} $\text{mbar}\,\text{l}/\text{s}$). In the connection from condenser to evaporator one high vacuum diaphragm valve is installed (He–leak rate $< 4\times10^{-9}$ $\text{mbar}\,\text{l}/\text{s}$).

- **Solenoid valves:** They are current–carrying in the open state. They short–circuit the pressure transducer with the selected component.

- **Vacuum pump:** For low temperature evaporation of the working fluid water a vacuum is necessary. The vacuum is generated by an oil–sealed double–staged rotary vane vacuum pump with an ultimate vacuum without gas ballast of 1.0×10^{-3} mbar. The disadvantage of this kind of pump is that contamination with pump oil of the vacuum system cannot be completely ruled out. An excellent alternative without any oil contamination might be a scroll dry vacuum pump.
  The single–adsorber facility has two connection points for the vacuum pump. The first is installed between the evaporator and adsorber in order to allow evacuating the evaporator and to degas a new filled–in working fluid, and the second is placed between the adsorber and the condenser, and allows to evacuate the adsorber only or both the adsorber and condenser.

- **Baths:**

  - The closed circulator heated bath provides the finned tube heat exchanger with temperatures between 20° and maximum 400°C. To the closed bath, a water cooling unit was adapted controlled by a solenoid valve.
  - The refrigerated open bath could be used in a temperature range of -45° up to 150°C. It is connected to the evaporator.
  - The coolant temperature of the condenser is regulated by a temperature controlled recirculator which has a working temperature range from -25° up to 80°C.

Chapter 7

Experiments with the Single–Adsorber System and their Assessment

7.1 Experimental Progression of Adsorption– and Desorption–Sequences

The heat exchanger (see Fig. 6.4(a)) is completely filled with adsorptive material (see Fig. 6.4(b)) and inserted in the adsorber (see Fig. 6.4(c)). The evaporator is filled up with degassed working fluid. Since water is used as working fluid, the whole experimental unit must be evacuated. The vacuum–tightness has been controlled by a leak detector. After the whole system is evacuated and the three baths are stabilized to their initial temperatures, we start progressing a first and sometimes a second complete operating cycle before the recording computer program will be launched. During one desorption/adsorption–cycle the following steps have to be carried out:

Desorption

1. All three valves are closed.
2. The adsorber will be heated, and valve 2 opened as soon as the working fluid pressure in the adsorber exceeds the condensation pressure.
3. After reaching the final desorption temperature in the adsorber, valve 2 will be closed, and valve 3 opened in order to guide the condensed working fluid back to the evaporator without causing pressure compensation between both tanks, and afterwards closed.

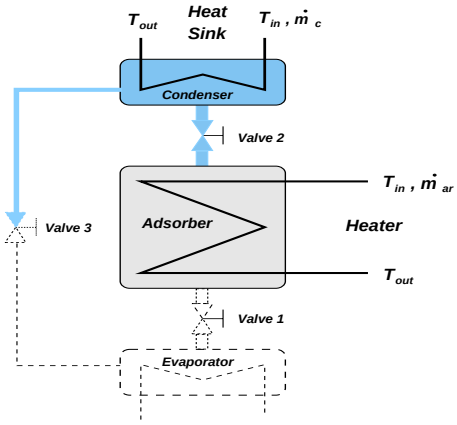

Adsorption

1. The adsorber will be cooled down by connecting it to the heat sink.
2. As soon as the pressure in the adsorber drops below the evaporation pressure, valve 1 will be opened. The adsorption process is started.
3. When the desired heat sink temperature is reached, valve 1 must be closed, and we can proceed with additional desorption/adsorption–sequences.

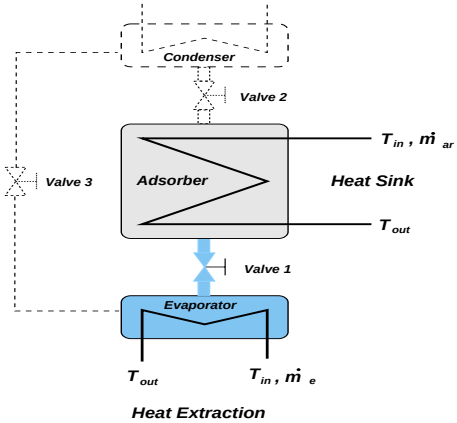

Normally three successive desorption/adsorption–sequences are measured. Fig. 7.1 shows one desorption/adsorption–cycle. The adsorption/desorption heat flux, the heat flux of the condenser, and the pressure in the adsorber are plotted as function of time. Unfortunately the heat flux of the evaporator is not determinable, because the evaporator contains too much working fluid reacting too sluggish on small temperature changes.

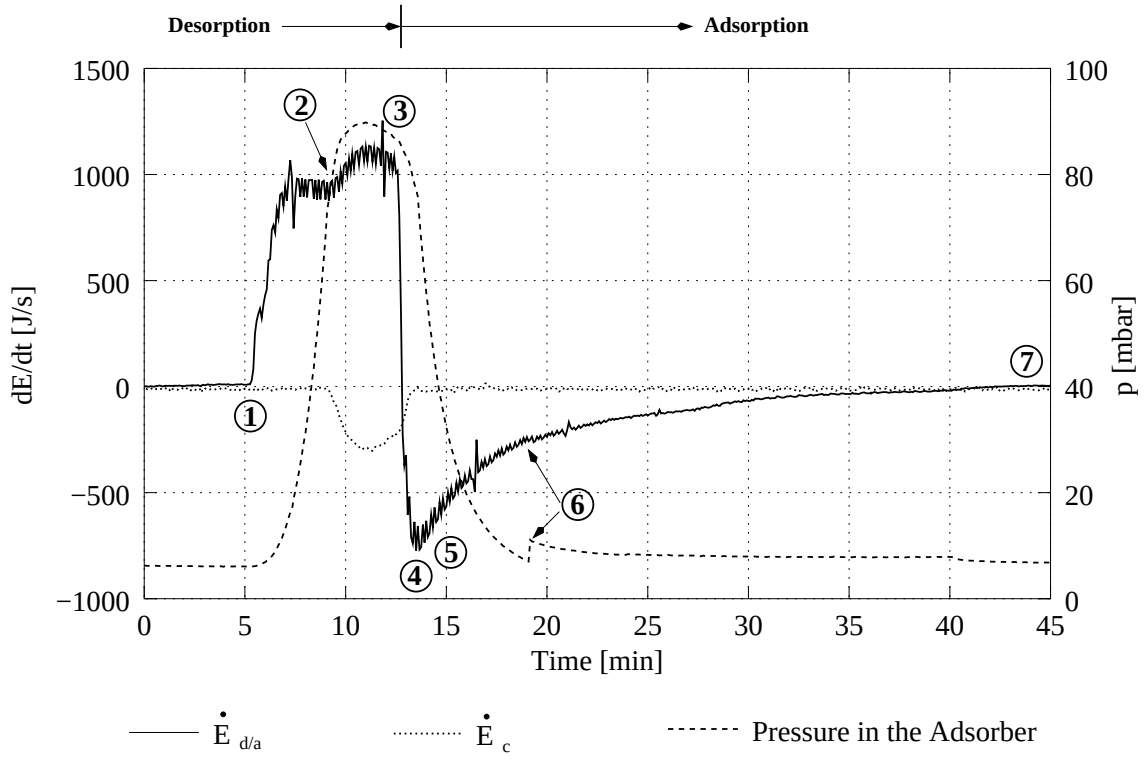

① ... adsorber heating started
② ... opening of valve 2 (condensation begins)
③ ... closing of valve 2 and opening of valve 3
④ ... cooling adsorber
⑤ ... closing of valve 3
⑥ ... opening of valve 1 (adsorption begins)
⑦ ... closing valve 1

Figure 7.1: One desorption/adsorption–cycle plotted together with the condensation heat flux. The right y–axis indicates the pressure in the adsorber.

7.2 Heat Flux Determination

The heat flux of the sorption heat exchanger $\dot{E}_{d/a}$ and the condensation heat flux $\dot{E}_c$ are calculated from the experimental data by the equation

$$\dot{E} = \rho(T_{mean})\,\dot{V}\,c_{htf}(T_{mean})\,\Delta T. \tag{7.1}$$

In order to avoid including the sensible heat of the coolant, ΔT is not the temperature difference between inlet and outlet at the same time t, but the temperature difference between an inlet tem-

perature at time t and outlet temperature at time $t + \Delta t$. The increment of time Δt is the period a fluid molecule needs to move from inlet to outlet; its velocity is assumed constant for Δt.

$$\Delta T = T_{in}(t) - T_{out}(t + \Delta t) \quad \text{with } \Delta t = \frac{A\,l}{\dot{V}} \tag{7.2}$$

T_{mean} is the arithmetical mean of the inlet temperature at time t and the outlet temperature at time $t + \Delta t$. By this procedure the sensible heat of the coolant is taken into account.

7.3 The Heat Loss of the Adsorber

Normally in an ideal process the adsorption and desorption heat are approximately of the same amount. In the experiment the adsorption and desorption heat differ from each other because of heat losses to the environment from the sorption heat exchanger. This heat loss is mainly caused by the sensible heat of the adsorber tank surrounding the heat exchanger. In our case its mass is more than twice as high as the heat exchanger and the adsorbent masses together. Furthermore the heat loss depends on the duration since the adsorption process is normally much slower than the desorption.

But how can we determine the heat loss coefficients? One possibility is to measure the heat flux while successively heating and cooling the closed (neither evaporation nor condensation occur) sorption heat exchanger. Then this system might be described by the expression

$$\text{input heat flux} = \text{output heat flux} + \text{heat loss},$$

which is a set of linear algebraic equations containing the unknown coefficients. A unique solution exists if there are as many equations as unknown coefficients, but in our case the situation occurs that we have more equations than unknowns, i.e. the system is over–determined; a least–squares solution is required.

The heat flux provided by an external heater to the system and as well the heat flux released from the system to the ambient consists of two parts. One part is stored in the heat exchanger and the adsorbent, and the other is transferred by convection, conduction and radiation to the adsorber tank, there partly stored, and partly transported through the insulation to the ambient. The heat stored in the heat transfer fluid is far from being negligible, but the approach of the adsorber heat flux $\dot{E}_{d/a}$ considers this circumstance (see previous § 7.2). The heat flow of the system *adsorber* might be described by heat resistances and capacities as shown in Fig. 7.2 following Kirchhoffs rules for electrical networks. The heat flux path is mathematically expressed by the linear differential equation (no radiation is considered):

$$\begin{aligned}
\dot{E}_{d/a} &= \dot{E}_{hxat} + \dot{E}_{hx\to sc} \\
&= \dot{E}_{hxat} + \dot{E}_{sc} + \dot{E}_{is} + \dot{E}_{sc\to amb} \\
&= (m_{hx}\,c_{hx} + m_{at}\,c_{at})\,\frac{dT_{hx}}{dt} + c_{sc}\,m_{sc}\,\frac{dT_{sc}}{dt} + \rho_{is}\,V_{is}\,c_{is}\,\frac{dT_{is}}{dt} \\
&\quad + \underbrace{h_{sc\to amb}}_{\frac{1}{R^k_{is}} + \frac{1}{R^h_{is\to amb}}}\,A_{sc}\,(T_{sc} - T_{amb})
\end{aligned} \tag{7.3}$$

Eq. 7.3 deals only with the one unknown coefficient ($h_{sc\to amb}\,A_{sc}$) which represents the heat transfer coefficient from the adsorber tank wall to the ambient. All other coefficients, the specific

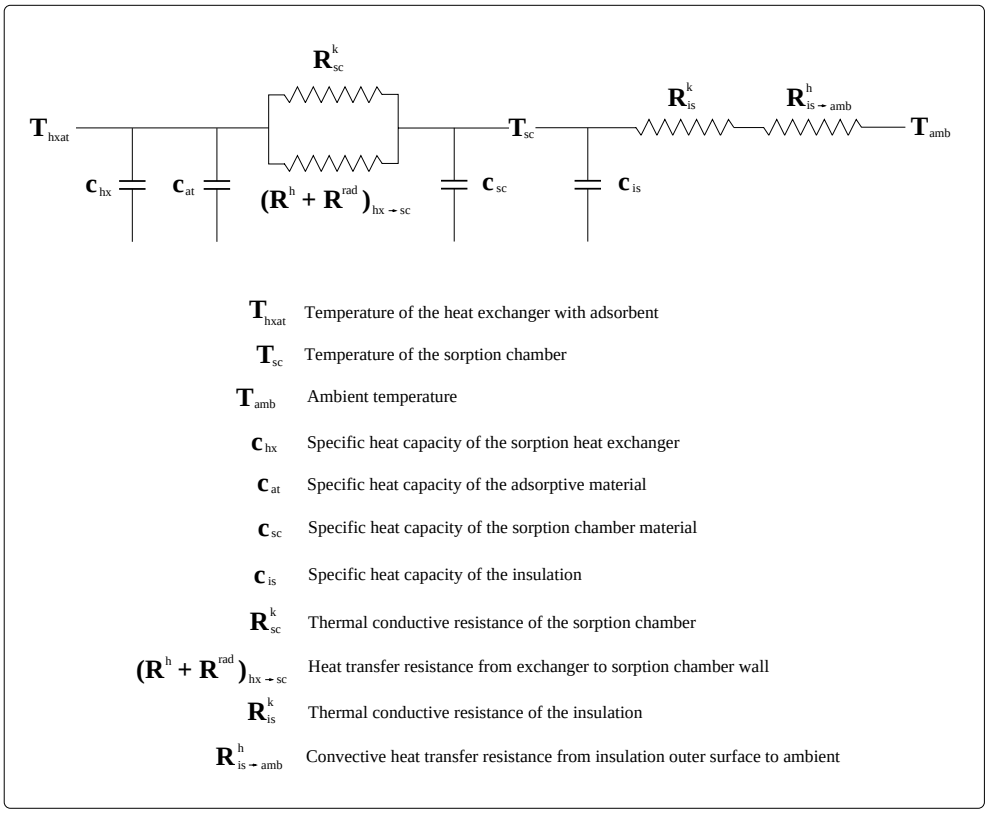

Figure 7.2: The physical modelling of the heat capacities and resistances of the adsorber.

heat capacities of the heat exchanger c_{hx}, of the adsorber tank c_{sc}, of the adsorbent c_{at} and of the insulation material c_{is} are well known:

$$c_{hx} = 383\,\frac{J}{kg\,K} \quad \text{(material: copper)}$$
$$c_{sc} = 477\,\frac{J}{kg\,K} \quad \text{(material: stainless steel)}$$
$$c_{at} = 1000\,\frac{J}{kg\,K} \quad \text{(material: silica gel)}$$
$$c_{is} = 840\,\frac{J}{kg\,K} \quad \text{(material: glass wool)}$$

The other variables in Eq. 7.3 have the following numerical values:

$$m_{hx} = 3.2\,kgK$$
$$m_{at} = 1.47\,kg$$
$$m_{sc} = 11.7\,kg$$
$$\rho_{is} = 75\,\frac{kg}{m^3}$$
$$V_{is} = 0.035\,m^3$$

Rearranging Eq. 7.3 yields to

$$\dot{E}_{d/a} - m_{hx}\, c_{hx}\, \frac{dT_{hx}}{dt} - \rho_{is}\, V_{is}\, c_{is}\, \frac{dT_{is}}{dt} - c_{at}\, m_{at}\, \frac{dT_{hx}}{dt} + c_{sc}\, m_{sc}\, \frac{dT_{sc}}{dt} = h_{sc\rightarrow amb}\, A_{sc}\, (T_{sc} - T_{amb}) \quad (7.4)$$

In a first approximation the derivatives $^{\mathrm{dT}}/_{\mathrm{dt}}$ are replaced by their finite–difference approximation

$$\frac{dT}{dt} = \frac{T(t) - T(t - \Delta t)}{\Delta t}, \quad (7.5)$$

where Δt is the incremental time between two measuring intervals.

Then Eq. 7.4 is valid for each measuring interval, no matter whether heating or cooling the *FTHX*, and we get a system of linear algebraic equations which is solved numerically by *Singular Value Decomposition* (Press et al. [74]), a method of choice for solving most linear least–squares problems.

Two measurements each of a number of successive heating/cooling–sequences with the Silica Gel Grace 125–water combination result in

$$h_{sc\rightarrow amb}\, A_{sc} = 0.7 \frac{W}{K} \quad \text{and} \quad h_{sc\rightarrow amb}\, A_{sc} = 0.67 \frac{W}{K}$$

The difference between these two values might be caused mainly by inaccuracies in measuring the adsorber wall and flange temperatures (the temperature sensors were not rigidly fastened to the wall).

A more precise determination of the loss coefficient will be achieved by

- better conductively fastened temperature sensors on the components or the installation of heat–flow–meters around the adsorber tank,
- increasing the number of temperature sensors and including the adjoining components and
- thermal control of the adsorber tank.

7.4 Measuring Errors

The average accuracy of the calculated desorption and adsorption heat flux, respectively, and the heat flow in the condenser

$$\dot{E} = \rho\, c_{htf}\, \dot{V}\, \Delta T \quad (7.6)$$

can be determined with Gauss' error propagation law

$$\overline{\Delta \dot{E}} = \sqrt{\left(\frac{\partial \dot{E}}{\partial \dot{V}}\, \overline{\Delta \dot{V}}\right)^2 + \left(\frac{\partial \dot{E}}{\partial T_{in}}\, \overline{\Delta T_{in}}\right)^2 + \left(\frac{\partial \dot{E}}{\partial T_{out}}\, \overline{\Delta T_{out}}\right)^2} = \rho\, c_p \sqrt{((T_{out} - T_{in})\, \overline{\Delta \dot{V}})^2 + \dot{V}^2\, (\overline{\Delta T_{in}^2} + \overline{\Delta T_{out}^2})} \quad (7.7)$$

where $\overline{\Delta\dot{V}}$, $\overline{\Delta T_{in}}$ and $\overline{\Delta T_{out}}$ are the maximum expected deviations of the measured value of the flow–meter and the inlet and outlet temperature sensors (see table below). The density ρ and the heat capacity c_{htf} of the coolant are assumed to be constant.

Measuring Device	Error
turbine flow–meter	$\pm 0.612\%$ of measured value
compact electromagnetic flow–meter	$\pm 0.5\%$ of measured value
inlet/outlet–Pt100 of *FTHX* (calibrated, class A)	± 0.1 K
inlet/outlet–Pt100 of evaporator and condenser ($^1/_3$ class B)	$\pm(0.10 + 0.0017\,\lvert T\rvert)\,^\circ$C

The measured values of the flow–meters are quite small and consequently the respective errors. For example the error of the turbine flow–meter measured up to maximum volume–flow rates of 5.5 $^1/_{\text{min}}$ is only 3.4×10^{-2} $^1/_{\text{min}}$. We conclude that the heat flux error is mainly affected by the temperature error.

$\overline{\Delta\dot{E}}$ is calculated for each measuring point, and then added up and averaged to determine $\overline{\Delta E}$. For a desorption sequence $\overline{\Delta E}$ is about 3%, and for an adsorption sequence about 10%. The reason why $\overline{\Delta E}$ is much higher for the adsorption sequence is, that the time derivatives of the temperature are much smaller over a long period which causes a large amount of quite high $\overline{\Delta\dot{E}}$ (see Fig. 7.3). This effect, but more intensified, can be regarded for the condensation temperature in Table 7.1. Since the condensation temperature differences from one measuring interval to another are small $\overline{\Delta\dot{E}}$ has high values, and summed up to $\overline{\Delta E}$ errors of about 50% are obtained.

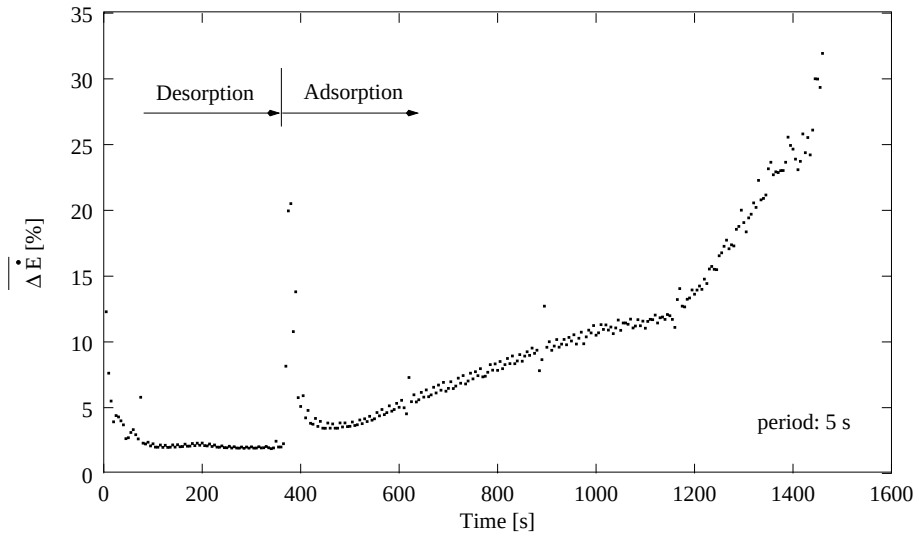

Figure 7.3: Average heat flux deviation distribution over one desorption/adsorption–sequence.

Mainly the different response–times of the temperature sensors are another error which depends on the measuring interval. This error is difficult to eliminate.

7.5 Energy Balance for one Cycle

The analyzed measurements with the single–adsorber experimental setup (see following § 7.6) will be compared with computer simulated results of the one cycle (see Fig. 7.4). For the computer simulations the same assumptions are used as for the simplified physical models of both multi–effect cycles in appendix A.1 and A.2. In the following energy balances we consider

- sensible heat of the working fluid and adsorbent,
- sensible heat of the heat exchanger, and
- latent heat of adsorption, including latent heat of vaporization L and binding energy ϕ.

Adsorption heat:

$$\begin{aligned} E_a = {} & m_{hx}\, c_{hx}\, (T_3 - T_1) \\ & + m_{at} \left[\int_{q_l}^{q_h} \big(T_e - T(p_c, q)\big)\, c_w(T)\, dq \right. \\ & \quad + (c_{at} + q_l\, c_{aw})\, (T_3 - T_4) + c_{at}\, (T_4 - T_1) + \int_{T_4}^{T_1} q(p_e, T)\, c_{aw}\, dT \\ & \quad \left. + \int_{q_l}^{q_h} \phi(q)\, dq + \int_{q_l}^{q_h} L(T_{(p_e,q)})\, dq \right] \end{aligned} \tag{7.8}$$

Desorption or driving heat:

$$\begin{aligned} E_d = {} & m_{hx}\, c_{hx}\, (T_3 - T_1) \\ & + m_{at} \left[(c_{at} + q_h\, c_{aw})\, (T_2 - T_1) + c_{at}\, (T_3 - T_2) + \int_{T_2}^{T_3} q(p_c, T)\, c_{aw}\, dT \right. \\ & \quad \left. + \int_{q_l}^{q_h} \phi(q)\, dq + \int_{q_l}^{q_h} L(T_{(p_c,q)})\, dq \right] \end{aligned} \tag{7.9}$$

Condensation heat:

$$E_c = m_{at} \left[(q_h - q_l)\, L(T_c) + \int_{q_l}^{q_h} \big(T(p_c, q) - T_c\big)\, c_w(T)\, dq \right] \tag{7.10}$$

Evaporation heat:

$$E_e = m_{at}\, (q_h - q_l)\, L(T_e) \tag{7.11}$$

The COP (for cooling) and COA (for heating) for the cycle are defined as:

$$\mathrm{COP} = \frac{|E_e|}{E_d} \quad \text{and} \quad \mathrm{COA} = \frac{|E_a + E_c|}{E_d} \tag{7.12}$$

7.6 Measurements and their Assessment

7.6.1 Presentation of the Results

The measurements are performed in the way described in section 7.1. The notations of the measured cycle with its input and output energies are given in Fig. 7.4 and explained as follows:

E^{exp} Heat calculated from experimental data, i.e the integration of the heat flux over a period of time (heat flux calculated by Eq. 7.1).

E_a^{exp}	adsorption heat
E_d^{exp}	desorption or regeneration heat
E_c^{exp}	condensation heat
E_e^{exp}	evaporation heat

E^{loss} Heat loss of the system during one desorption/adsorption–sequence calculated from experimental data taking into account the sensible heat of the adsorber tank and the insulation and the convection to the ambient (derived from Eq. 7.4):

$$E^{loss} = c_{sc}\, m_{sc}\, \frac{dT_{sc}}{dt} + \rho_{is}\, V_{is}\, c_{is}\, \frac{dT_{is}}{dt} + h_{sc\rightarrow amb}\, A_{sc}\, (T_{sc} - T_{amb}) \tag{7.13}$$

E^{calc} Calculated heat considering the initial temperatures obtained from the experiment. The calculations are based on the equations given in section 7.5, regarding only the sensible heat of the heat exchanger, the working fluid and the adsorbent.
Remark: Since the convective heat loss to the ambient is not taken into account, E^{calc} must be compared with $(E^{exp} + E^{loss})$.

Δq_{exp} The concentration difference is not measured, although it was possible to measure the amount of condensate, but only very inaccurately. Hence Δq_{exp} is calculated by dividing E_c^{exp} by the latent heat of vaporization of the working fluid and the adsorbent mass.

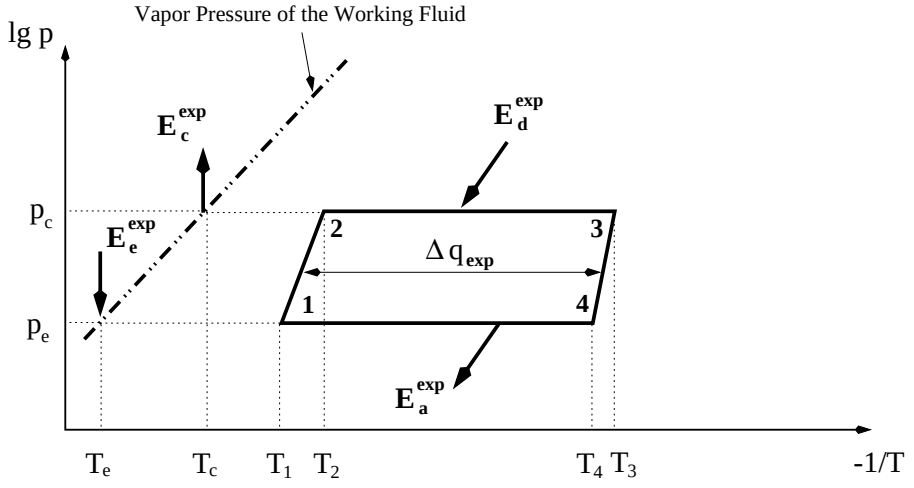

Figure 7.4: Notations for the measured cycle.

Remark 1: The evaporation heat E_e^{exp} cannot be accurately measured, because the evaporator was overdesigned and therefore reacted too sluggish. Since we are primarily interested in the COP, we set the evaporation heat E_e^{exp} approximately equal to the condensation heat E_c^{exp}, which is a rather good assumption.

Remark 2: The concentration change Δq_{exp} is not measured, but calculated. This means that there is no control about the amount of working fluid really evaporated and adsorbed, or desorbed and condensed. To weigh the evaporator before and after each evaporation would be a safe way to obtain accurate concentration data. Another way would be to measure the amount of condensate. But if parasitic condensation occurs in the tank or in its connections, and the condensate will not flow into the condenser, this measurement could be inaccurate.

Remark 3: The condenser is also overdesigned. It was observed that condensation took place on a very small fraction of the tubes compared to the overall tube length. It could be expected that the sensible heat of the tubes contributes significantly to the heat loss of the condenser, which could not be determined accurately. Therefore the heat transfer area, i.e. the area of the tubes where the working fluid condenses, which is proportional to the heat loss, is unknown.

			Silica Gel Grace 125 m = 1.47 kg				Zeolite 13X m = 1.52 kg
# of experiment			1	2	3	4	5
initial conditions	T_e (p_e)	[°C (mbar)]	7 (10)	7 (10)	7 (10)	10 (12.3)	5.5 (9)
	T_c (p_c)	[°C (mbar)]	38.4 (67.9)	43.6 (89.6)	48.1 (112.8)	43.2 (87.8)	85.1 (578.3)
	T_1	[°C]	34.7	39.8	44.8	39.7	106.2
	T_d	[°C]	118.5	118.5	122.3	115.3	272.5
	Δt_d	[min:s]	6:15	6:25	6:15	6:00	15:00
	Δt_a	[min:s]	45:20	33:10	33:20	39:10	27:16
experimental	E_d^{exp}	[kJ]	373 ±8	303 ±7	287 ±8	348 ±8	916 ±25
	E_a^{exp}	[kJ]	-301 ±31	-251 ±27	-230 ±28	-289 ±30	-734 ±36
	E_c^{exp}	[kJ]	-87 ±30	-40 ±21	-27 ±19	-82 ±29	-179 ±123
	$\mathbf{\Delta q_{exp}}$	[g/kg]	**24.6**	**11.5**	**7.7**	**23.2**	**45.2**
	COP_{exp}	[%]	0.23	0.13	0.09	0.24	0.20
	E_d^{loss}	[kJ]	-8	-8	-9	-9	-90
	E_a^{loss}	[kJ]	-49	-44	-46	-46	-100
calculated	E_d^{calc}	[kJ]	438	349	306	378	832
	E_a^{calc}	[kJ]	-432	-345	-303	-373	-821
	E_c^{calc}	[kJ]	-187	-121	-84	-154	-270
	$\mathbf{\Delta q_{calc}}$	[g/kg]	**50.7**	**32.7**	**22.7**	**41.8**	**70.1**
	COP_{calc}	[%]	0.43	0.35	0.27	0.41	0.32

Table 7.1: The tabulated results of four measurements with Silica Gel Grace 125/water and one with Zeolite 13X/water.

Table 7.1 presents four experiments with the material combination Silica Gel Grace 125/water, and one experiment with Zeolite 13X/water. These five experiments are chosen from a large number with the goal to connect the experiments 1 to 3 with 5 in order to approximate the performance of a double– or triple–effect AHP (approach see section 7.6.2).

In the first three experiments with silica gel only the heat sink temperature is varied, the most significant temperature affecting the efficiency of the proposed multi–effect cycles. Especially the experiment with zeolite was performed with a high heat sink temperature as it appears in the numerical simulations for the HT–cycle of the double– and triple–cycle presented in sections 4.2.2 and 4.1.2.

For each experiment Table 7.1 contains the energies derived from experimental data, and calculated assuming an ideal steady–state process based on a thermogravimetrically measured isosteric field. Both approaches use the initial conditions given in the head of Table 7.1.

There is a large difference between the experimentally determined concentration change Δq_{exp} and the calculated one Δq_{calc}, which is about two up to three times larger. Two reasons might be responsible for this large difference:

1. The regeneration heat determined from experiment ($E_d^{exp} + E_d^{loss}$) is in every case lower than the calculated one E_d^{calc}, which considers only equilibrium states. The experiments are performed in a way, that right after the heat exchanger reaches the given desorption temperature T_d, the heat transfer fluid is switched to cooling mode, i.e. the adsorber is not held at T_d for a while. This causes the adsorber to be in a non–equilibrium state at the end of desorption. Furthermore T_d is the mean temperature of the metallic heat exchanger. Due to the low thermal conductivity of the adsorbent a temperature drop is to be expected.

2. The high condensation temperatures of the presented experiments might favour parasitic condensation in the adsorber tank and its connection tubes to the condenser and to the pressure transducer (perhaps also in the large valve, located between the adsorber and evaporator). However, all connection tubes (not the adsorber tank) have been electrically heated above condensation temperature.

Furthermore we are able to prove from Table 7.1 that the heat loss determined through Eq. 7.13 fulfills the equation

$$|E_d^{exp} + E_d^{loss}| \approx |E_a^{exp} + E_a^{loss}| \tag{7.14}$$

in good approximation (except experiment 1). We can also state that the heat loss is nearly proportional to the sorption–period Δt, i.e.

$$\frac{\Delta t_a}{\Delta t_d} = \frac{|E_a^{loss}|}{E_d^{loss}} \tag{7.15}$$

7.6.2 Expanding the Single–Adsorber System Results to the Proposed Multi–Effect Cycles

The final goal of these experiments is to correlate them to a the triple– and double–effect adsorption heat pump cycle as presented in chapter 4.

To do so we combine the experiments 1, 2 and 3 *(silica gel)* with 5 *(zeolite)* which have nearly the same evaporation temperatures, and compare the obtained COPs ($\rightarrow \mathrm{COP}_{exp}$) with the corresponding numerical simulations based on the simple physical modelling as given in appendix A.1 and A.2, respectively ($\rightarrow \mathrm{COP}_{sim}$). For this comparison E_d^{exp} and E_a^{exp} have to be reduced by their heat losses as given in Table 7.1 and divided through their corresponding adsorbent mass. For the condensation heat E_c^{exp} a loss–factor cannot be determined.

$$\begin{aligned} e_d &= \frac{E_d^{exp} + E_d^{loss}}{m} \\ e_a &= \frac{E_a^{exp} + E_a^{loss}}{m} \\ e_c &= \frac{E_c^{exp}}{m} \approx e_e \end{aligned} \tag{7.16}$$

The specific energies $e_{d'}$, $e_{a'}$ and $e_{c'}$ are calculated in an analogous manner. Finally the COP for the **triple–effect cycle** yield to

$$\mathrm{COP} = \frac{|e_e + \frac{m'}{m}\, e_{e'}|}{e_d} \tag{7.17}$$

with its mass fraction

$$\frac{m'}{m} = \frac{|e_a + e_e|}{e_{d'}} \tag{7.18}$$

and for the **double–effect cycle** the COP is

$$\mathrm{COP} = \frac{|e_e + \frac{m'}{m}\, e_{e'}|}{e_d} \tag{7.19}$$

with its mass fraction

$$\frac{m'}{m} = \frac{|e_a|}{e_{d'}} \tag{7.20}$$

Table 7.2 presents three single–adsorber system experiment combinations which differ only by the condensation temperature of the LT–cycle $T_{c'}$ (38.4°C, 43.6°C and 48.1°C).

Comparing the experimentally determined COP_{exp} with the numerically simulated COP_{sim} we observe that COP_{exp} is for each case and both cycles significantly lower (between 40 and 50%), and its decrease with increasing condensation temperature $T_{c'}$ is smaller (see Fig. 7.5). The main reason for the lower efficiencies and mass fractions lies in the small condensation heat, especially for the silica gel measurements.

7.6.3 Characteristics of the Finned Tube Heat Exchanger

Effectiveness and Overall Heat Transfer Coefficient of the FTHX

A principal procedure for thermal analysis of a heat exchanger is the *NTU/effectiveness method*. The method involves the use of two concepts, the *heat exchanger effectiveness* ϵ and a grouping of parameters called the *number of transfer units NTU*. The heat–exchanger effectiveness is defined as

$$\epsilon = \frac{\text{actual heat transfer}}{\text{maximum possible heat transfer}}$$

exp. combination			1 + 5	2 + 5	3 + 5
$T_{c'}$ [°C] (LT–cycle)			38.4	43.6	48.1
energy/mass	e_d	[kJ/kg]	543.4	543.4	543.4
	e_a	[kJ/kg]	-548.7	-548.7	-548.7
	e_e	[kJ/kg]	-117.8	-117.8	-117.8
	$e_{d'}$	[kJ/kg]	248.3	200.7	189.1
	$e_{a'}$	[kJ/kg]	-238.1	-200.7	-187.8
	$e_{e'}$	[kJ/kg]	-49.2	-27.2	-18.4
triple–effect	COP_{exp}	[–]	0.46	0.38	0.34
	COP_{sim}	[–]	0.83	0.71	0.57
	$(\mathrm{m'/m})_{exp}$	[–]	2.7	3.3	3.5
	$(\mathrm{m'/m})_{sim}$	[–]	3.4	4.6	6.0
double–effect	COP_{exp}	[–]	0.42	0.35	0.32
	COP_{sim}	[–]	0.79	0.69	0.56
	$(\mathrm{m'/m})_{exp}$	[–]	2.2	2.7	2.9
	$(\mathrm{m'/m})_{sim}$	[–]	2.9	3.9	5.0

Table 7.2: The efficiencies of the proposed triple– and double–effect AHP's based on the single–adsorber system experimental results ($\rightarrow \mathrm{COP}_{exp}$) and those of the numerical simulation based on the initial conditions as given in Table 7.1 ($\rightarrow \mathrm{COP}_{sim}$).

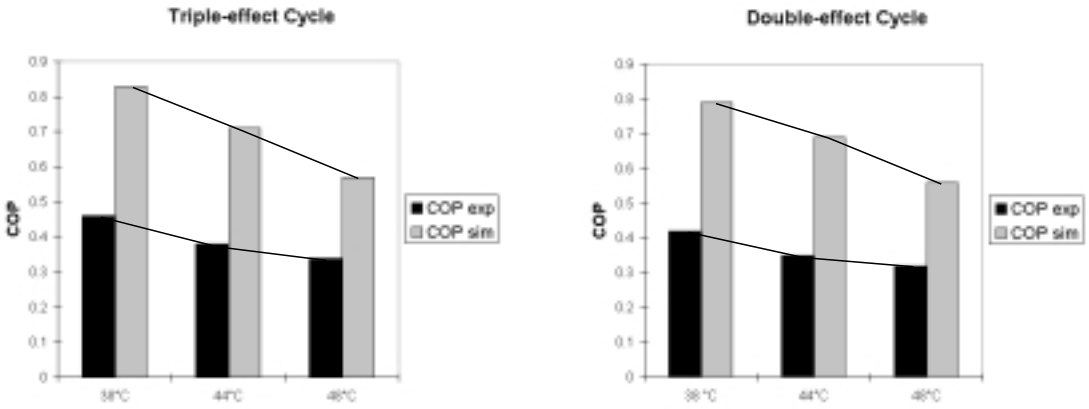

(a) (b)

Figure 7.5: Comparison of experimental and simulated COPs for (a) the triple–effect and (b) the double–effect AHP.

The actual heat transfer is the energy lost by the hot fluid or the energy gained by the cold fluid. It is the maximum possible heat transfer multiplied by the effectiveness ϵ, so that

$$\rho \dot{V} c (T_{hx}^{in} - T_{hx}) \epsilon = \rho \dot{V} c (T_{hx}^{in} - T_{hx}^{out}) \tag{7.21}$$

$$\Rightarrow \epsilon = \frac{T_{hx}^{in} - T_{hx}^{out}}{T_{hx}^{in} - T_{hx}} \tag{7.22}$$

The correlation between ϵ and NTU is

$$\epsilon = 1 - e^{-NTU} \tag{7.23}$$

with

$$NTU = \frac{U A}{\rho \dot{V} c} \tag{7.24}$$

U represents the overall heat transfer coefficient and A the exchange area or fin area, respectively.

Then,

$$U = -\ln(1 - \epsilon) \frac{\rho \dot{V} c}{A}. \tag{7.25}$$

Convection Heat Transfer of the Internal Flow

The convective heat transfer coefficient for the heat transfer between the coolant (thermal oil) and the inner surface of the exchanger tube can be calculated from the Nusselt number

$$Nu = \frac{h_{htf} d_i}{k_{htf}} \quad \Rightarrow \quad h_{htf} = Nu \frac{k_{htf}}{d_i} \tag{7.26}$$

The Nusselt number is given for fully turbulent flow ($2300 \lesssim Re \lesssim 10^6$) by the correlation [90]

$$Nu = \frac{\frac{f}{8}(Re - 1000) Pr}{1 + 12.7 \sqrt{\frac{f}{8}} (Pr^{2/3} - 1)} \left[1 + \left(\frac{d_i}{l}\right)^{2/3}\right] \tag{7.27}$$

with the friction factor

$$f = \frac{1}{(1.82 \log Re - 1.64)^2} \tag{7.28}$$

the Reynolds number is given by

$$Re = \frac{v d_i}{\nu} \tag{7.29}$$

and the Prandtl number is given by

$$Pr = \frac{\mu\, c_p}{k} = \frac{\nu}{\alpha} \tag{7.30}$$

During one desorption/adsorption–sequence with a fully developed turbulent flow in the heat exchanger tubes, the overall heat transfer coefficient of the FTHX–filled with Zeolite 13X varies between 26 and 46 $^{\mathrm{W}}/_{\mathrm{m}^2\,\mathrm{K}}$ (see Fig. 7.6). Douss et al. [16] have found for their two–adsorber unit an overall heat transfer coefficient of 18 $^{\mathrm{W}}/_{\mathrm{m}^2\,\mathrm{K}}$ or 360 $^{\mathrm{W}}/_{\mathrm{K}}$ for an area of 20 m^2.

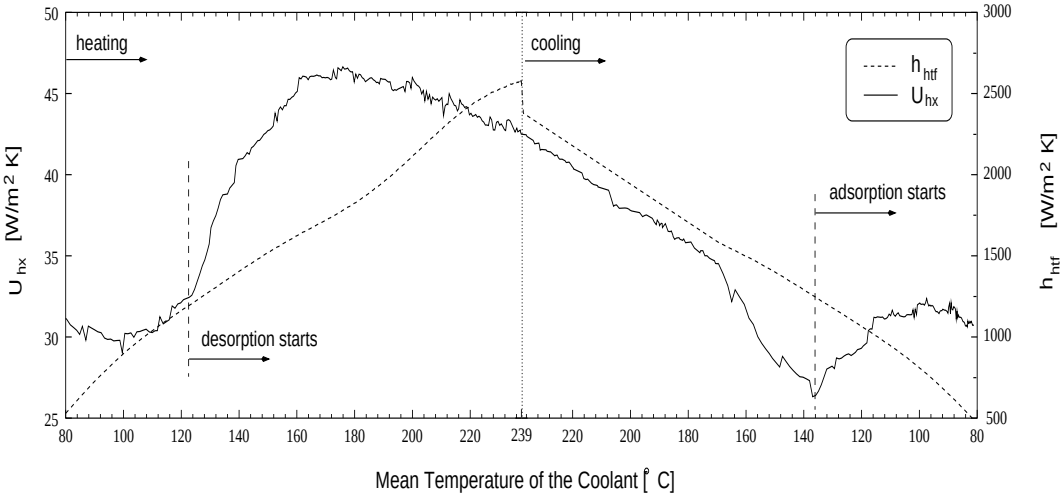

Figure 7.6: Overall heat transfer coefficient of the heat exchanger (solid line) and heat transfer coefficient of the coolant (dashed line) plotted versus the mean coolant temperature for one desorption/adsorption–sequence (Zeolite 13X and water).

Chapter 8

Conclusion

Higher efficiencies of adsorption heat pumps are mainly achieved by transferring heat and mass between multiple adsorbers. From the first part of this report we can conclude that, compared to single–adsorber heat pumps, multi–effect adsorption heat pumps have significantly higher efficiencies. Normally systems with high COPs are complicated and need a lot of special and additional components. This is true for the triple–effect AHP, but not for the double–effect AHP. The latter has only a few more components than the single–adsorber system and an equal number of sequences (see Table 5.2). Besides, the efficiency of the double–effect system is hardly smaller than that of the triple–effect system. Another advantage of the double–effect system compared to the single–effect system is the continuous heat output at the heat sink and the continuous cooling production at the evaporator.

The main purpose of building up a single–adsorber experimental facility as presented in the second part of this dissertation was to become acquainted with the new working field using adsorption process for heating and cooling established at Fraunhofer–ISE. For lack of experience and financial funds a lot of problems to fight with came up when building and operating the facility, and finally in analysing the measurements. A special problem was to detect the significant heat losses of the experimental setup, which was not completely solved. But accurate results were necessary for deriving the efficiencies of multi–effect systems from those of the single–adsorber facility.

The calculated efficiencies of the proposed multi–effect cycles indicate their suitability for low temperature residential heating systems ($\leq 50°C$). But to achieve these high COPs for real machines and to get them competitive on the market three future research goals should be reached:

- The heat transfer between the adsorptive material and the heat exchanger and the heat exchanger and the coolant, respectively, should be improved.
- To obtain a large amount of adsorption heat an adsorptive material is needed which has a large gradient of concentration change within the operating temperature range of the adsorption heat pump.
- High efficiency cycles should be simplified as far as possible using commercially available, simple and lightweight, but mechanically stable components.

Part III

Dynamic Simulations

Chapter 9

Dynamic Simulation of the Double–Effect AHP–Cycle

In this chapter the double–effect AHP–cycle is simulated dynamically with a numerical method. Important: The following numerical simulations consider the consolidated adsorbent tested and measured intensely at the *Laboratoire d'Informatique pour la Mécanique et les Sciences de l'Ingénieur* (LIMSI, France). The heat exchanger/adsorbent–combination as presented in chapter 6 is not regarded. The data for $\mathbf{q}$, $\mathbf{T}$, $\mathbf{p}$ and $\mathbf{\Delta H}$ of the adsorbent Zeolite 13X are experimental data provided by LIMSI and not the values used in the steady–state numerical simulations (chapter 4 and appendix B).

The numerical simulation program is based on a dynamic adsorption heat pump process of the double–effect cycle assuming uniform temperature, pressure and concentration for each adsorber during each time interval. Heat and mass transfer resistances are regarded. The computer program written in Pascal was developed by Jean–Jacques Guilleminot (LIMSI, France), utilized and described by Poyelle [73], and translated to C and modified to handle the double–effect cycle with two mass recoveries by the author.

9.1 Physical Model

The physical model for the double–effect cycle uses the following assumptions:

- Periodic (time–depending) heat and mass transfer.
- Adsorption equilibrium $\rightarrow q = f(p, T)$
- The adsorbent in both adsorbers is the compact composite material developed by Guilleminot et al. [33], [34], [35], [72], [73], Mauran et al. [50] and Mazet et al. [52]. This consolidated material is a homogeneous mixture composed of zeolite powder and expanded natural graphite (see Fig. 9.1).
- The consolidated adsorbents are characterized by their pressures p_{at}, $p_{at'}$, their temperatures T_{at}, $T_{at'}$ and concentrations q_{at}, $q_{at'}$.
- The mass transfer in the interior of the adsorbent is only in radial direction.
- Each adsorber tank is characterized by its temperature T_{ar} and $T_{ar'}$, respectively. The interior volume contains the heat exchanger tubes surrounded by the consolidated adsorbent, and a dead volume. The pressures of the dead volumes p_{ar}, $p_{ar'}$ are different from the pressures in the respective adsorbent matrix (p_{at}, $p_{at'}$).

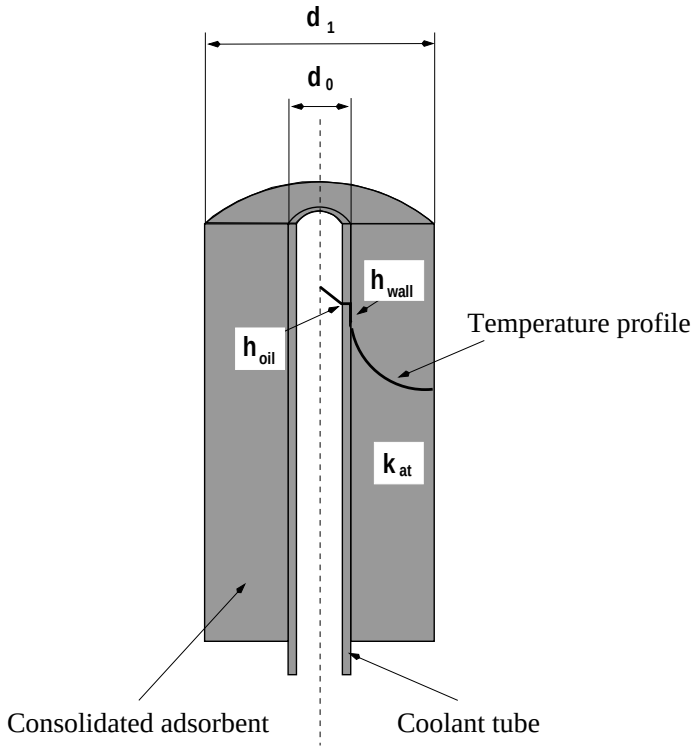

Figure 9.1: Schematic of adsorber with consolidated adsorbent.

- The evaporator and the condenser are characterized by their saturation temperatures T_e and T_c, respectively.
- All heat exchangers in the four tanks, evaporator, condenser, and two adsorbers are characterized by their coolant inlet temperatures T^{in}_{ehx}, T^{in}_{chx}, T^{in}_{hxat} and $T^{in}_{hxat'}$, and their mass flow rates $\dot{m}_{ehx}$, $\dot{m}_{chx}$, $\dot{m}_{hxat}$ and $\dot{m}_{hxat'}$.
- Each sequence is terminated by a short mass recovery between both adsorbers (see Fig. 3.5). The pressures of the dead volumes of both adsorbers equilibrate. They are calculated with the ideal gas equation:

$$p_{ar} = p_{ar'} = \frac{\Re}{M_w} \frac{m_e T_e}{V_{dv} + V_{dv'}} \tag{9.1}$$

where m_e is the vapor mass of the adsorber dead volumes $V_{dv} + V_{dv'}$.

9.2 Mathematical Description

9.2.1 Energy Conservation

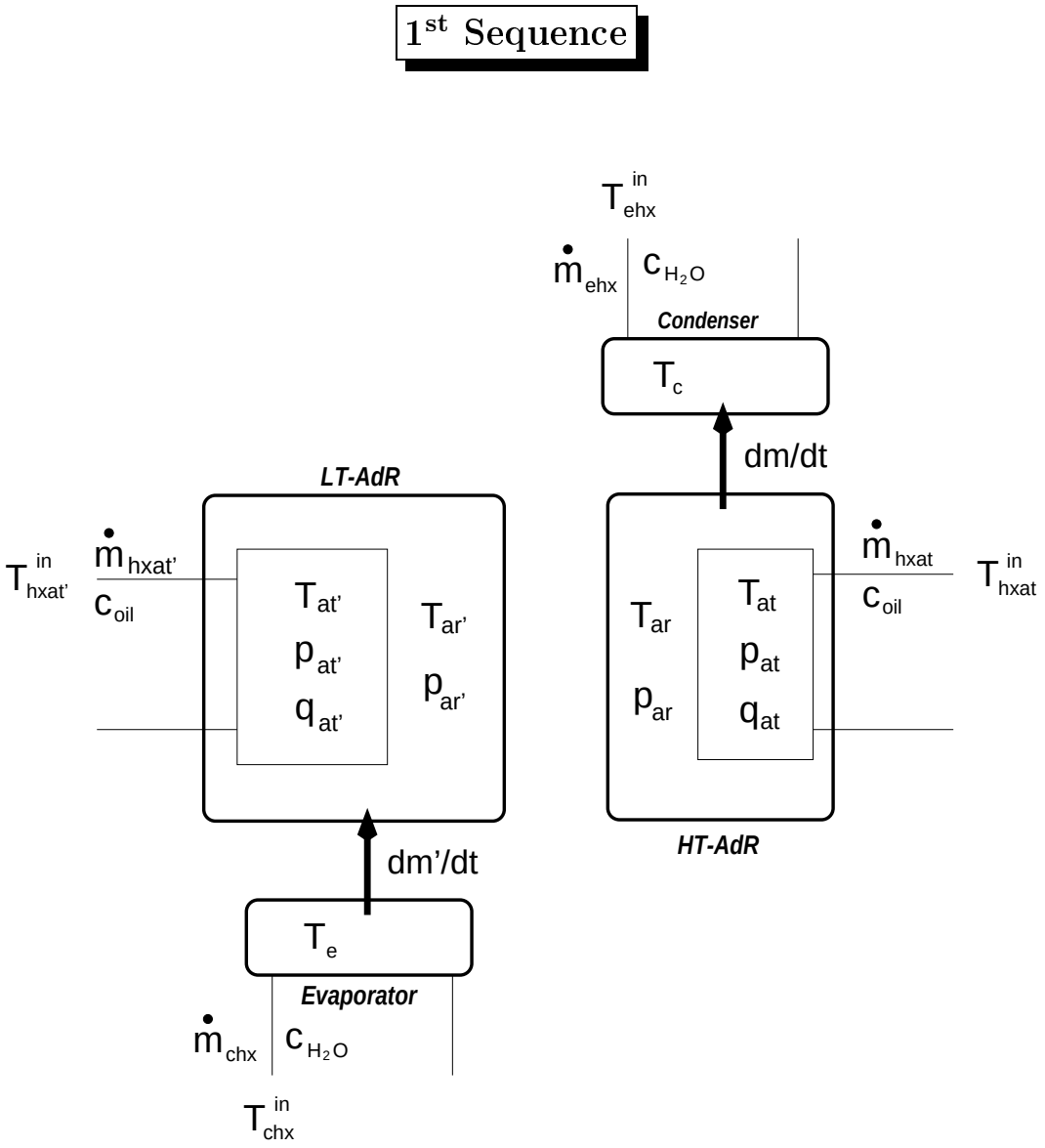

Figure 9.2: The parameters of the 1^{st} sequence.

HT–adsorbent → temperature evolution:

$$[m_{at}\, c_{at} + m_{oil}\, c_{oil} + m_{eng}\, c_{eng} + m_{hx}\, c_{hx} + m_{at}\, c_{at}\, q_{at}(T_{at}, p_{at})]\, \frac{dT_{at}}{dt} + m_{at}\, \Delta H\, \frac{dq_{at}}{dt}$$

$$= \dot{m}_{oil}\, c_{oil}\, \epsilon_{arhx}\, (T^{in}_{arhx} - T_{at}) + H_{ar}\, (T_{ar} - T_{at}) \quad (9.2)$$

with the heat exchanger effectiveness of a fully developed turbulent flow in smooth tubes, developed by Petukhov [66], also published by Holman [38] (empirical relation)

$$\epsilon_{arhx} = 1 - exp\left(-\frac{U_{arhx}\, A_{arhx}}{\dot{m}_{oil}\, c_{oil}}\right) \tag{9.3}$$

$$\frac{1}{U_{arhx}} = \frac{1}{h_{at}} + \frac{d_0 - 2\,\Delta r}{d_0\, h_{oil}} \tag{9.4}$$

$$\frac{1}{h_{at}} = \frac{1}{h_{wall}} + \frac{a}{1-a^2}\left[\frac{1+a^2}{4} + \left(\frac{\ln\left(\frac{1}{a}\right)}{1-a^2} - 1\right)\right]\frac{d_0}{2\,k_{at}} \quad \text{(Poyelle et al. [72])} \tag{9.5}$$

$$a = \frac{d_0}{d_1} \tag{9.6}$$

$$h_{oil} = Nu\,\frac{k_{oil}}{d_{hx}} \tag{9.7}$$

$$Nu = \frac{(f/8)\,Re\,Pr}{1.07 + 12.7\,\sqrt{f/8}\,(Pr^{2/3} - 1)} \tag{9.8}$$

$$f = \frac{1}{(1.82\,\log Re - 1.64)^2} \tag{9.9}$$

LT–adsorbent → temperature evolution:

$$\left[m_{at'}\, c_{at'} + m_{oil}\, c_{oil} + m_{eng}\, c_{eng} + m_{hx}\, c_{hx} + m_{at'}\, c_{at'}\, q_{at'}(T_{at'}, p_{at'})\right]\frac{dT_{at'}}{dt} + m_{at'}\,\Delta H\,\frac{dq_{at'}}{dt}$$
$$= \dot{m}_{oil}\, c_{oil}\, \epsilon_{arhx'}\,(T^{in}_{arhx'} - T_{at'}) + H_{ar'}\,(T_{ar'} - T_{at'}) \tag{9.10}$$

with the heat exchanger effectiveness $\epsilon_{arhx'} = \epsilon_{arhx}$, if the same adsorbent is used in the LT–adsorber, else the parameter corresponding to the LT–adsorbent must be replaced in Eqs. 9.3 till 9.7.

HT–heat exchanger → inlet temperature evolution:

$$m_{oil}\, c_{oil}\,\frac{dT^{in}_{arhx}}{dt} = P_z \tag{9.11}$$

LT–heat exchanger → inlet temperature evolution:

$$\frac{dT^{in}_{arhx'}}{dt} = 0 \quad \Rightarrow \quad T^{in}_{arhx'} = \text{const.} \tag{9.12}$$

HT–adsorber → temperature evolution:

$$m_{ar}\, c_{ar}\,\frac{dT_{ar}}{dt} = H_{ar}\,(T_{at} - T_{ar}) + H_{loss}\,(T_{amb} - T_{ar}) \tag{9.13}$$

LT–adsorber → temperature evolution:

$$m_{ar'}\, c_{ar'}\,\frac{dT_{ar'}}{dt} = H_{ar'}\,(T_{at'} - T_{ar'}) + H_{loss}\,(T_{amb} - T_{ar'}) \tag{9.14}$$

Evaporator (connected to LT–adsorber) → temperature evolution:

$$m_e\, c_w\, \frac{dT_e}{dt} = \dot{m}_{H_2O}\, c_{H_2O}\, \epsilon_{ehx}\, (T_{ehx}^{in} - T_e) + m'\, \frac{dq_{at'}}{dt}\, \left[L(T_e) - c_w\, (T_c - T_e)\right] \tag{9.15}$$

with the heat exchanger effectiveness

$$\epsilon_{ehx} = 1 - exp\left(-\frac{U_{ehx}\, A_{ehx}}{\dot{m}_{H_2O}\, c_{H_2O}}\right) \tag{9.16}$$

$$U_{ehx} = \frac{Nu\, k_{H_2O}}{d_{ehx}} \tag{9.17}$$

$$Nu = Re^{0.6}\, Pr^{0.36} \tag{9.18}$$

$$Re = \frac{\rho_{H_2O}\, v_{max}\, d_{ehx}}{\mu} \tag{9.19}$$

Condenser (connected to HT–adsorber) → temperature evolution:

$$m_c\, c_w\, \frac{dT_c}{dt} = \dot{m}_{H_2O}\, c_{H_2O}\, \epsilon_{chx}\, (T_{chx}^{in} - T_c) + m\, \frac{dq_{at}}{dt}\, L(T_c) \tag{9.20}$$

with the heat exchanger effectiveness

$$\epsilon_{chx} = 1 - exp\left(-\frac{U_{chx}\, A_{chx}}{\dot{m}_{H_2O}\, c_{H_2O}}\right) \tag{9.21}$$

$$U_{chx} = \frac{Nu\, k_{H_2O}}{d_{chx}} \tag{9.22}$$

$$Nu = 0.023\, \frac{4\, \dot{m}_{H_2O}}{\pi\, d_{chx}\, \mu_{H_2O}} \tag{9.23}$$

2nd Sequence

For the 2^{nd} sequence, the heat recovery sequence, only the equations determining both adsorber heat exchanger coolant temperatures are different from the 1^{st} sequence:

HT–heat exchanger → inlet temperature evolution: (Douss et al. [16])

$$m_{oil}\, c_{oil}\, \frac{dT_{arhx}^{in}}{dt} = \dot{m}_{oil}\, c_{oil}\, \left[\epsilon_{arhx}\, T_{at} + \epsilon_{arhx'}\, (1.0 - \epsilon_{arhx})\, T_{at'} - (\epsilon_{arhx} + \epsilon_{arhx'}(1.0 - \epsilon_{arhx}))\, dT_{arhx}^{in}\right] \tag{9.24}$$

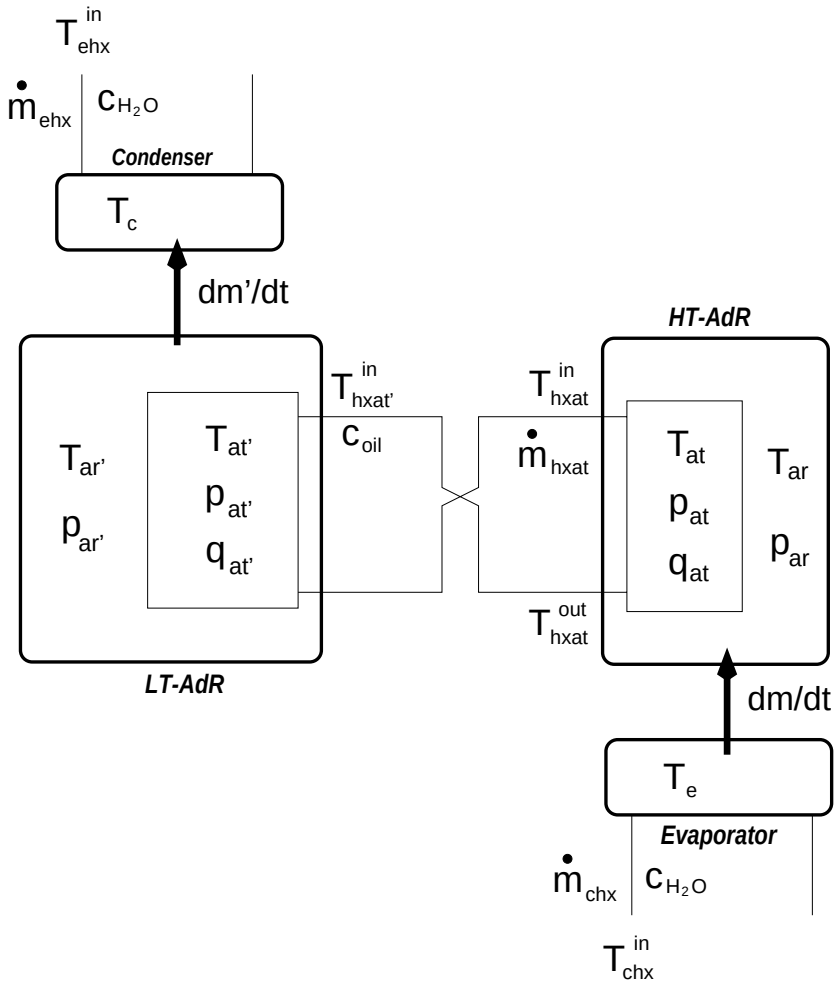

Figure 9.3: The parameters of the 2^{nd} sequence.

LT–heat exchanger → inlet temperature for each time interval:

We assume that the outlet temperature of the HT–adsorber T^{out}_{hxat} which can be expressed in terms of its inlet temperature T^{in}_{hxat} is equal to the inlet temperature of the LT–adsorber $T^{in}_{hxat'}$.

$$T^{in}_{arhx'} = T^{out}_{arhx} = T^{in}_{arhx} + \epsilon_{arhx}\,(T_{at} - T^{in}_{arhx}) \tag{9.25}$$

with the heat exchanger effectiveness ϵ_{hxat} as calculated by Eq. 9.3.

Evaporator (connected to HT–adsorber) → temperature evolution:

$$m_e\,c_w\,\frac{dT_e}{dt} = \dot{m}_{H_2O}\,c_{H_2O}\,\epsilon_{ehx}\,(T^{in}_{ehx} - T_e) + m\,\frac{dq_{at}}{dt}\,[L(T_e) - c_w\,(T_c - T_e)] \tag{9.26}$$

Condenser (connected to LT–adsorber) → temperature evolution:

$$m_c\,c_w\,\frac{dT_c}{dt} = \dot{m}_{H_2O}\,c_{H_2O}\,\epsilon_{chx}\,(T^{in}_{chx} - T_c) + m'\,\frac{dq_{at'}}{dt}\,L(T_c) \tag{9.27}$$

The heat exchanger effectivenesses ϵ_{ehx} and ϵ_{chx} are expressed by Eq. 9.16 and Eq. 9.21, respectively.

9.2.2 Mass Conservation

The mass conservation of each adsorber is expressed by

$$\varepsilon \frac{\partial c_c}{\partial t} + \rho_{at} \frac{\partial q}{\partial t} = -\nabla \cdot \mathbf{J} \tag{9.28}$$

with the mass transfer flux

$$\mathbf{J} = c_c \, \mathbf{v} - D \, \nabla c \tag{9.29}$$

The creeping flow $\mathbf{v}$ through a porous media can be described by *Darcy's Law* employing the permeability K:

$$\mathbf{v} = -\frac{K}{\mu} \nabla p_{at} \tag{9.30}$$

The pressure inside the adsorbent bed p_{at} as well as the temperature T_{at} and the concentration q_{at} are calculated using the *Theory of Dubinin* as given by Poyelle [73]. The pressure p_{ar} in the dead space of each adsorber which is different from p_{at} is calculated by the ideal gas equation during the isosteric phases

$$p_{ar} = c_c \frac{\Re}{M_w} T \tag{9.31}$$

During the evaporation or condensation phase, p_{at} becomes equal to the saturation pressure p_s of the working fluid.

9.2.3 Efficiency

The COP for the double–effect cycle (see section 4.2.2) is defined as sum of the evaporation heat divided by the driving heat of the HT–cycle. Since we take heat losses into account, the driving heat E_z is not only the sensible heat of adsorbent and working fluid and the latent heat of adsorption, but additionally consists of heat losses due to the adsorber, the tubes and the heat transfer fluid.

$$\mathrm{COP} = \frac{|E_{e'} + E_e|}{E_z} \tag{9.32}$$

with the energies E summarized over the simulation time

$$E_{e'} = \sum_t m' \, L(T_e) \, \left(q'(t) - q'(t + \Delta t) \right) \tag{9.33}$$

$$E_e = \sum_t m \, L(T_e) \, \left(q(t) - q(t + \Delta t) \right) \tag{9.34}$$

$$\begin{aligned} E_z = \sum_t \Bigg[& \underbrace{m \, c_{sens} \, \left(T_{at}(t + \Delta t) - T_{at}(t) \right) - m \, \Delta H \, \left(q(t + \Delta t) - q(t) \right)}_{\text{sensible heat and latent heat of adsorption}} \\ & + \underbrace{m_{oil} \, c_{oil} \, \left(T^{in}_{hxat}(t + \Delta t) - T^{in}_{hxat}(t) \right)}_{\text{sensible heat of adsorber heat transfer fluid}} \\ & + \underbrace{m_{hx} \, c_{hx} \, \left(T_{at}(t + \Delta t) - T_{at}(t) \right) \Bigg]}_{\text{sensible heat of heat exchanger tubes}} \\ & + \underbrace{H_{loss} \, \left(T_{ar}(t) - T_{amb}(t) \right) \, dt}_{\text{heat loss of adsorber to ambient}} \end{aligned} \tag{9.35}$$

The term $(m\,c_{sens})$ summarizes the capacitive masses of the consolidated adsorbent

$$(m\,c_{sens}) = m_{at}\,c_{at} + m_{oil}\,c_{oil} + m_{eng}\,c_{eng} + m_{hx}\,c_{hx} + m_{at}\,c_{at}\,q_{at}(T_{at}, p_{at})$$

9.3 Numerical Solver

The method for numerically integrating ordinary differential equations of the type $y' = f(x, y)$ as given in § 9.2 is the predictor–corrector method of Gear–Nordsiek.

9.4 Initial Conditions

Adsorber	
adsorbent in both adsorbers	Zeolite 13X powder mixed with expanded natural graphite as composite
specific heat capacity of both adsorbers c_{ar}, $c_{ar'}$	836 $^{\mathrm{J}}/_{\mathrm{kg\,K}}$
specific heat capacity of heat exchanger tubes c_{hx}	460 $^{\mathrm{J}}/_{\mathrm{kg\,K}}$
heat loss of the tank H_{loss}	1.6 $^{\mathrm{W}}/_{\mathrm{K}}$
convective heat loss H_{ar}, $H_{ar'}$	8 $^{\mathrm{W}}/_{\mathrm{K}}$
dead volume of each adsorber V_{dv}	20 l
Oil Heat Exchanger	
heat loss of the oil circuit H_{oil}	2 $^{\mathrm{W}}/_{\mathrm{K}}$
heat transfer coefficient of the thermal oil h_{oil}	1800 $^{\mathrm{W}}/_{\mathrm{m^2\,K}}$
mass flow rate of thermal oil $\dot{m}_{oil}$	3 $^{\mathrm{m^3}}/_{\mathrm{h}}$
Consolidated Adsorbent	
specific heat capacity of expanded natural graphite c_{eng}	950 $^{\mathrm{J}}/_{\mathrm{kg\,K}}$
permeability K	1.3×10^{-12} $\mathrm{m^2}$
diffusivity D	3.0×10^{-4} $^{\mathrm{m^2}}/_{\mathrm{s}}$
thermal conductivity k	5 $^{\mathrm{W}}/_{\mathrm{m\,K}}$
wall heat transfer coefficient h_{wall} for cooling	500 $^{\mathrm{W}}/_{\mathrm{m^2\,K}}$
wall heat transfer coefficient h_{wall} for heating	1000 $^{\mathrm{W}}/_{\mathrm{m^2\,K}}$
latent heat of adsorption ΔH	3×10^{6} $^{\mathrm{J}}/_{\mathrm{kg}}$
internal diameter d_0	16 mm
external diameter d_1	42 mm
Evaporator	
coolant	water
$m_e \cdot c_e$	16744 $^{\mathrm{J}}/_{\mathrm{K}}$
$\dot{m}_{H_2O} \cdot c_e$	2209 $^{\mathrm{W}}/_{\mathrm{K}}$
Condenser	
coolant	water
$m_c \cdot c_c$	4186 $^{\mathrm{J}}/_{\mathrm{K}}$

$\dot{m}_{H_2O} \cdot c_c$	2791 $^{W}/_{K}$
Additional Parameters	
power of the external heater P_z	4000 W
working fluid	water
Cyle Parameters	
mass of HT–adsorbent m_{at}	6 kg
mass of LT–adsorbent $m_{at'}$	8 kg
evaporation temperature T_e	6°C
condensation temperature T_c	42°C
maximum desorption temperature T_{max}	200°C
inlet temperature of LT–adsorber heat exchanger during 1^{st} sequence $T^{in}_{hxat'}$	42°C
period of the 1^{st} sequence without mass–recovery	1800 s
period of mass–recovery	60 s

The heat recovery sequence (2^{nd} sequence) is not limited by a fixed period, but is terminated when the temperatures of the adsorbents T_{at} and $T_{at'}$ equilibrate, i.e the temperature difference $|T_{at} - T_{at'}|$ becomes lower than 1.0 K.

9.5 Simulation Results

The evolution of the adsorbent temperatures T_{at}, $T_{at'}$, the inlet heat transfer fluid temperatures of the heat exchangers T^{in}_{arhx}, $T^{in}_{arhx'}$, and the pressures p_{at}, $p_{at'}$ with time for the initial data listed in the previous section is shown in Fig. 9.4. The first sequence period is 1860 seconds including the mass recovery, and one complete cycle is about 4700 seconds (1h:18m) long. The inlet heat transfer fluid temperatures of both heat exchangers are treated as follows:

1^{nd} Sequence: T^{in}_{arhx} follows Eq. 9.11 while $T^{in}_{arhx'}$ is held constant on the initial condensation temperature T_c (here: 42°C).

2^{nd} Sequence: At the very beginning of the heat recovery we assumed that the inlet of the HT–exchanger will be provided by the outlet temperature of the LT–exchanger which will be at the end of the first sequence a little higher than the condensation temperature T_c, and calculated through

$$T^{in}_{arhx} = T^{out}_{arhx'} = T^{in}_{arhx'} + \epsilon_{arhx'} \left(T_{at'} - T^{in}_{arhx'}\right) \tag{9.36}$$

For this simulation T^{in}_{arhx} will become about 44°C. So T^{in}_{arhx} will drop from final desorption temperature of 200°C down to 44°C. That is what we can observe at time 1900 seconds. Finally $T^{in}_{arhx'}$ is calculated by Eq. 9.25, and starts here at 114°C. The equilibrium temperature T_1 or $T_{3'}$, respectively, finishing the heat recovery sequence, is 104°C.

The shown cycle has a COP of 0.48. The mass of working fluid pumped in the HT–cycle is 450 g and in the LT–cycle 280 g water.

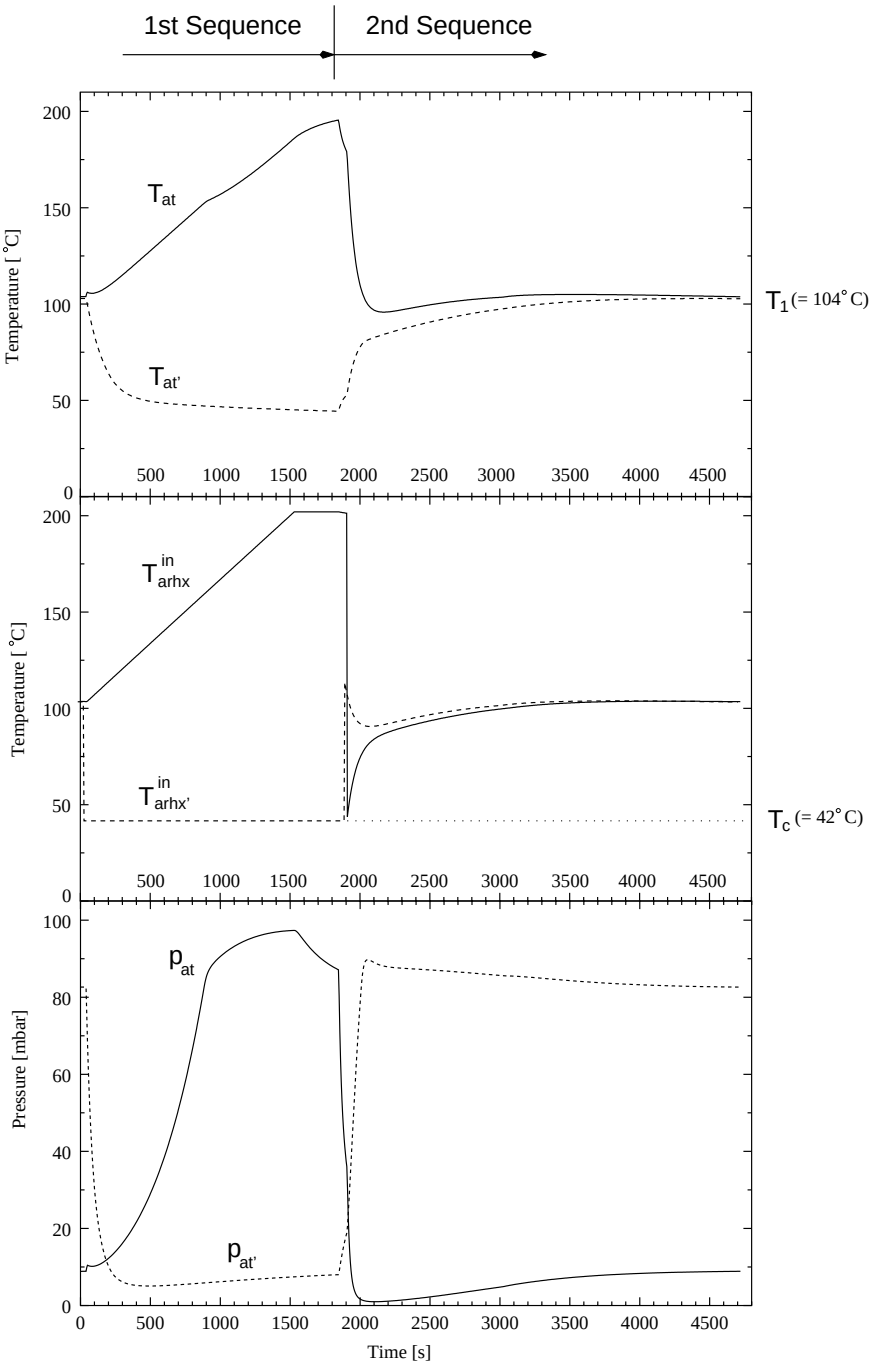

Figure 9.4: Temperature and pressure evolution in both adsorbers during one complete cycle with two mass recoveries.

In Fig. 9.5 the LT– and HT–cycles are depicted in a Clapeyron–diagram.

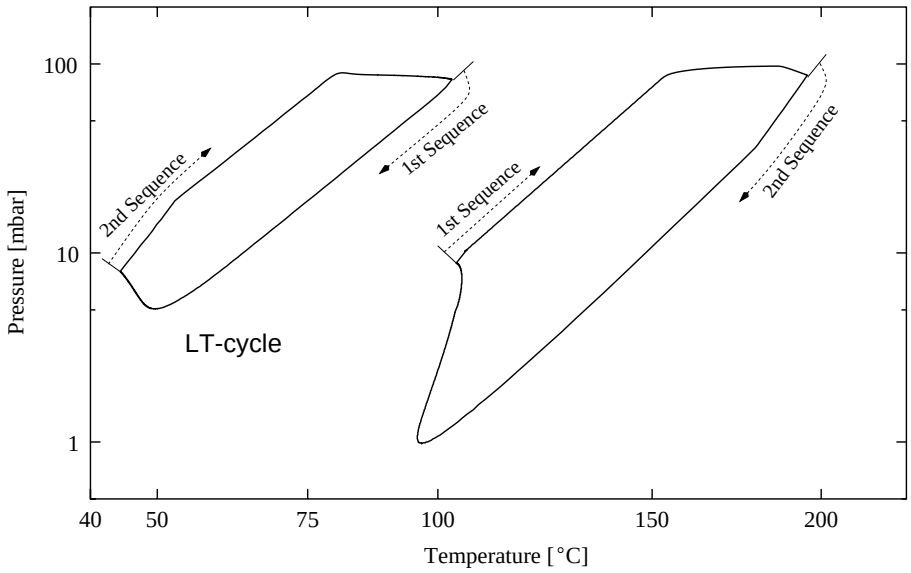

Figure 9.5: The cycle of Fig. 9.4 plotted in a Clapeyron-diagram.

9.5.1 Influence of the Evaporation Temperature on COP

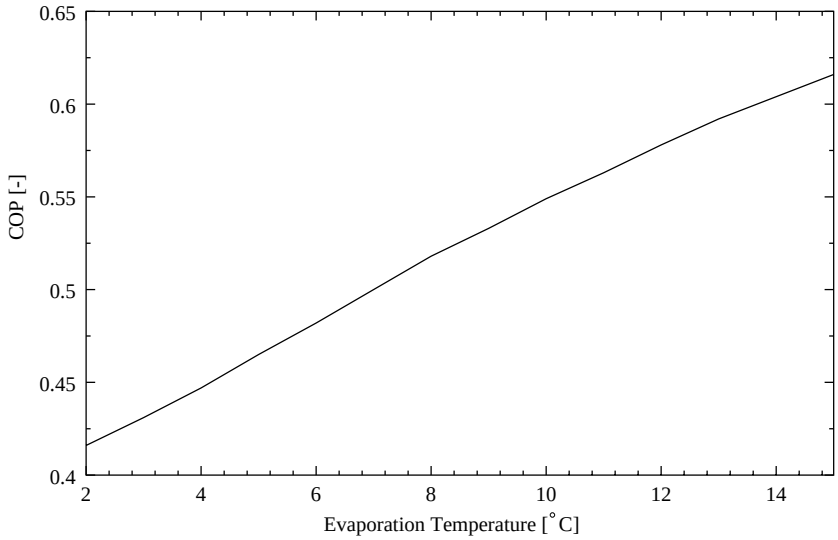

Figure 9.6: COP as function of the evaporation temperature.

In Fig. 9.6 the evaporation temperature (remaining equal for both cycles) is varied from 2°C up to 15°C. The other parameters as given in section 9.4 are left unchanged. The COP varies between 0.42 and 0.62.

9.5.2 Influence of the Condensation Temperature on COP

In Fig. 9.7 the COP is plotted against the condensation temperature (heat sink temperature) which was changed from 30° up to 65°C. The other parameters as given in section 9.4 are left unchanged.

The COP is decreasing approximately linearly from 0.63 down to 0.18.

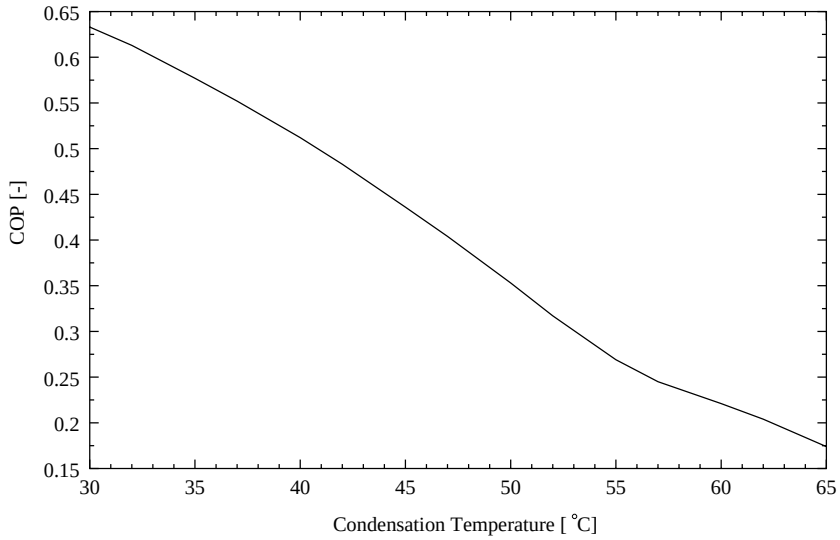

Figure 9.7: COP as function of the condensation temperature.

9.5.3 Influence of the HT–Regeneration Temperature on COP

Comparing Fig. 9.8 with Fig. 4.18 we recognize a very similar behaviour of the COP depending from the maximum desorption temperature of the HT–cycle. The COP–curve starts with a steep gradient before the it remains constant with increasing temperature. The maximum COP for the dynamic simulation of 0.49 is reached at a temperature of about 220°C.

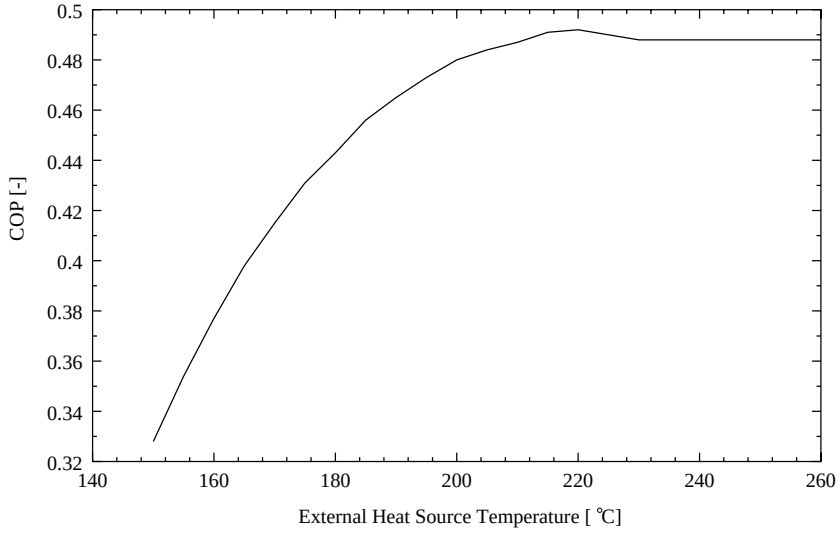

Figure 9.8: COP as function of the HT–cycle regeneration temperature.

9.5.4 Influence of the Adsorbent Mass Fraction on COP and Cycle Shape

For Fig. 9.9 and the table below we simulated the COP for three different mass fractions, keeping all initial conditions of section 9.4 constant, but changing the HT–adsorbent mass from 1.5 kg to 3 kg and up to 6 kg (LT–adsorbent mass = 8 kg). It is obvious that decreasing the HT–adsorbent mass contracts the LT–cycle because the HT–cycle releases less latent heat of adsorption, although the HT–cycle will be widened. Since the maximum desorption temperature is fix, enlarging the HT–cycle causes the decrease of T_1. Although the temperature swing from T_3 down to T_1 during the adsorbing phase is larger, the period of heat recovery decreases instead of increasing because the period is mainly determined by the lower mass of the HT–adsorbent. The COP will be doubled by enlarging the HT–adsorbent mass four times.

m'/m [–]	5.33	2.67	1.33
time for heat recovery [s]	1750	2070	2820
cycled mass HT [g]	127	249	447
cycled mass LT [g]	43	153	278
T_1 [°C]	80	92	104
COP	0.24	0.39	0.48

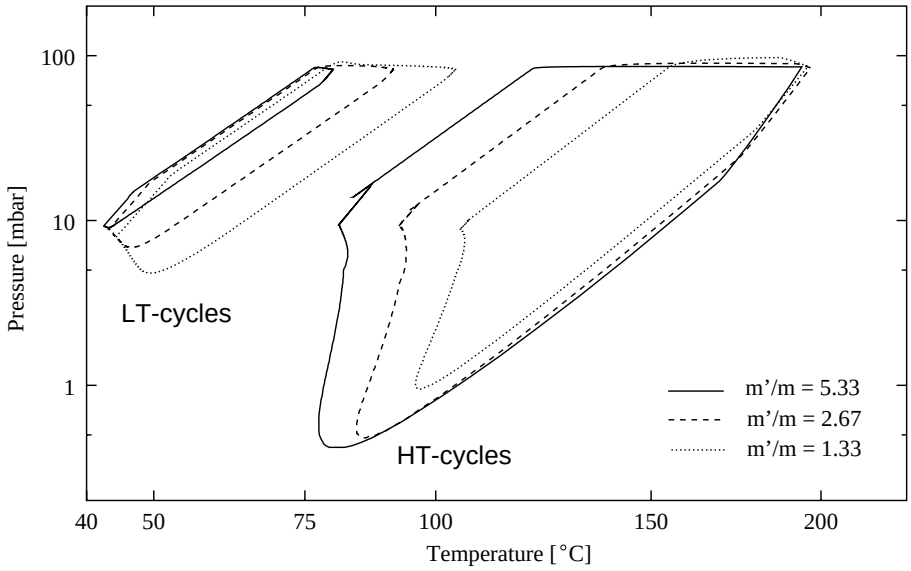

Figure 9.9: LT–cycle and HT–cycle for three mass fractions plotted in a Clapeyron-diagram.

9.5.5 Influence of the Permeability on COP

Increasing the permeability about ten times has only a small effect on COP, viz. increase by about 6%.

K $[m^2]$	1.3×10^{-12}	6.5×10^{-12}	1.3×10^{-11}
cycled mass HT [g]	447	461	468
cycled mass LT [g]	278	297	311
COP	0.48	0.50	0.51

9.5.6 Influence of the Heat Transfer Parameters on COP

Since a consolidated adsorbent with higher heat transfer coefficients is tested at LIMSI (France), Poyelle [73] suggested to enlarge the thermal conductivity k from 5 to 20 $^{W}/_{m\,K}$, and the wall heat transfer coefficient h_{wall} for heating and cooling up to 3500 $^{W}/_{m^2\,K}$ (experimentally obtained value with thermal oil). The other parameters are left constant as given in section 9.4. The table below presents the COPs and cycled masses for two different permeabilities and four different adsorbent diameters. The values typed in boldface represent the simulation results based on the heat transfer coefficients (1000 and 500 $^{W}/_{m^2\,K}$) and thermal conductivity (5 $^{W}/_{m\,K}$) as given in section 9.4 and used for all earlier simulations.

permeability	$\mathbf{K = 1.3 \times 10^{-12}}$ m^2					$\mathbf{K = 1.3 \times 10^{-11}}$ m^2				
external diameter d_1 [mm]	**42**	42	60	80	100	**42**	42	60	80	100
cycled mass HT [g]	**447**	485	447	425	415	**468**	501	478	471	446
cycled mass LT [g]	**278**	389	246	233	190	**311**	425	303	292	200
COP [%]	**0.48**	0.57	0.44	0.32	0.19	**0.51**	0.59	0.49	0.39	0.27

Comparison of the COPs for $d_1 = 42\ mm$ shows that the larger heat transfer coefficients and thermal conductivity increase the COP by about 19% and 16%.

Furthermore we can observe a strong COP decrease with increasing adsorbent diameter. Doubling the diameter from 42 mm to 80 mm will reduce the COP by about 33%, but rising the permeabilitiy to $K = 1.3 \times 10^{-11}\ m^2$ reduces this amount to 24%.

9.6 Conclusion

The numerical dynamic adsorption heat pump process simulations of the double–effect AHP–cycle with two mass recoveries as proposed in Fig. 3.5 have been performed successfully with obtaining credible results. For these simulations the well measured consolidated adsorbent was regarded instead of the FTHX filled with adsorbent (presented in chapter 6) because the required properties, such as permeability, diffusivity, specific heat capacity, etc., were known and available. Therefore the results are not quantitatively comparable with the results obtained by the steady–state simulations, as presented in chapter 4. But the influence of the evaporation and regeneration temperature on the COP are very similar to the steady–state simulations. The condensation temperature, however, has a much weaker influence on the COP than predicted by the steady–state simulations. Furthermore the dynamic simulations show that the COP is also strongly influenced by the mass fraction of the two adsorbents and the heat transfer parameters, especially the thermal conductivity of the adsorbent and the wall heat transfer coefficient between adsorbent and heat exchanger.

Bibliography

[1] Abdallah, K; Grenier, Ph.; Sun, L.M.; Meunier, F.: Nonisothermal adsorption of water by synthetic NaX zeolite pellets, *Chemical Engineering Science*, Vol. 43, No. 10 (1988), pp. 2633–2643

[2] Adamson, A.W.: *Physical chemistry of surfaces*, John Wiley & Sons, Inc., 1976, Chap. 14

[3] Alefeld, G.; Radermacher, R.: *Heat conversion systems*, CRC Press, Inc., 1994

[4] Ben Amar, N.; Sun, L.M.; Meunier, F.: Pressure and thermal fronts propagation in adsorbers, *Proceedings of Solid Sorption Refrigeration Symposium, Paris, France* (1992), pp. 64–73

[5] Ben Amar, N.; Sun, L.M.; Meunier, F.: Numerical analysis of adsorptive temperature wave regenerative heat pump, *Applied Thermal Engineering*, Vol. 16, No. 5 (1996), pp. 405–418

[6] Bering, B.P.; Dubinin, M.M.; Serpinsky, V.V.: Theory of volume filling for vapor adsorption, *Journal of Colloid and Interface Science*, **21** (1966), pp. 378–393

[7] Bjurström, H.; Karawack, E.; Carlsson, B.: Thermal conductivity of a microporous particulate medium: moist silica gel, *Int. J. Heat Mass Transfer*, Vol. 27, No. 11 (1984), pp. 2025–2036

[8] Blüh, O.; Stark, N.: *Die Adsorption*, Friedr. Vieweg Verlag, 1929

[9] Breck, D.W.: *Zeolite molecular sieves*, John Wiley & Sons, Inc., 1974

[10] Brunauer, S.; Emmett, P.H.; Teller, E.: *J. Am. Chem. Soc.*, **60** (1938), 309

[11] Critoph, R.E.: A forced convection regenerative cycle using the ammonia–carbon pair, *Proceedings of Solid Sorption Refrigeration Symposium, Paris, France* (1992), pp. 80–85

[12] Critoph, R.E.: Gas–fired air conditioning using a carbon–ammonia convective thermal wave cycle, *Proceedings International Ab–Sorption Heat Pump Conference, Montreal, Canada* (1996), pp. 353–360

[13] Critoph, R.E.: Forced convection adsorption cycles, *Applied Thermal Engineering*, Vol. 18, (1998), pp. 799–807

[14] Dehouche, Z.; de Jong, W.; Willers, E.; Isselhorst, A.; Groll, M.: Modelling and simulation of heating/air–conditioning systems using the thermal wave cascade concept, *Applied Thermal Engineering*, Vol. 18, No. 6 (1998), pp. 457–480

[15] Delgado, R.; Choisier, A.; Grenier, Ph.; Ismail, I.; Meunier, F.; Pons, M.: Etude du cycle intermittent charbon actif–méthanol en vue de la réalisation d'une machine à frabiquer de la glace fonctionnant à l'énergie solaire, *Proceedings of IIF Meeting, Jerusalem* (1982), pp. 181–187

[16] Douss, N.; Meunier, F.; Sun, L.M.: Predictive model and experimental results for a two–adsorber solid adsorption heat pump, *Ind. Eng. Chem. Res.*, Vol. 27, No. 2 (1988), pp. 310–316

[17] Douss, N.; Abdallah, K.; Grenier, Ph.; Guilleminot, J.J.; Gurgel, J.; Sun, L.M.; Sahnoune, H.; Meunier, F.: *Dynamic study of solid adsorption heat pumps: Experimental and numerical simulation; Economic analysis for development*, CNRS, Contract# EN3E–00097–F, 1989

[18] Douss, N.; Meunier, F.: Effect of operating temperatures on the coefficient of performance of active carbon methanol systems, *Journal Heat Recovery Systems & CHP*, Vol. 8–5 (1989), pp. 383–392

[19] Douss, N.; Meunier, F.: Experimental study of cascading adsorption cycles, *Chemical Engineering Science*, Vol. 44 (1989), pp. 225–235

[20] Dubinin, M.M.: Theory of the physical adsorption of gases and vapors and adsorption properties of adsorbents of various natures and porous structures, *Bulletin of the Division of Chemical Sciences* (1960), pp. 1072–1078

[21] Dubinin, M.M.: Adsorption in micropores, *Journal of Colloid and Interface Science*, **23** (1967), pp. 487–499

[22] Dubinin, M.M.; Astakhov, V.A.: Description of adsorption equilibria of vapors on zeolites over wide ranges of temperature and pressure, *Advances in Chemistry, Series 102* (1971), pp. 69–85

[23] Fowler, R.H.: *Proc. Camb. Phil. Soc.*, **31** (1935), 260

[24] Fowler, R.H.; Guggenheim, E.H.: *Statistical thermodynamics*, Cambridge University Press, 1952

[25] Fuller, T.A.; Wepfer, W.J.; Shelton, S.V.; Miles, D.J.: A two–temperature model of the regenerative solid–vapor heat pump, *J. Energy Res. Technol., Trans. ASME*, **116** (1994), pp. 297–304

[26] Goosens, M.; Mittelbach, F.; Samarin, A.: *The LaTeX companion*, Addison–Wesley Publishing Company, 1994

[27] Goosens, M.; Rahtz, S.; Mittelbach, F.: *The LaTeX graphics companion*, Addison–Wesley Publishing Company, 1997

[28] Grenier, P.; Guilleminot, J.J.; Meunier, F.; Pons, M.: Solar powered solid adsorption cold store, *Journal of Solar Energy Engineering*, Vol. 110 (1988), pp. 192–197

[29] Groll, M.: Reaction beds for dry sorption machines, *Proceedings of Solid Sorption Refrigeration Symposium, Paris, France* (1992), pp. 207–214

[30] Guilleminot, J.J.; Meunier, F.; Mischler, B.: Etude de cycles intermittents à adsorption solide pour la réfrigération solaire, *Rev. Phys. Appl.*, Vol. 15 (1980), pp. 441–452

[31] Guilleminot, J.J.; Meunier, F., Pakleza, J.: Heat and mass transfer in a non–isothermal fixed bed solid adsorbent reactor: a uniform pressure non–uniform temperature case, *Int. J. Heat Mass Transfer*, Vol. 30 (1987), pp. 1595–1606

[32] Guilleminot, J.J.; Choisir, A.; Chalfen, J.B.; Nicolas, S.; Reymonet, J.L.: Heat transfer intensification in fixed bed adsorbers, *Proceedings of Solid Sorption Refrigeration Symposium, Paris, France* (1992), pp. 215–220

[33] Guilleminot, J.J.; Choisir, A.; Chalfen, J.B.; Nicolas, S.; Reymonet, J.L.: Amélioration des transferts thermiques dans les adsorbeurs à lits fixes consolidés, *Journal Heat Recovery Systems & CHP*, Vol. 13, No. 4 (1993), pp. 297–300

[34] Guilleminot, J.J.; Chalfen, J.B.; Choisir, A.: Heat and mass transfer characteristics of composites for adsorption heat pumps, *International Absorption Heat Pump Conference*, ASME, AES–31 (1993), pp. 401–406

[35] Guilleminot, J.J.; Chalfen, J.B.; Poyelle, F.: Transferts de mass et de chaleur dans les composites adsorbants consolides. Influence sur les performances d'une pompe à chaleur à adsorption solide., *19th International Congress of Refrigeration*, 1995, pp. 261–268

[36] Guilleminot, J.J.; Poyelle, F.; Meunier, F.: La climatisation par adsorption, *Revue générale de Thermique*, Janvier–Février (1995), pp. 34–39

[37] Haar, L.; Gallagher, J.S.; Kell, George S.: *NBS/NRC Wasserdampftafeln*, Springer Verlag, 1988

[38] Holman, J.P.: *Heat transfer*, McGraw–Hill Book Company, Inc., 1990

[39] Hückel, E.: *Adsorption und Kapillarkondensation*, Akademische Verlagsgesellschaft mbH, 1928

[40] Irvine Jr., Thomas F.; Liley, Peter E.: *Steam and gas tables with computer equations*, Academic Press, Inc., 1984

[41] Jones, J.: Sorption refrigeration research at JPL/NASA, *Heat Recovery Systems and CHP*, **13** (1193), pp. 363–372

[42] Kärger, J.; Ruthven, D.M.: *Diffusion in zeolites and other microporous solids*, John Wiley & Sons, Inc., 1992

[43] Kast, W.: *Adsorption aus der Gasphase*, VCH Verlagsgesellschaft, 1988

[44] Kernighan, B.W.; Ritchie, D.M.: *Programmieren in C*, Carl Hanser Verlag, 1990

[45] Kerr, G.T.: Synthetic zeolites, *Scientific American*, No. 7 (1989), pp. 82–87

[46] Lacher, I.: *Proc. Roy. Soc.*, **A161** (1937), 525

[47] Langmuir, I.: *J. Amer. Chem. Soc.*, **40** (1918), 1361

[48] Lävemann, E.; Hessel, H.E.; Schneewind, R.; Khelifa, N.; Sizmann,R., : *Energiespeicherung in absorptiven Systemen, Anwendung zur Klimatisierung*, Ludwig–Maximilians–Universität München, 1988

[49] Lindon, T.: *Heat transfer*, Prentice Hall, Inc, 1993

[50] Mauran, S.; Prades, P.; L'Haridon, F.: Transfert de chaleur et de masse en milieux réactifs consolidés pour systèmes thermochimiques, *Proceedings Symposium Le froid par adsorption solide, Paris* (1992), pp. 239–244

[51] Mauran, S.; Prades, P.; L'Haridon, F.: Heat and mass transfer in consolidated reacting beds for thermochemical systems, *Heat Recovery Systems*, **13**, (1993), pp. 315–319

[52] Mazet, N.; Meyer, P.; Neveu, P.; Spinner, B.: Concept and study of a double effect refrigeration machine based on the sorption of solid ammonia gas and controlled by heat pipes, *Proceedings International Absorption Heat Pump Conference, New York* (1993), pp. 407–412

[53] Meunier, F.: Utilisation des cycles à sorption pour la production de froid par l'énergie solaire, *Cahier de l'AFEDES*, no. 5 (1978), pp. 57–67

[54] Meunier, F.: Second law analysis of a solid adsorption heat pump operating on reversible cascade cycles:application to the zeolite–water pair, *J. Heat Recovery Systems*, Vol. 5 , No. 2 (1985), pp. 133–141

[55] Meunier, F.: Theoretical performances of solid adsorbent cascading cycles using the zeolite–water and active carbon–methanol pairs: Four case studies, *J. Heat Recovery Systems*, Vol. 5 (1986), pp. 491–498

[56] Meunier, F.: Thermal swing adsorption refrigeration (heat pump), *Separation Technology.*, Vol. 3, July (1963), pp. 143–150

[57] Meunier, F.: Solid Sorption: an alternative to CFC's, *Journal Heat Recovery Systems & CHP*, Vol. 13 (1993), pp. 289–295

[58] Meunier, F.: Sorption solar cooling, *Renewable Energy*, Vol. 5, Part I (1994), pp. 622–629

[59] Meunier, F.; Poyelle, F.; LeVan, M.D.: Entropic analysis of regenerative adsorptive refrigeration cycles, *5th International Conference Fundamentals of Adsorption*, Pacific Grove, California (1995), pp. 627–634

[60] Meunier, F.; Kaushik, S.C.; Neveu, P.; Poyelle, F.: A comparative thermodynamic study of sorption systems: second law analysis, *Int. J. Refrig.*, Vol. 19, No. 6 (1996), pp. 414–421

[61] Meunier, F.; Poyelle, F.; LeVan, M.D.: Second–law analysis of adsorptive refrigeration cycles: The role of thermal coupling entropy production, *Applied Thermal Engineering*, Vol. 17, No. 1 (1997), pp. 43–55

[62] Meunier, F.: Solid sorption heat powered cycles for cooling and heat pumping applications, *Applied Thermal Engineering*, Vol. 18, (1998), pp. 715–729

[63] Meyer; C.A.: Thermodynamic and transport properties of steam : comprising tables and charts for steam and water; calculated using the 1967 IFC Formulation for Industrial Use; in conformity with the 1963 International Skeleton Tables as adopted by the 6. International Conference on the Properties of Steam, *American Soc. of Mechanical Engineers ASME*, 1993

[64] Miles, D.J.; Shelton, S.V.: Coupled heat transfer and thermodynamic adsorption heat pump analysis, *Heat Pump Design, Analysis and Application* (1991), pp. 33–38, ASME

[65] Miles, D.J.; Sanborn, D.M.; Nowakowski, G.A.; Shelton, S.V.: Gas fired sorption heat pump development, *Proceedings of Solid Sorption Refrigeration Symposium, Paris, France* (1992), pp. 74–79

[66] Petukhov, B.S.: Heat transfer and friction in turbulent pipe flow with variable physical properties, in J.P. Hatnett and T.F. Irvine, (eds.), *Advances in Heat Transfer*, Academic Press, Inc., pp. 504–664, 1970

[67] Pons, M.: Global analysis of adsorption cycles with thermal regeneration, *Proceedings International Ab–Sorption Heat Pump Conference, Montreal, Canada* (1996), pp. 153–160

[68] Pons, M.: Optimized internal vapour transports for adsorption cycles with thermal regeneration, *Proceedings International Ab–Sorption Heat Pump Conference, Montreal, Canada* (1996), pp. 421–428

[69] Pons, M.; Laurent, D.; Meunier, F.: Experimental temperature fronts for adsorptive heat pump applications, *Applied Thermal Engineering*, Vol. 16, No. 5 (1996), pp. 395–404

[70] Pons, M.: Second law analysis of adsorption cycles with thermal regeneration, *Journal of Energy Resources Technology*, Vol. 118 (1997), pp. 229–236

[71] Pons, M.: Analysis of the adsorption cycle with thermal regeneration based on the entropic mean temperatures, *Applied Thermal Engineering*, Vol. 17, No. 7 (1997), pp. 615–627

[72] Poyelle, F.; Guilleminot, J.J.; Meunier, F.: Analytical study of a gas–fired adsorptive air–conditioning system, *ASHRAE Transaction*, **102**, Part I (1996)

[73] Poyelle, F.: *Etude des systèmes énergétiques à adsorption modulés en température – application à la réfrigération*, Thèse de Doctorat, Université de Paris XI, Orsay, 1996

[74] Press, W.H.; Flannery, B.P.; Teukolsky, S.A.; Vetterling, W.T.: *Numerical recipes in C*, Cambridge University Press, 1994

[75] Puppe, L.: Zeolites – properties and practical applications, *Chemie in unserer Zeit*, Vol. 20, No. 4 (1986), pp. 117–127

[76] Recknagel; Sprenger; Schramek: *Taschenbuch für Heizung und Klimatechnik 94/95*, R. Oldenbourg Verlag, 1994

[77] Reid, R.C.; Prausnitz, J.M.; Poling, B.E.: *The properties of gases and liquids*, McGraw–Hill Book Company, 1986

[78] Rockenfeller, U.; Kirol, L.; Sarkisian, P.; Ryan, W.: Advanced heat pump staging for complex compound chemi–sorption systems, *Proceedings of Solid Sorption Refrigeration Symposium, Paris, France* (1992), pp. 153–159

[79] Rudzinski, W.; Everett, D.H.: *Adsorption of gases on heterogeneous surfaces*, Academic Press, Inc., 1992

[80] Ruthven, D.M.: *Principles of adsorption and adsorption processes*, John Wiley & Sons, 1984

[81] Saha, B.B.; Kashiwagi, T.: Performance evaluation of advanced adsorption cycle driven by near–environmental temperature waste heat–comparison with conventional cycle, *Proceedings International Ab–Sorption Heat Pump Conference, Montreal, Canada* (1996), pp. 277–284

[82] Sahnoune, H.; Grenier, P.H.: Mesure de la conductivité thermique d'une zéolithe, *The Chemical Engineering Journal*, Vol. 40 (1989), pp. 45–54

[83] Shelton, S.V.: Residential space conditioning with solid sorption technology, *Heat Recovery Systems and CHP*, **13** (1993), pp. 353–361

[84] Shelton, S.V.; Wepfer, W.J.; Miles, D.J.: Ramp wave analysis of the solid vapor heat pump, *J. Energy Res. Technol., Trans. ASME*, **112** (1990), pp. 69–78

[85] Sun, L.M.; Ben Amar, N.; Meunier, F.: Numerical study on coupled heat and mass transfers in an adsorber with external fluid heating, *Journal Heat Recovery Systems & CHP*, Vol. 15, No. 1 (1995), pp. 19–29

[86] Sun, L.M.; Ben Amar, N.; Meunier, F.: Numerical investigation of adsorptive heat pump systems with thermal wave heat regeneration under uniform–pressure conditions, *Int. J. Heat Mass Transfer*, Vol. 40, No. 2 (1995), pp. 281–293

[87] Suzuki, M.: *Adsorption engineering*, Kodansha LTD and Elsevier Science Publishers, 1990

[88] Tchernev, D.I.: Solar refrigeration utilizing zeolites *14th Inter. Conv. Eng. Conf., Amer. Chem. Soc.* (1979), pp. 2070

[89] Vargaftik, N.B.: *Handbook of physical properties of liquids and gases*, Hemisphere Publishing Corporation, 1975

[90] VDI: *VDI–Wärmeatlas*, VDI–Verlag GmbH, 1991

[91] Völkl, J.: Heat conduction in zeolite beds, *7th International Heat Transfer Conference*, Munich (1982), pp. 105–107

[92] Yanagi, H.; Komatu, F.; Ino, N.: Prototype test of adsorption refrigerator using silicagel–water pairs, *Proceedings of Solid Sorption Refrigeration Symposium, Paris, France* (1992), pp. 100–105

[93] Yang, R.T.: *Gas separation by adsorption processes*, Butterworths Publishers, 1987

[94] Zanife, T.; Meunier, F.: Experimental results of a zeolite–water heat pump installed in a slaughter house, *Journal Heat Recovery Systems & CHP*, Vol. 12–2 (1992), pp. 131–142

[95] Zheng, W.; Worek, W.M.; Nowakowski, G.: Effect of design and operating parameters on the performance of two–bed sorption heat pump systems, *J. Energy Res. Technol., Trans. ASME*, **117** (1995), pp. 67–74

[96] Zheng, W.; Worek, W.M.; Nowakowski, G.: Performance of multi–bed sorption heat pump systems, *International Journal of Energy Research*, Vol. 20 (1996), pp. 339–350

Part IV

Appendices

Appendix A

Mathematical Concepts

A.1 Mathematical Formulation of the Efficiency of the Two–Stage Triple–Effect Adsorption Cycle

The simplified numerical simulation program which approximates the efficiency of the two–stage triple–effect adsorption heat pump considers a steady–state adsorption heat pump process *(assuming uniform temperatures, pressures and concentrations)* taking into account the sensible heats of the liquid and adsorbed working fluid and the adsorbents, the latent heat of adsorption ΔH and furthermore the sensible heat of a copper heat exchanger assuming a mass ratio of two units exchanger mass per unit adsorbent mass ($\rightarrow\ 2\,c_{hx}\,\Delta T$). This mass ratio was realized by the finned tube heat exchanger presented in § 6.1. But no heat transfer coefficients are regarded. The thermodynamic cycles are assumed as ideal *(isobaric, isosteric and adiabatic processes)*.

The latent heat of adsorption ΔH is used in these equations in a slightly uncommon way, because it is not assumed as constant value, but composed of the latent heat of vaporization L of the working fluid and the binding energy ϕ. The binding energy ϕ is the amount which results from the intermolecular forces, and is here expressed in terms of the concentration q (see appendix B.1, Eq. B.17). The latent heat of vaporization of the working fluid L is calculated in dependence of the temperature T which is a function of concentration q and pressure p.

Adsorption heat of HT–adsorbent:

$$
\begin{aligned}
e_a = \quad & \underbrace{2\,c_{hx}\,(T_3 - T_1)}_{\text{sensible heat of heat exchanger}} \\
& \underbrace{+\int_{q_l}^{q_h} \big(T_e - T(p_e, q)\big)\, c_w(T)\, dq}_{\text{sensible heat of working fluid}} \\
& \underbrace{+(c_{at} + q_l\, c_{aw})\,(T_3 - T_4) + c_{at}\,(T_4 - T_1) + \int_{T_4}^{T_1} q(p_e, T)\, c_{aw}\, dT}_{\text{sensible heat of adsorbent and adsorbed working fluid}} \\
& \underbrace{+\int_{q_l}^{q_h} \phi(q)\, dq + \int_{q_a}^{q_r} L(T_{(p_e,q)})\, dq}_{\text{latent heat of adsorption}}
\end{aligned}
\tag{A.1}
$$

Desorption heat for HT–adsorbent (provided by an external heat source):

$$\begin{aligned} e_z = & \underbrace{2\,c_{hx}\,(T_5 - T_1)}_{\text{sensible heat of heat exchanger}} \\ & \underbrace{+(c_{at} + q_h\,c_{aw})\,(T_2 - T_1) + c_{at}\,(T_5 - T_2) + \int_{T_2}^{T_5} q(p,T)\,c_{aw}\,dT}_{\text{sensible heat of adsorbent and adsorbed working fluid}} \\ & \underbrace{+\int_{q_3}^{q_h} \phi(q)\,dq + \int_{q_3}^{q_h} L(T_{(p,q)})\,dq + \int_{q_l}^{q_3} \phi(q)\,dq + \int_{q_l}^{q_3} L(T_{(p,q)})\,dq}_{\text{latent heat of adsorption}} \end{aligned} \tag{A.2}$$

Evaporation heat while adsorbing HT–adsorbent:

$$e_e = \underbrace{(q_h - q_l)\,L(T_e)}_{\text{latent heat of working fluid}} \tag{A.3}$$

Condensation heat transferred to LT–adsorbent while desorbing HT–adsorbent:

$$e_c = \underbrace{\int_{q_l}^{q_h} L(T_{(p,q)})\,dq}_{\text{latent heat of working fluid}} + \underbrace{\int_{q_l}^{q_h} \big(T(p,q) - T_c\big)\,c_w(T)\,dq}_{\text{sensible heat of working fluid}} \tag{A.4}$$

Condensation heat transferred to heat sink while desorbing HT–adsorbent (isothermal desorption):

$$e_c^{5\to 3} = \underbrace{\int_{q_l}^{q_3} L(T_s)\,dq}_{\text{latent heat of working fluid}} + \underbrace{\int_{q_l}^{q_3} \big(T_3 - T_s(p_{s(T_3,q_3)}) - T_c\big)\,c_w(T_s)\,dq + \int_{T_{1'}}^{T_c} c_w(T)\,dT}_{\text{sensible heat of working fluid}} \tag{A.5}$$

Adsorption heat of LT–adsorbent:

$$\begin{aligned} e_{a'} = & \underbrace{2\,c_{hx}\,(T_{3'} - T_{1'})}_{\text{sensible heat of heat exchanger}} \\ & \underbrace{+\int_{q_{l'}}^{q_{h'}} \big(T_e - T(p_e,q)\big)\,c_w(T)\,dq}_{\text{sensible heat of working fluid}} \\ & \underbrace{+(c_{a'} + q_{l'}\,c_{aw})\,(T_{3'} - T_{4'}) + c_{a'}\,(T_{4'} - T_{1'}) + \int_{T_{4'}}^{T_{1'}} q(p_e,T)\,c_{aw}\,dT}_{\text{sensible heat of adsorbent and adsorbed working fluid}} \\ & \underbrace{+\int_{q_{l'}}^{q_{h'}} \phi(q)\,dq + \int_{q_{l'}}^{q_{h'}} L(T_{(p_e,q)})\,dq}_{\text{latent heat of adsorption}} \end{aligned} \tag{A.6}$$

Desorption heat for LT–adsorbent:

$$
\begin{aligned}
e_{d'} = \quad & \underbrace{2\,c_{hx}\,(T_{3'} - T_{1'})}_{\text{sensible heat of heat exchanger}} \\
& \underbrace{+(c_{a'} + q_{h'}\,c_{aw})\,(T_{2'} - T_{1'}) + c_{a'}\,(T_{3'} - T_{2'}) + \int_{T_{2'}}^{T_{3'}} q(p_{c'}, T)\,c_{aw}\,dT}_{\text{sensible heat of adsorbent and adsorbed working fluid}} \\
& \underbrace{+ \int_{q_{l'}}^{q_{h'}} \phi(q)\,dq + \int_{q_{l'}}^{q_{h'}} L(T_{(p_{c'},q)})\,dq}_{\text{latent heat of adsorption}}
\end{aligned}
\tag{A.7}
$$

Evaporation heat while adsorbing LT–adsorbent:

$$
e_{e'} = \quad \underbrace{(q_{h'} - q_{l'})\,L(T_e)}_{\text{latent heat of working fluid}} \tag{A.8}
$$

Condensation heat while desorbing LT–adsorbent:

$$
e_{c'} = \quad \underbrace{(q_{h'} - q_{l'})\,L(T_{c'})}_{\text{latent heat of working fluid}} \quad + \underbrace{\int_{q_{l'}}^{q_{h'}} \big(T(p_{c'}, q) - T_{c'}\big)\,c_w(T)\,dq}_{\text{sensible heat of working fluid}} \tag{A.9}
$$

The mass fraction of both adsorbents $^{\mathrm{m'}}/_{\mathrm{m}}$ is expressed through the energy conservation of both interacting cycles, viz. that the adsorption plus the condensation heat of the HT–cycle should be equal to the necessary desorption heat of the LT–cycle.

$$
m\,|e_a + e_c| = m'\,e_{d'} \quad \Rightarrow \quad \frac{m'}{m} = \frac{|e_a + e_c|}{e_{d'}} \tag{A.10}
$$

The efficiency of the adsorption heat pump is expressed by the COP *(Coefficient of Performance)* and the COA *(Coefficient of Amplification)* which are defined as:

$$
\underbrace{\mathrm{COP} = \frac{\text{refrigeration}}{\text{net work}} = \frac{|e_e + \frac{m'}{m}\,e_{e'}|}{e_z}}_{\text{used for cooling}} \quad \text{and} \quad \underbrace{\mathrm{COA} = \frac{\text{heat out}}{\text{net work}} = \frac{|\frac{m'}{m}\,(e_{a'} + e_{c'}) + e_c^{5\to 3}|}{e_z}}_{\text{used for heating}} \tag{A.11}
$$

We are able to express both efficiencies COP and COA independent of the mass fraction, and only in terms of the efficiency of each individual cycle. For the approach we insert Eq. A.10 in Eqs. A.11 and assume that $|e_a| \approx e_z$ and $e_c \approx e_e$, then we receive

$$\mathrm{COP} = \frac{\left| e_e + \dfrac{e_z + e_e}{e_{d'}}\, e_{e'} \right|}{e_z} = \frac{|e_e|}{e_z} + \frac{|e_{e'}|}{e_{d'}}\,\frac{|e_z + e_e|}{e_z} = \underbrace{\frac{|e_e|}{e_z}}_{\mathrm{COP}_{HT}} + \underbrace{\frac{|e_{e'}|}{e_{d'}}}_{\mathrm{COP}_{LT}} \left(1 + \underbrace{\frac{|e_e|}{e_z}}_{\mathrm{COP}_{HT}}\right)$$

$$= \mathrm{COP}_{HT} + \mathrm{COP}_{LT}\,(1 + \mathrm{COP}_{HT}) \tag{A.12}$$

and

$$\mathrm{COA} = \frac{\dfrac{|e_z + e_e|}{e_{d'}}\,|e_{a'} + e_{c'}| + |e_c^{5\to 3}|}{e_z} = \frac{|e_{a'} + e_{c'}|}{e_{d'}} + \frac{|e_e\,(e_{a'} + e_{c'})|}{e_{d'}\,e_z} + \frac{e_c^{5\to 3}}{e_z}$$

$$= \underbrace{\frac{|e_{a'} + e_{c'}|}{e_{d'}}}_{\mathrm{COA}_{LT}} \left(1 + \underbrace{\frac{|e_e|}{e_z}}_{\mathrm{COP}_{HT}}\right) + \underbrace{\frac{|e_c^{5\to 3}|}{e_z}}_{\mathrm{COA}_{HT}} \tag{A.13}$$

$$= \mathrm{COA}_{LT}\,(1 + \mathrm{COP}_{HT}) + \mathrm{COA}_{HT}$$

The simulation program is based on the energy conservations which are calculated independently from each other. This fact makes it necessary to check if the condensation heat of the HT–cycle with its maximum temperature T_c is equal to the heat released from desorption of LT–adsorbent until T_c was reached multiplied by the mass fraction.

$$|e_c(T_c)| = \frac{m'}{m} e_{d'}(T_c) \tag{A.14}$$

A.2 Mathematical Formulation of the Efficiency of the Single–Stage Double–Effect Adsorption Cycle

The equations for the single–stage double–effect adsorption heat pump are based on the same assumptions as for the two–staged triple–effect system, see section A.1. Since the following equations are nearly identical with those in section A.1 no detailed descriptions are given.

Adsorption heat of HT–adsorbent:

$$\begin{aligned} e_a =& \, 2\, c_{hx}\,(T_3 - T_1) \\ &+ \int_{q_l}^{q_h} \big(T_e - T(p_e, q)\big)\, c_w(T)\, dq \\ &+ (c_{at} + q_l\, c_{aw})\,(T_3 - T_4) + c_{at}\,(T_4 - T_1) + \int_{T_4}^{T_1} q(p_e, T)\, c_{aw}\, dT \\ &+ \int_{q_l}^{q_h} \phi(q)\, dq + \int_{q_a}^{q_r} L(T_{(p_e,q)})\, dq \end{aligned} \tag{A.15}$$

Desorption heat for HT–adsorbent (provided by an external heat source):

$$\begin{aligned} e_z =& \, 2\, c_{hx}\, (T_3 - T_1) \\ &+ (c_{at} + q_h\, c_{aw})\, (T_2 - T_1) + c_{at}\, (T_3 - T_2) + \int_{T_2}^{T_3} q(p,T)\, c_{aw}\, dT \\ &+ \int_{q_l}^{q_h} \phi(q)\, dq + \int_{q_l}^{q_h} L(T_{(p,q)})\, dq \end{aligned} \tag{A.16}$$

Evaporation heat while adsorbing HT–adsorbent:

$$e_e = (q_h - q_l)\, L(T_e) \tag{A.17}$$

Condensation heat of HT–adsorbent:

$$e_c = \int_{q_l}^{q_h} L(T_{(p,q)})\, dq + \int_{q_l}^{q_h} \big(T(p,q) - T_c\big)\, c_w(T)\, dq \tag{A.18}$$

Adsorption heat of LT–adsorbent:

$$\begin{aligned} e_{a'} =& \, 2\, c_{hx}\, (T_{3'} - T_{1'}) \\ &+ \int_{q_{l'}}^{q_{h'}} \big(T_e - T(p_e,q)\big)\, c_w(T)\, dq \\ &+ (c_{at'} + q_{l'}\, c_{aw})\, (T_{3'} - T_{4'}) + c_{at'}\, (T_{4'} - T_{1'}) + \int_{T_{4'}}^{T_{1'}} q(p_e,T)\, c_{aw}\, dT \\ &+ \int_{q_{l'}}^{q_{h'}} \phi(q)\, dq + \int_{q_{l'}}^{q_{h'}} L(T_{(p_e,q)})\, dq \end{aligned} \tag{A.19}$$

Desorption heat for LT–adsorbent:

$$\begin{aligned} e_{d'} =& \, 2\, c_{hx}\, (T_{3'} - T_{1'}) \\ &+ (c_{at'} + q_{h'}\, c_{aw})\, (T_{2'} - T_{1'}) + c_{at'}\, (T_{3'} - T_{2'}) + \int_{T_{2'}}^{T_{3'}} q(p_c,T)\, c_{aw}\, dT \\ &+ \int_{q_{l'}}^{q_{h'}} \phi(q)\, dq + \int_{q_{l'}}^{q_{h'}} L(T_{(p_c,q)})\, dq \end{aligned} \tag{A.20}$$

Evaporation heat while adsorbing LT–adsorbent:

$$e_{e'} = (q_{h'} - q_{l'})\, L(T_e) \tag{A.21}$$

Condensation heat while desorbing LT–adsorbent:

$$e_{c'} = (q_{h'} - q_{l'})\, L(T_c) + \int_{q_{l'}}^{q_{h'}} \big(T(p_c, q) - T_c\big)\, c_w(T)\, dq \tag{A.22}$$

The mass fraction of both adsorbents $^{\mathrm{m'}}/_{\mathrm{m}}$ is expressed by the energy conservation of both interacting cycles, viz. that the adsorption plus the condensation heat of the HT–cycle should be equal to the necessary desorption heat of the LT–cycle.

$$m\,|e_a| = m'\, e_{d'} \quad \Rightarrow \quad \frac{m'}{m} = \frac{|e_a|}{e_{d'}} \tag{A.23}$$

The efficiency of the adsorption heat pump is expressed by the COP *(Coefficient of Performance)* and the COA *(Coefficient of Amplification)* which are defined as:

$$\mathrm{COP} = \frac{\text{refrigeration}}{\text{net work}} = \frac{|e_e + \frac{m'}{m}\, e_{e'}|}{e_z} \quad \text{and} \quad \mathrm{COA} = \frac{\text{heat out}}{\text{net work}} = \frac{|\frac{m'}{m}\,(e_{a'} + e_{c'}) + e_c|}{e_z} \tag{A.24}$$

used for cooling — used for heating

Both Eqs. A.24 can be expressed independent of the mass fraction and in the form that the COP (COA) is equal to the sum of the COPs (COAs) of each individual cycle, $\mathrm{COP} = \mathrm{COP}_{LT} + \mathrm{COP}_{HT}$ ($\mathrm{COA} = \mathrm{COA}_{LT} + \mathrm{COA}_{HT}$). Inserting Eq. A.23 in Eqs. A.24 and assuming $|e_a| \approx e_z$, we receive

$$\mathrm{COP} = \frac{|e_e + \frac{e_a}{e_{d'}}\, e_{e'}|}{e_z} = \underbrace{\frac{|e_{e'}|}{e_{d'}}}_{\mathrm{COP}_{LT}} + \underbrace{\frac{|e_e|}{e_z}}_{\mathrm{COP}_{HT}} \tag{A.25}$$

and

$$\mathrm{COA} = \frac{\frac{e_a}{e_{d'}}\,|e_{a'} + e_{c'}| + |e_c|}{e_z} = \underbrace{\frac{|e_{a'} + e_{c'}|}{e_{d'}}}_{\mathrm{COP}_{LT}} + \underbrace{\frac{|e_c|}{e_z}}_{\mathrm{COP}_{HT}} \tag{A.26}$$

Appendix B

The Thermogravimetrical Measurement Device

B.1 Thermogravimetrical Measurements and their Assessment

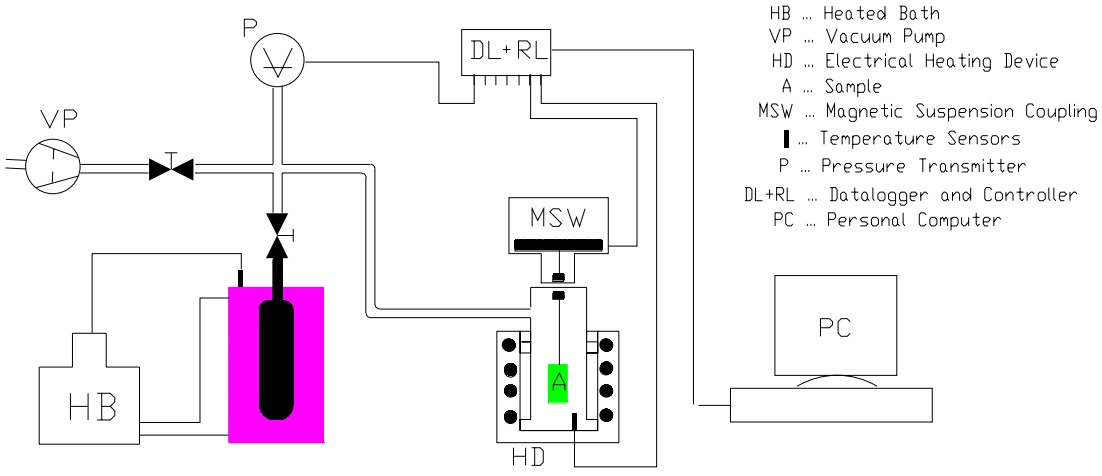

Figure B.1: Thermogravimetrical measuring device.

The thermogravimetrical measuring device shown in Fig. B.1 consists of a high–accuracy balance with a magnetic suspension coupling. The sample is placed in a vacuum and pressure tight cell which can be heated by an electric oven and cooled with nitrogen, water or compressed air. The measuring cell is separated from the balance through a magnetic coupling in order to allow the use of corrosive process gases like ammonia for example and of high pressures without a special high–precision balance becoming necessary. The mass of the sample can be measured very accurately in a wide temperature ($-40°$ up to 400°C) and pressure range ($1.0\times\ 10^{-5}$ up to 20 bar) under almost any process gas. The sample mass is limited to 20 g and can be determined with an accuracy of $\pm 10\mu$g. The cell is connected to the working fluid tank which is completely submerged in an externally heated bath. The bath temperature controls the vapor pressure of the working fluid. The measuring data are recorded by two pressure transducers, one for high and the other for low pressures, three temperature sensors, one placed in the cell and the other in the bath and the balance. Data recording and storage and partly the measuring process are controlled by a personal computer.

An isobaric desorption measurement (isothermal measurements are possible too) with water or alcohol as working fluid (then vacuum is necessary) will proceed as follows:

1. The sample will be placed in the cell which is to be closed vacuum–tight and evacuated.
2. The sample is heated up to a high temperature depending on the kind of adsorptive material (silica gels about 240°C and zeolites about 360°C), while evacuating the cell the working fluid concentration of the sample is reduced when no further mass reduction is observed, the sample is dry, and its mass is recorded.
3. Afterwards the cell will be cooled down to initial temperature, and the externally heated bath will be stabilized at its initial temperature also given by the chosen vapor pressure. The initial cell (sample) temperature must be adjusted slightly above the saturation temperature of the working fluid in order to start measuring very close to the point of maximum concentration and to prevent the gaseous working fluid from condensing on the sample.
4. The cell oven will be controlled by a temperature program which increases the temperature in chosen increments.
5. When initial conditions are reached the valve installed between the bath and the cell will be opened.
6. The sample adsorbs the gaseous working fluid till saturation is achieved.
7. Now the desorption proceeds by heating the sample with temperature increments (controlled by the temperature program). After each increment the temperature will be held constant until mass equilibrium (mass variation becomes zero) is obtained (see the top left diagram in Fig. B.2).
8. During the whole measurement the mass variations, the temperature of the sample, and the pressure are recorded and stored for further analysis.

Apart from the isobaric measurements, isotherms can be measured, too, by holding the sample at a constant temperature and varying the vapor pressure of the working fluid.

For achieving a comprehensive knowledge about the thermodynamic equilibria of the regarded adsorptive material/working fluid–pair with a small number of measurements, the Dubinin theory of micropore volume filling (Dubinin[20], Bering et al. [6] and Lävemann et al. [48]) is employed. The theory is to reduce the three–dimensional isosteric field *($q = f(p,T)$ with sorbate concentration q, pressure p and temperature T)* into a two–dimensional problem with one degree of freedom. Therefore Dubinin defined the adsorption volume W

$$W = \frac{q}{q_{max}} W_0 = \frac{q}{\varrho(T)} \qquad \text{with} \quad \varrho(T) \ldots \text{density of the sorbate} \tag{B.1}$$

and the change of free energy ΔF during a reversible isothermal transfer of a mole of the adsorbate from a bulk liquid to an infinitely large amount of adsorbent

$$\Delta F = R_i\, T\, ln \left(\frac{p_s(T)}{p} \right) \tag{B.2}$$

The density of the sorbate $\varrho(T)$ is normally unknown and can be approximated in first order by the density of the saturated liquid. p_s denotes the saturation pressure and R the specific gas

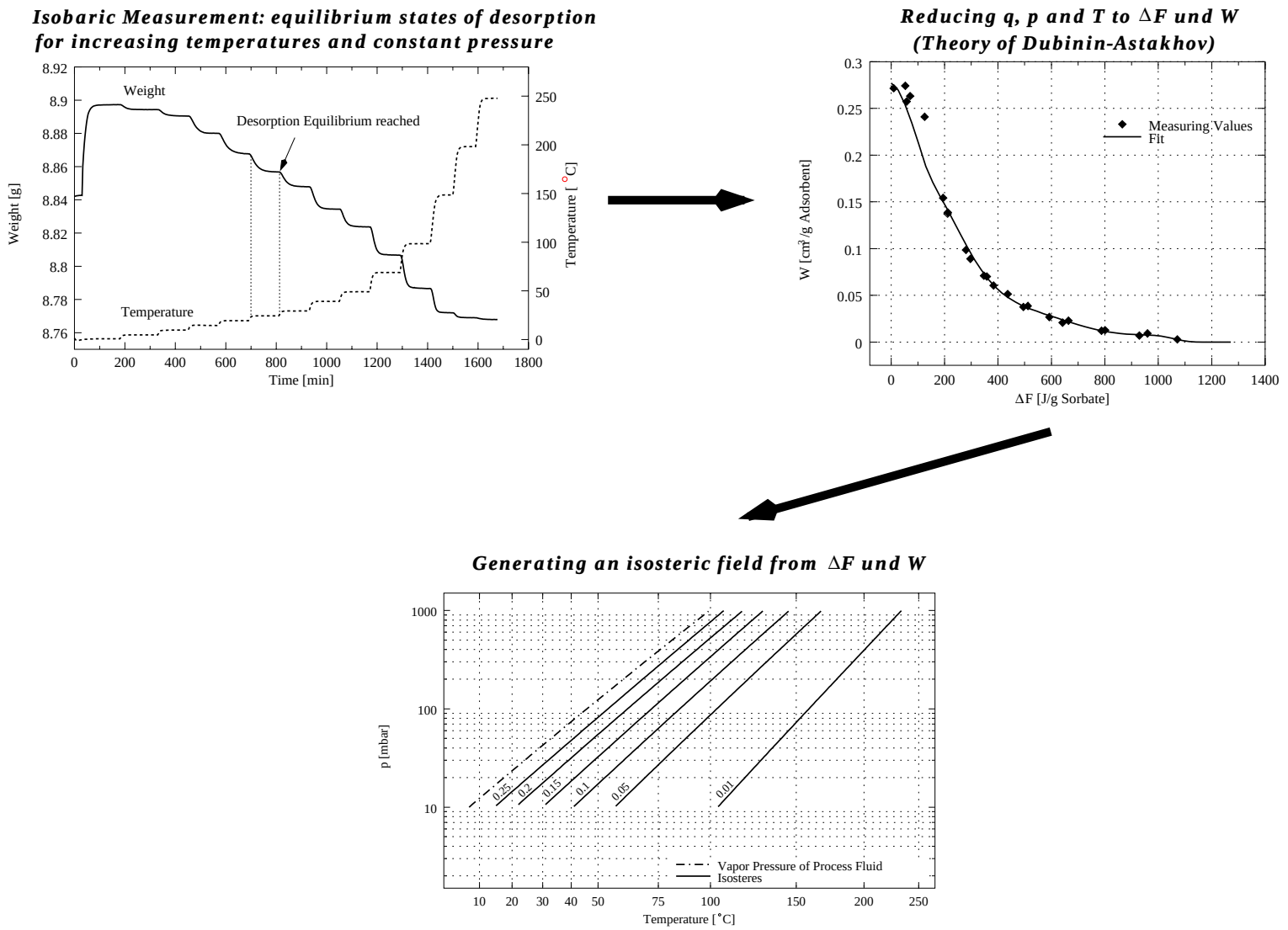

Figure B.2: Analysis of the measured data with the theory of Dubinin–Astakhov.

constant of the working fluid. If the pressure is be varied for different temperatures, both W and ΔF will change dependently on each other, but nearly independent of the temperature T. With this functional dependence

$$\Delta F = \Delta F(W,T) \approx \Delta F(W) \tag{B.3}$$

the isosteric field is almost entirely described. This function is called the *characteristic curve* and has to be obtained experimentally by a suitable fit of the measured data. But the Dubinin theory is only appropriate to describe the intermediate range of concentrations. The boundary regions of the *characteristic curve* where the assumed temperature–independence of ΔF seems no longer to be negligible, i.e in the range of low sorbate concentrations where sorption forms a monomolecular layer and of high concentrations where capillary condensation dominates, must be detected by additional measurements and then described by other theories in order to receive an accurate entire description of the sorptive equilibrium of a sorptive system.

The procedure of thermogravimetrical measurement analysis with the Dubinin theory as shown in Fig. B.2 is as follows:

1. The thermogravimetrical measurements provide the measuring triple pressure, temperature and mass difference independent of the kind of measurement, isothermal or isobaric, respectively. The concentration will be ascertained with the dry mass of the sample which precedes each series of measurements. With the final triple pressure, temperature and concentration, ΔF and W can be easily calculated by:

$$W = \frac{q}{\varrho(T)} \tag{B.4}$$

$$\Delta F = R_i\, T\, ln\left(\frac{p_s(T)}{p}\right) \tag{B.5}$$

2. This two–dimensional assemblage of points with one degree of freedom, the *characteristic curve* $W(\Delta F)$, might be fitted for example by the approximating function proposed by Lävemann et al. [48]

$$W = exp\left(\sum_{i=0}^{n} a_i\, \Delta F^i\right) \tag{B.6}$$

or by any other function or composite function (see top right diagram of Fig. B.2). Problems occur on the left boundary (high concentrations) and right boundary (low concentrations) for lack of measuring points. Perhaps the application of theories handling monomolecular layers in case of low sorbate concentrations and capillary condensation in case of high sorbate concentration, respectively, is more appropriate and much more convenient.

3. With help of the three equations

$$W = \frac{q}{\varrho(T)} \tag{B.7}$$

$$\Delta F = R_i\, T\, ln\left(\frac{p_s(T)}{p}\right) \tag{B.8}$$

$$W = f(\Delta F) \tag{B.9}$$

and assuming that the density of the sorbate $\varrho(T)$ is equal to the density of the saturated liquid, the isosteric field of the regarded adsorbent–working fluid pair can be determined (see bottom diagram of Fig. B.2).

Depending which variable, q, p or T, is unknown

case	given	unknown
1	p, T	q
2	q, p	T
3	q, T	p

three cases can be distinguished to calculate the unknown variable from W and ΔF:

Case 1

$$\Delta F = R_i\, T\, ln\left(\frac{p_s(T)}{p}\right) \tag{B.10}$$

$$q = W(\Delta F)\, \varrho(T) \tag{B.11}$$

Case 2

The equation

$$W(_{\Delta F(T)}) - \frac{q}{\varrho(T)} = 0 \tag{B.12}$$

must be solved numerically for T with a root finding method. The lower boundary for root finding should be a value of T for which $\Delta F = 0$. This happens for $p_s(T) = p$. The upper boundary might be set to the critical temperature of the working fluid.

Case 3

At first we calculate

$$W = \frac{q}{\varrho(T)} \tag{B.13}$$

and afterwards ΔF from the relationship

$$W(\Delta F) - W = 0 \tag{B.14}$$

With the knowledge of ΔF the pressure p will be determined by solving the equation

$$\Delta F = R_i\, T\, ln\left(\frac{p_s(T)}{p}\right) \tag{B.15}$$

$$\Rightarrow p = p_s(T)\, e^{-\frac{\Delta F}{R_i\, T}} \tag{B.16}$$

4. The last step is the calculation of the differential binding enthalpy ϕ_d from the *Dubinin–Theory*:

$$\phi_d = \Delta F - T\,\frac{\partial \Delta F}{\partial T} - T\,\alpha\,\frac{\partial \Delta F}{\partial W} \tag{B.17}$$

Assuming that the *characteristic curve* is independent of temperature, the equation above can be simplified to:

$$\phi_d = \Delta F - T\,\alpha\,\frac{1}{\frac{\partial W}{\partial \Delta F}} \tag{B.18}$$

β is the expansion coefficient of the saturated working fluid and will be calculated in terms of the density ϱ:

$$\beta = -\frac{1}{\varrho}\,\frac{d\varrho}{dT}. \tag{B.19}$$

The integral binding enthalpy ϕ_i is obtained by integrating ϕ_d from 0 up to a concentration q:

$$\phi_i = \int_0^q \phi_d\,dq \tag{B.20}$$

B.2 Properties of some Analysed Adsorbents

The numerical simulations and the experiments with the single–adsorber setup are based on two different types of adsorbents, silica gels for weak affinity and zeolites for strong affinity. The following requirements for an adsorbent utilized in the proposed multi–effect adsorption heat pumps should be met:

- high adsorption capacity ($\left[\frac{g_{sorbate}}{kg_{adsorbent}}\right]$) in a specific temperature and pressure range
  - large specific surface area
  - porous structure
- adsorbent with weak affinity (wide pore diameters) and an adsorbent with high affinity (narrow pore diameters)
- couple hydrophilic silica gels and zeolites with a polar working fluid (e.g. water, alcohol or ammonia) and hydrophobic active carbon with an apolar working fluid (e.g. propane or butane)
- chemical, mechanical and thermal durability (cycle stability and retention of the maximum adsorption capacity)

Silica gel has the nominal chemical formula $SiO_2 \bullet xH_2O$ and is a solid, amorphous for hydrous silicon dioxide distinguished by its microporosity and hydroxylated surface. The structure of silica gel is an interconnected random array of ultimate polymerized silicate particles, called micelles, which are spheroidal of 20–100 Å in diameter (resulting in high specific surface areas of about 300–1000 m^2/g SiO_2). The properties of silica gel are a result of the silica micelles, their state of aggregation, and the chemistry of the micelle surface. In contrary to zeolites, silica gels possess no ordered crystal structure and consequently the pores are nonuniform.

Zeolites are crystalline hydrated aluminosilicates formed by nature or synthesized and based on an infinitely extending three–dimensional network of AlO_4 and SiO_4 tetrahedras linked to each other by sharing all of the oxygen atoms. Zeolite molecular sieves have pores of uniform size in a range of 3 up to 10 Å which are uniquely determined by the unit structure of the crystal. These pores will completely exclude molecules which are larger than their diameter. The pore size distribution for a zeolite in comparison to a silica gel is illustrated schematically in Fig. B.3. A comprehensive description of zeolites is given by Breck [9], Kärger/Ruthven [42], Puppe [75] and Kerr [45].

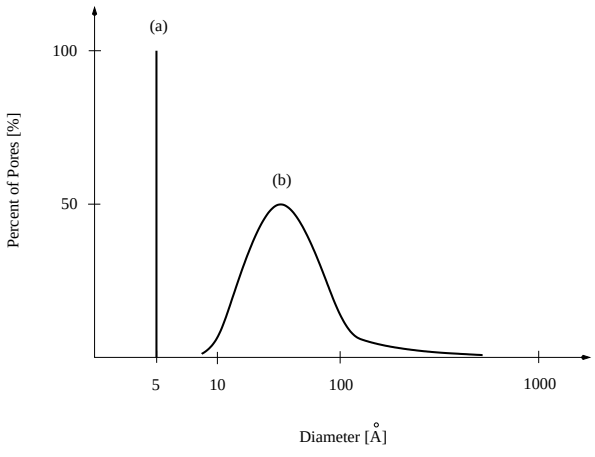

Figure B.3: Pore size distribution of a customary zeolite (a) and silica gel (b).

All isosteric fields presented in the following subsections are based on thermogravimetric isobaric measurements of the desorption process, knowing that in the region of capillary condensation a hysteresis of the apparent equilibrium pressure in adsorption and desorption experiments might occur depending on the sorptive material. But for all calculations no hysteresis was assumed.

B.2.1 Silica Gel Grace 123 + Water

Silica Gel 123 is a narrow pore, granular form of silica and produced by Grace GmbH (Germany). With its high water–binding capacity it is mainly applied in refrigerant drying solid cores, in desiccators and as desiccant in insulating glass units.

The *characteristic curve* $W(\Delta F)$ is fitted by a non–linear equation of type *Lorentzian Cumulative* (valid in the range 17 $^{J}/_{g} < \Delta F < 1940$ $^{J}/_{g}$):

$$W(\Delta F) = d + \frac{a}{\pi}\left[arctan\left(\frac{\Delta F - b}{c}\right) + \frac{\pi}{2}\right]$$

$$\begin{aligned} a &= \ \ 5.072313 \times 10^{-1} \\ b &= \ \ 1.305531 \times 10^{2} \\ c &= -8.492403 \times 10^{1} \\ d &= \ \ 4.128962 \times 10^{-3} \end{aligned}$$

The following properties are given by the manufacturer:

Property	Specification
Chemical composition	pure SiO_2
Specific surface area	750 $^{m^2}/_{g}$
Specific pore volume	0.4 $^{ml}/_{g}$
Specific heat capacity	1.0 $^{kJ}/_{kg\,K}$
Thermal conductivity	0.12 $^{W}/_{m\,K}$
Average pore diameter	21 Å (2.1 nm)
True particle density	2.2 $^{g}/_{cm^3}$
Apparent particle density	1.25 $^{g}/_{cm^3}$
Diameter	0.5 ÷ 1.25 mm
Bulk density	650 $^{g}/_{l}$

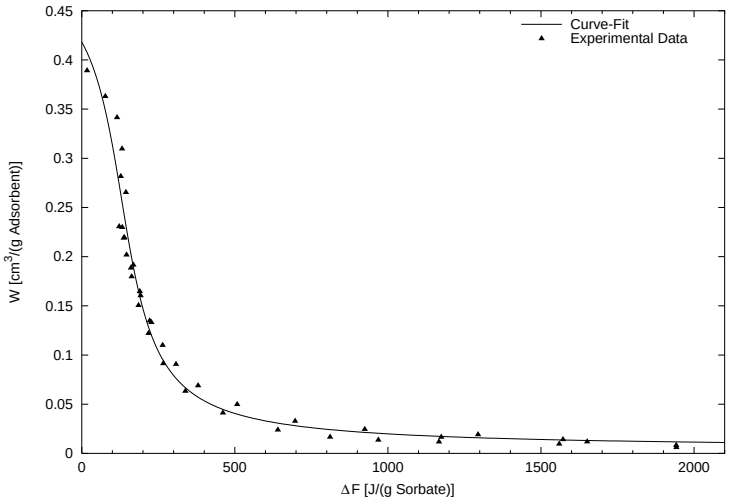

Figure B.4: Experimental data fitted to the *characteristic curve* $W(\Delta F)$.

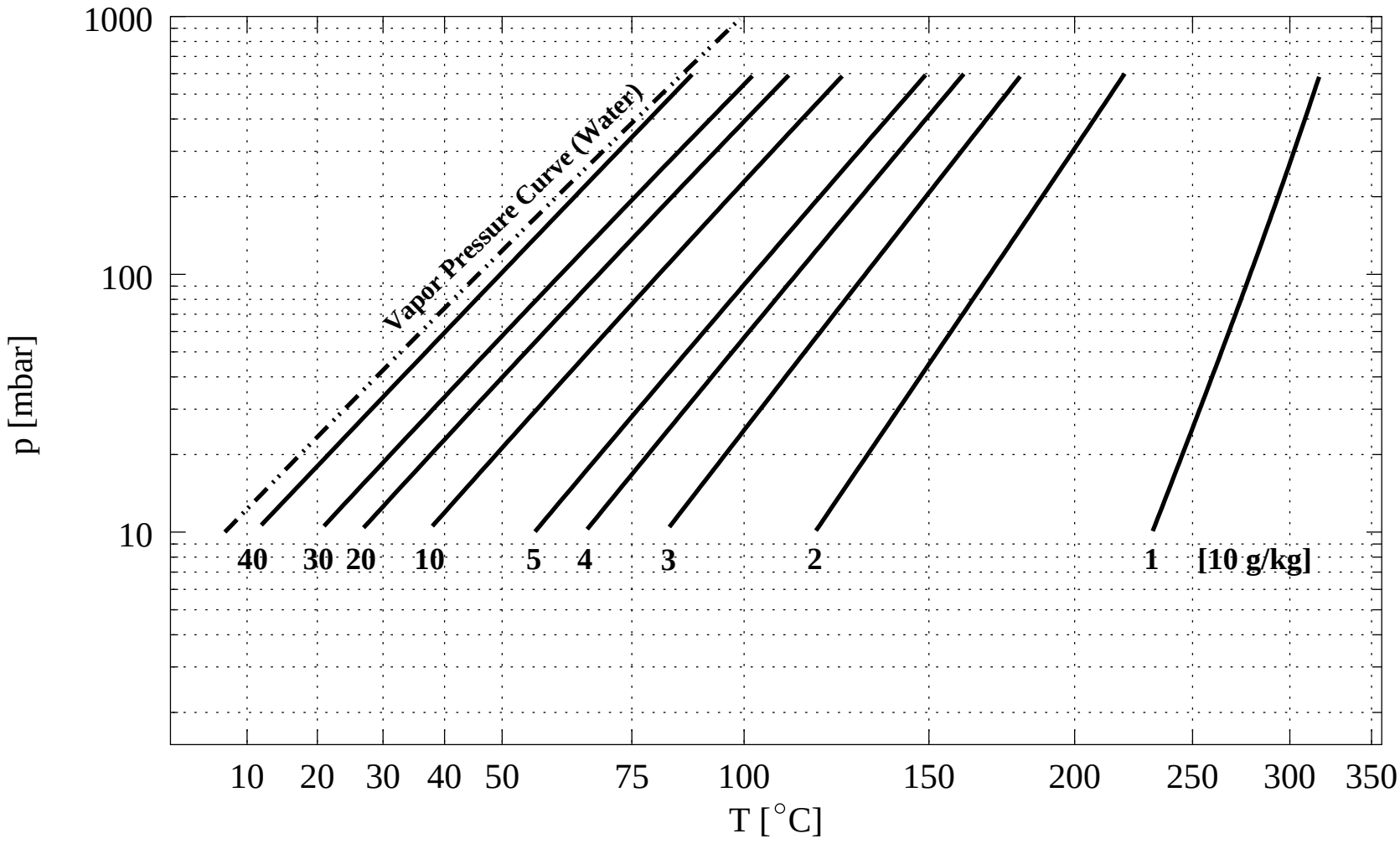

Figure B.5: Isosteric field of Silica Gel Grace 123.

B.2.2 Silica Gel Grace 125 + Water

Silica Gel 125 is a narrow pore, granular form of silica and produced by Grace GmbH (Germany). It is used in various gas and liquid dehydration applications like in desiccant bags for protection against moisture, mildew and odor in packaging.

The *characteristic curve* $W(\Delta F)$ is fitted by a non–linear equation of type *Lorentzian Cumulative* (valid in the range $20\ {}^{\mathrm{J}}/_{\mathrm{g}} < \Delta F < 1570\ {}^{\mathrm{J}}/_{\mathrm{g}}$):

$$W(\Delta F) = d + \frac{a}{\pi}\left[arctan\left(\frac{\Delta F - b}{c}\right) + \frac{\pi}{2}\right] \qquad \begin{aligned} a &= \ \ 4.527805 \times 10^{-1} \\ b &= \ \ 1.229005 \times 10^{2} \\ c &= -8.847167 \times 10^{1} \\ d &= \ \ 6.034706 \times 10^{-4} \end{aligned}$$

The following properties are given by the manufacturer:

Property	Specification
Chemical composition	pure SiO_2
Specific surface area	750 ${}^{\mathrm{m}^2}/_{\mathrm{g}}$
Specific pore volume	0.4 ${}^{\mathrm{ml}}/_{\mathrm{g}}$
Specific heat	1.0 ${}^{\mathrm{kJ}}/_{\mathrm{kg\,K}}$
Thermal conductivity	0.12 ${}^{\mathrm{W}}/_{\mathrm{m\,K}}$
Average pore diameter	21 Å (2.1 nm)
True particle density	2.2 ${}^{\mathrm{g}}/_{\mathrm{cm}^3}$
Apparent particle density	1.25 ${}^{\mathrm{g}}/_{\mathrm{cm}^3}$
Diameter	1.0 ÷ 3.15 mm
Bulk density	690–760 ${}^{\mathrm{g}}/_{\mathrm{l}}$

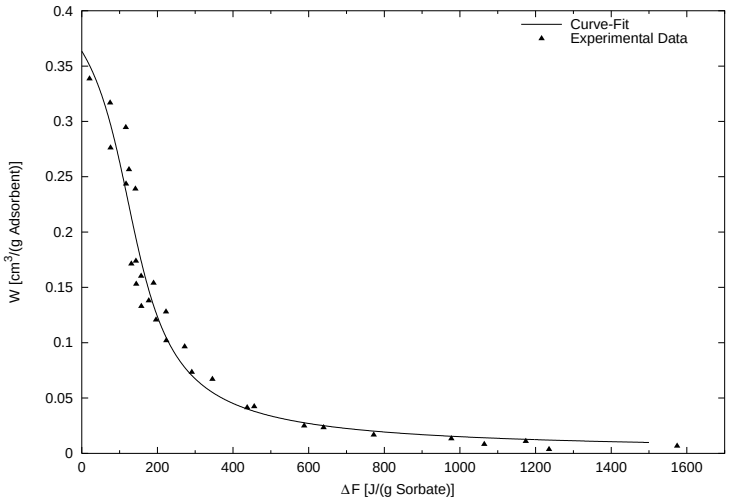

Figure B.6: Experimental data fitted to the *characteristic curve* $W(\Delta F)$.

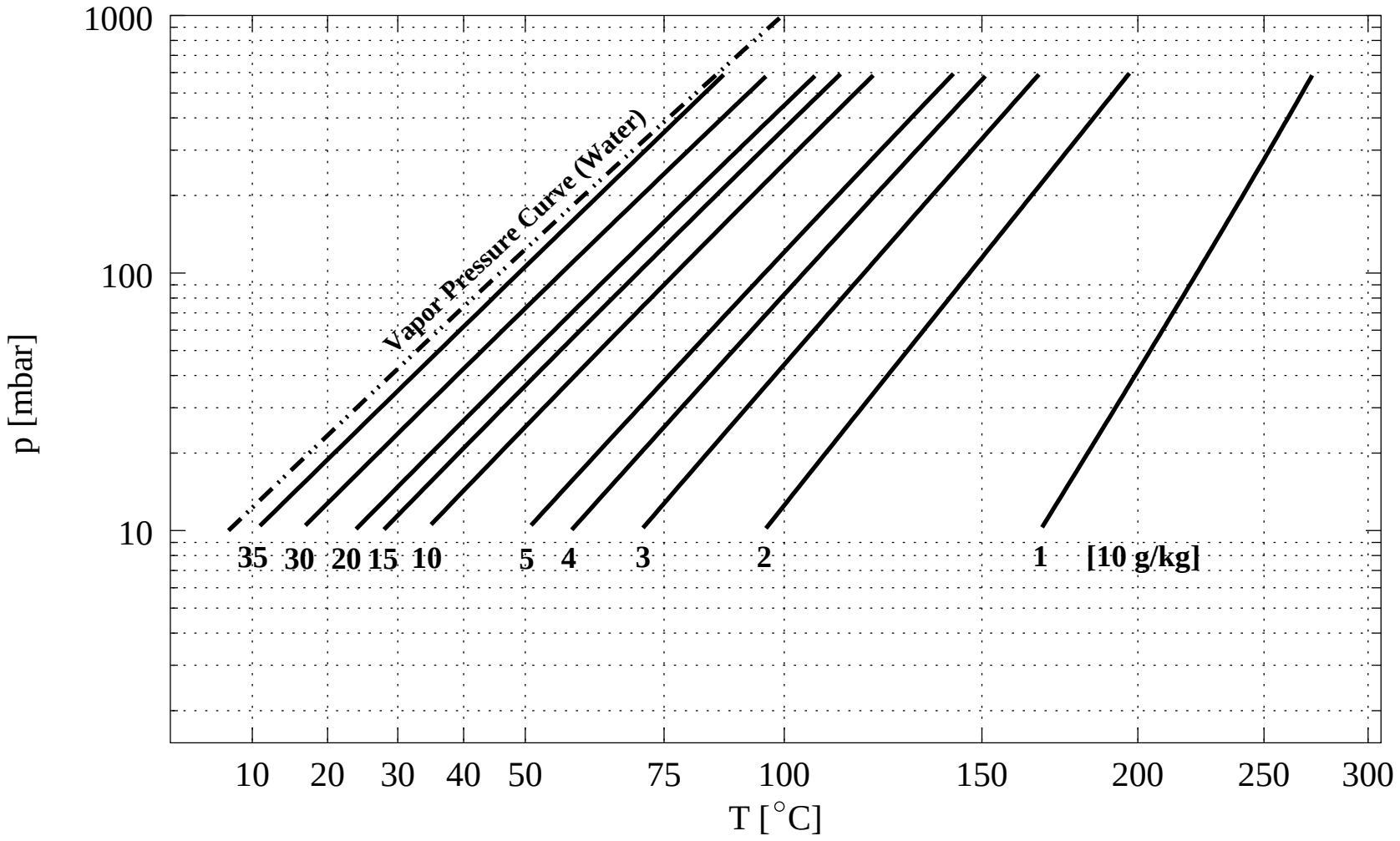

Figure B.7: Isosteric field of Silica Gel Grace 125.

B.2.3 Silica Gel NAC + Water

This granular silica gel comes out of an adsorption cooling device of type NAK, which is manufactured by the Japanese company Nishiyodo Air Conditioning Co. Ltd. (Japan). The producer of the silica gel is unknown, as well the physical properties.

The *characteristic curve* $W(\Delta F)$ is fitted by a linear function in the range $10\ {}^{\mathrm{J}}/_{\mathrm{g}} < \Delta F < 1070\ {}^{\mathrm{J}}/_{\mathrm{g}}$):

$$\frac{1}{W(\Delta F)} = a + b\,\Delta F^2 \ln \Delta F + c\,\Delta F^3$$

with the coefficients:

$$\begin{aligned} a &= 3.570644 \\ b &= 8.569149 \times 10^{-6} \\ c &= 9.597209 \times 10^{-8} \end{aligned}$$

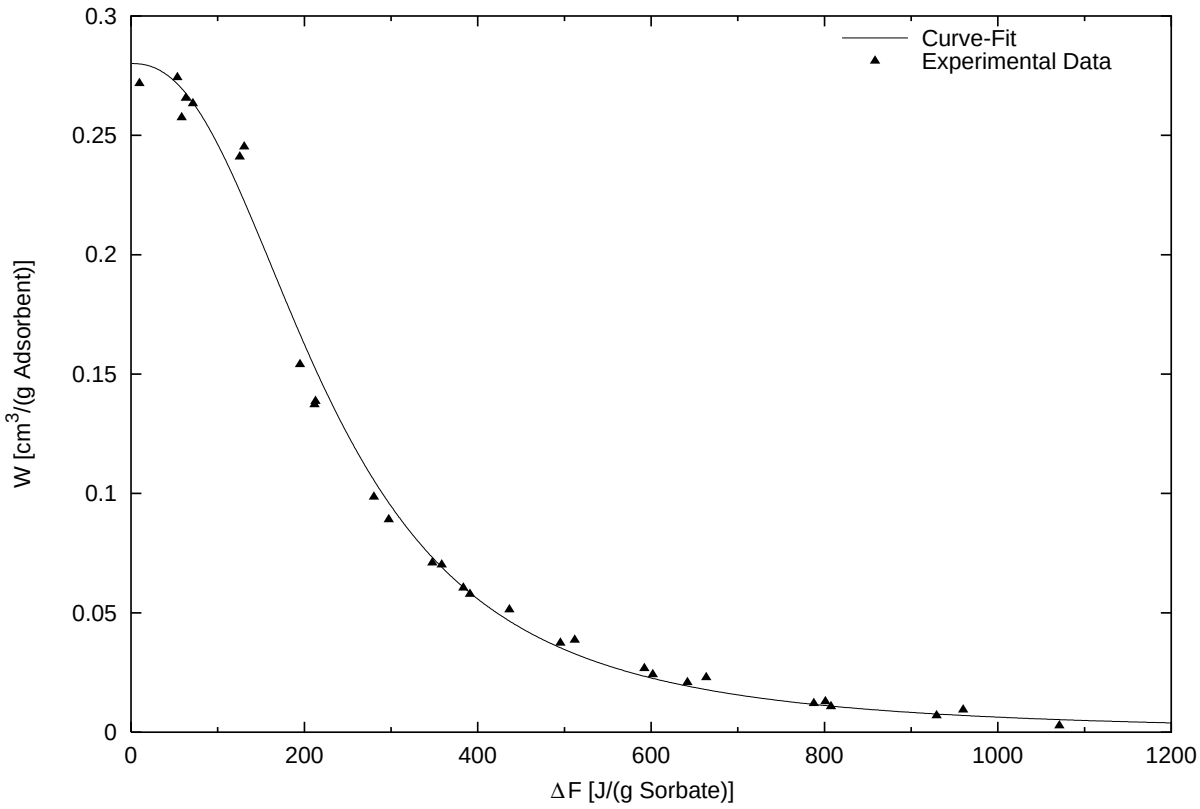

Figure B.8: Experimental data fitted to the *characteristic curve* $W(\Delta F)$.

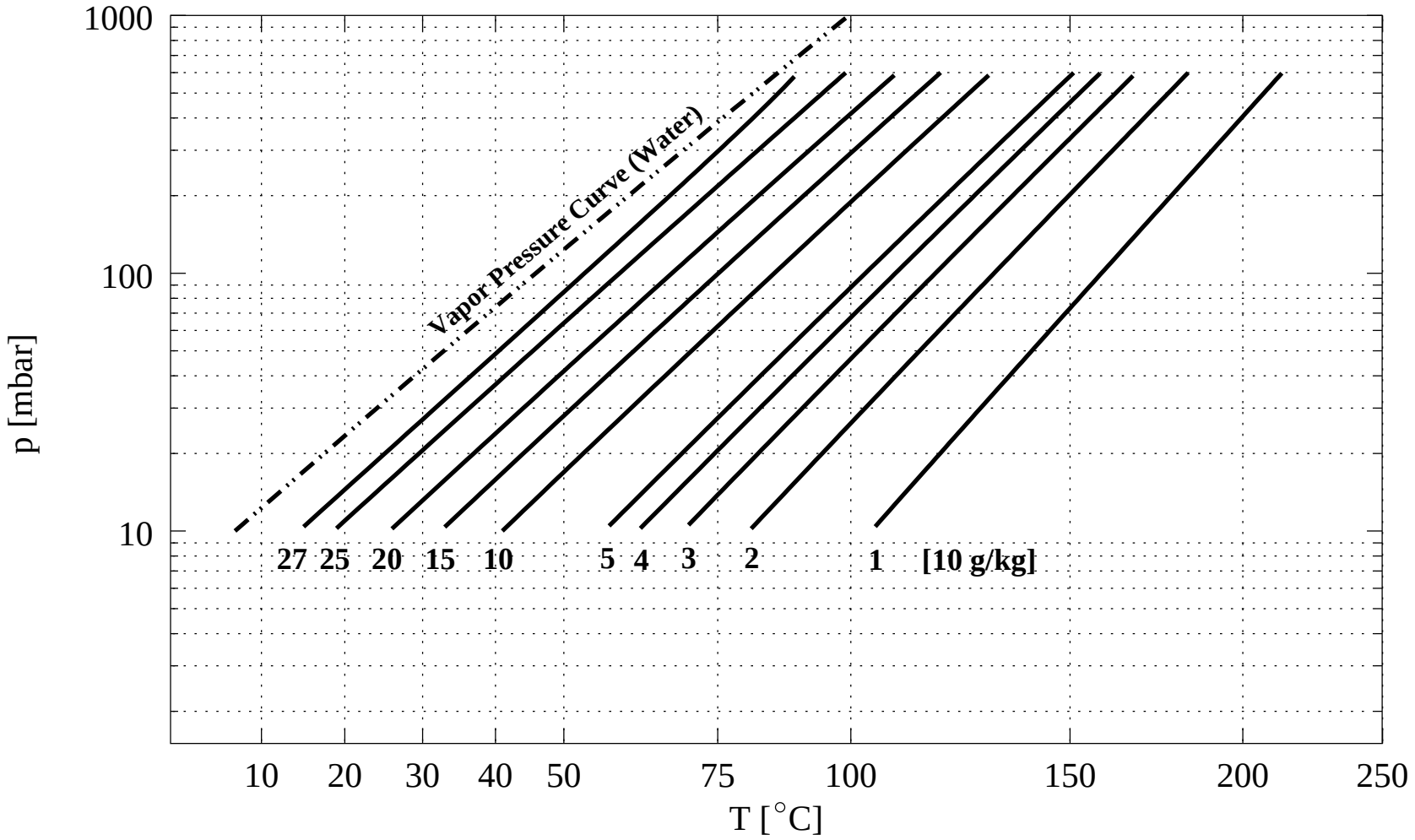

Figure B.9: Isosteric field of Silica Gel NAC.

B.2.4 Silica Gel Fuji + Water

This silica gel is an A–type 60–200 Mesh and is distributed by Fuji Silysia Chemical LTD (Japan).

The *characteristic curve* $W(\Delta F)$ is fitted by a non–linear equation of type *Lorentzian Cumulative* (valid in the range $7\ {}^{\mathrm{J}}/_{\mathrm{g}} < \Delta F < 2020\ {}^{\mathrm{J}}/_{\mathrm{g}}$):

$$W(\Delta F) = \frac{a}{\pi}\left[arctan\left(\frac{\Delta F - b}{c}\right) + \frac{\pi}{2}\right]$$

with the coefficients:

$$\begin{aligned} a = &\quad 3.857567 \times 10^{-1} \\ b = &\quad 1.262497 \times 10^{2} \\ c = &-9.919397 \times 10^{1} \end{aligned}$$

The following properties are given by the manufacturer:

Property	Specification
BET surface area	$589\ {}^{\mathrm{m}^2}/_{\mathrm{g}}$
Specific pore volume	$0.31\ {}^{\mathrm{ml}}/_{\mathrm{g}}$

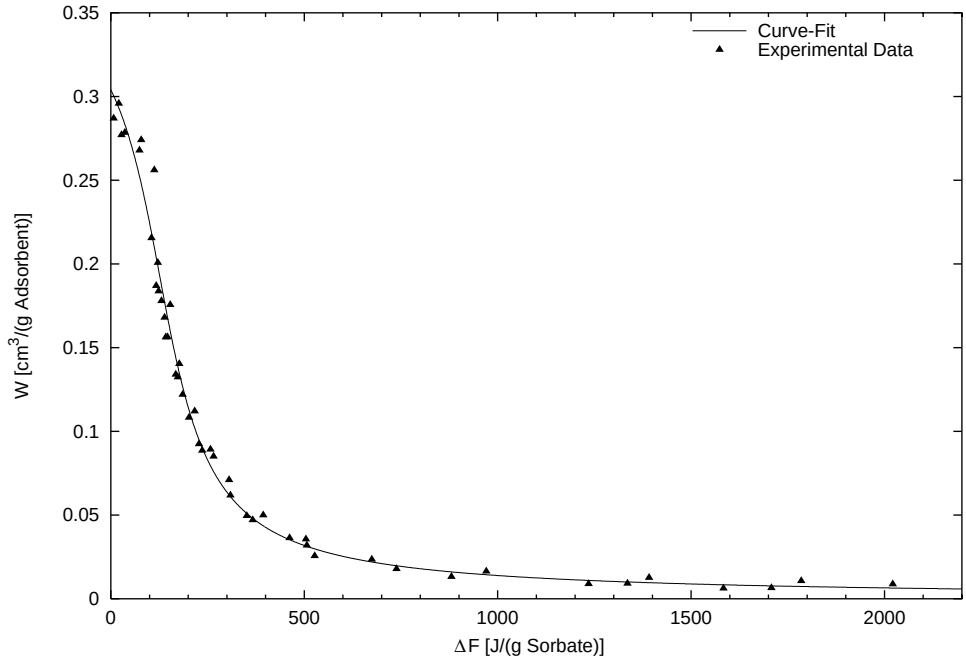

Figure B.10: Experimental data fitted to the *characteristic curve* $W(\Delta F)$.

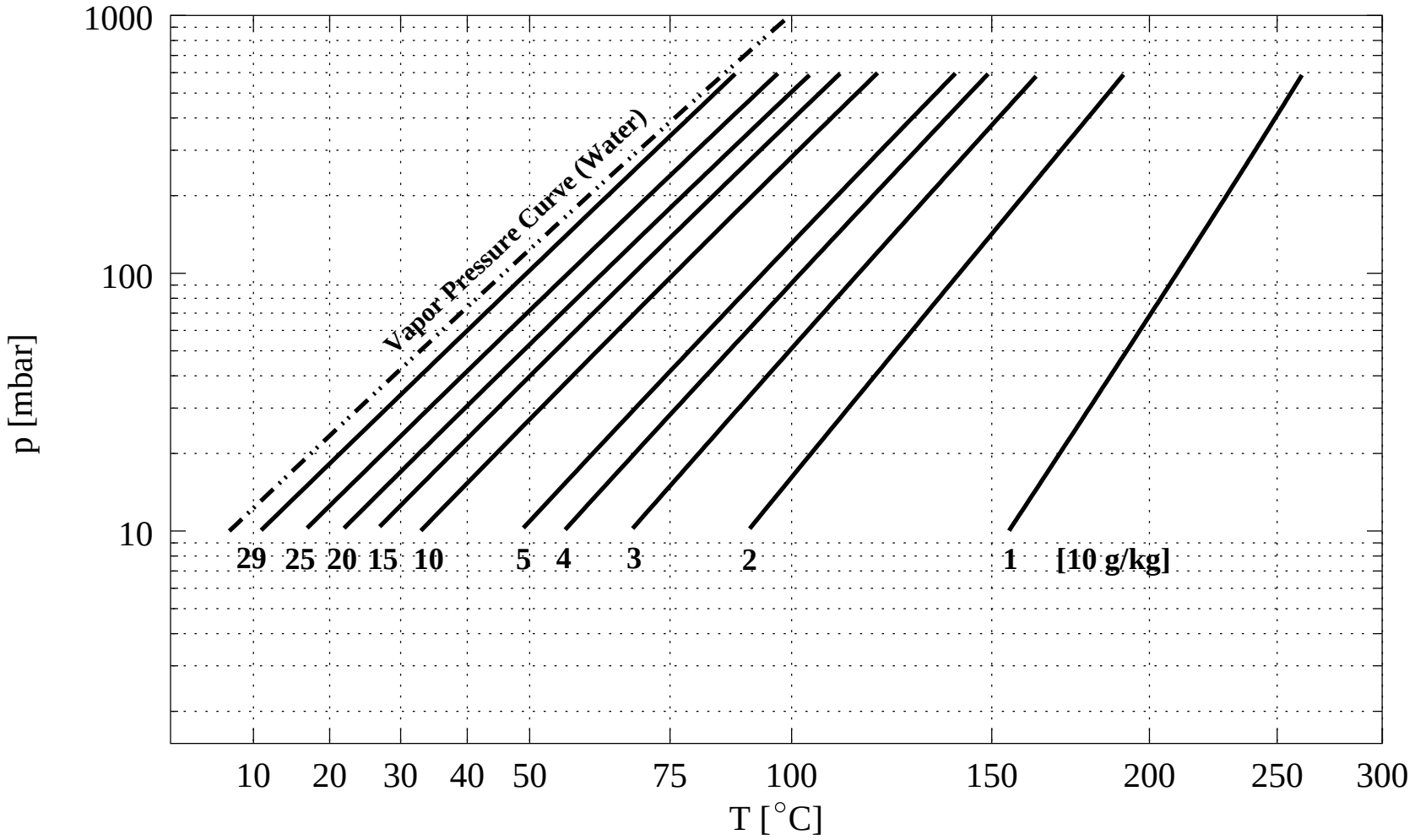

Figure B.11: Isosteric field of Silica Gel Fuji.

B.2.5 Silica Gel N + Water

Silica Gel N from Engelhard Process Chemicals GmbH (Germany) is an adsorbent with an above–average drying capacity, on account of its high specific area.

The *characteristic curve* $W(\Delta F)$ is fitted by a non–linear equation of type *Pearson IV* (valid in the range $14\ {}^{\mathrm{J}}/_{\mathrm{g}} < \Delta F < 860\ {}^{\mathrm{J}}/_{\mathrm{g}}$):

$$W(\Delta F) = a + \frac{b\,(1+n^2)^{-e}\ exp\left[-f\left(arctan(n) + arctan\left(\frac{f}{2\,e}\right)\right)\right]}{\left(1+\frac{f^2}{4\,e^2}\right)^{-e}}, \quad n = \frac{\Delta F - \frac{d\,f}{2\,e} - c}{d}$$

with the coefficients:

$$\begin{aligned} a &= -7.689279 \times 10^{-1} & d &= 4.244922 \times 10^{1} \\ b &= \ \ 1.176831 & e &= 2.207797 \times 10^{-2} \\ c &= \ \ 1.485965 \times 10^{1} & f &= 1.146067 \times 10^{-1} \end{aligned}$$

The following properties are given by the manufacturer:

Property	Specification
Chemical composition	97% SiO_2 and 3% Al_2O_3
BET surface area	750 ${}^{\mathrm{m}^2}/_{\mathrm{g}}$
Specific pore volume	0.37 ${}^{\mathrm{ml}}/_{\mathrm{g}}$
Specific heat capacity	1.0 ${}^{\mathrm{kJ}}/_{\mathrm{kg\,K}}$
Thermal conductivity	0.2 ${}^{\mathrm{W}}/_{\mathrm{m\,K}}$
Average pore diameter	20 Å (2.0 nm)
Bulk density	800 ${}^{\mathrm{g}}/_{\mathrm{l}}$

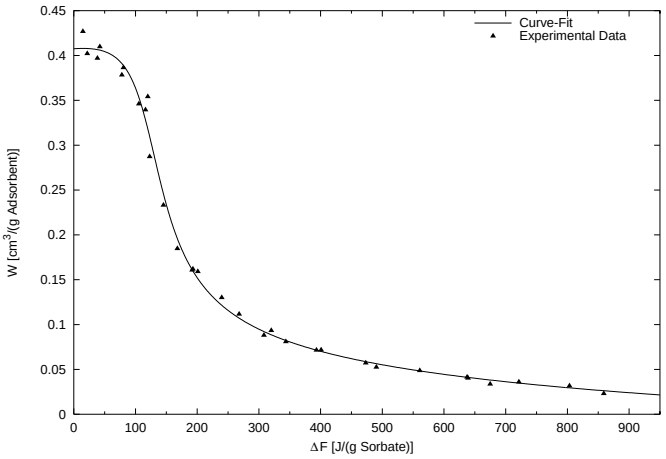

Figure B.12: Experimental data fitted to the *characteristic curve* $W(\Delta F)$.

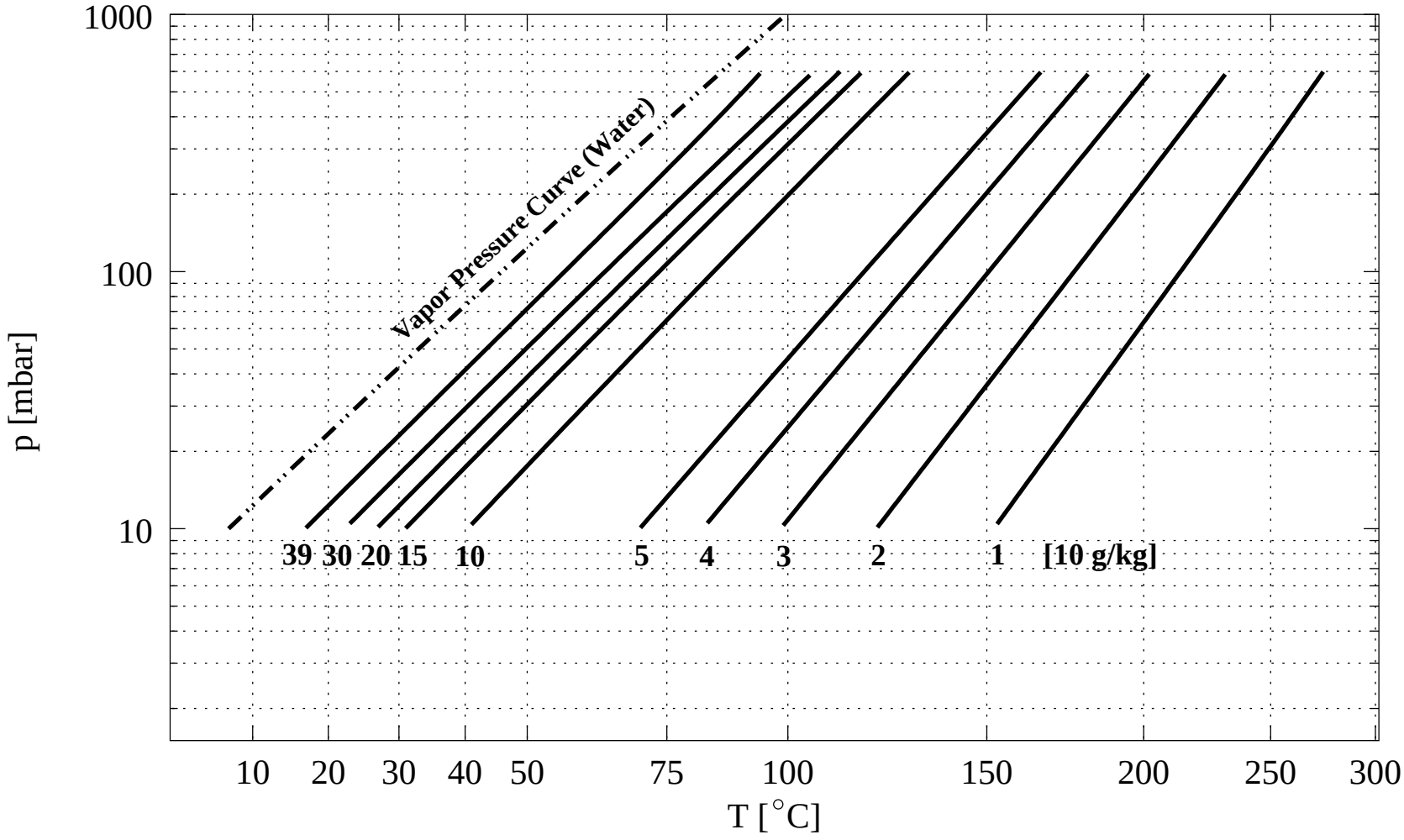

Figure B.13: Isosteric field of Silica Gel N.

B.2.6 Silica Gel WS + Water

Silica Gel WS is a water–resistant, narrow pore silica gel distributed by Engelhard Process Chemicals GmbH (Germany).

The *characteristic curve* $W(\Delta F)$ is fitted by a non–linear equation of type *Lorentzian Cumulative* (valid in the range $7\ {}^{\mathrm{J}}/_{\mathrm{g}} < \Delta F < 1080\ {}^{\mathrm{J}}/_{\mathrm{g}}$):

$$W(\Delta F) = \frac{a}{\pi}\left[arctan\left(\frac{\Delta F - b}{c}\right) + \frac{\pi}{2}\right]$$

with the coefficients:

$$\begin{aligned} a = &\quad 5.046468 \times 10^{-1} \\ b = &\quad 1.002140 \times 10^{2} \\ c = &-7.264229 \times 10^{1} \end{aligned}$$

The following properties are given by the manufacturer:

Property	Specification
Form	pellet
Chemical composition	97% SiO_2 and 3% Al_2O_3
BET surface area	650 ${}^{\mathrm{m}^2}/_{\mathrm{g}}$
Specific pore volume	0.4 ${}^{\mathrm{ml}}/_{\mathrm{g}}$
Specific heat capacity	1.0 ${}^{\mathrm{kJ}}/_{\mathrm{kg\,K}}$
Thermal conductivity	0.2 ${}^{\mathrm{W}}/_{\mathrm{m\,K}}$
Average pore diameter	25 Å (2.5 nm)
Bulk density	700 ${}^{\mathrm{g}}/_{\mathrm{l}}$

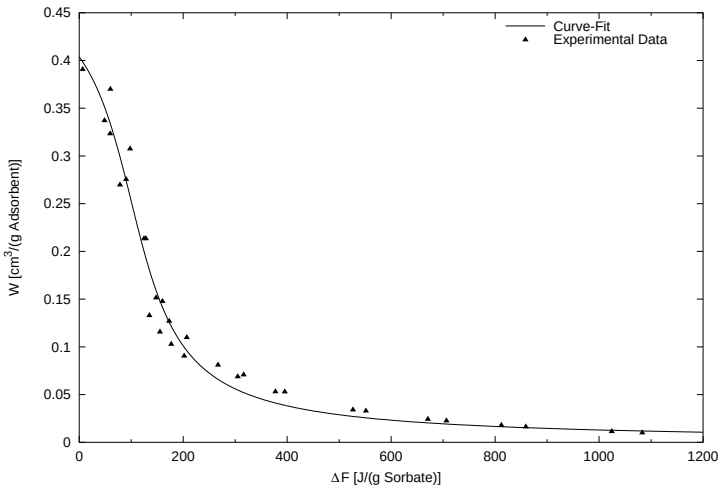

Figure B.14: Experimental data fitted to the *characteristic curve* $W(\Delta F)$.

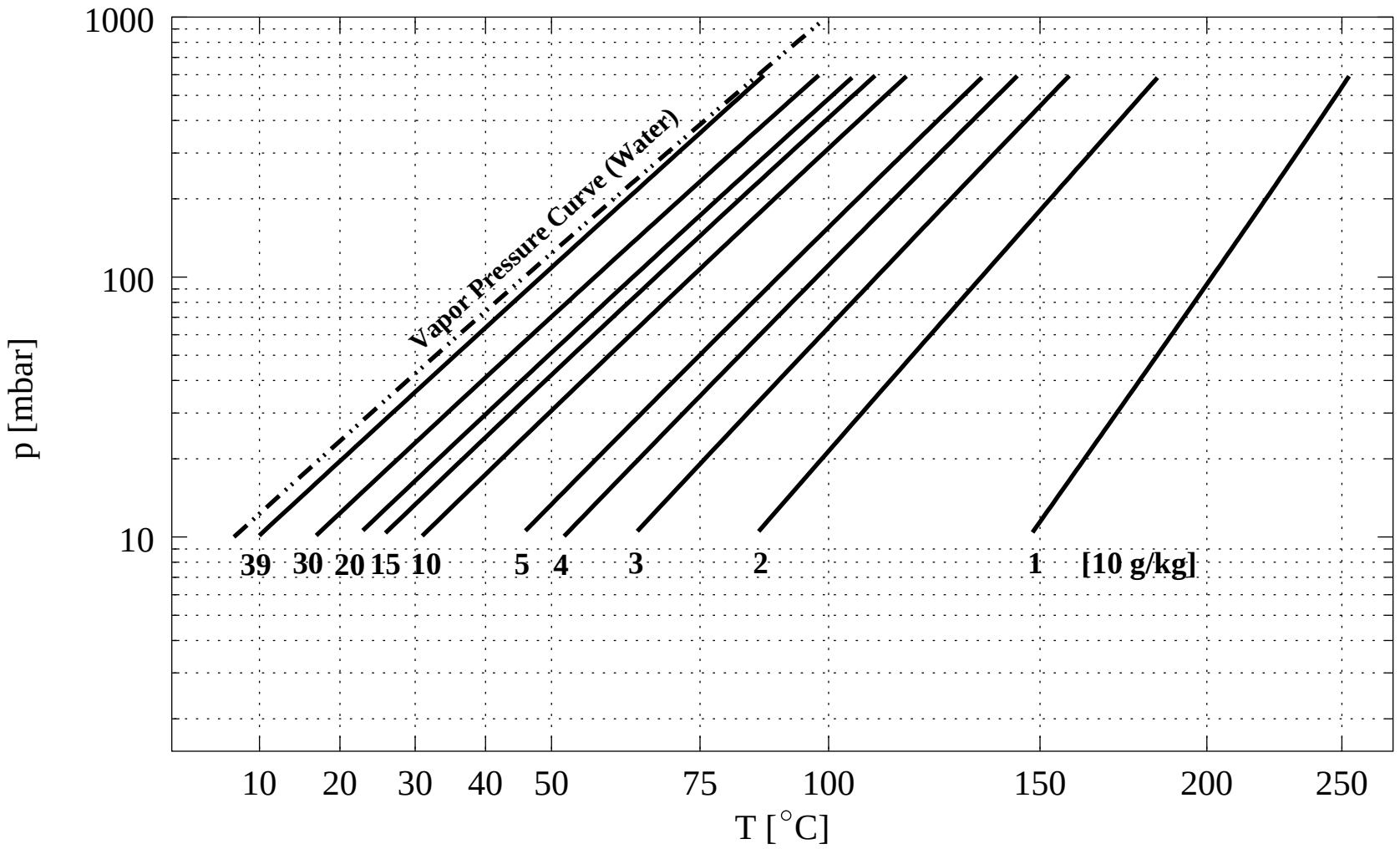

Figure B.15: Isosteric field of Silica Gel WS.

B.2.7 Silica Gel LE–32 + Water

Silica Gel LE–32 is a product of Engelhard Process Chemicals GmbH (Germany).

The *characteristic curve* $W(\Delta F)$ is fitted by a non–linear equation of type *Pearson IV* (valid in the range 15 $^{\mathrm{J}}/_{\mathrm{g}} < \Delta F < 530$ $^{\mathrm{J}}/_{\mathrm{g}}$):

$$W(\Delta F) = a + \frac{b\,(1+n^2)^{-e}\; exp\left[-f\left(arctan(n) + arctan\left(\frac{f}{2\,e}\right)\right)\right]}{\left(1+\frac{f^2}{4\,e^2}\right)^{-e}}, \quad n = \frac{\Delta F - \frac{d\,f}{2\,e} - c}{d}$$

with the coefficients:

$$\begin{aligned} a &= -1.044288 \times 10^{-1} & d &= 3.327467 \times 10^{1} \\ b &= \;\; 7.154669 \times 10^{-1} & e &= 1.201645 \times 10^{-1} \\ c &= -2.345348 \times 10^{1} & f &= 5.058059 \times 10^{-1} \end{aligned}$$

The following properties are given by the manufacturer:

Property	Specification
Chemical composition	pure SiO_2
BET surface area	750 $^{\mathrm{m}^2}/_{\mathrm{g}}$
Specific pore volume	0.5 $^{\mathrm{ml}}/_{\mathrm{g}}$
Specific heat capacity	1.0 $^{\mathrm{kJ}}/_{\mathrm{kg\,K}}$
Thermal conductivity	0.2 $^{\mathrm{W}}/_{\mathrm{m\,K}}$
Average pore diameter	25 Å (2.5 nm)
Bulk density	700 $^{\mathrm{g}}/_{\mathrm{l}}$

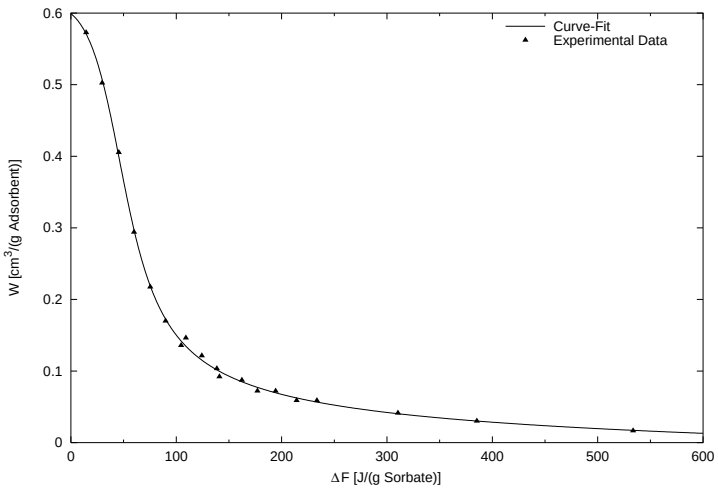

Figure B.16: Experimental data fitted to the *characteristic curve* $W(\Delta F)$.

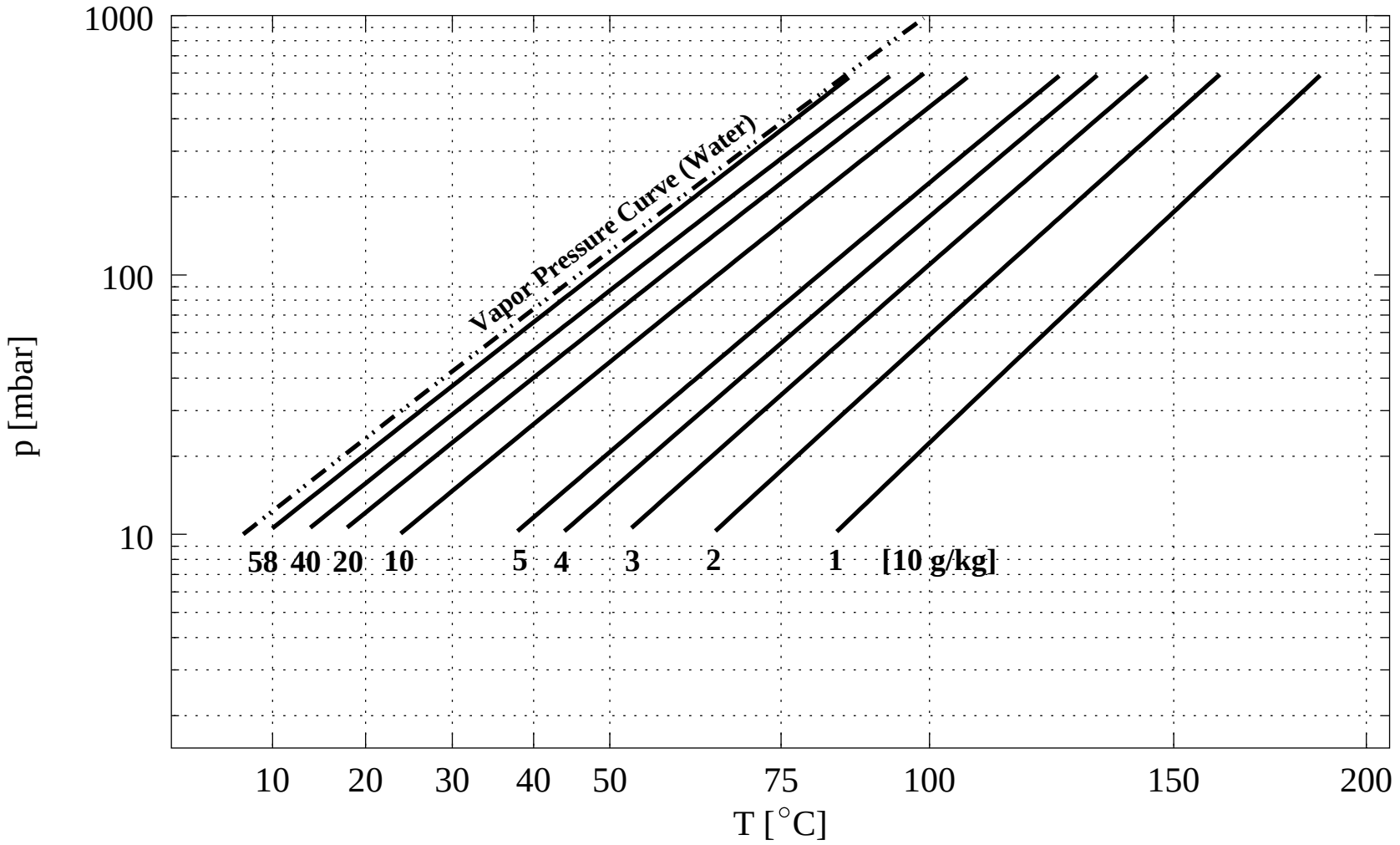

Figure B.17: Isosteric field of Silica Gel LE 32.

B.2.8 Silica Gel H + Water

Silica Gel H, an adsorbent of Engelhard Process Chemicals GmbH (Germany) is normally used for the recovery of the higher hydrocarbons from natural gas. The drying of the natural gas is carried out at the same time.

The *characteristic curve* $W(\Delta F)$ is fitted by a non–linear equation of type *Pearson IV* (valid in the range 16 $^{J}/_{g} < \Delta F <$ 1210 $^{J}/_{g}$):

$$W(\Delta F) = a + \frac{b\,(1+n^2)^{-e}\; exp\left[-f\left(arctan(n) + arctan\left(\frac{f}{2\,e}\right)\right)\right]}{\left(1+\frac{f^2}{4\,e^2}\right)^{-e}}, \quad n = \frac{\Delta F - \frac{d\,f}{2\,e} - c}{d}$$

with the coefficients:

$$\begin{aligned} a &= -2.243367 \times 10^{-1} & d &= 3.678460 \times 10^{1} \\ b &= \;\; 7.354090 \times 10^{-1} & e &= 7.419258 \times 10^{-2} \\ c &= \;\; 1.044776 \times 10^{1} & f &= 2.927265 \times 10^{-1} \end{aligned}$$

The following properties are given by the manufacturer:

Property	Specification
Chemical composition	97% SiO_2 and 3% Al_2O_3
BET surface area	750 $^{m^2}/_{g}$
Specific pore volume	0.47 $^{ml}/_{g}$
Specific heat capacity	1.0 $^{kJ}/_{kg\,K}$
Thermal conductivity	0.2 $^{W}/_{m\,K}$
Average pore diameter	25 Å (2.5 nm)
Bulk density	700 $^{g}/_{l}$

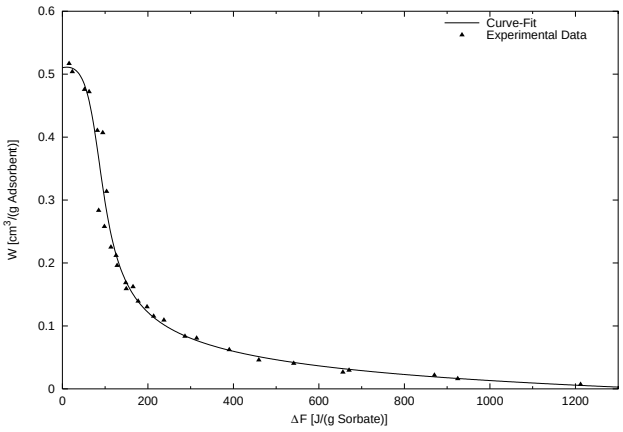

Figure B.18: Experimental data fitted to the *characteristic curve* $W(\Delta F)$.

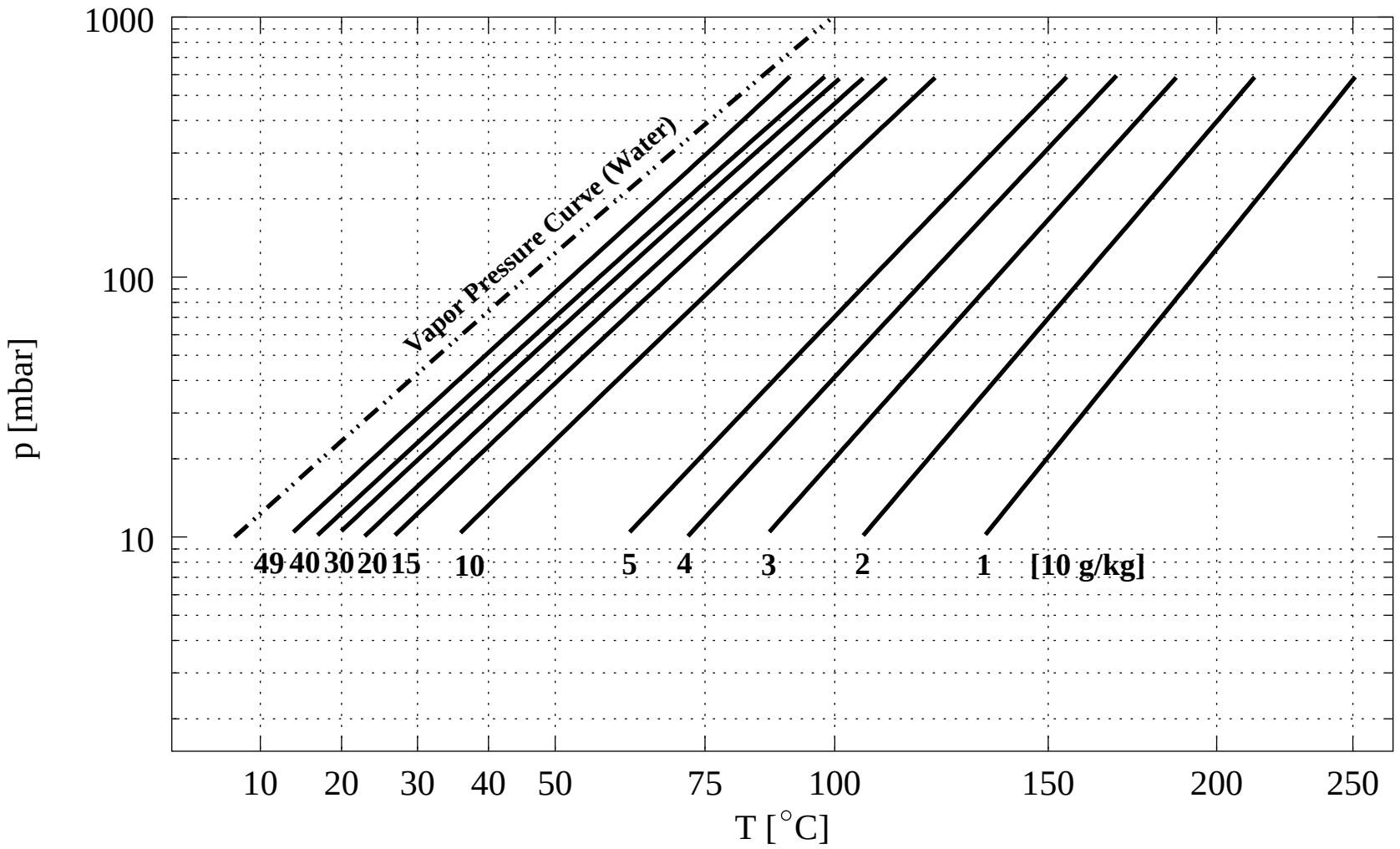

Figure B.19: Isosteric field of Silica Gel H.

B.2.9 Silica Gel AF–25 + Water

Silica Gel AF–25 is a bead–shaped alumina–free desiccant. The bead size provides an even gas distribution and avoids channelling and nest formation. It is distributed by Engelhard Process Chemicals GmbH (Germany).

The *characteristic curve* $W(\Delta F)$ is fitted by a non–linear equation of type *Lorentzian Cumulative* (valid in the range 6 $^{J}/_{g} < \Delta F < 1580$ $^{J}/_{g}$):

$$W(\Delta F) = \frac{a}{\pi}\left[arctan\left(\frac{\Delta F - b}{c}\right) + \frac{\pi}{2}\right]$$

with the coefficients:

$$\begin{aligned} a = &\quad 6.452704 \times 10^{-1} \\ b = &\quad 8.979911 \times 10^{1} \\ c = &-7.845557 \times 10^{1} \end{aligned}$$

The following properties are given by the manufacturer:

Property	Specification
Chemical composition	99.7% SiO_2 and 0.3% Al_2O_3
BET surface area	750 $^{m^2}/_{g}$
Specific pore volume	0.5 $^{ml}/_{g}$
Specific heat capacity	1.0 $^{kJ}/_{kg\,K}$
Thermal conductivity	0.2 $^{W}/_{m\,K}$
Average pore diameter	25 Å (2.5 nm)
Bulk density	600 $^{g}/_{l}$

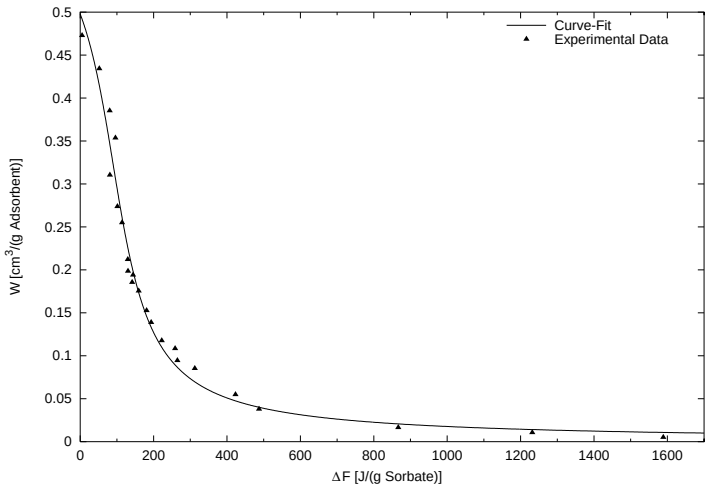

Figure B.20: Experimental data fitted to the *characteristic curve* $W(\Delta F)$.

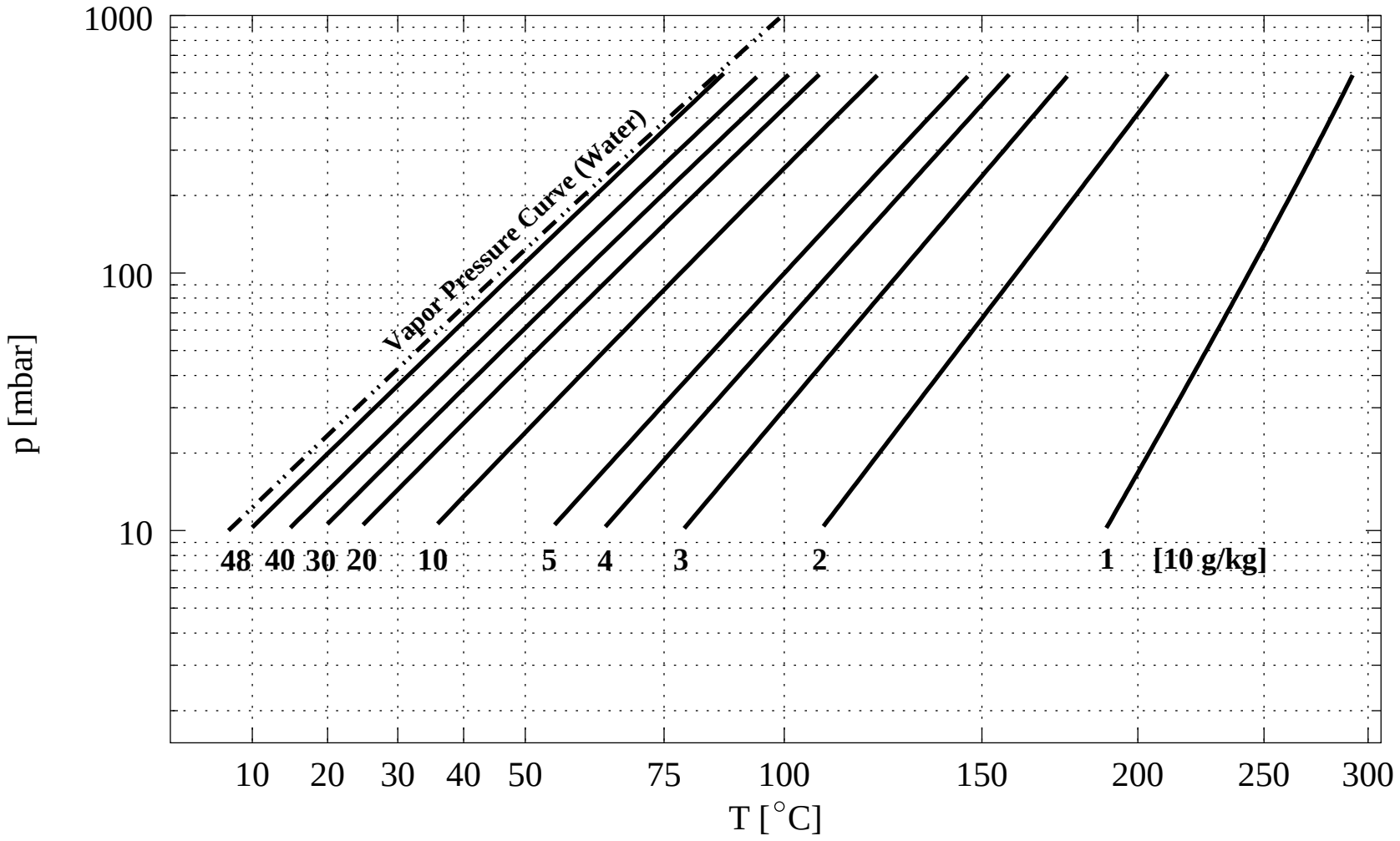

Figure B.21: Isosteric field of Silica Gel AF25.

B.2.10 Sizeo 15 + Water

Sizeo 15 is a mixture of crystalline aluminosilicates and amorphous silicon dioxide and no longer produced.

The *characteristic curve* $W(\Delta F)$ is fitted by a non–linear equation of type *Pearson IV* (valid in the range $38\ {}^{\mathrm{J}}/_{\mathrm{g}} < \Delta F < 1200\ {}^{\mathrm{J}}/_{\mathrm{g}}$):

$$W(\Delta F) = a + \frac{b\,(1+n^2)^{-e}\ exp\left[-f\left(arctan(n) + arctan\left(\frac{f}{2\,e}\right)\right)\right]}{\left(1+\frac{f^2}{4\,e^2}\right)^{-e}}, \quad n = \frac{\Delta F - \frac{d\,f}{2\,e} - c}{d}$$

with the coefficients:

$$\begin{aligned} a &= -5.798998 \times 10^{-1} & d &= 3.586237 \times 10^{1} \\ b &= \ \ 9.685636 \times 10^{-1} & e &= 3.214072 \times 10^{-2} \\ c &= \ \ 1.313229 \times 10^{1} & f &= 1.179455 \times 10^{-1} \end{aligned}$$

The following properties are given by the manufacturer:

Property	Specification
BET surface area	491 ${}^{\mathrm{m}^2}/_{\mathrm{g}}$
Specific pore volume	0.42 ${}^{\mathrm{ml}}/_{\mathrm{g}}$
Average pore diameter	34.2 Å (3.42 nm)
Bulk density	660 ${}^{\mathrm{g}}/_{\mathrm{l}}$

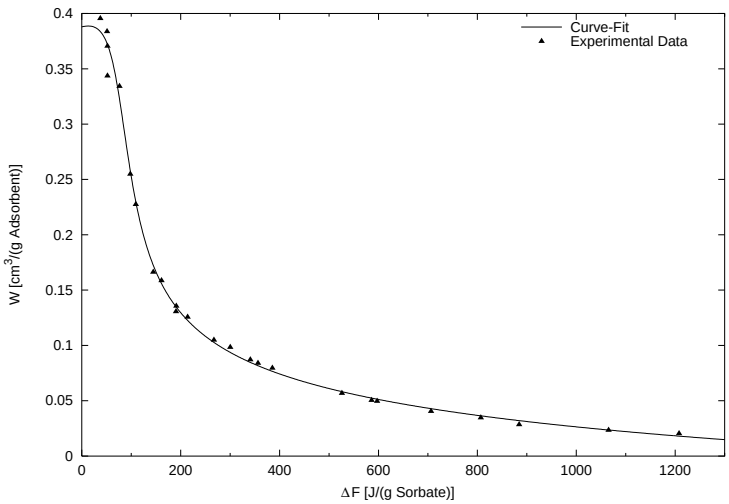

Figure B.22: Experimental data fitted to the *characteristic curve* $W(\Delta F)$.

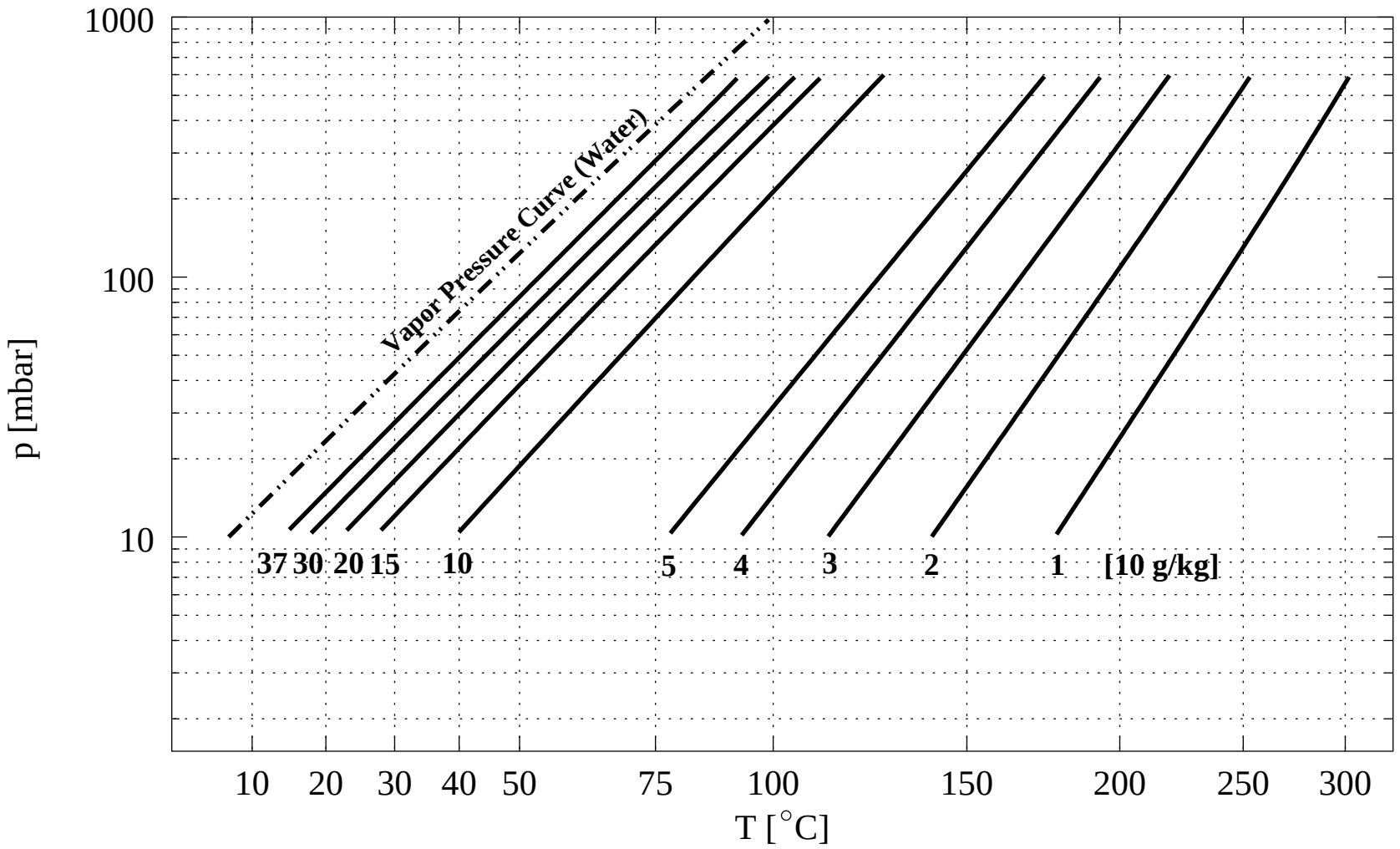

Figure B.23: Isosteric field of Sizeo 15.

B.2.11 Zeolite 13X + Water

Zeolite 13X was obtained under the trade name Baylith WE 592 from Bayer AG (Germany).

The *characteristic curve* $W(\Delta F)$ is fitted by a linear function in the range 10 $^{J}/_{g} < \Delta F <$ 1970 $^{J}/_{g}$):

$$W(\Delta F) = \frac{a + c\sqrt{\Delta F} + e\,\Delta F + g\,x\sqrt{\Delta F}}{1 + b\sqrt{\Delta F} + d\,x + f\,x\sqrt{\Delta F}}$$

$$\begin{aligned} a &= 3.083531 \times 10^{-1} \\ b &= -5.415506 \times 10^{-2} \\ c &= -1.969937 \times 10^{-2} \\ d &= 8.174501 \times 10^{-4} \\ e &= 4.362905 \times 10^{-4} \\ f &= 2.339058 \times 10^{-6} \\ g &= -3.199002 \times 10^{-6} \end{aligned}$$

The following properties are given by the manufacturer:

Property	Specification
Type of zeolite	type X in the Na–form
Pore size	9 Å(0.9 nm)
Form supplied	spherical beads
Particle size	1.5 – 2.5 mm
Bulk density	≈670 $^{g}/_{l}$
Settled bulk density	≈680 $^{g}/_{l}$
Bead density	≈1.05 $^{g}/_{cm^3}$
pH–5% aqueous suspension	≈9–10
Maximum H_2O heat	3767 $^{kJ}/_{kg}$
Specific heat capacity	920 $^{J}/_{kg\,K}$

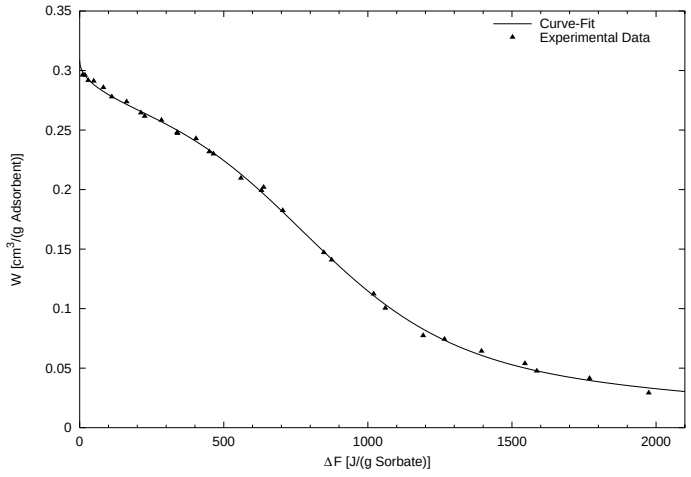

Figure B.24: Experimental data fitted to the *characteristic curve* $W(\Delta F)$.

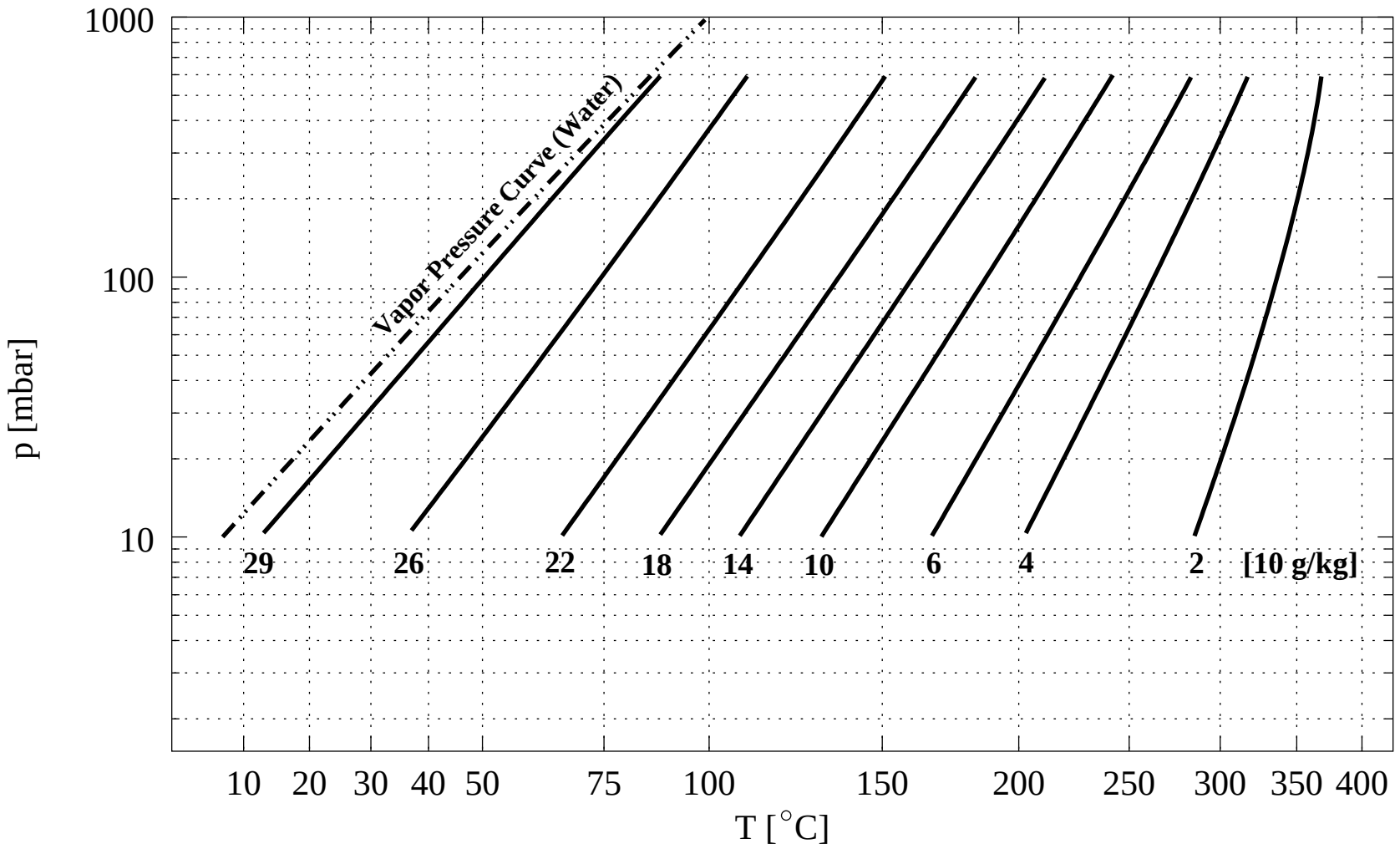

Figure B.25: Isosteric field of Zeolite 13X.

B.2.12 Na–Zeolite Y + Water

Na–Zeolite Y was obtained under the trade name Baylith CP 190 from Bayer AG (Germany).

The *characteristic curve* $W(\Delta F)$ is fitted by a constrained non–linear fit SVD–rational (valid in the range 28 $^{J}/_{g} < \Delta F < 1770$ $^{J}/_{g}$):

$$W(\Delta F) = \frac{a + c\sqrt{\Delta F} + e\,\Delta F}{1 + b\sqrt{\Delta F} + d\,\Delta F + f\,\Delta F\sqrt{\Delta F}}$$

with the coefficients:

$$\begin{aligned} a &= 3.393156 \times 10^{-1} & d &= -2.448014 \times 10^{-3} \\ b &= 8.766651 \times 10^{-3} & e &= 9.055743 \times 10^{-5} \\ c &= -1.104630 \times 10^{-2} & f &= 6.243287 \times 10^{-5} \end{aligned}$$

The following properties are given by the manufacturer:

Property	Specification
Type of zeolite	Na–Zeolite Y
molar ratio SiO_2/Al_2O_3	4.8
Na_2O/Al_2O_3	0.9 ± 0.2
Pore size	9 Å(0.9 nm)
Form supplied	powder
Particle size	1.5 – 3 mm
Bulk density	≈400–500 $^{g}/_{l}$
BET surface area	800 $^{m^2}/_{g}$
pH–5% aqueous suspension	≈10.5

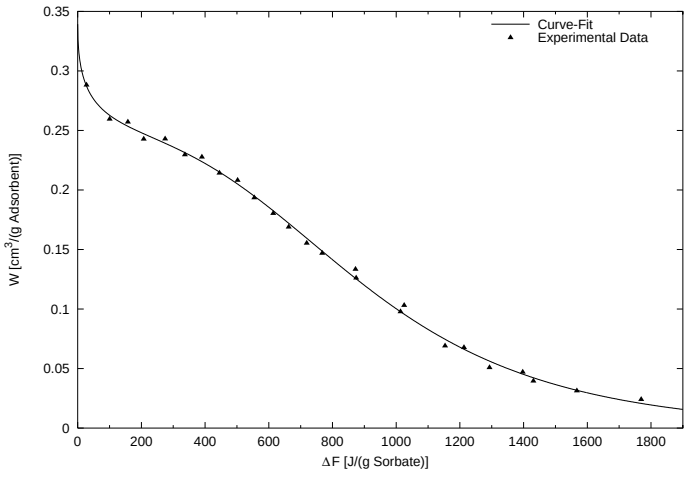

Figure B.26: Experimental data fitted to the *characteristic curve* $W(\Delta F)$.

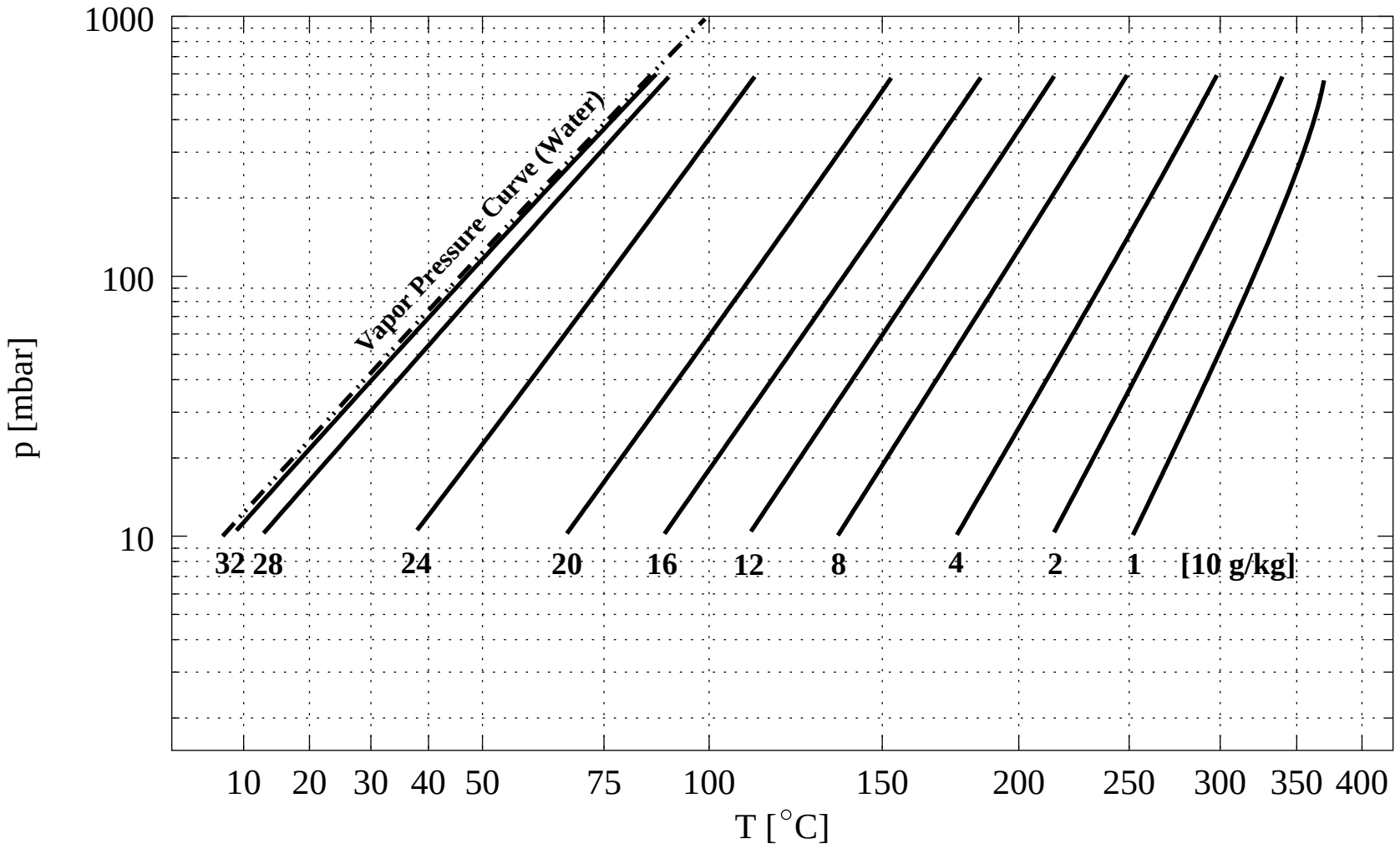

Figure B.27: Isosteric field of Zeolite CP 190 (Na–Zeolite Y).

B.2.13 Zeolite Type A + Water

Zeolite Type A was obtained under the trade name Baylith KE–154 from Bayer AG (Germany).

The *characteristic curve* $W(\Delta F)$ is fitted by a Chebyshev series rational order 3/3 (valid in the range 8 $^{J}/_{g} < \Delta F < 2120$ $^{J}/_{g}$):

$$W(\Delta F) = \frac{a + c\,x + e\,(2\,x^2 - 1) + g\,(4\,x^3 - 3\,x)}{1 + b\,x + d\,(2\,x^2 - 1) + f\,(4\,x^3 - 3\,x)}, \quad x = \frac{\Delta F - 1061.930}{1065.595}$$

with the coefficients:

$$\begin{aligned} a &= 3.472616 \times 10^{-2} & e &= 1.350676 \times 10^{-3} \\ b &= 1.322831 & f &= 1.313913 \times 10^{-1} \\ c &= 9.401171 \times 10^{-3} & g &= -1.926730 \times 10^{-4} \\ d &= 5.760414 \times 10^{-1} \end{aligned}$$

The following properties are given by the manufacturer:

Property	Specification
Type of zeolite	type A in the Ca–Na–form
Pore size	5 Å(0.5 nm)
Form supplied	spherical beads
Particle size	1.5 – 3 mm
Bulk density	≈740 $^{g}/_{l}$
Settled bulk density	≈760 $^{g}/_{l}$
Bead density	≈1.2 $^{g}/_{cm^3}$
pH–5% aqueous suspension	≈8–9
Maximum H_2O heat	3767 $^{kJ}/_{kg}$
Specific heat capacity	920 $^{J}/_{kg\,K}$

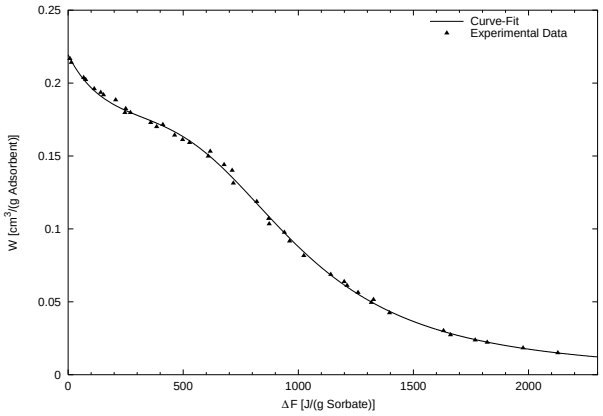

Figure B.28: Experimental data fitted to the *characteristic curve* $W(\Delta F)$.

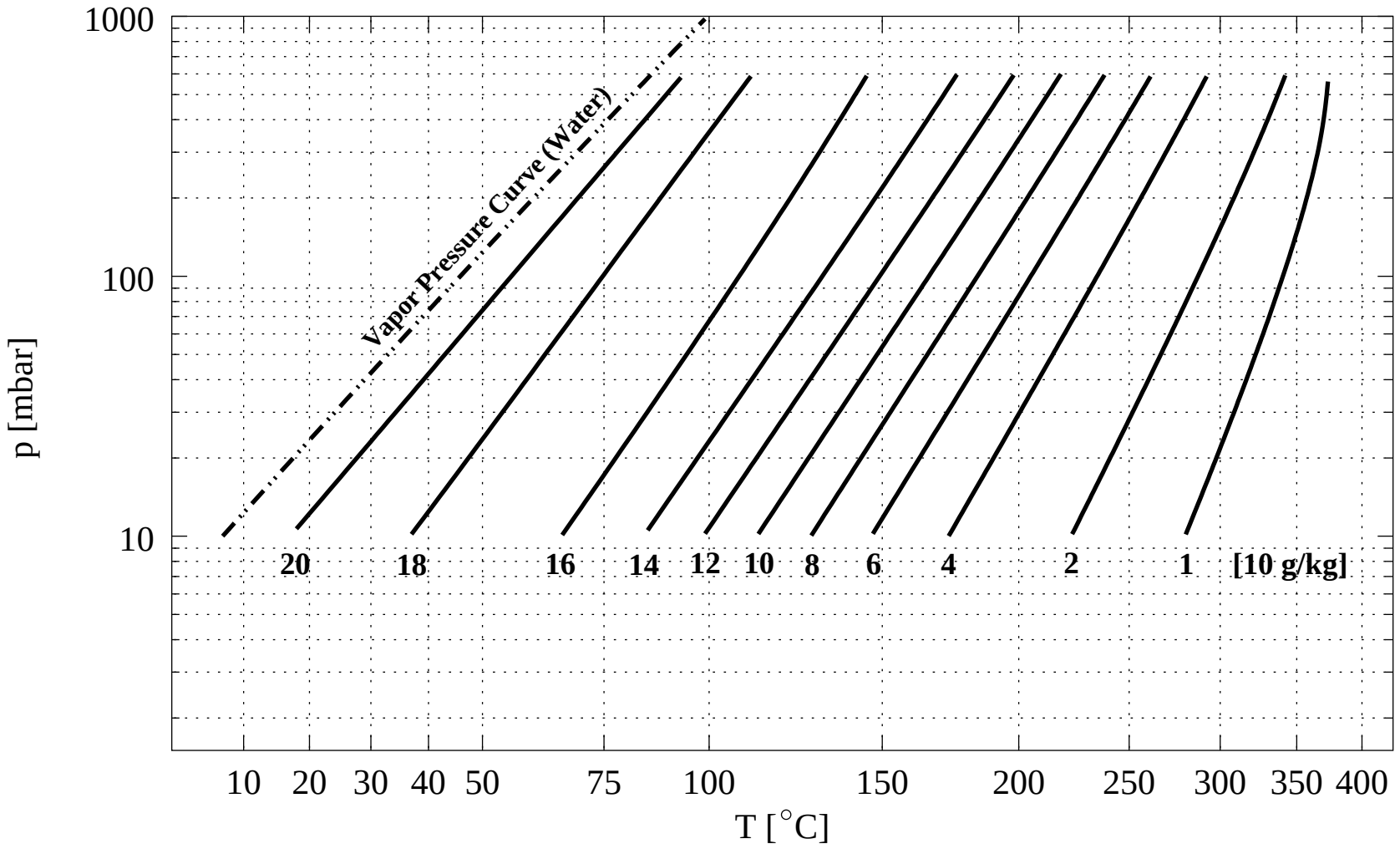

Figure B.29: Isosteric field of Zeolite KE 154 (Zeolite A).

Appendix C

Working Fluids and their Properties

In recent years working fluids became of great ecological significance due to the problems of CFC causing atmospheric pollution. Therefore and for high efficiencies the working fluids should be able to meet several of the following demands:

- low or no *Ozone Depletion Potential* (ODP)
- low or no *Global Warming Potential* (GWP)
- no harmful effect on the human organism
- non–explosive in connection with oxygen
- vapor pressure above atmospheric pressure, else vacuum necessary
- high latent heat of vaporization
- high stability with respect to materials (adsorptive and component material) and sealings
- no catalytic decomposition
- low dynamic (absolute) viscosity
- high heat transfer characteristics
- polarity and hydrophilic behaviour should suite to the adsorptive material (e.g. zeolite–water is a good choice but not zeolite–methanol)
- simple and cost–effective commercial production
- trouble–free disposal or recycling

Water, fulfilling nearly all these requirements, becomes the best choice, but it needs low pressures to evaporate and has a high freezing point. Working fluids with zero ODP and GWP are:

- **Water**
  - \+ high latent heat of vaporization
  - \+ high stability
  - \+ non–toxic
  - \+ unlimited available
  - \+ economical

+ relatively non–corrosive
– limited temperature range ⇒ high triple point, but can be decreased by dissolving salts or propylene glycol (effects of the dissolved component on the adsorptive material should be studied)
– for evaporation at low temperatures a vacuum is necessary

- **Methanol and Ethanol**
  + latent heat of vaporization is relatively high
  + low freezing point
  – for evaporation at low temperatures a vacuum is necessary
  – methanol toxic and ethanol slightly toxic
  – poor stability at high temperatures
- **Propane and iso–Butane** (saturated hydrocarbons)
  + non–toxic
  + for evaporation at low temperatures no vacuum is necessary
  – low latent heat of vaporization
  – flammable
- **Ammonia**
  + latent heat of vaporization is relatively high
  + high stability
  + very low freezing temperature
  + no vacuum is necessary
  – toxic
  – high pressures, depending on the condensation temperature

The table below presents the main physical properties of the working fluids listed above:

	Water H_2O (R718)	Methanol CH_4O	Ethanol C_2H_6O	Ammonia NH_3 (R717)	Propane C_3H_8 (R290)	iso–Butane $CH(CH_3)_3$ (R600a)
CASRN	7732–18–5	67–56–1	64–17–5	7664–41–7	74–98–6	75–28–5
MolWt	18.015	32.042	46.069	17.031	44.094	58.124
ϱ	0.998‡	0.80‡	0.79‡	0.77*	2.01*	2.70*
$\mathbf{T_{fp}}$	273.15	175.5	159.1	195.4	85.5	113.6
$\mathbf{h_s}$	335.0	103.0	108.0	339.0	80.0	80.0
$\mathbf{T_b}$	373.15	337.7	351.4	239.8	231.1	261.4
L	2257.0	1100.0	846.0	1369.0	426.0	386.0
$\mathbf{c_p}$	4.182	2.495	2.395	4.74	2.592	2.48
$\mathbf{T_{crit}}$	647.3	512.6	513.9	405.5	369.8	408.2
$\mathbf{p_{crit}}$	221.2	80.9	61.4	113.5	42.5	36.5
$\mathbf{v_{crit}}$	57.1	118.0	167.1	72.5	203.0	263.0
$\boldsymbol{\varrho_{crit}}$	322.0	272.0	276.0	234.7	217.0	228.0
Dipm $\mu_\mathbf{D}$	1.8	1.7	1.7	1.5	0.0	0.1

CAS RN	...	Chemical Abstracts Service Registry Number
MolWt	...	molecular weight $[g/mol]$
$\boldsymbol{\varrho}$	...	density at (20°C, 1013 mbar)‡ and (0°C, 1013 mbar)* $[kg/m^3]$
$\mathbf{T_{fp}}$	...	normal freezing point $[Kelvin]$
$\mathbf{h_s}$	...	enthalpy of fusion $[kJ/kg]$
$\mathbf{T_b}$	...	normal boiling point $[Kelvin]$
L	...	latent heat of vaporization $[kJ/kg]$ at T_b
$\mathbf{c_p}$	...	specific heat capacity of the liquid state at constant atmospheric pressure 1013 mbar and 20°C $[kJ/kg\,K]$
$\mathbf{T_{crit}}$	...	critical temperature $[Kelvin]$
$\mathbf{p_{crit}}$	...	critical pressure $[bar]$
$\mathbf{v_{crit}}$	...	critical volume $[cm^3/mole]$
$\boldsymbol{\varrho_{crit}}$	...	critical density $[kg/m^3]$
Dipm $\mu_{\mathbf{D}}$	...	dipole moment (temperature independent) $[Debye]$

For computer calculations the properties mostly as function of temperature are available in form of empirical equations found in the literature or tabulated values which are fitted best by any equation.

C.1 Water

C.1.1 Vapor Pressure

Irvine et al. [40] present an equation for the saturated vapor pressure p_v [MPa] which is valid for the temperature range $273.15\,K \leq T_s \leq 647.3\,K$.

$$ln(p_v) = \sum_{i=0}^{9}(c_i\,T_s^i) + \frac{c_{10}}{T_s - c_{11}} \tag{C.1}$$

with the coefficients:

$$\begin{aligned}
c_0 &= 0.104592 \times 10^{2} & c_6 &= 0.903668 \times 10^{-15}\\
c_1 &= -0.404897 \times 10^{-2} & c_7 &= -0.199690 \times 10^{-17}\\
c_2 &= -0.417520 \times 10^{-4} & c_8 &= 0.779287 \times 10^{-21}\\
c_3 &= 0.368510 \times 10^{-6} & c_9 &= 0.191482 \times 10^{-24}\\
c_4 &= -0.101520 \times 10^{-8} & c_{10} &= -0.396806 \times 10^{4}\\
c_5 &= 0.865310 \times 10^{-12} & c_{11} &= 0.395735 \times 10^{2}
\end{aligned}$$

C.1.2 Saturation Temperature

The saturation temperature T_s [K] can be calculated from the known saturated vapor pressure p_v [MPa]. An equation is reported by Irvine et al. [40]:

$$T_s = c_0 + \frac{c_1}{ln\,p_v + c_2} \tag{C.2}$$

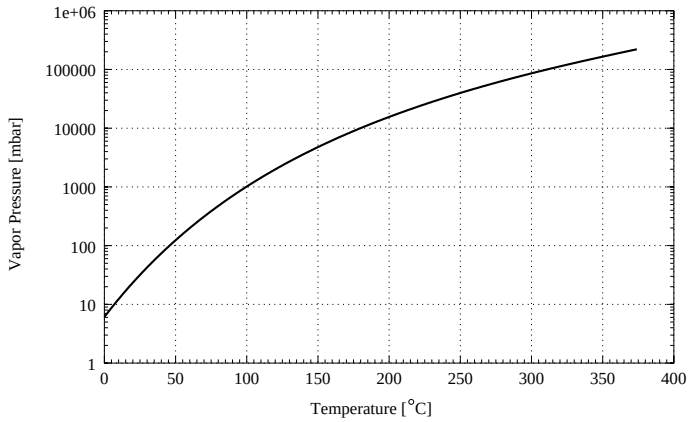

Figure C.1: Vapor pressure of water/steam.

The coefficients c_1, c_2 and c_3 are given for two pressure and temperature ranges:

$0.00611\ bar \leq p_v \leq 123.3\ bar$	$123.3\ bar \leq p_v \leq 221.0\ bar$
$273.16\ K \leq T_s \leq 600.0\ K$	$600.0\ K \leq T_s \leq 647.3\ K$

$$
\begin{aligned}
c_0 &= 0.426777 \times 10^2 & c_0 &= -0.387592 \times 10^3 \\
c_1 &= -0.389200 \times 10^4 & c_1 &= -0.125875 \times 10^5 \\
c_2 &= -0.948654 \times 10^1 & c_2 &= -0.152578 \times 10^2
\end{aligned}
$$

C.1.3 Latent Heat of Vaporization

An equation for the calculation of the latent heat of vaporization L [J/g] *(difference between the vapor saturation enthalpy and the liquid saturation enthalpy)* as function of the saturation temperature T_s [K] is made available by Irvine et al. [40].

$$\frac{L}{L_{tp}} = c_0 + c_1 T^{\frac{1}{3}} + c_2 T^{\frac{5}{6}} c_3 T^{\frac{7}{8}} + \sum_{i=4}^{8} c_i T^i \tag{C.3}$$

with

$$T = \frac{T_{crit} - T_s}{T_{crit}}$$

The coefficients c_i and the value of the latent heat of vaporization at triple point L_{tp} are:

$$
\begin{aligned}
c_0 &= 0.0 & c_5 &= 2.94553 \\
c_1 &= 7.79221 \times 10^{-1} & c_6 &= -8.06395 \\
c_2 &= 4.62668 & c_7 &= 1.15633 \times 10^1 \\
c_3 &= -1.07931 & c_8 &= -6.02884 \\
c_4 &= -3.87446 & r_{tp} &= 2.5009 \times 10^3
\end{aligned}
$$

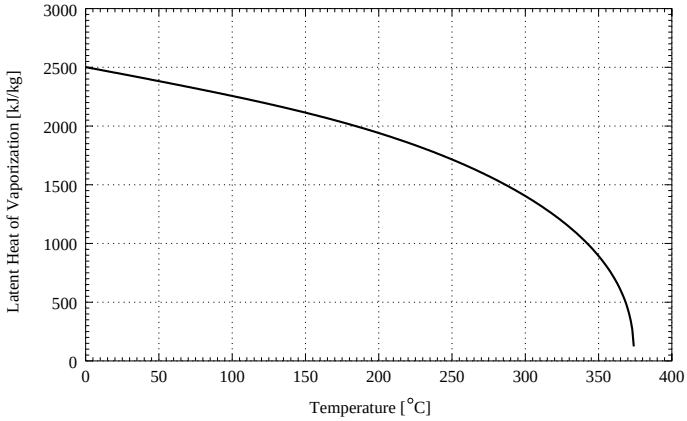

Figure C.2: Latent heat of vaporization of water/steam.

C.1.4 Specific Volume = 1/Density

The *International Formulation Committee IFC of the Sixth International Conference on the Properties of Steam* published in [63] beside others a formulation for the specific volume υ $[\frac{m^3}{kg}]$ of water in the temperature range of $273.16 \leq T \leq 1073.15\ K$ and pressure range of $0 \leq p \leq 1000\ bar$:

$$\begin{aligned}\chi =& I_1 \frac{\theta}{\beta} - \sum_{i=1}^{5} \left(i\, \beta^{i-1} \sum_{j=1}^{n(i)} C_{ij}\, y^{u(i,j)} \right) - \sum_{i=6}^{8} \frac{(i-2)\, \beta^{1-i} \sum_{j=1}^{n(i)} C_{ij}\, y^{u(i,j)}}{\left(\beta^{2-i} + \sum_{k=1}^{l(i)} c_{ik}\, y^{w(i,k)} \right)^2} \\ &+ 11 \left(\frac{\beta}{\beta_L} \right)^{10} \sum_{i=0}^{6} C_{9i}\, y^i \end{aligned} \tag{C.4}$$

with

$$\begin{aligned} y &= e^{c\,(1-\theta)}, \\ \beta_L(\theta) &= \frac{(\theta_2 - \theta)\, \beta_1 + (\theta - \theta_1)\, \beta_2 - L\, (\theta_2 - \theta)\, (\theta - \theta_1)}{\theta_2 - \theta_1}, \\ \chi &= \frac{\upsilon}{\upsilon_c}, \\ \theta &= \frac{T}{T_c}, \\ \beta &= \frac{p}{p_c}. \end{aligned}$$

The numerical values of the coefficients C_{ij} and c_{ij}, the derived constants of the reduced temperature θ_1 and θ_2, the reduced pressures β_1 and β_2, the reduced gas constant of the ideal gas I_1 and the values of the L–function L, L_0, L_1 and L_2 are listed in the table below:

$$
\begin{aligned}
C_{11} &= 6.670376 \times 10^{-2} & C_{90} &= 1.936588 \times 10^{2} \\
C_{12} &= 1.388984 & C_{91} &= -1.388522 \times 10^{3} \\
C_{21} &= 8.390104 \times 10^{-2} & C_{92} &= 4.126607 \times 10^{3} \\
C_{22} &= 2.614671 \times 10^{-2} & C_{93} &= -6.508212 \times 10^{3} \\
C_{23} &= -3.373439 \times 10^{-2} & C_{94} &= 5.745984 \times 10^{3} \\
C_{31} &= 4.520919 \times 10^{-1} & C_{95} &= -2.693088 \times 10^{3} \\
C_{32} &= 1.069037 \times 10^{-1} & C_{96} &= 5.235719 \times 10^{2} \\
C_{41} &= -5.975337 \times 10^{-1} & c &= 7.633333 \times 10^{-1} \\
C_{42} &= -8.847536 \times 10^{-2} & c_{61} &= 4.006074 \times 10^{-1} \\
C_{51} &= 5.958052 \times 10^{-1} & c_{71} &= 8.636082 \times 10^{-2} \\
C_{52} &= -5.159303 \times 10^{-1} & c_{81} &= -8.532323 \times 10^{-1} \\
C_{53} &= 2.075021 \times 10^{-1} & c_{82} &= 3.460209 \times 10^{-1} \\
C_{61} &= 1.190610 \times 10^{-1} & \theta_1 &= 9.626912 \times 10^{-1} \\
C_{62} &= -9.867174 \times 10^{-2} & \theta_2 &= 1.333462 \\
C_{71} &= 1.683999 \times 10^{-1} & \beta_1 &= 7.475192 \times 10^{-1} \\
C_{72} &= -5.809438 \times 10^{-2} & \beta_2 &= 4.520796 \\
C_{81} &= 6.552390 \times 10^{-3} & I_1 &= 4.260321 \\
C_{82} &= 5.710219 \times 10^{-4} & L &= 7.160998
\end{aligned}
$$

Furthermore the number of terms $n(i)$ and $l(i)$, and the exponents $u(i,j)$ and $w(i,j)$ are given as follows:

i	n(i)	$u(i,j)$			l(i)	$w(i,k)$	
		$j=1$	$j=2$	$j=3$		$k=1$	$k=2$
1	2	13	3	–	–	–	–
2	3	18	2	1	–	–	–
3	2	18	10	–	–	–	–
4	2	25	14	–	–	–	–
5	3	32	28	24	–	–	–
6	2	12	11	–	1	14	–
7	2	24	18	–	1	19	–
8	2	24	14	–	2	54	27

Alternatively and in a less complicated way the density of the saturated liquid can be calculated by a self–fitted function based on the data pairs (T, ϱ) which are taken from the NBS/NRC Steam Tables [37]. As fitted density function $\varrho(T_s)$ $[\frac{kg}{m^3}]$ depending on the saturation temperature T_s $[K]$ the rational function

$$\varrho = \frac{c_0 + c_2\,T_s^2 + c_4\,T_s^4 + c_6\,T_s^6}{1 + c_1\,T_s^2 + c_3\,T_s^4 + c_5\,T_s^6 + c_7\,T_s^8} \tag{C.5}$$

was chosen with its coefficients

$$
\begin{aligned}
c_0 &= \quad 1.208088 \times 10^{3} & c_4 &= \quad 1.513557 \times 10^{-7} \\
c_1 &= -3.267456 \times 10^{-5} & c_5 &= -2.389353 \times 10^{-17} \\
c_2 &= -0.038724 & c_6 &= -1.573137 \times 10^{-13} \\
c_3 &= \quad 9.808551 \times 10^{11} & c_7 &= -9.152471 \times 10^{-23}
\end{aligned}
$$

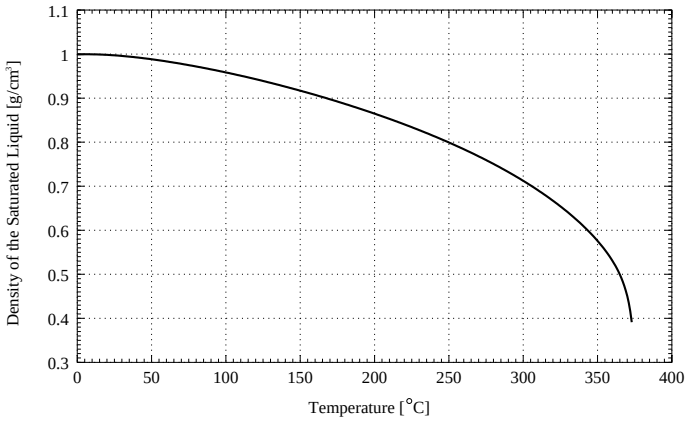

Figure C.3: Density of saturated liquid water.

C.1.5 Specific Heat Capacity

For the calculation of the specific heat capacity at constant pressure of saturated steam c_p $[^{\mathrm{kJ}}/_{(\mathrm{kg\,K})}]$ as function of the saturation temperature T_s, Glück [76] presents an equation valid in the temperature range of $273.15\,K \leq T_s < 647.3\,K$:

$$c_p = 1.862 + 2.858485 \times 10^{-4}\,T_s + 6.148483 \times 10^{-7}\,T_s^2 - 2.060606 \times 10^{-10}\,T_s^3 \qquad \text{(C.6)}$$

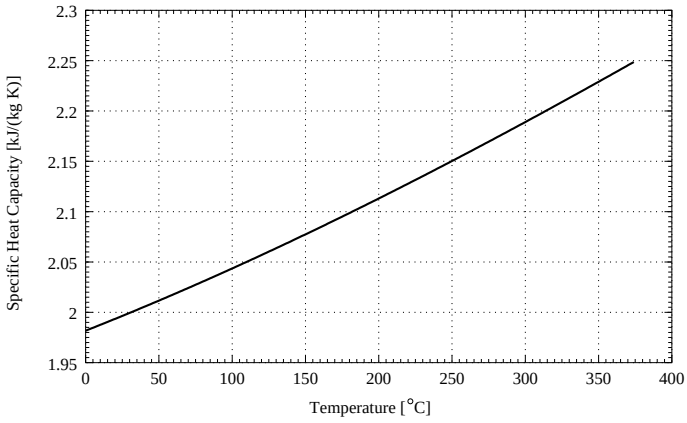

Figure C.4: Specific heat capacity of water/steam.

Appendix D

Heat Transfer Fluid Properties

The single–adsorber experimental setup as well as the theoretically proposed two–bed adsorbers or multi–effect adsorption heat pumps will be provided with two different heat transfer fluids (coolants). The evaporator and the heat sink are supplied with water or a mixture of water with polypropylene glycol, if the evaporator operates below the freezing point of water. Water is an excellent heat transfer medium because it is cheap, available in nearly all parts of the world, non–toxic, relatively non–corrosive or otherwise not harmful to many materials. Water combines the physical properties of high latent heat of vaporization, high thermal conductivity, high specific heat, and high density with moderate viscosity (properties are listed in appendix C), which allows a large amount of heat to be carried away at high rates of heat transfer with only moderate pumping work required. Using the good heat–transfer characteristics of liquid water at temperatures above its boiling point of 100°C it must be pressurized, i.e. for a temperature of 320°C maximally needed to desorb zeolite, a pressure of nearly 115 bar is necessary. Thus for heat supply of the adsorber, for heat transfer between the adsorbers, and for heat output of the latent heat of adsorption thermal oils are necessary. Such a thermal oil which has a vapor pressure below the atmospheric pressure of 860 hPa at 360°C is *Marlotherm SH* from Hüls AG (Germany).

D.1 Thermal Oil

Marlotherm SH is a high–performance synthetic, organic heat transfer medium for use in the liquid phase in closed circulation systems. It can be used over the whole working range without being kept under pressure. This oil is advantageously used in the temperature range from 250°C to 340°C. The upper limit corresponds to a maximum film temperature of 380°C for a prolonged period. From the chemical point of view Marlotherm SH is a clear liquid–based isomeric dibenzyltoluene containing minimal amounts of homologous structures. The properties are given below.

Property	Value
Boiling range at 1013 mbar	385–395°C
Density at 20°C	1044 $\frac{kg}{m^3}$
Kinematic viscosity at 20°C	47 $\frac{mm^2}{s}$
Ignition temperature	$\approx$ 450°C
Permissible heater outlet temperature	350°C
Permissible film temperature	380°C
Pumpability limit temperature	-5°C

D.1.1 Liquid Density

The density ρ [kg/m^3] as linear function of the temperature T [K] in the range of 293.15 K up to 633.15 K:

$$\rho = 58.821 \times 10^4 * T \tag{D.1}$$

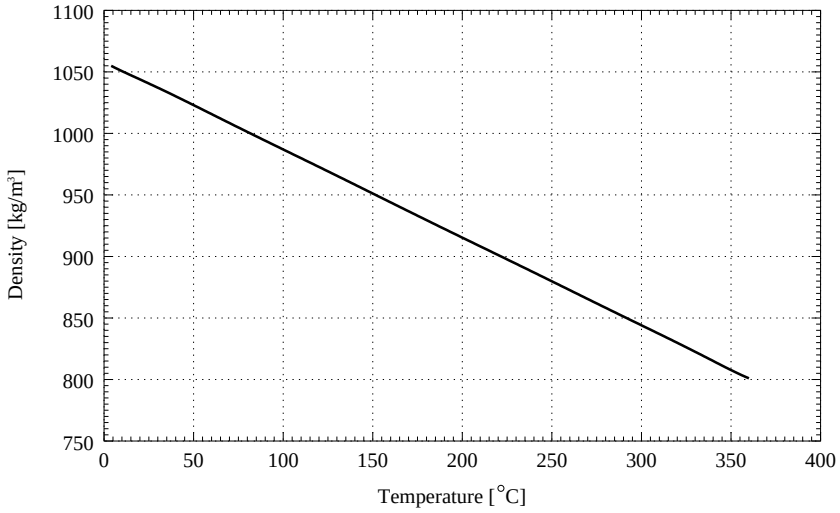

D.1.2 Specific Heat

The specific heat c_p [J/(gK)] of the liquid thermal oil as function of the temperature T [K] (range: $293.15\,K \leq T \leq 633.15\,K$) is described by a Chebyshev Polynomial of order 11:

$$c_p = \sum_{i=0}^{i=11} c_i * F_i(T') \tag{D.2}$$

where T' represents the mapping of the temperature T in the range of -1 to 1

$$T' = \frac{T - 453.150}{180.0}$$

The Chebyshev Functions $F_i(T')$ are

$$F_i(T') = cos(i\, arccos(T'))$$

and can be combined with trigonometric identities to yield explicit expressions for $F_i(T')$

$$F_{i+1}(T') = 2\,T'\,F_i(T') - F_{n-1}(T') \qquad \text{for} \quad n \geq 1$$

The coefficients for (D.2) are given as:

$$
\begin{aligned}
c_0 &= 2.145875 \\
c_1 &= 6.695702 \times 10^{-1} \\
c_2 &= 2.274028 \times 10^{-3} \\
c_3 &= -1.277471 \times 10^{-3} \\
c_4 &= 1.452723 \times 10^{-3} \\
c_5 &= -7.364749 \times 10^{-4} \\
c_6 &= 7.428131 \times 10^{-4} \\
c_7 &= -1.198653 \times 10^{-6} \\
c_8 &= 7.618788 \times 10^{-4} \\
c_9 &= 1.625140 \times 10^{-3} \\
c_{10} &= -1.156713 \times 10^{-3} \\
c_{11} &= 7.947980 \times 10^{-4}
\end{aligned}
$$

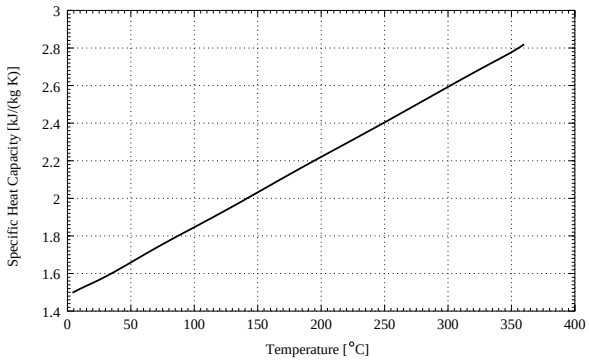

D.1.3 Thermal Conductivity

The fitted expression for the thermal conductivity k [W/(mK)] of the liquid thermal oil as function of the temperature T [K] valid from 293.15 K up to 633.15 K is given by a Fourier Series Polynomial of 5th order

$$k = c_0 + \sum_{i=1}^{i=5} c_{2\,i-1}\, cos(i\,T') + c_{2\,i}\, sin(i\,T') \tag{D.3}$$

where T' is

$$T' = \frac{T - 293.150}{108.225361}$$

The coefficients for (D.3) are given as:

$$
\begin{aligned}
c_0 &= 7.931626 \times 10^{-2} \\
c_1 &= 1.322260 \times 10^{-2} \\
c_2 &= 5.382802 \times 10^{-2} \\
c_3 &= 3.763841 \times 10^{-2} \\
c_4 &= 9.783270 \times 10^{-3} \\
c_5 &= 1.204579 \times 10^{-2} \\
c_6 &= -2.006787 \times 10^{-2} \\
c_7 &= -7.457715 \times 10^{-3} \\
c_8 &= -6.608146 \times 10^{-3} \\
c_9 &= -1.748311 \times 10^{-3} \\
c_{10} &= 1.607589 \times 10^{-3}
\end{aligned}
$$

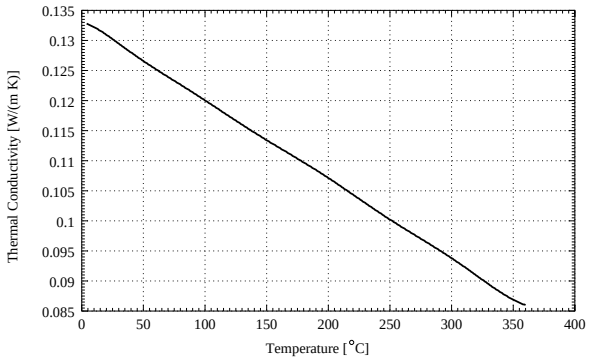

D.1.4 Kinematic Viscosity

Another Fourier Series Polynomial of 7th order is used to calculate the kinematic viscosity ν [mm^2/s] of the thermal oil depending on temperature (range: $293.15\,K \leq T \leq 633.15\,K$):

$$\nu = c_0 + \sum_{i=1}^{i=7} c_{2\,i-1}\, cos(i\,T') + c_{2\,i}\, sin(i\,T') \tag{D.4}$$

where T' is

$$T' = \frac{T - 293.150}{108.225361}$$

The coefficients for (D.4) are given as:

$$\begin{aligned}
c_0 &= 9.463364 \times 10^{2} \\
c_1 &= 3.494670 \times 10^{2} \\
c_2 &= -1.673998 \times 10^{3} \\
c_3 &= -1.159631 \times 10^{3} \\
c_4 &= -4.995025 \times 10^{2} \\
c_5 &= -4.280962 \times 10^{2} \\
c_6 &= 620.775325 \times 10^{-5} \\
c_7 &= 2.479469 \times 10^{2} \\
c_8 &= 2.546990 \times 10^{2} \\
c_9 &= 1.057274 \times 10^{2} \\
c_{10} &= -6.850451 \times 10^{1} \\
c_{11} &= -1.099214 \times 10^{1} \\
c_{12} &= -2.827088 \times 10^{1} \\
c_{13} &= -3.758226 \\
c_{14} &= 5.721241 \times 10^{-1}
\end{aligned}$$

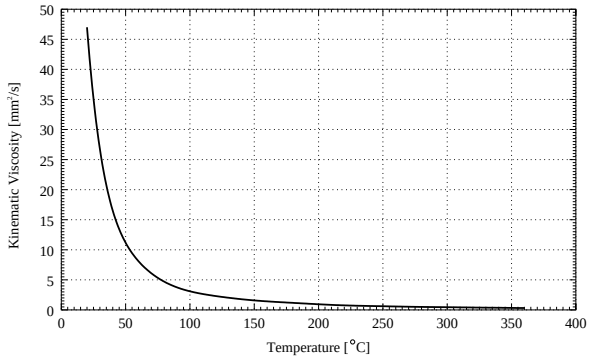

D.1.5 Prandtl Number

The fitting equation for the Prandtl number Pr [–] as function of the temperature T [K] valid from 293.15 K up to 633.15 K is represented by an inverse polynomial of order 9:

$$Pr = \sum_{i=0}^{i=9} \frac{c_i}{T^i} \tag{D.5}$$

where the coefficients are given as follows:

$$\begin{aligned}
c_0 &= -8.526948 \times 10^{5} \\
c_1 &= 3.402260 \times 10^{9} \\
c_2 &= -5.986761 \times 10^{12} \\
c_3 &= 6.098774 \times 10^{15} \\
c_4 &= -3.964678 \times 10^{18} \\
c_5 &= 1.706043 \times 10^{21} \\
c_6 &= -4.860824 \times 10^{23} \\
c_7 &= 8.845244 \times 10^{25} \\
c_8 &= -9.331314 \times 10^{27} \\
c_9 &= 4.349904 \times 10^{29}
\end{aligned}$$